DEVELOPMENT OF SUSTAINABLE STRUCTURAL MATERIALS USING BASALT FIBER AND AGRICULTURAL WASTE IN CEMENTITIOUS SYSTEM FOR GROUND IMPROVEMENT

「セメント系における玄武岩繊維と農業廃棄物を利用した持続可能な地盤改良用構造材料の開発」

A dissertation submitted in partial fulfillment of the requirements of the degree of Doctor of Philosophy in the Department of Environmental Science and Technology of Mie University

By

OWINO ALEX OTIENO

Soil Resources Engineering Laboratory

Department of Environmental Science and Technology

Graduate School of Bioresources

Mie University Mie, Japan

September 2023

DEVELOPMENT OF SUSTAINABLE STRUCTURAL MATERIALS USING BASALT FIBER AND AGRICULTURAL WASTE IN CEMENTITIOUS SYSTEM FOR GROUND IMPROVEMENT

「セメント系における玄武岩繊維と農業廃棄物を利用した持続可能な地盤改良用構造材料の開発」

A dissertation submitted in partial fulfillment of the requirements of the degree of Doctor of Philosophy in the Department of Environmental Science and Technology of Mie University

By

OWINO ALEX OTIENO

Examined and approved as to style and contents by

_____

Prof. Dr. Zakaria Hossain
Chairman of the Examination Committee

_____

Prof. Dr. Kenji Okajima
Co-chair of the Committee

_____

Prof. Dr. Kunio Watanabe
Co-chair of the Committee

Soil Resources Engineering Laboratory

Department of Environmental Science and Technology

Graduate School of Bioresources

Mie University Mie, Japan

September, 2023

SPECIAL DEDICATION TO

MY PARENTS AND BELOVED FAMILY

WITH LOTS OF GRATITUDE TO

MY SUPERVISOR:

PROF. DR. ZAKARIA HOSSAIN

ACKNOWLEDGEMENTS

First and foremost, I humbly acknowledge and express my sincere gratitude to the Almighty God for enabling me to commence and successfully complete my Ph.D. Research.

I express my heartfelt gratitude to my family, without whom this achievement would not have been possible. Their unwavering love, encouragement, and support have sustained me through the ups and downs of my academic journey. I am particularly grateful to my parents for instilling in me a love for learning and for their sacrifices that enabled me to pursue my academic goals.

I also express my sincere gratitude and appreciation to my research supervisor and mentor, Prof. Dr. Zakaria Hossain, for his priceless guidance and insightful suggestions throughout this program and for his earnest support and mentorship throughout my Doctoral Research period. I extend my sincere thanks to my academic advisors, Prof. Dr. Kenji Okajima, Prof. Dr. Kunio Watanabe, Prof. Dr. Toshinori Sakai, Prof. Dr. Kajisa Takamitsu, Prof. Dr. Ohno, Prof. Dr. Narioka Hajime, whose guidance, feedback, and support were essential in shaping my research and shaping me into the scholar I am today. Their expertise, passion for research, and unwavering dedication to my success have inspired and motivated me throughout my doctoral studies.

I am also grateful to my colleagues within my research group and beyond, who have provided me with a supportive and intellectually stimulating academic environment. Their willingness to engage in discussions, provide feedback on my work, and share their expertise has enriched my research and contributed to my personal growth as a scholar.

I acknowledge the financial support provided by the Japanese Government-Sponsored Scholarship-MEXT (MONBUKAGAKUSHO) and Make Integrated Technology (M.I.T) Limited, Osaka, Japan, which made it possible for me to carry out my research and attend conferences and workshops. This support not only provided me with the resources needed to pursue my research but also enabled me to connect with other scholars and professionals in my field, enriching my research experience.

I am also indebted to the individuals who assisted me in various aspects of my research, including data collection, analysis, and interpretation. I am particularly grateful to my laboratory mates for their tireless efforts in helping me collect and analyze data. I want to thank my proofreaders and editors, whose careful review and feedback helped me refine and improve the quality of my publications and dissertation. Their commitment to excellence and attention to detail ensured that my publications and dissertation met the highest standards of scholarship.

Finally, I would like to thank the faculty and staff of the Department of Environmental Science and Technology, Graduate School of Bioresources at Mie University, Japan, whose commitment to teaching and research has provided me with a stimulating and supportive academic environment. Their dedication to fostering a culture of intellectual curiosity, rigorous scholarship, and collaboration has shaped my academic journey and prepared me for a career in academia and beyond. This dissertation would not have been possible without their support and encouragement. I hope to continue to build on the foundation they have helped me lay and make meaningful contributions to my field in the coming years.

ABSTRACT

With the increase in the built environment due to urbanization and industrialization, there is a rising demand for infrastructure development in marginalized areas with weak expansive soils, which are considered unsuitable. Expansive soils have been analyzed to possess weak shear strength and high compressibility and pose numerous challenges to civil and geotechnical engineers when constructing any engineering structures. The instability of the expansive soil is due to the high clay contents, which tend to shrink or expand when subjected to moisture content variation. Building on expansive soils can lead to considerable damage to foundations, embankments, and pavements, increasing the cost of constructing durable and safe structures.

Stabilizing and reinforcing the expansive soils to improve their geotechnical properties is vital to curb these challenges. Conventionally, the addition of additives such as cement, lime, and lime-cement mixtures has been practiced extensively. However, the over-dependence on cement and lime has proven to degrade the environment, raising environmental concerns such as contributing to 8 to 10 percent of global anthropogenic CO_2 emission from the 4.1 billion metric tons produced yearly. In addition to the emissions of CO_2, the production of cement and lime can also lead to the depletion of natural resources. Cement production requires large amounts of raw materials such as limestone, clay, and sand. These resources are finite and can become depleted if not managed sustainably. Moreover, mining these raw materials can negatively impact the environment as their manufacture involves the crushing and grinding of raw materials, which can produce large amounts of dust that can negatively impact human health and local ecosystems.

In addition to the environmental drawbacks, cement and lime are susceptible to high plastic shrinkage and cracking, affecting the mechanical strength of the stabilized soil. To reduce these environmental concerns and enhance the geotechnical properties of expansive soils, the partial

replacement of cement and lime with pozzolanic additives such as rice husk ash (RHA) is gaining research attention. The potential use of RHA in soil stabilization can be attributed to; the abundance of rice husks generated worldwide from rice processing and particularly the presence of highly active amorphous silica (SiO_2) produced during the production process of rice husk ash. However, during the soil stabilization phase, the pozzolanic reactions between the additives and the soil form cementitious systems that need further reinforcements to avoid cracking and excessive settlement problems when subjected to extensive loads.

Recently, fibers have been used with cementitious additives to arrest the formation of weak planes in the stabilized soil and to influence the strength of the stabilized composite material. However, in the available literature, most research articles are limited to the reinforcement material used, the soil tested, and the type of stabilizing agent used. To date, few pieces of research have been carried out on expansive soils with no scientific studies on the combined action of RHA, minimal cement dosages, and basalt fiber, particularly its effect on consolidation settlement, volume change, shear strength, bearing capacity, microstructural development, and ultimate permeability.

In this context, the present study aimed to investigate the influences on bearing capacity, shear strength, consolidation coefficients, permeability, and micro and macrostructure of different specified specimen combinations of stabilized and reinforced expansive soils. Each specified specimen combination constituted a mixture of varying basalt fiber lengths and varied dosages of RHA-cement mixtures in their proposed proportions. In addition, the investigation proposed a material combination scheme with superior properties that could be used as a fill or subbase material for engineering structures such as embankments, pavements, and foundations.

In this research, a series of Oedometer tests, Compaction tests, Consolidated-drained (CD) Triaxial tests, Unconfined Compression Strength tests (UCS) tests, Constant head permeability tests, and

microstructural analysis tests (SEM and XRD) were conducted on expansive soil reinforced with different basalt fiber lengths (3mm, 6mm, and 12mm) and stabilized with RHA (5%,10%, and 15%)-cement (3%) mixtures in their specified combinations. Furthermore, scanning electron microscopy (SEM) tests and X-ray diffraction (XRD) analysis were conducted to examine the microstructural modifications and chemical composition developments within the stabilized and reinforced soil composite. The results were presented graphically with correlation equations and pictorial forms to provide additional data and to act as a benchmark for providing solutions to challenges encountered by civil, geotechnical, and geo-environmental engineers working with the new composite material.

Based on the experimental results obtained in this study, it was concluded that adding RHA, minimal dosages of cement, and basalt fiber reinforcements to expansive soil significantly improved its compatibility, bearing capacity, and shear strength, reduced the rate of consolidation settlements, and enhanced the microstructure development. The increased strength enhanced its stability and suitability when used in geotechnical engineering applications.

TABLE OF CONTENTS

LIST OF TABLES

LIST OF FIGURES

List Of Published Scientific Papers

i. Owino, A.O., Nahar, N., Hossain, Z. and Tamaki, N., 2022. Effects of basalt fibres on strength and permeability of rice husk ash-treated expansive soils. Journal of Agricultural Engineering, 53(1). https://doi.org/10.4081/jae.2022.1315

ii. Owino, A.O., Nahar, N., Hossain, Z. and Tamaki, N., 2022. Dimensional influence of basalt fiber reinforcements on the consolidation behaviour of rice husk ash stabilized soils. Construction and Building Materials, 339, p.127686. https://doi.org/10.1016/j.conbuildmat.2022.127686

iii. Owino, A.O. and Hossain, Z., 2023. The influence of basalt fiber filament length on shear strength development of chemically stabilized soils for ground improvement. Construction and Building Materials, 374, p.130930. https://doi.org/10.1016/j.conbuildmat.2023.130930

iv. Owino, A.O. and Hossain, Z., 2023. Correlation between one-dimensional consolidation coefficients and different basalt fiber lengths and RHA-cement contents in fiber-reinforced stabilized expansive soils. Soils and Foundations, 63(4), p.101351. https://doi.org/10.1016/j.sandf.2023.101351

List Of Conference Proceedings

i. Owino, A.O., Ovia, J. U., Shiau, J. and Hossain, Z., 2020. Solar panel foundations on sloping land and offshore ~ A Review, Proc. of 10th International Conference on Geotechnique, Construction Materials and Environment, RMIT University, Melbourne, Australia, 11-13 November 2020, ISBN: 978-4-909106049 C3051, Vol.10, pp. 432-442, 2021.

ii. Owino, A.O., Nahar, N., Sayful, K. K., Hossain, Z. and Tamaki, N., 2021. Effects of basalt fiber on strength and permeability of RHA treated expansive soils, Proc. of 11th International Conference on Geotechnique, Construction Materials and Environment, Kyoto, Japan, 3-5 November 2021, ISBN: 978-4-909106063 C3051, Vol.11, pp. 279-287, 2021.

iii. Owino, A.O. and Hossain, Z., 2022. A Correlation Between One-Dimensional Consolidation Coefficients with Basalt Fiber Length and RHA Content in Fiber-Reinforced Stabilized Expansive Soils, Proc. of 12th International Conference on Geotechnique, Construction Materials and Environment, Bangkok, Thailand, 22-24 November 2022, ISBN: 978-4-909106087 C3051, Vol.12, pp. 288-301, 2022.

iv. Owino, A.O. and Hossain, Z., 2022. The effects of rice husk ash dosage on compressibility and microstructural development of stabilized calcite-rich river sludge, Proc. of 8th International Conference on Structure, Engineering and Environment, Yokkaichi, Mie, Japan, 10-12 November 2022, ISBN: 978-4-909106094 C3051, Vol.12, pp. 282-290, 2022.

CHAPTER 1 : INTRODUCTION

1.1 Research Background

Soil stabilization techniques have been used for centuries to improve soil strength, durability, and stability for various construction projects (Afrin, 2017). The history of soil stabilization techniques can be traced back to ancient civilizations, where natural materials such as lime and clay were used to improve soil quality for construction purposes (Karatai et al., 2017; Galán-Marín et al., 2010). In the early 19th century, using hydraulic lime and pozzolanic materials became popular for soil stabilization (Grist et al., 2013). However, the development of cement in the mid-19th century led to the widespread use of cement-based soil stabilization techniques revolutionizing the soil stabilization field (Zhou et al., 2020). In the 20th century, other soil stabilization techniques were developed, such as bituminous stabilization, chemical stabilization, and geotextile reinforcement. Bituminous stabilization involves mixing bitumen with soil to improve its strength and durability (Zheng et al., 2013); chemical stabilization involves adding chemicals such as lime, cement, and fly ash to the soil to enhance its properties (Jalal et al., 2020; Chen et al., 2021), while geotextile reinforcement involves using synthetic materials such as geotextiles and geogrids to reinforce the soil and improve its stability (Mishra et al., 2022). With the development of new materials and technologies, soil stabilization techniques continued to evolve and improve. Today, a wide range of these soil stabilization techniques are still available, including mechanical stabilization, chemical stabilization, and geosynthetic stabilization. These techniques are widely used in various construction projects such as roads, embankments, bridges, buildings, and airports to improve the quality and durability of soils.

To develop a fundamental understanding of how soils behave under different environmental conditions, which is essential for the design of civil engineering structures and infrastructure projects, an in-depth analysis of the stabilized soil mechanics is paramount. Soil mechanics is a branch of

engineering that deals with the study of the behavior of soils under different loading conditions. It involves the analysis of the physical and mechanical properties of soils, such as their composition, density, porosity, permeability, shear strength, and deformation characteristics. These properties of soil are influenced by various factors, such as the mineral composition of the soil, the amounts of stabilizers added, the degree of compaction, the amount of moisture content, and the type of loading applied during the loading processes. Based on the properties, soils can be categorized into three main types: cohesive, non-cohesive, and organic. Cohesive soil is characterized by high clay content, non-cohesive soil has low clay content, and organic soil is mainly composed of decomposed plant and animal matter.

Conventionally, non-cohesive soils, known as granular soils (including sand, gravel, and crushed rock), are commonly used in engineering construction works because they are generally more stable than cohesive soils. Using cohesive soils, such as clay, in engineering practice during construction is often discouraged due to the low bearing capacity, meaning they cannot support heavy loads or structures leading to settlement, which can cause structural damage and instability. Clay soils are also highly compressible and hence can easily deform under load. The high water content associated with clay soils can cause them to become unstable when wet leading to landslides, slope failures, and other problems. Nevertheless, cohesive soils have low permeability, making it difficult to drain water leading to standing water, which can cause stability problems.

When cohesive soils are unavoidable, engineers must take special precautions and use appropriate techniques to mitigate the risks associated with their use. This challenge has led to the development of soil stabilization techniques aimed at altering soil properties to increase its strength, durability, and resistance to deformation and other ground improvement processes to improve the engineering properties of soil to support civil engineering structures and infrastructure. Some of the common soil stabilization techniques include soil compaction, chemical stabilization, cement stabilization, lime

stabilization, and asphalt stabilization. On the other hand, ground improvement techniques include; (i) soil densification to apply pressure on the soil (Mishra, 2016), (ii) grouting by injecting a fluid material into the soil to fill the voids (Kazemain, 2012), (iii) deep mixing of soil with cement, lime, or other stabilizing agents (Kitazume, 2013), (iv) vibro-compaction using vibratory equipment (Duan, 2019), and (v) soil reinforcement using geosynthetic materials such as geotextiles and geogrids (Suriya, 2020) - all aimed at improving the density, stability, and strength of the soil.

Out of all these methods listed above, the primary soil stabilization and ground improvement methods are soil compaction using rollers or other heavy equipment to compress the soil and chemical stabilization by adding chemicals such as lime, cement, or fly ash to the soil. The latter has been used successfully in many projects (Andavan and Pagadala, 2020; Nguyen and Phan, 2021; Firoozi et al., 2017). However, they are some limitations, such as environmental damage from cement and lime manufacture and high costs incurred when they are used in engineering projects (Santos et al., 2021; Spence and Mulligan, 1995; Obuzor et al., 2012; Formoso et al., 2002). For instance, cement manufacture utilizes approximately 1.7 tons of raw material, yielding about 1 ton of CO_2 during combustion (Van Oss and Padovani, 2002; Akan et al., 2017). Therefore, alternative approaches in binder choices are under study to partially or fully reduce cement and lime usage (Ali et al., 2011). According to a report published in 2020 by the Global Cement and Concrete Association (GCCA), the global production of supplementary cementitious materials (SCMs), including natural pozzolans such as rice husk ash, sugarcane bagasse ash, and palm oil fuel ash, was estimated at around 400 million tons per year. However, large portions remain unused due to unawareness of their potential as a sustainable alternative to cement or the absence of appropriate infrastructure for their utilization in the construction industry.

Recently, efforts have been made to promote using natural cementitious materials from agricultural waste, including research on their properties and the development of standards and guidelines for

their use. Additionally, there is a growing interest in sustainable construction practices that prioritize using environmentally friendly materials and reducing the carbon footprint of construction projects (Basack et al., 2021). In literature, the development of sustainable high-strength cementitious composites using cement substitutes like RHA is rising, but higher cement percentages (>5%) in these stabilized composites require further examination (Zhang et al., 2021; Sensale et al., 2008; Yoobanpot and Jamsawang, 2014; Attah et al., 2021). Consequently, potential soil composite combinations using rice husk ash (RHA) mixed with nominal cement dosages are gaining research attention (Nahar et al., 2021a; Nahar et al., 2021b). The mixture is considered a highly reactive pozzolanic material when amorphous silica (SiO_2) and Al_2O_3 in the RHA react with CaO in cement in the presence of water. The hydration process leads to the formation of a cementitious compound called calcium aluminosilicate hydrate, also known as CSH Gel (Yu et al., 1999; Xu ae al., 2016; Givi et al., 2010; Patel and Shah, 2018; Ali et al., 1992). However, cementitious bonds became brittle during loading at the post-peak strength state, and the residual shear strength significantly diminished (Lorenzo and Bergado, 2006; Panda and Rao, 1998; Porbaha et al., 2000; Yin, 2001).

In this context, using randomly oriented fibers (ROF) to reinforce the cementitious structure of chemically stabilized soil composites is gaining research attention (de Lima et al., 2022). Various types of fibers have recently been used for this purpose, including polypropylene (Vakili et al., 2022), glass (Ateş, 2016), steel (Jamsawang, 2018), and coir fibers (Meena, 2021). The main advantage of ROF reinforcements is the elimination of weak zones in the stabilized soil structure compared to other conventional reinforcement methods (Dhar and Hussain, 2019; Soleiman and Janalizadeh, 2017). Also, fibers are easily mixed with the soil hence a more reliable option for ground improvement in terms of workability (Wang et al., 2020). Even though efforts have been made to study the potential of various fibers in soil stabilization, most studies have only investigated the effects of fiber inclusions in cemented cohesionless soils, with few researchers conducting studies

on weak clay soils (Tang et al., 2007; Chen et al., 2015). In addition, there is limited research on how high-strength fiber filaments that are environmentally friendly (such as basalt fiber) can influence the ultimate shear strength, bearing capacity, compressibility, permeability, and microstructural development of RHA-cement stabilized cohesive soils.

Furthermore, the interaction between basalt fibers and sustainable stabilization techniques using RHA with nominal cement dosages is also scarce. The superiority of basalt fibers over conventional fibers is derived from the high tensile strength and its natural occurrence from basalt rocks which gives it more versatility in enhancing the compressive capabilities of expansive soil composites. Therefore, analyzing stabilized and reinforced weak expansive soils with basalt fibers is necessary to ensure its validation for vast applications due to the enhanced geotechnical behavior. On the other hand, using RHA as a sustainable means of chemically stabilizing expansive soils addresses the environmental pollution concern (For instance, pollution from excessive cement manufacture and pollution from rice husk disposal methods) while maintaining sustainable geotechnical applications in engineering construction works.

1.2 Research Scope

Soil stabilization is a crucial aspect of civil engineering, as it is necessary to ensure the durability and longevity of any infrastructure built on it. Various methods have been developed over the years to achieve this objective. Recent research has shown that using rice husk ash as a cement-reducing aggregate and fiber as a reinforcing material can effectively stabilize the soil. In this context, this research investigated the effectiveness of rice husk ash and basalt fiber in soil stabilization.

The study aimed to provide a comprehensive understanding of the geotechnical properties and characteristics of the stabilized and reinforced soil, the effect of the addition of different dosages of rice husk ash and varied lengths of basalt fiber on the properties of the soil, and the optimum proportion of rice husk ash and basalt fiber to be used for effective soil stabilization. Also, an

investigative approach to the effectiveness of using rice husk ash as a cement-reducing aggregate and basalt fiber as a reinforcing material in soil stabilization was considered through the analysis of the strength development at low cement usage compared to the values obtained from conventional stabilization methods. Moreover, the research on soil stabilization using rice husk ash as a cement-reducing aggregate and basalt fiber as a reinforcing material is also related to the Sustainable Development Goals (SDGs 9, 12, 13, and 15) adopted by the United Nations General Assembly in 2015.

To achieve the research objectives, a review of relevant literature on soil stabilization using conventional binders and other potential silica-based binders mixed with different types of fiber for soil stabilization was essential. This provided a basis for understanding the previous work done in this field, identifying the gaps in knowledge, and providing a framework for the research.

Next, experimental investigations were performed to assess the effects of adding rice husk ash, nominal cement dosages, and varied lengths of basalt fiber to determine the optimum ratio for effective soil stabilization. Aggregates analysis tests (Soil, RHA, and basalt fiber), Standard Proctor compaction tests, Oedometer tests, Unconfined compressive strength (UCS) tests, Consolidated-Drained (CD) Triaxial compression tests, and Constant Head Permeability tests were performed on a wide range of specimen composites under laboratory conditions. Furthermore, a visual and chemical analysis of the new soil composite structure using scanning electron microscopy (SEM) and X-ray diffraction (XRD) was conducted to provide insights into the hybrid mechanisms of soil stabilization and reinforcement techniques at the micro and macro levels. In conclusion, the findings of this research will contribute to the development of a theoretical framework for using rice husk ash and basalt fiber in soil stabilization and provide insights into the intended application areas in civil and geotechnical engineering works.

1.3 Research Objectives

Soil stabilization and reinforcement processes can be achieved through various methods, including using conventional fibers, cement, lime, or other chemical stabilizers. However, these methods can be expensive and have negative environmental impacts during production and utilization. Therefore, alternative methods have gained interest in recent years, such as using rice husk ash (RHA) as a cement-reducing aggregate and basalt fiber as a sustainable and natural reinforcing material. The primary objectives of this research study are outlined as follows:

- To determine the optimum percentage of RHA that can be used as a cement-reducing aggregate. This procedure will involve conducting laboratory tests to evaluate the compressive strength and other relevant properties of the stabilized soil samples with varying percentages of RHA.
- To evaluate the effectiveness of basalt fiber dimensions as a reinforcing material in the stabilized soil. This assessment will involve conducting laboratory tests to value the impact of different basalt fiber lengths on the mechanical properties of stabilized soil composites, such as compressive strength, consolidation characteristics, permeability, and shear strength.
- To compare the performance of the hybridized Soil-RHA-Cement-Basalt fiber stabilized and reinforced soil composites with unreinforced composites made using RHA and cement only. This methodology will involve conducting laboratory tests to evaluate the ultimate strength and load-bearing capacity of proposed soil composites under different loading conditions, including micro and macro-structural investigation.
- To develop a new hybrid composite material for ground improvement using RHA, Cement, and Basalt fiber that is environmentally friendly and follows the set sustainable development goals.

1.4 Research Significance

The type of fiber, fiber filament length, and the amounts of sustainable soil stabilizers in cementitious soil composites can effectively improve the geotechnical properties of weak expansive soils. The

problem associated with the soil failure phenomenon, consolidation behavior, permeability, bearing capacity, and shear response of fiber-reinforced stabilized soils under various loading conditions has been studied quite extensively in the past. However, despite the volume of research available, very little or no research is reported on the developments of the shear strength, permeability, consolidation response, and relatable physical, chemical, and structural behavior of hybridized soil stabilization techniques using environmentally friendly materials. Even though it presents considerable versatility in developing fiber and RHA-reinforced cementitious systems for ground improvement. Most soil reinforcements today involve low tensile strength fibers and are degradable with time. Additionally, these fibers are being used together with well-established stabilizers like cement, which has proven hazardous to the global carbon footprint and is uneconomical considering construction costs. For optimal response, therefore, the utilization of natural high-strength fibers and sustainable stabilizers to produce hybrid fiber-reinforced cementitious systems is necessary. Also, it is paramount to investigate the civil and geotechnical properties development in such composites and to identify the synergistic effects between the blend combinations if present. Additionally, using recyclable aggregates such as RHA can reduce cement usage and disposal problems in an economical and environmentally friendly way through their incorporation into developing new innovative material composites.

1.5 Thesis Outline

Chapter 1 encompasses the research background, scope, objectives, significance, and thesis outline.

Chapter 2 describes the literature review on expansive soils, relatable Sustainable Development Goals, conventional soil Stabilization techniques, environmental concerns in the current built environment, sustainable soil stabilization techniques, and sustainable soil stabilization and reinforcement mechanisms.

Chapter 3 explains the materials used in this research, including; soil, RHA, basalt fibers, and cement.

Chapter 4 shows the research methodologies used in the study, including; the methods of evaluating the properties of materials and laboratory experimental methods.

Chapter 5 details the results and discussions concerning the research methodologies illustrated in Chapter 4.

Chapter 6 describes the areas of applicability of the current research.

Chapter 7 includes the conclusions and recommendations by summarising the research findings.

Chapter 8 explains future research.

Chapter 9 contains the references used during the study period to support the hypothesis.

Chapter 10 shows copies of the printed publications during the study period.

CHAPTER 2 : LITERATURE REVIEW

2.1 Understanding and Overcoming the Challenges of Expansive Soils

Expansive soils are a significant challenge in civil and geotechnical engineering due to their ability to cause severe damage to structures and infrastructure (Puppala, 2021). In recent years, there has been an increasing amount of research on the topic, as well as new approaches and technologies to mitigate the effects of expansive soils (Taher et al., 2020; Puppala et al., 2019; Mostafiz et al., 2021). Expansive soils are soils that have the ability to swell and shrink significantly with changes in moisture content. These soils are prevalent in many parts of the world and are typically formed from clay minerals such as smectite, which have a high surface area and a strong ability to attract water molecules (Kumari and Mohan, 2021). When the moisture content of the soil increases, the clay particles absorb water and expand, leading to soil heave. Conversely, the clay particles shrink when the soil dries out, leading to soil settlement (Al-Rawas and Goosen, 2006).

One of the critical challenges posed by expansive soils is the potential damage they can cause to infrastructure. When buildings or other structures are built on expansive soils, the soil can push against the foundation, causing it to heave and potentially crack. This heaving effect can significantly damage the structure and cause potential safety hazards. In addition, expansive soils can also cause damage to roads, bridges, embankments, and other infrastructure, leading to increased maintenance costs and potential safety risks.

One common approach developed to mitigate the effects of expansive soils is to use deep foundations, such as piles or caissons, that penetrate the expansive soil layer and transfer the load to a more stable layer below (Alnmr et al., 2023; Nelson et al., 2017). Another approach is to use soil stabilization techniques, such as adding lime or cement, to improve the strength and stability of the soil. In recent years, there has been increasing research on using sustainable binders and geosynthetics, such as geogrids, fibers, or geocells, to reinforce the soil and prevent heave, as discussed in the previous

section. In addition to these traditional approaches, there has also been an increasing amount of research on new technologies to mitigate the effects of expansive soils. For example, some researchers have explored the use of electrokinetics, which involves applying an electric field to the soil to improve its strength and stability (Mosavat et al., 2012; Malekzadeh et al., 2016; Mohammad et al., 2022). Others have investigated the use of chemical treatments, such as the addition of surfactants, to alter the behavior of the clay minerals and reduce heave (Mironova and Ilyin, 2018; Novikau and Lujaniene, 2022; Kuhnt, 1993).

Despite these efforts, much is still to be learned about expansive soils and how best to mitigate their effects. One area of ongoing research is the development of new testing methods to understand the behavior of expansive soils better and predict their potential outcomes on infrastructure. In addition, there is a need for further research on the long-term performance of different mitigation techniques, as well as the cost-effectiveness of different approaches. Moreover, as will be discussed in the next section, the relevance of these mitigation measures should follow the Sustainable Development Goals (SDGs) guidelines, also known as the Global Goals, adopted by the United Nations in 2015.

2.2 Sustainable Development Goals on Resilient Infrastructure and Environment

The world today faces the daunting challenge of balancing the needs of economic growth with the necessity of protecting the environment. In recent years, there has been a growing concern about the impact of infrastructure development on the environment, especially regarding the depletion of natural resources, increased pollution, and climate change. In response, the United Nations launched the Sustainable Development Goals (SDGs), a set of 17 interconnected goals to achieve a sustainable future for all and promote sustainable development globally, as shown in Figure 1 (UN General Assembly, 2015; Adshead et al., 2019). These goals served as a blueprint for global development efforts toward a sustainable future. Each SDG had specific targets to achieve by 2030, and progress was tracked through indicators (Hák et al., 2016). The SDGs aimed to address a range of global

challenges, including poverty, hunger, health, education, gender equality, clean water and sanitation, renewable energy, economic growth, sustainable infrastructure, reducing inequality, sustainable cities, responsible consumption and production, climate change, sustainable use of marine resources, sustainable use of land and ecosystems, peace, justice, and strong institutions, and partnerships for sustainable development.

Figure 1 The 17 Sustainable Development Goals (UN General Assembly, 2015).

This research focused on the importance of resilient infrastructure and environment in achieving SDG 9, which aims to provide universal access to reliable, affordable, and modern energy services, increase the share of renewable energy in the global energy mix, and promote sustainable industrialization and innovation. The following are the targets of SDG 9:

- Develop quality, reliable, sustainable, and resilient infrastructure: This target aims to develop infrastructure such as transportation, water and sanitation, and telecommunications that is of good quality, reliable, sustainable, and resilient.
- Promote inclusive and sustainable industrialization: This target aims to increase the share of industry in employment and gross domestic product (GDP) while reducing its environmental

impact. It also seeks to enhance the competitiveness of small and medium-sized enterprises and promote the development of sustainable industries in developing countries.

- Increase access to financial services: This target aims to increase access to financial services, including affordable credit, for small and medium-sized enterprises in developing countries.
- Upgrade infrastructure and retrofit industries to make them sustainable: This target aims to retrofit industries and upgrade infrastructure to reduce their environmental impact, increase energy efficiency, and promote the use of renewable energy sources.
- Enhance research and development and increase the number of people employed in research and development: This target aims to increase investment in research and development and promote innovation in developing countries.
- Facilitate sustainable and resilient infrastructure development in developing countries: This target aims to support the development of sustainable and resilient infrastructure in developing countries, including through technology transfer and capacity building.
- Increase access to affordable, reliable, sustainable, and modern energy services: This target aims to provide universal access to affordable, reliable, sustainable, and modern energy services, including through the use of renewable energy sources.
- Increase the share of renewable energy in the global energy mix: This target aims to increase the share of renewable energy in the global energy mix to promote sustainable development and reduce greenhouse gas emissions.
- Promote sustainable urbanization: This target aims to promote sustainable urbanization through the development of compact, connected, and resilient cities that are energy-efficient and have sustainable infrastructure and transport systems.

By achieving these targets, SDG 9 will contribute to achieving several other SDGs, including SDG 7 on affordable and clean energy, SDG 8 on decent work and economic growth, and SDG 11 on

sustainable cities and communities. Resilient infrastructure is the backbone of sustainable development, and it is essential to ensure that infrastructure is resilient to climate change and other environmental factors. This present study focused on developing new structural materials for soil stabilization and ground improvement by utilizing environmentally friendly soil reinforcing materials and recycled industrial and agricultural wastes in cementitious systems for sustainable development. All were aimed at maximizing sustainable construction benefits and realizing SGD 9.

2.3 Conventional Soil Stabilization Techniques

With the increased built environment due to urbanization and industrialization, there is a rising demand for infrastructure development in marginalized areas with weak expansive soils, which are considered unsuitable. Expansive soils have been analyzed to possess weak shear strength and high compressibility and pose numerous challenges to civil and geotechnical engineers when constructing any engineering structures. Building on expansive soils can lead to considerable damage to foundations, embankments, and pavements, increasing the cost of constructing durable and safe structures. Stabilizing and reinforcing the expansive soils to improve their geotechnical properties is vital to curb these challenges. Some of the methods employed to date to stabilize and reinforce these weak soils will be discussed in Sections 2.3, 2.5, and 2.6.

2.3.1 Mechanical/Physical Stabilization of Soil

Mechanical/physical stabilization is commonly used to improve the stability of soils prone to erosion, such as coastal regions, slopes, and embankments. It is also helpful in constructing highways, airfields, and other infrastructure projects. One of the most common mechanical/physical stabilization techniques is compaction. Compaction involves using heavy machinery to compress soil particles, resulting in denser soil that is less susceptible to settling and erosion. According to a study by Bahar et al. (2004), compaction can improve the strength of soils by up to 50%.

Another technique used for mechanical/physical stabilization is soil reinforcement. This technique uses geosynthetics such as geo-textiles, geogrids, and geocells to reinforce the soil structure. The geosynthetics work by increasing the soil's tensile strength, which reduces deformation and improves stability. A review by Biswas and Krishna (2017) found that soil reinforcement with geosynthetics significantly improved soil shear strength and deformation behavior. Soil nailing is another mechanical/physical stabilization technique that involves the insertion of steel bars (nails) into the soil to improve its stability. The nails are typically installed at an angle and grouted into place, creating a reinforced soil structure and effectively improving slope stability and deformation characteristics (Sharma et al., 2019).

The jet grouting technique that involves injecting high-pressure water and cement into the soil to create a column of reinforced soil has also been practiced extensively. The method commonly stabilizes soil in construction projects such as tunnels, retaining walls, and bridge foundations by improving the compressive and shear strength of the soil (Njock et al., 2018).

2.3.2 Chemical Stabilization of Soil

Conventionally, cement and lime are the two common chemical stabilizing agents that have been used extensively in soil stabilization. Cement is a hydraulic binder that reacts with water to form a hard and durable material. Lime, on the other hand, is a chemical stabilizer that reacts with soil particles to form stable compounds, thus improving the strength and durability of the soil. According to a study by Chenarboni et al. (2021), adding cement (6, 8, 10, and 12%) to expansive soil increased the soil's unconfined compressive strength (UCS). The study also found that the optimum cement dosage for soil stabilization depended on several factors, including amounts of admixtures and curing time. In another study, Liu et al. (2010) investigated the effect of Portland cement and calcium lime on the engineering properties of soil during freezing and thawing. The study found that the modified soils exhibited better performance than before modification, the cement-modified clay was superior

to the lime-modified clay, and all of the soils' mechanical properties were visibly improved. Asgari et al. (2015) investigated the effect of using different amounts of lime and cement on the UCS of stabilized clayey soil. The study found that the UCS of the stabilized soil increased with increasing lime and cement content. The researchers also observed that the improvement in mechanical behaviors of the soil due to cement treatment was noticeably higher than lime treatment.

Similarly, Khemissa and Mahamedi (2014), while investigating the effect of cement (0-12%) and lime (0-12%) mixture stabilization of expansive overconsolidated clay, found that the bearing capacity improvement of the natural clay was translated by a significant increase in soil strength and durability. However, the best performances are obtained for a mixed treatment corresponding to 8% cement and 4% lime contents.

A study by Khazaei and Moayedi (2019) investigated the effect of quick lime on the compressive strength and stiffness of expansive soil. The researchers found that adding lime improved the geotechnical properties. In addition to the tests above, several studies have been conducted to investigate the behavior of cement or lime-stabilized soils using consolidation tests. Bushra and Robinson (2009) investigated the effect of cement content on the consolidation behavior of stabilized marine clay using consolidation tests. The range of cement contents selected was 2.5 %, 5 %, 7.5 %, 10 %, 15 %, and 20 %, with a curing period of 28 days. The results showed that increasing the cement content of the soil decreased its compressibility and increased its stiffness and strength. The consolidation behavior of the stabilized soil was influenced by the curing time and the degree of saturation. Ouhadi et al. (2014) investigated the effect of lime content on the consolidation behavior of stabilized clayey soil using consolidation tests. The study illustrated that test results show that pozzolanic consolidation causes an increase in initial pre-consolidation stress of 70 kN/m^2 for soft clay soil to 375 kN/m^2 for stabilized soil with 6% lime and 385 kN/m^2 for stabilized soil with 6% cement.

Moreover, Nazari et al. (2021) investigated the effect of compaction delay and curing time on the consolidation behavior of cement-stabilized and lime-stabilized clayey soil using consolidation tests. Samples were mixed with 1.5, 3, 6, and 9% Portland cement and delayed for 120 minutes to achieve adequate curing before conducting one-dimensional consolidation tests. The studies found that increasing the curing time of the stabilized soil decreased its compressibility and increased its stiffness and strength. The researchers also noted that the cement content and the saturation degree influenced the stabilized soil's consolidation behavior.

Based on the labor requirements, project duration, costs incurred during mechanical stabilization, and high amounts of cement and lime utilized in the soil stabilization industry, as shown in the literature above, alternatives are under study to substitute or reduce their usage. Another factor driving intensive research on alternative stabilization methods is the uncontrolled environmental loads due to manufacturing these conventional binders, more so the carbon footprint. Some of these challenges will be discussed in Section 2.4.

2.4 Environmental Concerns of the Current Chemical Stabilization Techniques.

Based on data from the International Energy Agency (IEA), the cement industry is responsible for 27% of industrial CO_2 emissions, making it the second-largest emitter in 2014 (Guo et al., 2021). The over-dependence on cement and lime has proven to degrade the environment, raising environmental concerns such as contributing to 8 to 10 percent of global anthropogenic CO_2 emissions from the 4.1 billion metric tonnes produced yearly (Wang, 2020; Poudyal and Adhikari, 2021). Also, CO_2 emissions significantly contribute to global warming, natural resource depletion, and dust generation from their manufacturing processes (Ghadir and Ranjbar, 2018; Zhang et al., 2021; Bennett et al., 2022; Hussain et al., 2020; Mo et al., 2016; Blankendaal et al., 2014). The production of clinker in cement production creates CO_2 emissions through two primary sources. First, the thermal decomposition of limestone ($CaCO_3$) generates emissions, and second; energy is required

for the process, mainly provided through fossil fuel combustion. Despite advancements in energy efficiency and cement kiln technology, process emissions are estimated to still account for around 60% of total emissions. Therefore, reducing process emissions is critical for achieving climate action sustainable development goals (SDGs), which align with the "below 1.5°" climate target set by Rogelj et al. (2018).

Conventionally, adding additives such as cement, lime, and lime-cement mixtures has been practiced extensively in soil stabilization. The continued use and production of cement and lime can cause severe environmental concerns that should be addressed with a thorough agency. (Yi et al., 2015; Firoozi et al., 2014; Wang, 2002; Prusinski and Bhattacharja, 1999; Cuisinier et al., 2011; James and Pandian, 2016). In addition to the environmental drawbacks, cement and lime are susceptible to high plastic shrinkage and cracking, affecting the mechanical strength of the stabilized soil with time (Biswal et al., 2019).

2.5 Sustainable Soil Stabilization Techniques

Sustainable soil stabilization techniques are crucial in civil and geotechnical engineering practices. They provide a cost-effective, environmentally friendly, and durable solution to soil stabilization problems. Promoting sustainable soil stabilization techniques is paramount to reducing the negative impacts of conventional methods and effect sustainability in civil and geotechnical engineering practices. Sections 2.5.1 and 2.5.2 will elaborate on the current trials investigating the influence and the potential of some of these sustainable techniques.

2.5.1 Soil Stabilization using Recyclable Industrial/Agricultural Wastes.

Soil stabilization using recyclable industrial and agricultural wastes is an environmentally sustainable and cost-effective solution for civil and geotechnical engineering applications. These waste materials have proven to improve soil physical and chemical properties in various

experimental and construction projects. Utilizing these waste materials in the construction industry reduces waste disposal problems and negative environmental impacts, providing a more sustainable solution for soil stabilization in the construction industry. Table 1 below summarizes some of the typical industrial and agricultural waste materials researchers use in soil stabilization, indicating the dominant compositions that make them useful for soil stabilization processes.

Table 1 Typical industrial and agricultural waste materials used in soil stabilization.

Industrial Wastes					
Name	**Composition in %**				**Reference**
	SiO_2	**Al_2O_3**	**CaO**	**Fe_2O_3**	
Blast furnace slag	37.70	10.20	43.80	0.60	Wattez et al., 2021
Coal ash	65.60	25.00	1.78	6.00	Nath et al., 2017
Copper slag	34.00	2.00	6.50	47.00	Fakhrabadi et al., 2021
Fly ash	52.87	28.14	4.64	6.59	Cristelo et al., 2013
Municipal incinerator ash	55.37	9.20	19.39	4.93	Singh and Kumar, 2017
Quarry dust	63.48	17.72	5.56	1.77	Onyelowe et al., 2019
Granite dust	77.00	14.00	1.00	2.00	Igwe and Adepehin, 2017
Agricultural Waste Ashes					
Name	**Composition in %**				**Reference**
	SiO_2	**Al_2O_3**	**CaO**	**Fe_2O_3**	
Almond shell	10.70	2.70	10.50	2.80	Demirbaş, 2002
Coconut shell	4.64	1.39	6.26	1.39	Amu et al., 2011
Cow cattle manure	57.33	5.02	14.2	2.78	Yadav et al., 2017
Eucalyptus wood	27.00	23.60	21.5	2.70	Sefene, 2021

Groundnut shell	41.36	13.15	5.91	9.12	Olugbenga et al., 2021
Hazelnut shell	27.90	3.10	15.40	3.80	Demirbaş, 2002
Olive husk	29.40	8.40	14.50	6.30	Demirbaş, 2002
Olive tree pruning	22.20	4.50	30.40	2.50	Ureña et al., 2021
Palm oil fruit bunch	60.85	15.38	14.7	0.49	Otunyo and Chukuigwe, 2018
Rice husk	68.2	0.01	0.01	1.92	Fentaw et al., 2021
Sugarcane Bagasse	70.87	6.86	3.41	4.87	Yadav et al., 2017
Sugarcane straw	70.20	1.93	12.20	2.09	Amu et al., 2011
Sunflower shell	16.60	2.90	15.80	2.10	Demirbaş, 2002
Walnut shell	9.90	2.40	16.60	1.50	Demirbaş, 2002
Waste paper sludge ash	23.25	5.26	62.39	0.77	Khalid et al., 2012
Wheat straw	43.22	N/A	5.46	0.84	Singh et al., 2017

These industrial and agricultural waste materials work through pozzolanic reactions, which help to improve the physical and chemical strength and stability of the soil. Pozzolanic reactions are chemical reactions that occur between pozzolanic materials and calcium hydroxide in the presence of water. Pozzolanic materials are naturally occurring or artificial materials (mostly ash products) that do not have cementitious properties but can react with calcium hydroxide (in the soil or from cement and lime additives) to form compounds that bind with the soil particles (Basha et al., 2005; Malhotra and Mehta, 2004). The reaction produces a stable and durable material that improves the geotechnical properties of the soil. Notably, the ash products in Table 1 are rich in pozzolanic materials such as silica (SiO_2), alumina (Al_2O_3), calcium oxide (CaO), and iron oxide (Fe_2O_3). Therefore, when added to soil, they react with calcium hydroxide to form calcium silicate hydrate (CSH) and calcium alumino-silicate hydrate (CASH), which bind with the soil particles to improve their strength and stability.

Predominantly, one of the pozzolanic materials gaining much research attention in engineering practice today is rice husk ash (RHA), a by-product of the rice grain production process. Upon the controlled or open burning of rice husks, we obtain RHA, which is extensively used to improve the geotechnical properties of soil due to its abundance and is superiorly inexpensive compared to other conventional stabilizing agents such as cement and lime (Aprianti, 2015). Figure 2 shows the top rice-producing countries worldwide, primarily Asian countries topping the list. Moreover, global demand for rice is expected to increase by nearly 30% by 2050 because of the steadily growing population, especially in developing countries (Liu et al., 2022; FAOSTAT, 2020).

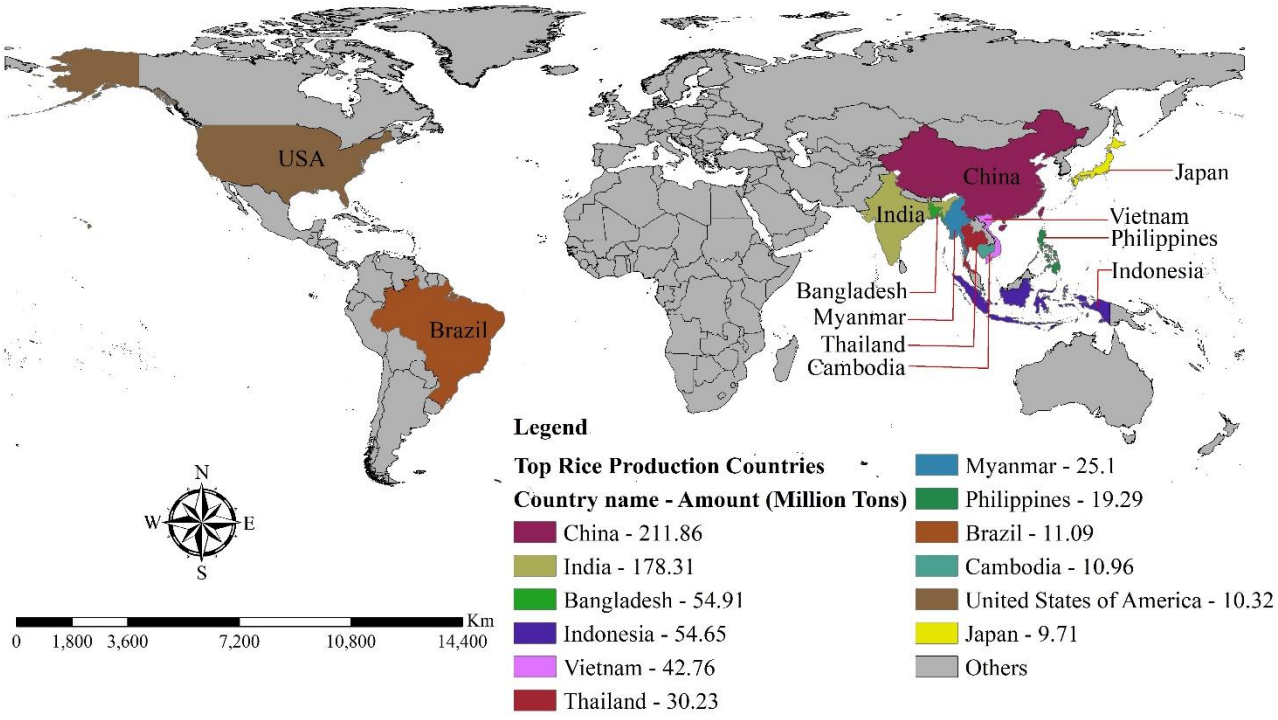

Figure 2 Top 10 rice-producing countries worldwide (Source: FAOSTAT, 2020).

According to the statistics by FAOSTAT (2020), global paddy rice production was estimated to be 756.7 million tons in 2020, producing approximately 172 million tons of rice husks. Annually, developing nations face significant environmental and health risks as a vast quantity of rice husks are left unutilized. The lack of alternative utilization procedures for rice husks leads to their disposal in landfills, riversides, and areas around the rice mills, as shown in Figure 3 (a Kenyan case study).

This statement is supported by several studies, including Saraswathy and Song (2007), Wang et al. (2011), Thomas et al. (2015), Kaur and Jha (2016), and Pode (2016). Therefore, developing alternative technologies to tackle this uncontrolled disposal problem is very crucial.

Figure 3 Uncontrolled rice husks disposal in Mwea Rice Mills, Kenya (Tom, J., 2012[Blog post]).

Many methods to produce high-quality rice husk ash from rice husks have been studied extensively in literature. The main factors that significantly impact the quality of rice husk ash for civil and geotechnical engineering use are burning temperature, burning duration, and silica content. Firstly, the burning temperature is crucial because it affects the degree of combustion of the rice husk, which, in turn, determines the quantity of silica that remains in the ash. Typically, a burning temperature of 600-800°C is preferred because it results in the highest degree of combustion and the highest amount of amorphous silica in the ash (Chen et al., 2021; Bie et al., 2015; Khassaf et al., 2014; Bahri et al., 2018; Venkatanarayanan and Rangaraju, 2015; Chindaprasirt et al., 2007).

Secondly, the burning duration is also a critical factor influencing the quality of rice husk ash. Longer burning durations typically result in higher-quality rice husk ash because they allow for a more thorough combustion process. This results in a more uniform distribution of silica in the ash, which makes it a more effective supplementary cementitious material. The listed publications in Table 2 suggested optimum burning conditions for RHA production.

Table 2 Optimum burning conditions for RHA production.

Type of burning	Burning temperature	Burning duration	Loss of ignition	Colour	References
Controlled burning	700°C	-	4.05	Grey	Bahri et al. (2018)
Open burning	-	60 mins	3.83	Grey	Mayooran et al. (2017)
Pyrolysis	800°C	40 mins	0.54	Off-white	Venkatanarayanan and Rangaraju (2015)
Open burning	600°C	-	-	Whitish grey	Chindaprasirt et al. (2007)
Controlled burning	650°C	60 mins	5.91	Whitish grey	Ramezanianpour et al. (2009)
Open burning	650°C	-	3.7	Grey	Chindaprasirt and Rukzon (2008)
Controlled burning	500-700°C	30 mins	3.21	White	Zain et al. (2011)
Controlled burning (Gas furnace)	800°C	-	-	White	Jaya et al. (2012)
Burning (Muffle furnace)	700°C	2 hrs	1.48	-	Bie et al. (2015)
Controlled burning	650°C	60 mins	2.10		Ganesan et al. (2008)
Controlled burning	600°C	3 hrs	-	White	Salas et al. (2009)

Open burning, also known as field burning (or uncontrolled burning), has been used as a traditional method of disposing rice husks in various regions worldwide. However, the ashes produced from this open burning or uncontrolled combustion in industrial furnaces contain non-reactive silica, such as crystobalite and tridymite (Sensale, 2010). Although this type of RHA has less reactive silica, there are still marginal improvements in properties when blended with construction products such as

cement and lime (Hadipramana et al., 2013). Additionally, RHA from uncontrolled combustion has a lesser loss on ignition (LOI), indicating a higher amount of unburned carbon, making the ash black (Ganesan et al., 2008). The presence of unburned carbon increases surface area but decreases workability.

Implementing highly effective and economical techniques to produce RHA under controlled conditions can improve the performance of RHA blended materials and also reduce the environmental issues of open or uncontrolled burning. Cyclonic furnace, muffle furnace, electric furnace, thermal gravimetric column, electric oven, tubular reactor, fixed bed reactor, fluidized bed reactor, torbed reactor, and rotary tube furnace are used for controlled burning of rice husk to obtain RHA (Nehdi et al., 2003; Rozainee et al., 2008; Venkatanarayanan and Rangaraju, 2013). Control burning increases the reactivity due to the high quantity of amorphous silica in RHA. Further, few researchers reported that silica in RHA burned above 900 °C showed crystalline nature (Behak and Núñez, 2013; Jaya et al., 2012). The properties of RHA also depend on the cooling rate and duration (Zain et al., 2011). The use of RHA obtained from the controlled burning (with 98% of amorphous silica) yielded materials with less permeability and higher resistance to acid attack than using RHA from uncontrolled burning (with 39% of amorphous silica) (Sensale, 2010).

Concerning the applicability of RHA in civil and geotechnical engineering, several experimental studies have been conducted to evaluate the influence of RHA on the compressibility, bearing capacity, permeability, and other geotechnical aspects necessary to justify its usage. Rahman (1986), in his research on the effects of rice husk ash alone on the unconfined compressive strength (UCS) of stabilized soils, showed that an increase of RHA to 20% increased the UCS of lateritic soils, after which they started to decrease. Noor (1993) also examined the RHA-cement ratios and how they positively influenced the proposed mix ratios, UCS, and durability. Muntohar's (2004) results showed that mixing RHA with 6% lime significantly reduced swelling and increased durability on

such improved soils. The literature also showed that RHA had an optimum percentage above which the UCS of improved soils decreased. Alhassan (2008a, 2008b) showed that adding RHA percentages between 0 to 4% to clay soils and lime specimens significantly increased the UCS value at specified lime contents while enhancing permeability. On the other hand, from the same research, increasing rice husk ash percentages from 6 to 8% decreased the UCS value considering the curing period in both cases.

Moreover, chemical additives such as cement and rice husk ash (RHA) have been used to enhance the soil structure of such expansive clay soils because of the associated pozzolanic activity during cation exchange between calcium and silica (Fattah et al., 2013; Rahman, 1987; Sarkar et al., 2012). Furthermore, stabilizing expansive soil using RHA and fly ash has also considerably reduced swelling between the foundation footing and subgrade (Brooks, 2009). Also, in literature, using RHA, lime, and gypsum as additives to expansive soil resulted in significant development in the strength characteristics of weak expansive soil (Koteswara et al., 2011). Eberemu and Sada (2013), in their research on one-dimensional consolidation of expansive soils treated with RHA only, found that the coefficient of volume change (m_v) and coefficient of consolidation (c_v) generally decreased with increased loading pressure and RHA treatment for up to 8%. Also, in the same study, the permeability coefficient (k) decreased with increased RHA content by up to 8%. These investigations disclosed that adding cement or lime to RHA might accelerate the strength properties. However, soils treated or stabilized with cementitious additives are more prone to shrinkage and cracking when used as a base course, affecting the mechanical strength of the stabilized soil (Biswal et al., 2019; Sebesta, 2005; Little, 1992). New research methodologies involving sustainable reinforcement materials, such as fibers, are currently under study to arrest the shrinkage and cracking failure planes, as discussed in Section 2.5.2.

2.5.2 Soil Stabilization using RHA, Cement/Lime, and Fibers

Fiber inclusion in a soil matrix has proved to add more intensification in the compressive abilities, significantly modifying and improving the mechanical behavior of soils due to the reinforcing effect between the soil particles (Gupta and Kumar, 2016; Casagrande et al., 2006; Consoli et al., 2007a; Consoli et al., 2007b; Fatahi et al., 2012; Divya and Viswananham, 2014; Li et al., 2014; Anggraini et al., 2015; Botero et al., 2015). Several pieces of research have been investigated considering different fibers and their applicability in enhancing soil strength. Kumar et al. (2006) studied the UCS gain on the soil by mixing polyester fibers and soft clay and observed that the compaction degree affected fiber reinforcement. Also, the unconfined compressive strength of clay increased with the addition of fibers, and it further increased when fibers were mixed in the clay-sand mixture.

Hossain and Awal (2011) also examined the structural improvement of cement-based matrices using varied carbon fiber lengths, improving durability and compressive strength. With the diversity in the fiber available for soil stabilization, polypropylene and recycled carpet have also been used before. Where bender element tests on 126 cylindrical specimens of cement-treated clay with various cement and fiber contents were analyzed to distinguish the relationships between fiber and cement content and the small-strain mechanical properties (Fatahi et al., 2013). Park (2009) further showed that compacting polyvinyl alcohol (PVA) fiber in different layers inside a cylindrical river sand specimen improved the compressive strength as the number of fiber layers increased. With fibers evenly distributed throughout the five layers, a reinforced model was twice as strong as a non-fiber-reinforced specimen. A more comparable study to this research was done by Cristelo et al. (2015). In their study, the influence of discrete fiber reinforcement on the uniaxial compression response found that sandy clay reinforced with polypropylene fibers and cement increased the stiffness, modulus of deformation, and compression strength of the mixtures for every cement content. Moreover, a study by Abdulhameed et al. (2020) investigated the effect of using different types of

fibers in conjunction with cement and lime on the UCS of stabilized soil. The study found that adding fibers increased the UCS of the stabilized soil and that the type of fiber used influenced the UCS of the stabilized soil.

To validate the effectiveness of the reinforcement and stabilization techniques using fiber and RHA, understanding the consolidation parameters, such as the coefficient of consolidation (c_v), coefficient of volume change(m_v), and the ultimate permeability coefficient (k), is critical. The consolidation rate is related to the c_v, while the settlement amount is related to the m_v. Based on experimental tests, researchers have realized that stabilization and fiber reinforcement techniques have increased strength, enhanced stability, and substantially reduced the rate of consolidation settlements. Abdi et al. (2008) found that increasing the fiber content and length significantly reduced consolidation settlements, swelling, and crack formation while working on fiber-reinforced soil. Das and Pal (2012) noted that the coefficient of consolidation (c_v) increased with the fly ash content while investigating the consolidation responses on silty clayey soils stabilized with fly ash in another study.

Regarding the coefficient of volume change (m_v), Kar and Pradhan (2011) studied the compressibility trends of polypropylene and coir fiber-reinforced local cohesive soils. The results showed that the m_v decreased significantly with increased fiber content. In addition, the study concluded that the coefficient of consolidation increased with fiber content. Considering triaxial tests, Lima et al. (1996), while working on cement and lime-stabilized soils, observed that the compressive strength significantly increased with the addition of fiber reinforcements. Random fibers have also been proven to improve soil stress-strain behavior (Consoli et al., 2003). The effects of adding rice husk ash, pond ash, cement, and polypropylene fiber on clay's compaction and strength behavior have also been studied. The literature showed that including fiber reinforcement within un-cemented and cemented soil caused an increase in the unconfined compressive strength, split tensile strength, and axial strain at failure (Ghorbani et al., 2018; Chen et al., 2021; Ghorbani and

Salimzadehshooiili, 2018). Also, fibers changed the brittle behavior of cemented soils to a more ductile one (Kumar and Gupta, 2016). Different types and configurations of natural and synthetic fibers used for soil reinforcement are shown in Table 3.

Table 3 Different types and configurations of natural and synthetic fibers used for soil reinforcement.

Natural Fibers					
Type	**Soil + additives used**	**Length (mm)**	**Fiber (%)**	**Tests conducted**	**References**
Coir fibers	Clay	15	0.1-1	Direct shear, UCS, Consolidation	Kar and Pradhan, 2011
Coir fibers	Clay + Lime 5%	5-15	0.5-2	Compaction, Tensile strength, UCS	Anggraini et al., 2015
Sisal fibers	Silty Clay	5-15	0.5	Triaxial CU,	Wu et al., 2014
Palm fibers	Sand	20-40	0-1	Compaction, UCS	Marandi et al., 2008
Jute fibers	Expansive soil	10	0.3-0.9	Direct shear, Triaxial,	Wang et al., 2017
Barley-straw fibers	Silty clay	10-500	1-3.5	Shrinkage, Flexual strength, Shear, Durability	Bouhicha et al., 2005
Synthetic Fibers					
Type	**Soil + additives used**	**Length (mm)**	**Fiber (%)**	**Tests conducted**	**References**
Polypropylene fibers	Clay, pond ash, Cement(0-6%)	3,6,12	0.5-2	UCS, STS, and CBR tests	Gupta and Kumar, 2016; Li et al., 2014
Polyester fibers	Clay soils + Nanosilica	20	0.1-0.5	UCS	Changizi and Haddad, 2015
Glass fibers	Expansive soil	30	0.25-1	UCS, ITS, CBR	Rabab'ah et al., 2021
Polyvinyl alcohol fibers	Sand+ + Cement(4%)	12	0.2-1	UCS	Park, 2009

Recycled carpet fibers	Soil+ Cement (5-15%)	0.4-18	0.5-1	UCS, ITS	Fatahi et al., 2012
Steel fibers					
Polypropylene carpet	Clay+ Cement (5-15%)	-	0.1-0.5	Shrinkage Test, UCS	Fatahi et al., 2013
Polypropylene fibers	Sand clay	12-49	0.1-0.25	UCS, SEM, and ultrasonic tests	Cristelo et al., 2015
Polypropylene fibers	Sandy clay Cement(2-16%)	6	0.2	UCS	Ghorbani et al., 2018
Polypropylene fibers	Clay+RHA+ Pondash+ Cement(4%)	6-12	0.5-1.5	UCS, Split tensile	Kumar and Gupta, 2016
Polypropylene fibers	Clays+Cement (5-15%)	5-10	0.1-0.5	Bender element tests,	Fatahi et al., 2013
Polypropylene fibers	Clay+RHA+ Cement(2-5%)	12	0.5	Compaction, UCS, Split tensile, Statistical analysis	Muñoz et al., 2021

The use of RHA, cement, and lime as stabilizing agents and fibers as reinforcing agents has attracted the attention of researchers who have found out that they have an advantageous effect in developing the geotechnical properties of the soils under study (Changizi and Haddad, 2015; Fatahi et al., 2013; Muñoz et al., 2021). However, in the available literature, most research articles are limited to the reinforcement material used, the soil tested, and the type of stabilizing agent used. Additionally, most studies used higher amounts (i.e., 5-50%) of conventional additives to the soil, raising concern about the projected environmental impacts of their continued manufacture and use. To date, few pieces of research have been carried out on expansive soils with no scientific studies on the combined action of RHA, cement, and basalt fiber, particularly its effect on consolidation settlement, volume change, and permeability. In addition, there is limited research on how high-strength fiber filaments made from natural basalt rock can influence the ultimate shear strength, UCS, permeability, and bearing

capacity of RHA-cement-stabilized soils. Based on these deficits, the present study aimed to evaluate the influence of basalt fiber filament lengths, considering its high tensile strength, on the shear strength development, consolidation response, permeability, and bearing capacity of the hybrid stabilized soils composite for ground improvement. Also, the present study investigated a correlation between the consolidation coefficients by adding different basalt fiber lengths and RHA-cement mixtures in expansive soils. Additionally, the study emphasized how natural fibers such as basalt fibers can be used with pozzolanic additives to arrest the formation of weak planes in the stabilized soil and control the consolidation rate while improving the strength when built upon them. The ultimate goal was to propose a material combination scheme with superior properties to use as a fill or subbase material for engineering structures such as embankments, pavements, and foundations.

2.6 Mechanisms of Sustainable Soil Stabilization and Reinforcement Techniques

2.6.1 Physical Soil Stabilization Mechanisms

Physical soil stabilization is a process that involves various methods to enhance the properties of soils to make them more stable and robust for multiple civil and geotechnical engineering applications. These methods involve mechanical and physical manipulation of the soil structure and properties to improve their performance. One highly practiced physical soil stabilization method is compaction. Compaction involves applying mechanical pressure to the soil to increase its density and strength.

During this process, the soil particles are rearranged to reduce the void spaces between them, resulting in a more compact and denser soil structure. The compacted soil is more stable and has increased resistance to deformation when subjected to structural loads. Types of equipment used for compaction include vibratory rollers, smooth wheel rollers, sheep foot rollers, and pneumatic rollers. Vibratory rollers are commonly used for compacting granular soils, while smooth wheel rollers are used for compacting cohesive soils.

2.6.2 Chemical Soil Stabilization Mechanisms

2.6.2.1 Lime/Cement Stabilization Reactions

In soil stabilization, adding additives like lime and cement has been found to have significant effects on the properties of the stabilized soil. However, before examining the impact of additives on soil stabilization, it is crucial to understand the chemical reactions that occur upon adding these additives to the soil. Lime is commonly added to soil to initiate several reactions, broadly classified into short- and long-term reactions. Short-term reactions include ion exchange, flocculation, and carbonation, while long-term pozzolanic reactions involve the formation of reaction products that affect the strength and compressibility of clays. Immediate ion exchange occurs when divalent calcium ions from lime replace univalent cations on the clay surface, and high-concentration ions replace those in lower concentrations. The short-term reactions improve soil plasticity, making it easier to work with, and enhance uncured strength and load-deformation properties (Bhuvaneswari et al., 2010; Metelková, 2012; Little, 1995). The short-term reaction can be expressed using Equations 1 and 2.

$$Ca(OH)_2 \rightarrow Ca^{2+} + 2(OH)^- \quad (1)$$

$$Ca^2 + \text{Clay Mineral-}M^+ \rightarrow \text{Clay Mineral-}Ca^{2+} + M^+ \quad (2)$$

Long-term pozzolanic reactions involve lime, water, soil silica, and alumina. High alkaline soil pH during lime treatment stimulates the dissolution of siliceous and aluminous compounds from the clay mineral structure. These dissolved compounds react with calcium ions (Ca^{2+}) in pore water to form calcium silicate hydrate (CSH) and calcium aluminate hydrate (CAH) gels, which cover the soil particles and later crystallize to link them. The long-term pozzolanic reactions are time-dependent, and curing is essential for developing strength and durability (Rajasekaran, 2005; Rao and Shivananda, 2005; Mallela et al., 2004; Pallanza and Matheson, 2023). The long-term reactions have been presented in Equations 3 and 4 below.

$Ca^{2+} + OH^{-} + SiO_2$ (Soluble Clay Silica) → CSH gel (3)

$Ca^{2+} + OH^{-} + Al_2O_3$ (Soluble Clay Alumina) → CAH gel (4)

On the other hand, Portland cement is composed of calcium silicates and calcium aluminates that hydrate to form the cementing compounds of CSH and CAH, as well as excess calcium hydroxide when combined with water. The pozzolanic reaction between calcium hydroxide released during hydration and silica and alumina of soil occurs in fine-grained clay soils and is essential to stabilizing these soils. Therefore, it can be observed that cement-soil reactions are similar to the pozzolanic reactions of lime with soil (Little et al., 2000). Figure 4 represents the CSH formation stages.

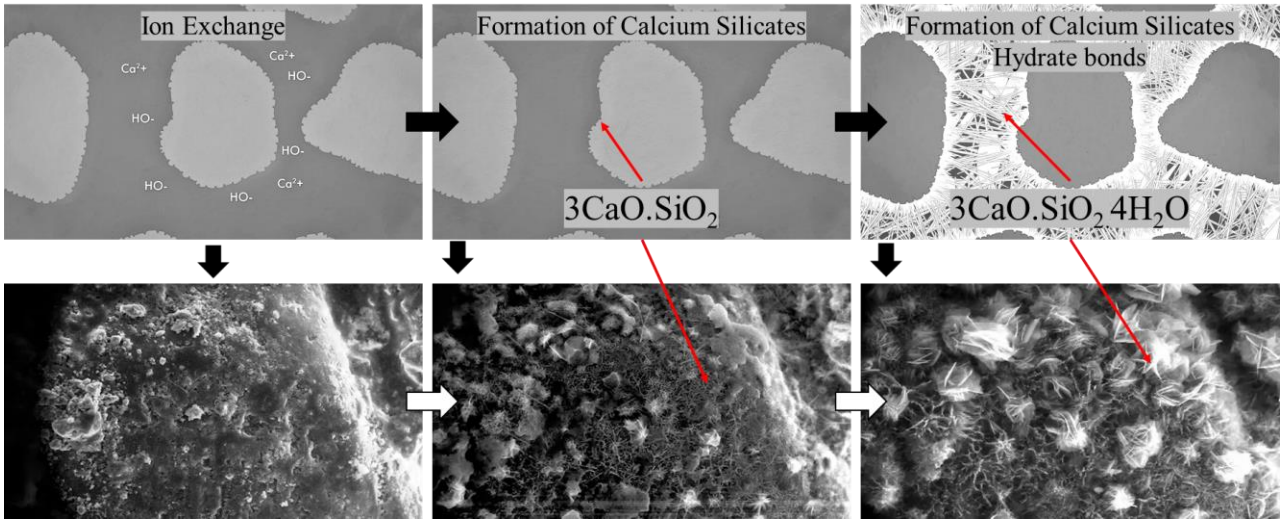

Figure 4 Illustration of the formation of CSH bonds in cementitious composites: SEM image scale x1000 (Modified from; Source; Veratisium, 2023).

In conclusion, the chemical reactions from adding additives to soil are crucial to understanding the effects of soil stabilization. Short-term reactions improve soil plasticity and uncured strength, while long-term pozzolanic reactions involve forming reaction products that affect the strength and compressibility of weak clays. The similarities between cement-soil reactions and pozzolanic reactions of lime with soil further emphasize the importance of understanding these chemical reactions in soil stabilization.

2.6.2.2 RHA(Pozzolan) and Lime/Cement Stabilization Reactions

Soil stabilization can be achieved using ashes, which is attributed to the pozzolanic reactions. When lime ($Ca(OH)_2$) is mixed with RHA and water is added, the pH of the mixture increases to above 12.4, releasing calcium ions (Ca^{2+}) (Rogers and Glendinning, 2000). Similarly, the hydration of CaO in cement increases pH to around 12.4, releasing hydroxyl (OH^-) ions. In this highly alkaline environment, the aluminum (Al^{3+}) and silicon (Si^{+4}) ions dissolve from the ash and react with the Ca^{2+} to produce calcium silicate hydrate gels (CSH) and calcium aluminosilicate hydrate gels (CASH) (Basha et al., 2005; Guney et al., 2007; Yong and Ouhadi, 2007; Solanki and Zaman, 2012). Equations 5 to 8 comprehensively represent the chemical reaction during pozzolanic reactions in chemically stabilized soils.

$$CaO + H_2O \rightarrow Ca(OH)_2\ ; \text{[Cement hydration]} \quad (5)$$

$$Ca(OH)_2 \rightarrow Ca^{2+} + 2(OH)^- \quad (6)$$

$$Ca^{2+} + 2(OH)^- + SiO_2 \rightarrow CSH;\ [(CaO)(SiO_2)_6\ 4(H_2O)] \quad (7)$$

$$Ca^{2+} + 2(OH)^- + SiO_2 + Al_2O_3 \rightarrow CASH;\ [(CaO)(Al_2O_3)(SiO_2)_6\ 4(H_2O)] \quad (8)$$

According to Little (2000), the products generated by pozzolanic reactions are primarily gels that cover and bond the soil grains, leading to strength gain. Over time, these gels crystallize into well-defined calcium silicate hydrates (CSH), further enhancing the strength of the soil. Pozzolanic reactions begin quickly, within a few hours of adding water to the mixture, and can persist for many years as long as there is enough lime/cement, silica, water, and a high pH. Ali et al. (1992) investigated the X-ray diffractograms (XRD) of mixtures of clayey sandy soil with RHA and lime that were cured for 7, 28, and 90 days. The results indicated new peaks of calcium aluminate hydrate (CAH) and CSH appearing after 7 days and continuing to form after 28 and 90 days, while peaks of

lime disappeared at 28 days. These gradual reactions have proven to result in a long-term increase in the strength of the stabilized soil.

2.6.3 Fiber Soil Reinforcement Mechanisms

Soil reinforcement involves introducing materials with desired properties to improve the engineering characteristics and behavior of soil, with the primary goal of enhancing its stability and reducing soil deformations (Hejazi et al., 2012). Civil and geotechnical engineering has seen a rise in the use of natural fibers for reinforcing soil due to its unique advantages. However, the limited effective lifespan of natural fibers in subsoil conditions poses a challenge (Gaw et al., 2011). In geotechnical applications, fiber content, length, textures, stiffness, and orientation are practical concerns among the varied forms and aspect ratios of fibers embedded in soil (Wang et al., 2017). Fiber-reinforced soil can be classified into two types based on their method of application: (i) Oriented Distributed Fiber-reinforced Soil (ODFS) and (ii) Randomly Distributed Fiber-reinforced Soil (RDFS) (Sharma et al., 2015; Bordoloi et al., 2017; Gowthaman et al., 2018).

ODFS is a well-known reinforcement mechanism that introduces natural fibers to the soil through planner systems in vertical, horizontal, or both directions. Mechanical enhancements of natural fibers can be achieved through modifications such as weaving, binding, combining, or punching, depending on the application requirements. The mechanism of ODFS is similar to conventional geosynthetic approaches, where materials are introduced to weaker planes of the soil as geo-grids, geo-cells, geo-mats, and geo-textiles. It is well understood that the ODFS technique mobilizes additional frictional strength along the fiber-reinforced planes. In contrast, un-reinforced zones rely on their own strength, but the possibility of generating failure planes through weaker un-reinforced zones still exists. Figure 5 clearly illustrates the schematic diagrams of ODFS and RDFS. This current study was focused on the RDFS due to the intense fiber connectivity throughout the stabilized soil composite.

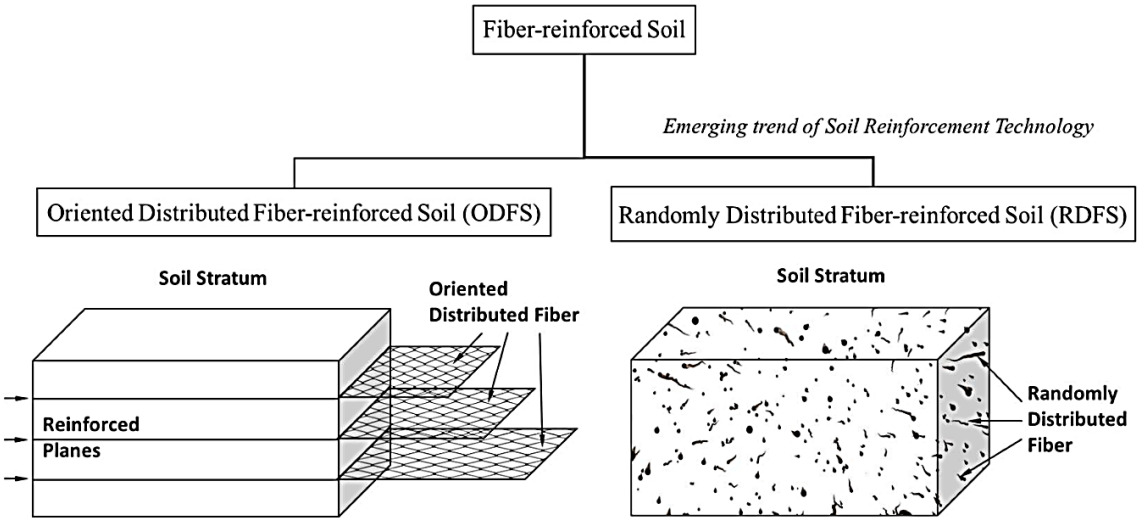

Figure 5 Classification of Fiber reinforcement mechanism of soil (Gowthaman et al., 2018).

On the other hand, RDFS is a well-recognized soil improvement technique in which fibers with desired properties and quantities are randomly assorted and compacted in situ (Sharma et al., 2015; Bordoloi et al., 2017). In recent times, the incorporation of RDFS has become more popular because short discrete fibers can be easily added and mixed randomly with the soil, similar to the addition of cement, lime, or other additives.

As a result, it can provide an isotropic increase in the strength of the soil composite without introducing continuous planes of weakness (Chauhan et al., 2008; Ahmad et al., 2010). The RDFS method exploits the similar behavior of plant roots, which strengthen the soil by contributing additional friction and interlocking (Pollen, 2007; Vannoppen et al., 2015; Gyssels et al., 2005). In Figure 6, a clear illustration of the mechanism of RDFS has been presented. Notably, distributed fibers subjected to tension contribute to the increase in the strength of specimens, as shown in Figure 6b (Hejazi et al., 2012; Wang et al., 2017).

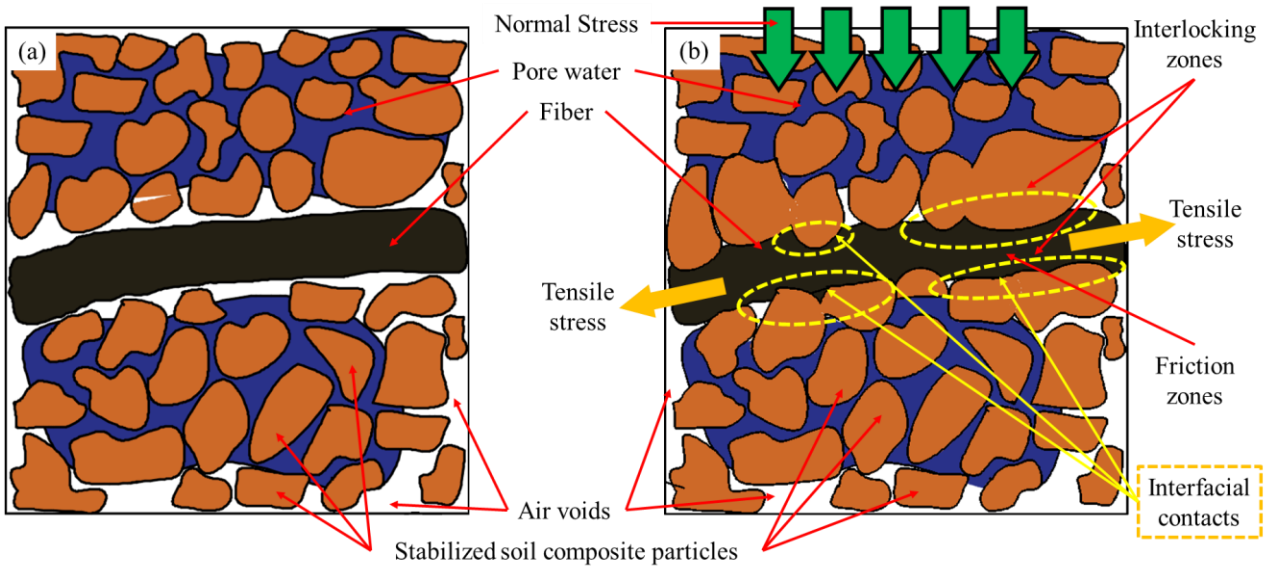

Figure 6 Illustration of a Randomly Distributed Fiber-reinforced Soil composite (RDFS): **(a)** Initial state before loading and **(b)** Deformation due to loading, indicating the interlocking zones, friction zones, and interfacial bonding zone that enhances tensile stress mobilization. (Modified from Gowthaman et al., 2018).

Initially, soil particles subjected to stresses attempt to densify [Figure 6 (a)], which persuades deformation of the fiber material. Subsequently, direct forces are generated on the fiber at the fiber-soil interlocking phases due to rotation and the direct impact of composite soil particles. Simultaneously, soil particles in contact with the fiber induce the development of frictional forces on fibers and interlocking forces through the interfacial contacts (Bordoloi et al., 2017). Eventually, the interlocking forces coupled with frictional forces tend to mobilize the tensile stress on the fiber material.

Moreover, the random distribution of fibers mobilizes fiber-soil adhesive bonding, which utilizes additional composite strength, and the interaction of the flexible fibers behaves as a structural mesh that holds the soil together, increasing the structural integrity of the stabilized and reinforced soil composite (Hejazi et al., 2012; Wang et al., 2017).

CHAPTER 3 : MATERIALS

3.1 Soil (S)

The materials used in this study included clay soil from the Handa area of Mie Prefecture, Japan. Soil sample collection is an essential process in civil engineering, geotechnical engineering, and environmental science. Collecting soil samples in bulk is a standard method used to collect soil samples for various purposes. The sampling location was rich in clayey soils, aligning with the investigated hypothesis. The site was cleared free of debris and other obstructions that could interfere with the sampling process. The collection process involved using a soil excavator to extract the soil in bulk. Afterward, the collected soil was transported to the research location and stored in holding tanks for drying. The soil was classified as A-7-5(2) clayey soils based on the American Association of State Highway and Transportation Officials (AASHTO). Detailed experimental methodologies to analyze the soil will be explained in Chapter 4. Figure 7 shows the location of the soil sample collection.

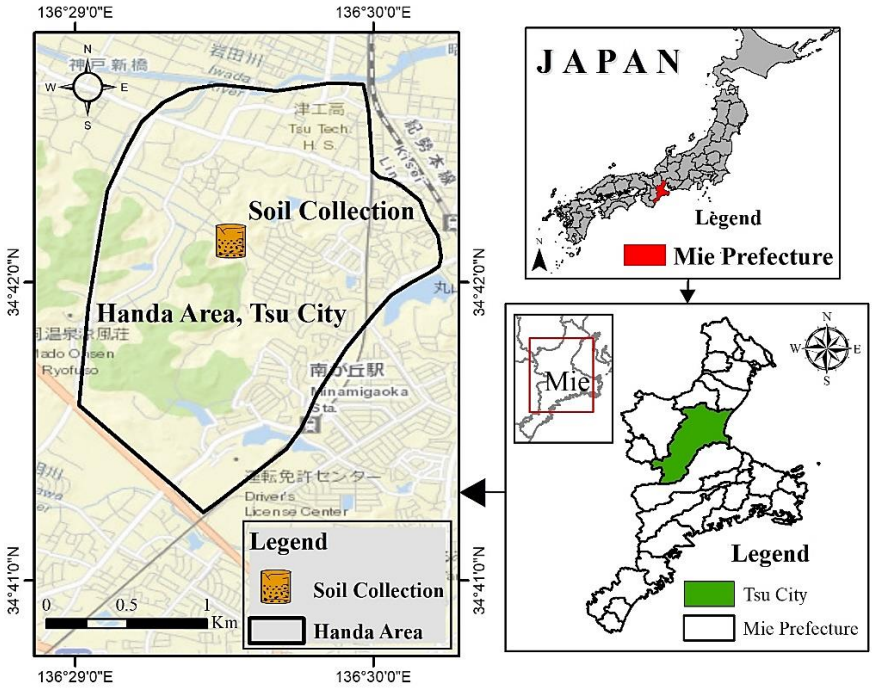

Figure 7 Soil sampling site.

3.2 Rice Husk Ash (RHA)

A controlled burned RHA at 650-700 °C with high silica content of 91.10% was provided by Make Integrated Technology Co., Ltd, Osaka, Japan. Plant-based RHA was fired from the rice husks of domestic rice using the Ethical Star ash production machine. Approximately 15-20% of high-purity amorphous silica was produced from 800-1000 kg dry rice husks. The RHA was produced by igniting a small methanol solid fuel as a pilot fire into the rice husk holding chambers leading to self-combustion, certifying it as an organic Japanese Agricultural Standards (JAS) material. After the ignition, combustion was controlled by a computer for 27 hours, and the operating status was monitored from a remote location. Afterward, the RHA was removed from the combustion chamber and left to cool naturally at room temperature. This monitoring system makes producing high-purity silica of approximately 85-90% possible.

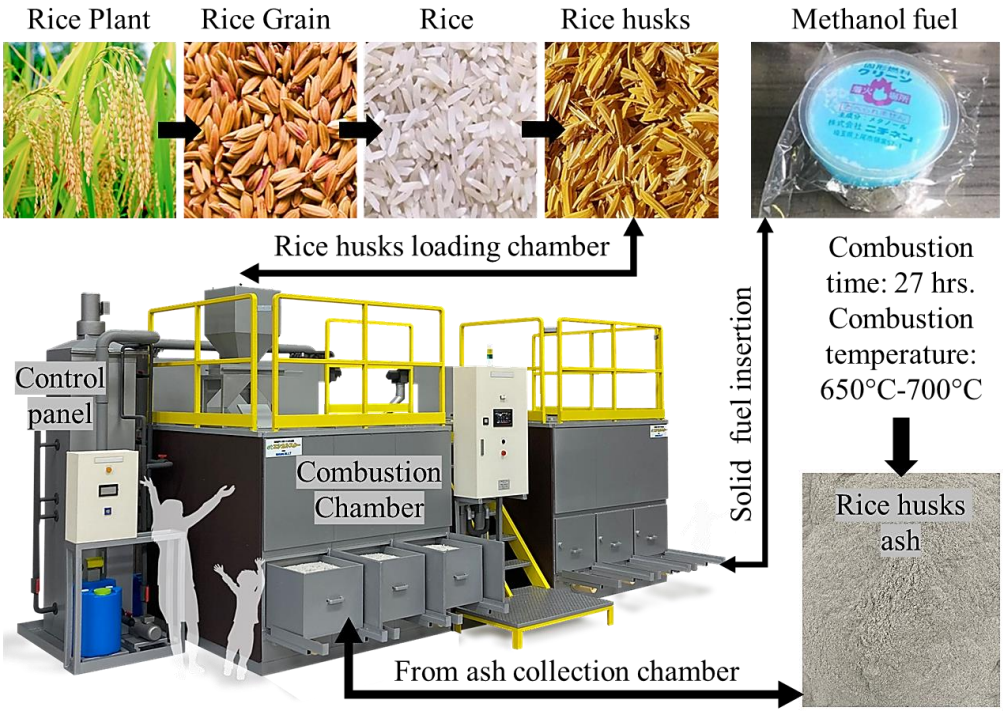

Figure 8 Flow diagram illustrating the Rice husk ash production process.

The production station was located in Higashi Osaka, facilitating proper production logistics and RHA acquisition, as shown in Figure 9.

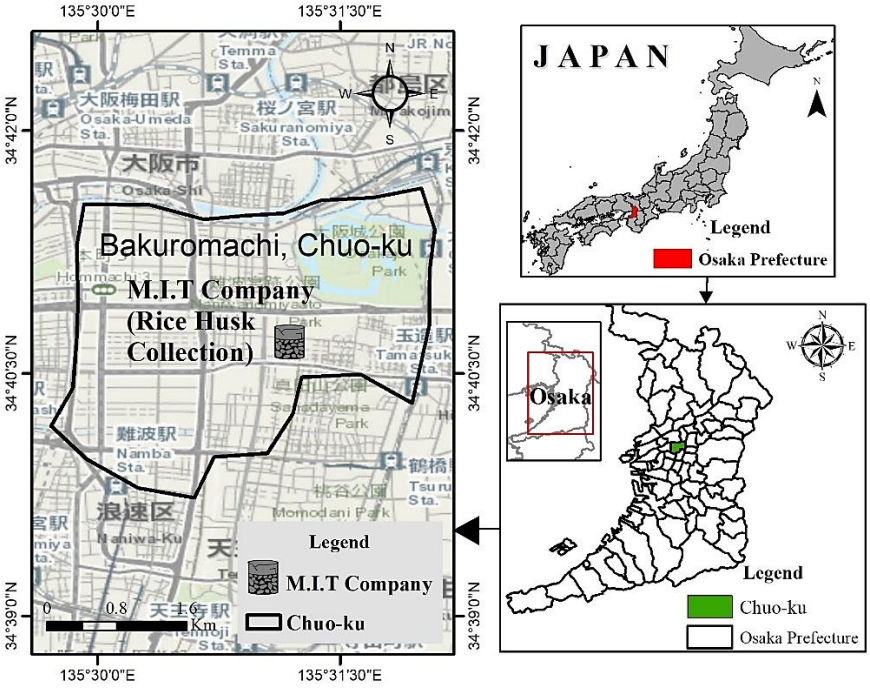

Figure 9 RHA production station.

3.3 Basalt Fiber

Basalt fiber is a material made from fine fibers of natural basalt rock. The production of BF is a one-stage process involving: the melting and homogenization of basalt rock and extrusion through small nozzles to produce continuous filaments of basalt fiber (Hu and Liu, 2010; Dhand et al., 2015). The first step in making basalt fibers is to obtain the basalt rock. Basalt is a volcanic rock commonly found in many parts of the world, including the United States, Europe, Africa, and Asia.

The quality of the basalt rock is crucial because it affects the properties of the final product. Once the basalt rock has been obtained, it is crushed and melted in a furnace at around 1,400°C to 1,600°C. This temperature is high enough to melt the basalt but not so high that it vaporizes. The molten basalt is then extruded through small nozzles to create continuous fiber filaments. As the fibers are extruded, they are stretched to align the molecules and improve their strength. Afterward, they are treated with resin, a coating that helps protect them and improve their adhesion to other materials. The resin sometimes contains additives that enhance the fibers' properties. The next step involves winding the

fibers onto a spool before transportation to another location for further processing. The spooling process is critical because it must be done carefully to avoid damaging the fibers. In this study, JCK Corporation provided the fibers in their standardized forms of 3mm, 6mm, and 12mm (http://www.j-c-k.co.jp).

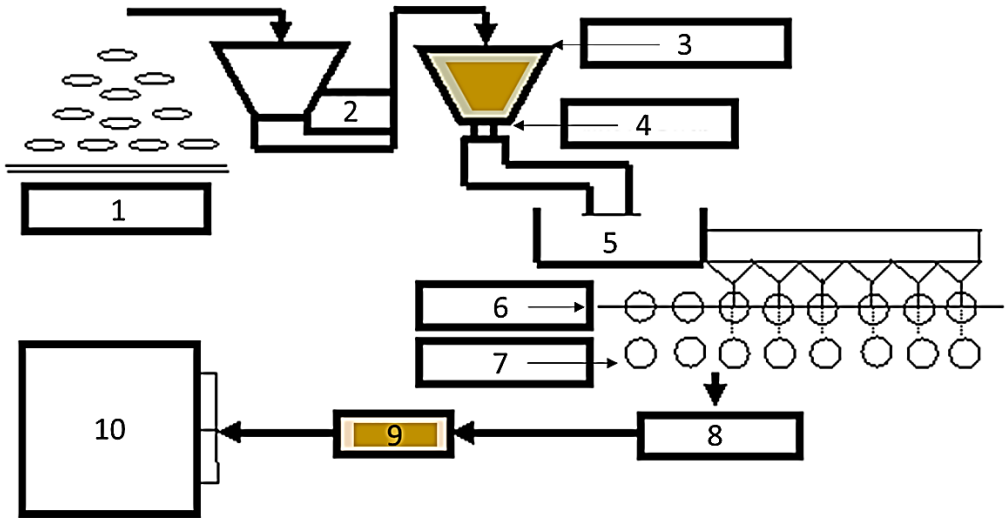

1. Basalt rock (Raw materials)
2. Measurements
3. Raw materials storage tank
4. Raw materials filling machine
5. Electric melting machine
6. Resin coating machine
7. Weaving machine
8. Filaments ejection
9. Drying
10. Basalt fiber products

Figure 10 Flow diagram showing the basalt fiber production process (Source: JCK corporation).

Basalt fiber dimensions of 3mm, 6mm, and 12mm were used to investigate a comprehensive parametric study on reinforcement capabilities in the soil, as shown in Figure 11.

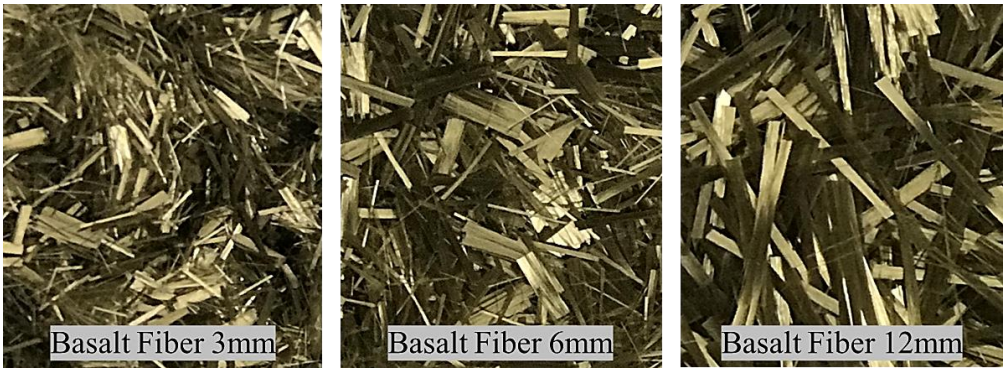

Figure 11 Basalt fiber dimensions (3mm, 6mm, and 12mm).

3.4 Ordinary Portland Cement (OPC)

Ordinary Portland Cement (OPC) is a crucial building material widely used in construction projects worldwide. Its manufacturing process involves a series of steps that transform raw materials into fine powder used in various construction applications. The first step in the production of OPC is mining the raw materials required for the manufacturing process, such as limestone, clay, and iron ore, from quarries. These materials are then crushed and ground into a fine powder called raw meal. The raw meal is then preheated in a preheater using hot gases from the kiln to reduce the amount of fuel required to heat the kiln. The preheated raw meal is then fed into a kiln, which is a long, rotating cylinder. The raw meal is heated to temperatures of up to 1450°C, causing a chemical reaction that produces clinker. The clinker is then cooled rapidly in a cooler by blowing air to reduce its temperature. The cooled clinker is then ground with a small amount of gypsum to produce the final product, Ordinary Portland Cement. Figure 12 shows the Ordinary Portland Cement used in this study.

Figure 12 Ordinary Portland Cement.

CHAPTER 4 : RESEARCH METHODOLOGIES

4.1 Evaluation of Material Properties

4.1.1 Soil Classification and Properties Evaluation

The soil used in this research was collected from Handa Area, Mie Prefecture, Japan. The soil was air-dried for 3 weeks and then sieved through the 200mm sieve, after which sieve analysis, hydrometer analysis, liquid limit, and plastic limit analysis were conducted to classify the soil. The liquid and plastic limits were 58.21% and 31.05%, respectively. The soil comprised 6.2% sand, 52.56% silt, and 41.24% clay. Based on the American Association of State Highway and Transportation Officials (AASHTO), the soil was classified as A-7-5(2) clayey soils. The soil compositions above rank the soil as expansive clay soil. Testing procedures followed Japan Industrial Standards JIS A 1204 for the sieve and hydrometer test and JIS A 1205 for the liquid and plastic limit tests. Additional geotechnical properties and index properties of the soil are shown in Table 4. Additionally, the particle size distribution is illustrated in Figure 13.

Table 4 Properties of soil

Materials	Property	Value
Soil Properties	Specific Gravity, g/cm^3	2.74
	Maximum dry density, g/cm^3	1.65
	Saturation, %	87.14
	Sand (75 μm - 2 mm), %	6.20
	Silt (5 - 75 μm), %	52.56
	Clay < 5 μm, %	41.24
	Liquid limit, LL, %	58.21
	Plastic limit, PL, %	31.05
	Plasticity Index, PI, %	27.16
	AASHTO classification	A-7-5(2)

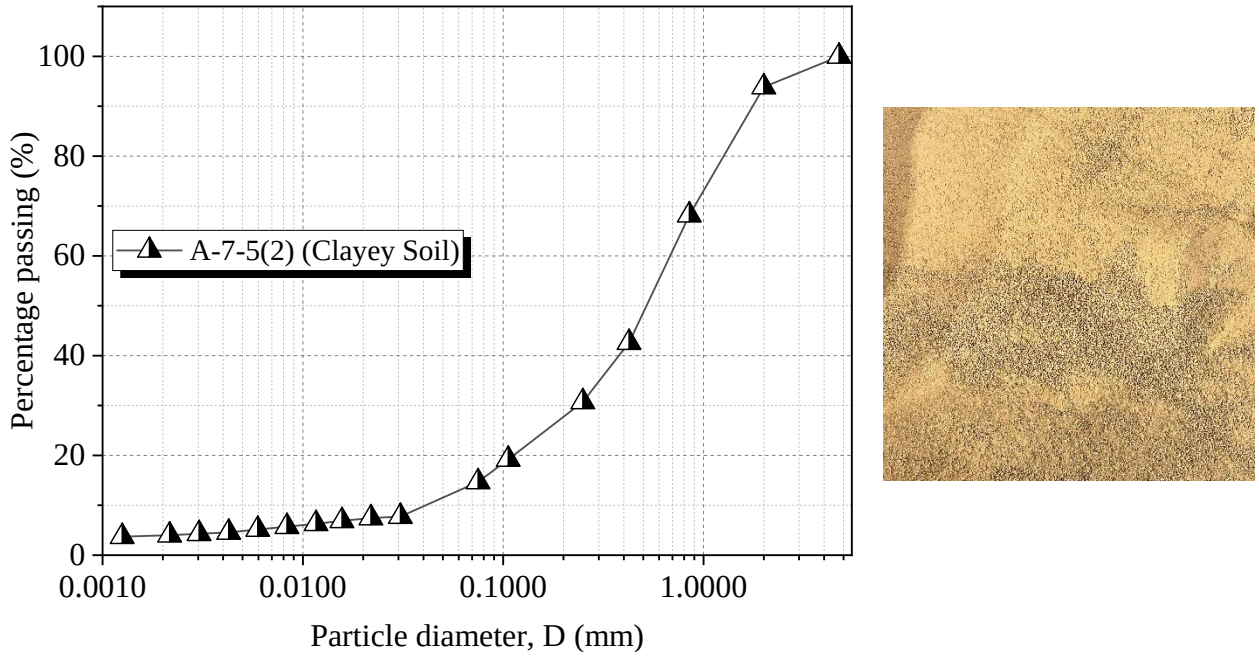

Figure 13 Particle size distribution for soil.

Soil samples were subjected to X-ray powder diffraction (XRD) analysis which quantitatively allowed for the determination of the chemical composition of the materials, as illustrated in Figure 14 (a). The soil had high crystal peaks of SiO_2 found in sedimentary soils, essential for the soil stabilization processes (de Jesús Arrieta Baldovino et al., 2020). Additionally, an individual granular structure of soil particles, observed using a scanning electron microscope (SEM) image, is shown in Figure 14 (b).

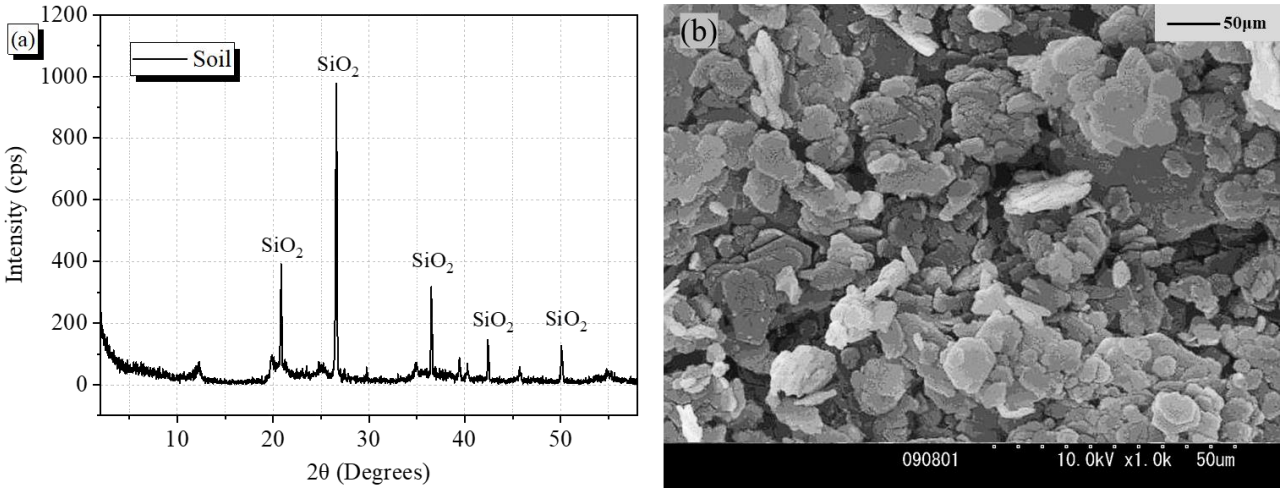

Figure 14 Microstructural examination of soil **(a)** X-ray diffraction (XRD) of soil **(b)** Scanning electron microscope (SEM) image of soil.

4.1.2 Rice husk ash (RHA): Physical and Chemical Properties

RHA, with a high silica content of 91.10%, was obtained from Make Integrated Technology Co., Ltd, Osaka, Japan. The high silica content was obtained by burning the rice husks for 27 hours in a computer-controlled industrial incinerator. A detailed grain size analysis for RHA is shown in Figure 15. Where RHA had grain sizes ranging from 0.00129 to 0.3 mm. RHA was subjected to X-ray powder diffraction (XRD) analysis which quantitatively allowed for the determination of the chemical composition of the materials, as illustrated in Figure 16 (a). RHA had an amorphous phase with a crystalline phase observed at a diffraction angle (2θ) of approximately 21°, corresponding to SiO_2. The crystalline phase in RHA indicated that the burning of rice husks was done at a temperature above 600°C. The amorphous phase was destroyed at these high temperatures, increasing pozzolanic properties (Chouksey and Kumari, 2019; Muñoz et al., 2021). A detailed physical and chemical property chart for rice husk ash is illustrated in Table 5.

Table 5 Physical and Chemical Properties of RHA.

Physical properties	
Property	**Values**
Specific gravity	1.47
Average particle size (mm)	0.001 to 0.30
Loss of ignition	4.00 to 6.00
Chemical properties	
Oxide compounds	**Values (%)**
Silica (SiO_2)	91.10
Carbon dioxide (CO_2)	4.35
Potassium Oxide (K_2O)	2.40
Calcium Oxide (CaO)	0.57
Iron Oxide (Fe_2O_3)	0.05
Alumina (Al_2O_3)	0.03
Others	1.50

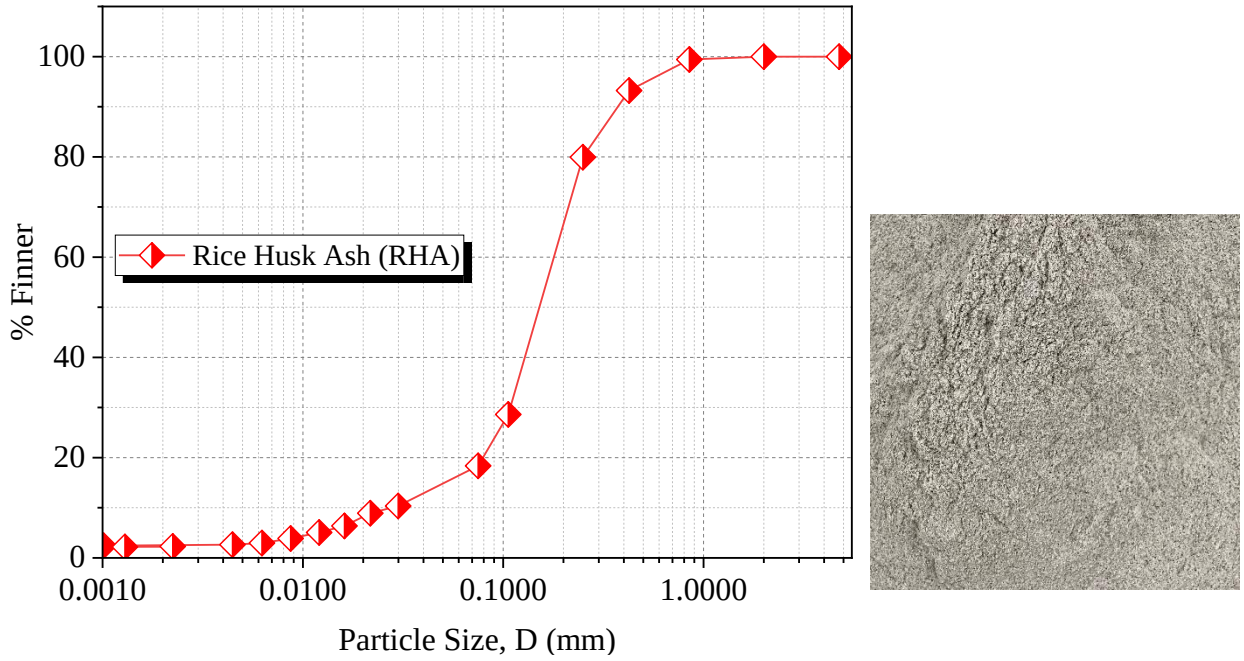

Figure 15 Particle size distribution for RHA.

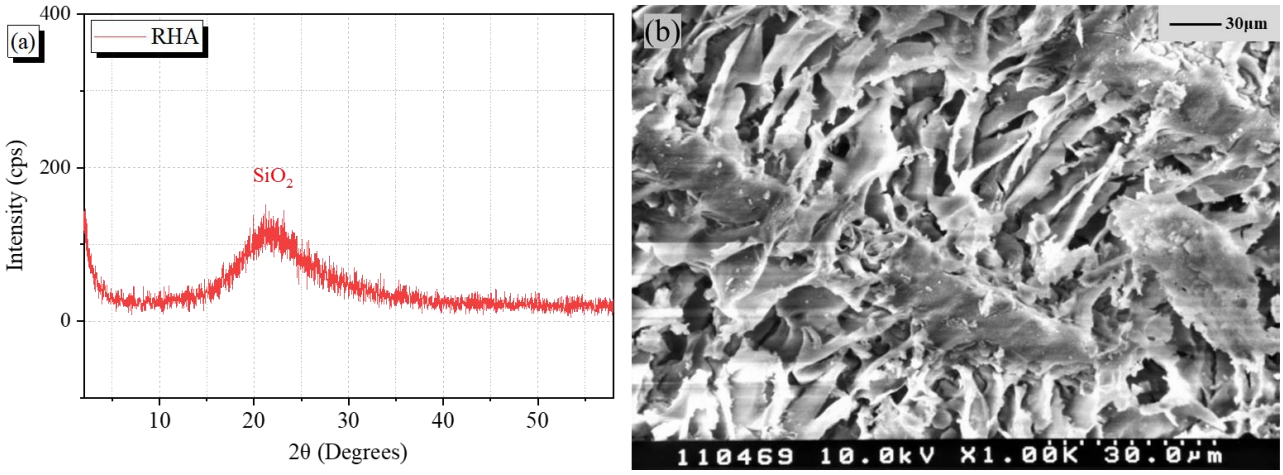

Figure 16 Microstructural examination of RHA **(a)** X-ray diffraction (XRD) of RHA **(b)** Scanning electron microscope (SEM) image of RHA.

4.1.3 Basalt fiber (BF): Physical and Chemical Properties

Basalt fibers are an environmentally friendly material made from melted basalt rock at a high temperature of 1500 °C and then quickly morphed into a continuous fiber by extrusion through 6-30 µm filament nozzles. The superiority of BF compared to the other conventional fibers is derived from the high tensile strength (4100~4840MPa), high elastic modulus (93.1~111.0GPa), long-term durability, thermal stability, and alkali resistance (Sim and Park, 2005). Additionally, basalt fibers

have a fracture elongation rate of 3.1%. JCK Corporation provided the fibers in their standardized forms of 3mm, 6mm, and 12mm (http://www.j-c-k.co.jp). Detailed physical, thermal, and chemical properties of the BF used in this study are shown in Table 6. Figure 17 (a) shows the standardized lengths of basalt fibers, and Figure 17 (b) shows the scanning electron microscope (SEM) image of Basalt fiber at a magnification of x1000.

Table 6 Physical and Chemical Properties of Basalt Fiber.

Physical Properties	
Properties	**Values**
Fiber diameter (μm)	6~30
Fiber length (mm)	3, 6 & 12
Density (g/cm^3)	2.63~2.80
Tensile strength (MPa)	4100~4840
Elastic modulus (GPa)	93.10~110
Fracture elongation rate (%)	3.1
Thermal properties	Values
Heat resistance temperature (°C)	-269~650
Thermal conductivity (W/mk)	0.03~0.04
Melting temperature (°C)	1450
Softening temperature (°C)	1050
Chemical properties	
Oxides composition	**Values (%)**
Silicon oxide (SiO_2)	51.6~59.3
Aluminum oxide (Al_2O_3)	14.6~18.3
Iron oxides (Fe_2O_3)	9.00~14.0
Calcium oxide (CaO)	5.90~9.40
Magnesium oxide (MgO)	3.00~5.30
Others	0.09~0.13

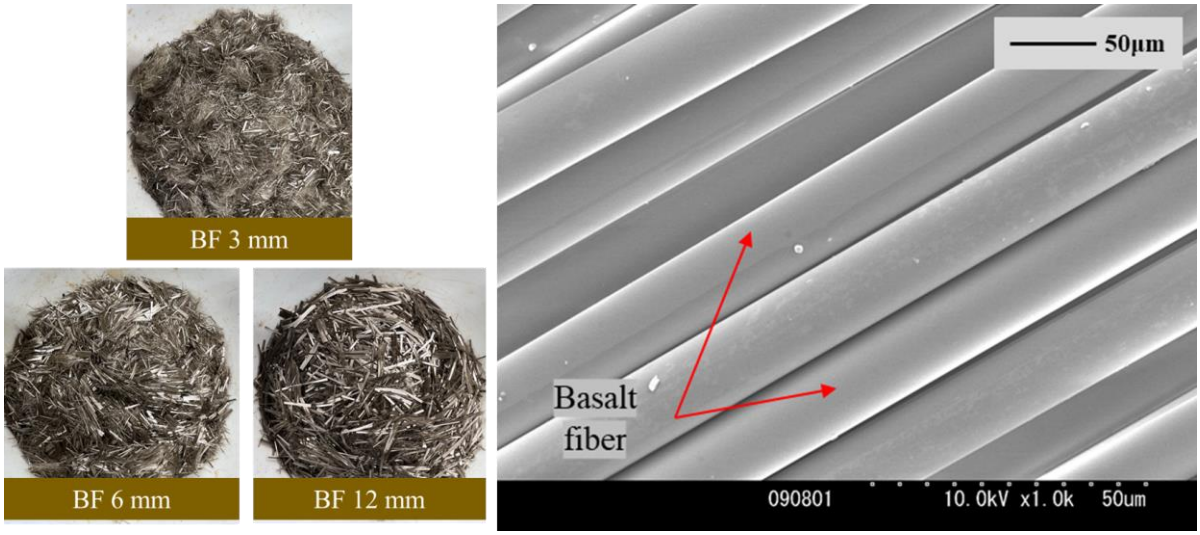

Figure 17 Basalt fiber **(a)** Standardized lengths of basalt fibers **(b)** Scanning electron microscope (SEM) image of Basalt fiber.

4.1.4 Ordinary Portland Cement (OPC): Physical and Chemical Properties

The properties of OPC are shown in Table 7. Also, a detailed particle size distribution is shown in Fig. 18. The cement had a composition of alite (Ca_3SiO_5), a major chemical component in OPC that defined its high strength as shown in the X-ray powder diffraction (XRD) analysis results in Figure 19 (a). Additional microstructural analysis was also done using SEM imagery, revealing highly irregularly shaped particles with sharp edges, as shown in Figure 19 (b).

Table 7 Physical and Chemical Properties of OPC

Physical properties	
Properties	**Values**
Initial setting time (minutes)	170
Final setting time (minutes)	225
Specific gravity (g/cm^3)	3.15
Specific surface area (m^2/kg)	340
28-day compressive strength (MPa)	33~ 53
Loss of ignition (%)	<4
Chemical properties	
Oxides composition	**Values (%)**

Calcium Oxide (CaO)	63.40
Silicon dioxide (SiO_2)	21.60
Iron Oxide (Fe_2O_3)	5.35
Alumina (Al_2O_3)	4.45
Magnesium oxide (MgO)	1.65
Others	3.55

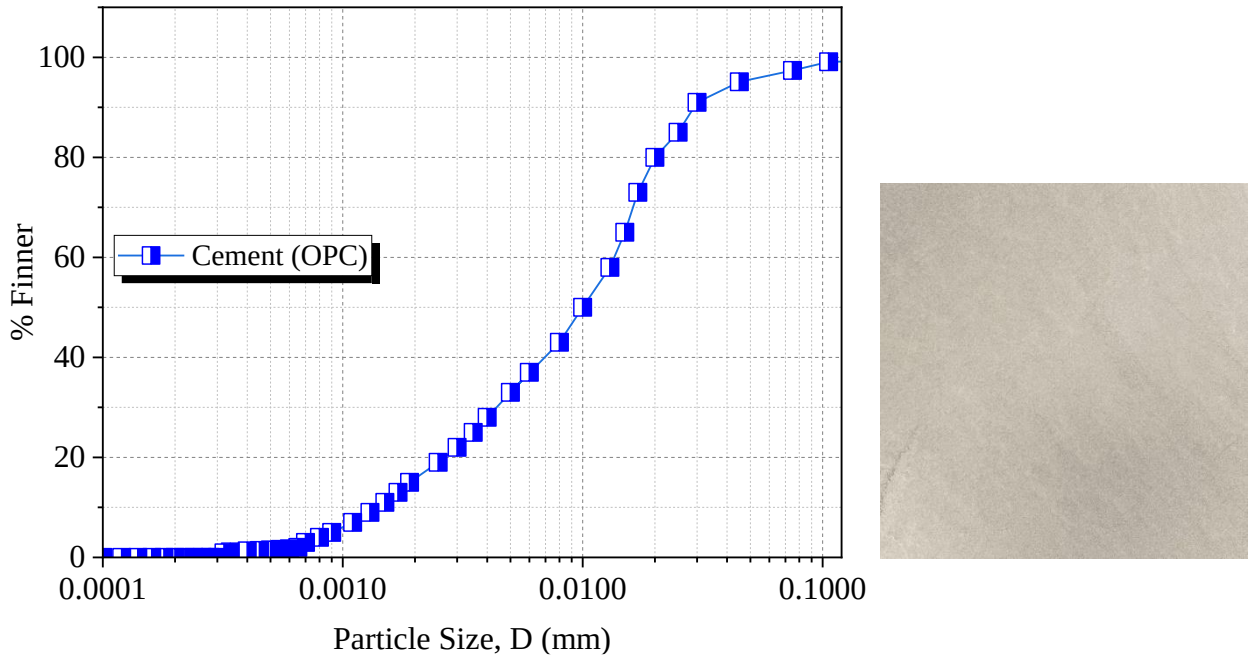

Figure 18 Particle size distribution for OPC

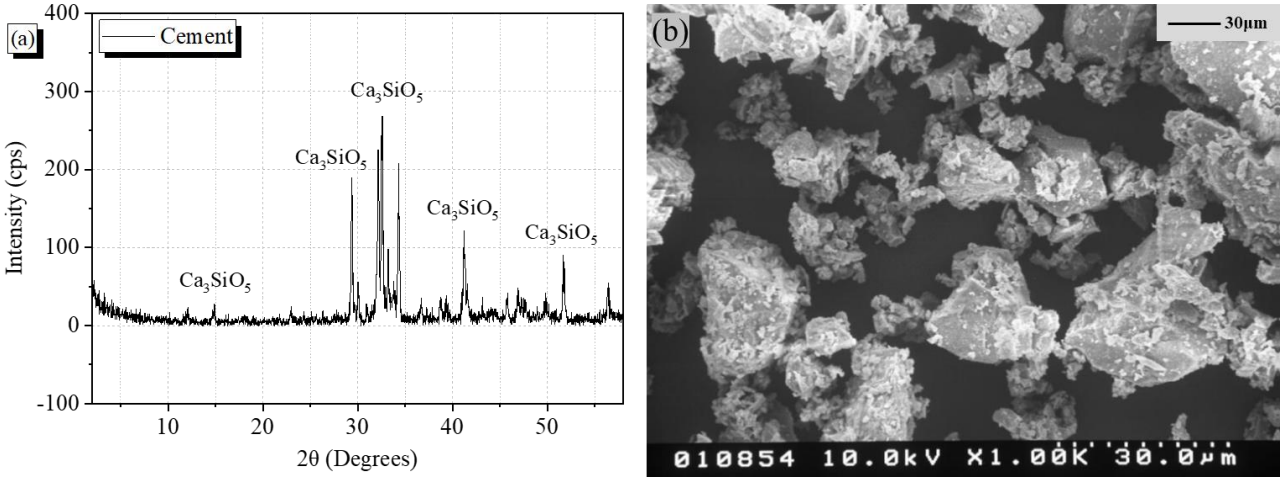

Figure 19 Microstructural examination of OPC: **(a)** X-ray diffraction (XRD) of OPC **(b)** Scanning electron microscope (SEM) image of OPC.

4.2 Experimental Specimen Codes and Specified Combination Schemes

Each specimen was prepared using soil, RHA (5%, 10%, or 15% dry weight of soil), cement (3% dry weight of soil), and basalt fiber (3, 6, or 12mm length: 1% dry weight of soil for each length) in their specified combination schemes as shown in Table 8. In this study, RHA dosages were set between 5 to 15% because the optimal strength of RHA-stabilized soils is achieved when the RHA content is between 5-15% (Owino et al., 2022b). This range provides the best balance between strength and cost-effectiveness regarding cement reduction costs, soil stabilization costs, and RHA disposal costs. Additionally, the rate of adding RHA also depends on the properties of the soil. Soils with high plasticity and low permeability require higher rates of RHA addition to improve their strength and stability. Therefore, the range provided in this study ensured a detailed parametric study on RHA dosage during expansive soil stabilization.

On the other hand, a minimal dosage of OPC was used as the pozzolanic reaction activator by providing the calcium oxide ions and as a binder element. Additionally, the minimum dosage of 3% cement was typically used for the following reasons; (i) Higher cement dosages can have negative environmental impacts, such as increased carbon emissions and depletion of natural resources during their production processes. (ii) Using 3% cement dosage is a cost-effective solution for achieving the required strength and stability if other binding aggregates with cementitious properties, such as RHA, are used. (iii) cohesive soils, such as expansive soils, require less cement than non-cohesive soils like sand. As discussed in the previous sections, the minimal dosages of cement can reduce the overdependence on OPC and enable the application of sustainable cement-reducing alternatives.

The superiority of BF compared to the other conventional fibers was derived from the high tensile strength (4100~4840MPa), high elastic modulus (93.1~111.0GPa), and its environmental friendliness since it is made from natural materials.

Table 8 Specimen codes and specified combination schemes.

No.	Specimen Code	Soil, S (%)	BF (mm)	BF (%)	RHA (%)	Cement, C (%)
1	S-Control	100	0	0	0	0
2	S:5R	100	0	0	5	0
3	S:10R	100	0	0	10	0
4	S:15R	100	0	0	15	0
5	S:5R:3C	100	0	0	5	3
6	S:10R:3C	100	0	0	10	3
7	S:15R:3C	100	0	0	15	3
8	S:5R:3C:1BF3	100	3	1	5	3
9	S:10R:3C:1BF3	100	3	1	10	3
10	S:15R:3C:1BF3	100	3	1	15	3
11	S:5R:3C:1BF6	100	6	1	5	3
12	S:10R:3C:1BF6	100	6	1	10	3
13	S:15R:3C:1BF6	100	6	1	15	3
14	S:5R:3C:1BF12	100	12	1	5	3
15	S:10R:3C:1BF12	100	12	1	10	3
16	S:15R:3C:1BF12	100	12	1	15	3
NOTE: S-Soil, R-RHA, C-Cement, BF-Basalt fiber						

4.3 Experimental Methods

4.3.1 Standard Proctor Compaction test

The Standard Proctor Compaction Test, also known as the Modified Proctor Test, is a widely used laboratory test to determine the optimum moisture content (w_{opt}) and maximum dry density (ρ_{dmax}) of soils. The w_{opt} is the moisture content at which the soil is the most workable and can be compacted to its maximum dry density, while the ρ_{dmax} is the density achieved when the soil is compacted to its maximum potential under a specified compaction energy. This test is essential in geotechnical engineering as it helps in densifying soil by reducing its voids content, making it more stable and able to support heavy loads. In construction projects, compacted soils are used as a base layer for

roads, embankments, and foundations. A well-compacted soil can resist deformation and prevent settlement, which can cause structural damage. The test results are useful in selecting the appropriate compaction equipment and the number of passes required to achieve the desired density. The test also helps assess soil suitability for a specific project by comparing the results with the required specifications. The Standard Proctor Compaction testing equipment, including the mold, collar, and rammer, is shown in Figure 20.

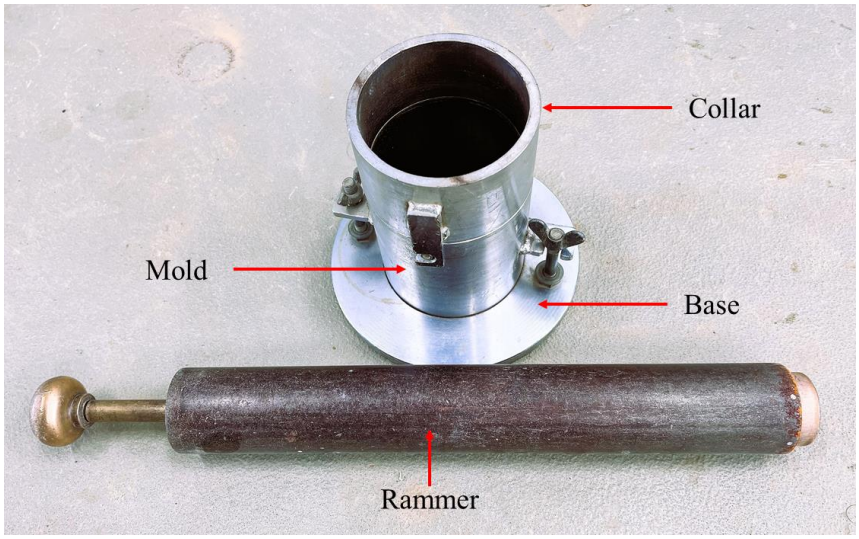

Figure 20 The Standard Proctor Compaction testing equipment.

4.3.1.1 Material Preparation and Testing Procedure

Considering the material combinations shown in Table 8, each combination scheme (2500g after mixing dry aggregates) was compacted into a cylindrical mold measuring 10 cm in diameter and 12.73 cm in height using a 2.5 kg rammer at a falling height of 30 cm while maintaining a constant compaction effort for each of the three layers. This process was repeated for variously known moisture contents, and the dry densities were calculated for each. The plots of the dry density to the moisture content also called the compaction curves, were then used to obtain the peak points representing the maximum dry density and the optimum moisture content. All testing procedures followed the Japan Industrial Standards (JIS) A 1210 standards.

4.3.2 Soil Consolidation Test

Soil consolidation test, also known as the oedometer test, is a standard laboratory procedure used to determine the rate and magnitude of soil compression over time under a specified load. This test is commonly used in civil and geotechnical engineering to estimate the settlement of structures built on compressible soil layers. The experimental equipment used in this study is presented in Figure 21.

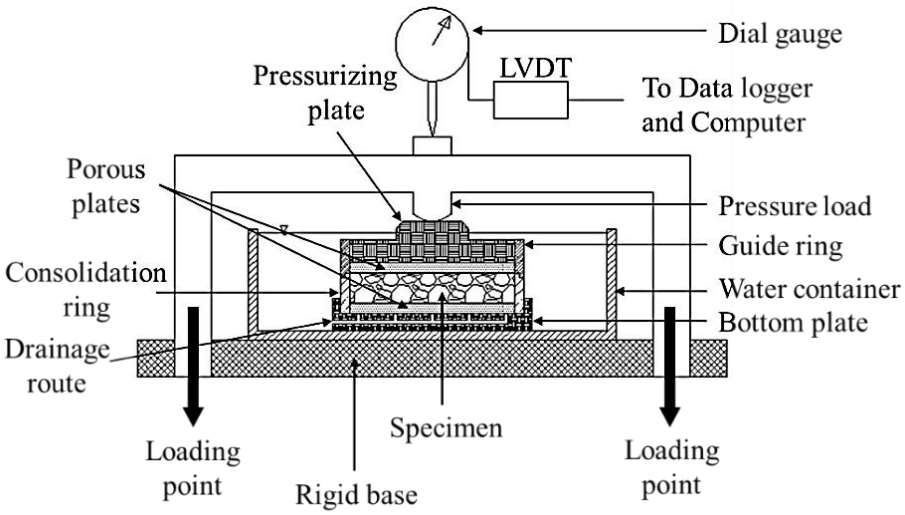

Figure 21 Components of the oedometric cell apparatus.

It consisted of an oedometric cell on a rigid base, a loading lever arm, and a dial gauge combined with LVDT (Linear Variable Differential Transformer). The oedometric cell included a water container, a pressurizing plate fitted with a porous plate at the bottom, a guide ring, a consolidation ring, and a bottom plate equipped with a porous media. The guide ring and the consolidation rings were made of stainless steel with a uniform diameter of 60 mm and a height of 20 mm. They were inserted into the bottom plate to ensure high rigidity, capable of minimizing the expansions in the radial direction during loading. The porous media on the pressurizing plate and the bottom plates allowed proper drainage through the specimens during one-dimensional consolidation.

Specimen Preparation Procedure; During specimen preparation, one of the primary considerations was achieving the maximum effects of the fibers and ensuring their random installation in the soil

composite. The dry materials were dry-mixed manually using a spatula before adding water. The dry-mixing process ensured the random distribution of fibers and aided in preventing the fiber balling effect, which was checked through physical observation of the mixture before adding water. It is important to note that many factors, including the type, fiber stiffness, concentration of fibers, and specimen preparation method and time, can influence the distribution of fibers in a soil specimen. Therefore, it is essential to carefully control these factors to ensure accurate results. In this case, visual inspection of the fiber distribution was possible due to the stiffness of the basalt fibers that enabled the random distribution of individual fibers in the soil.

Each specimen was prepared using soil (200g), RHA (5%, 10%, or 15% dry weight of soil), cement (3% dry weight of soil), and basalt fiber (3, 6, or 12mm length: 1% dry weight of soil for each length) in their specified combination schemes as shown in Table 8. Water was added to an initial water content of 47.81%, 51.53%, and 55.62% for 5%RHA, 10%RHA, and 15% RHA, respectively. The difference in the initial water contents was due to the high-water affinity for the higher percentages of RHA when mixed with soil, as observed through optimum moisture content evaluation in a related study (Owino et al., 2022b). The stipulated water contents, just below the liquid limit of the clay soil, enhanced the handling and formability of the soil composites. The added water increased the specimens' water content to within the range of the liquid limit of medium plastic clay (40-60%) hence simulating pore water pressures similar to clay in its natural state (Sridharan and Nagaraj, 2004; Owino et al., 2022a). Preparing the specimens within this liquid limit was essential mainly because it is considered the limiting water content above which the soil is almost flowing, and it's one of the main parameters dictating the compressibility of soil. Next, the materials were mixed for 10 minutes using a spatula to obtain a homogeneous paste, rolled by hand to a 30 mm thick cylindrical shape, then placed in a desiccator for 24 hours to achieve maximum moisture equilibration. Afterward, the specimens were trimmed using the cutting rings (diameter=60mm;

height= 20 mm), and the excess soil was cut off using a cutting wire before transferring to the soil consolidation rings, as shown in Figure 22.

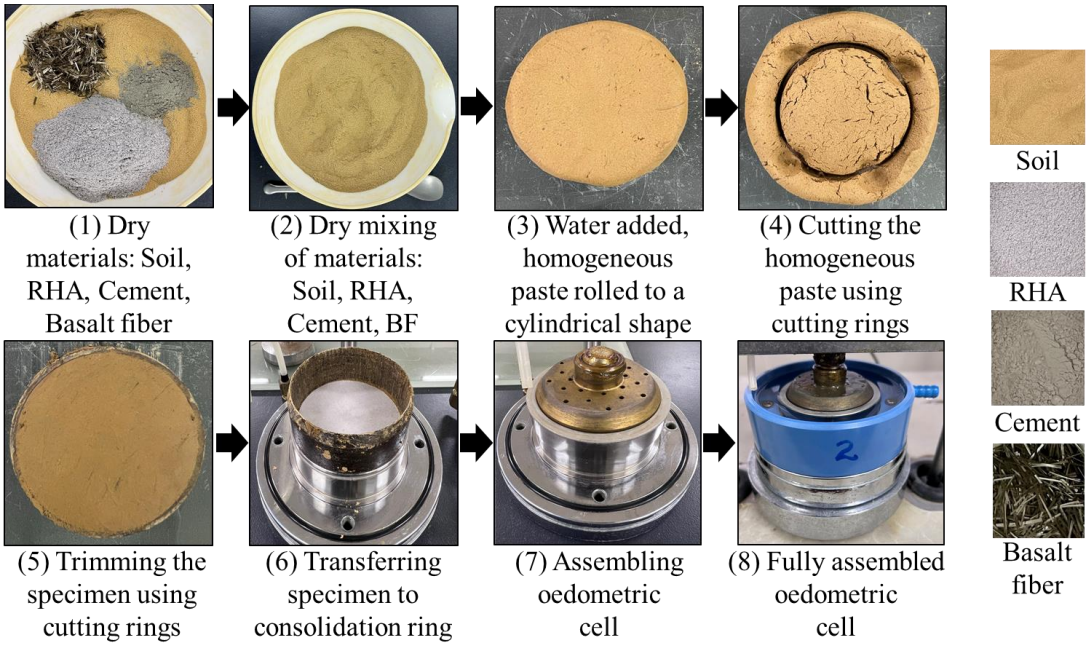

Note: The surface cracks on the rolled 30 mm thick cylindrical shape in item (4) were removed by cutting the extra 10 mm, reducing the sample thickness to 20 mm. This procedure ensured a very minimum disturbance effect in the specimen structure.

Figure 22 Specimen preparation procedure and the oedometric cell assembly.

The dimensions of the initial cylindrical composites were maintained for each combination scheme to minimize the scalability errors for each prepared specimen. The trimmed soil composites were used to evaluate the initial specimen water content.

Concerning the specimen preparation procedures above, it should be noted that the scale effect of basalt fiber length on the mechanical properties of the specimens is dependent on the dimensions of the soil specimen being tested. In general, longer basalt fibers can provide more reinforcement to the soil composite and can lead to improved mechanical properties. However, the effect of fiber length on the mechanical properties of basalt fiber-reinforced soils may not be consistent across different specimen sizes. This is because the fiber length ratio to specimen size can affect how the fibers interact with the soil matrix and with each other. Therefore, it is essential to consider the specimen

dimensions, basalt fiber dosage percentages, and length when designing and testing basalt fiber-reinforced soils to ensure that the chosen fiber length is appropriate for the scale of the specimen. Additionally, the void ratio, density, and degree of saturation of the specimens were calculated, as will be discussed in the subsequent section. Filter papers with similar dimensions to the consolidation rings were placed at the top and bottom of the specimen to prevent the soil composite from clogging the porous plates during the loading and drainage processes. A detailed specimen preparation procedure for all ten combinations is shown in Figure 22. The preparation procedure for the control specimen (specimen 1) followed the same steps from 1-8 minus the additives in steps 1 and 2.

4.3.2.1 Experimental procedure

After transferring the specimen into the consolidation rings, the initial weight and dimensions were determined. These two measurements were used to evaluate the initial specimen condition, as will be discussed in the next section. The oedometric cell was assembled and filled with water, as shown in Figure 22 [item (8) Fully assembled oedometric cell]. Afterward, the mechanical loading-unloading cycles were performed in steps with incremental loads of 9.8, 19.6, 39.2, 78.5, 157, 314, 628, and 1256 kPa during the loading cycle and 628, 314, 157, 78.5, 39.2, 19.6 and 9.8 kPa during the unloading cycle.

All the load increments/reductions were kept constant for 24 hours until the primary consolidation had seized and the excess pore water pressure dissipated completely (Ferrari et al., 2016). Meanwhile, the settlement of the specimen with time was measured using an electronic dial gauge combined with an LVDT and connected to a data logger and computer to maintain accuracy in the data sets obtained. Each specimen was consolidated for 16 days, after which it was weighed and oven-dried to calculate the final water content. Finally, a piece of each specimen was collected for SEM analysis. Figure 23 shows the soil consolidation testing equipment. The testing procedures followed the Japan Industrial Standards (JIS) (JIS A 1217, 2010; JIS A 1227, 2010).

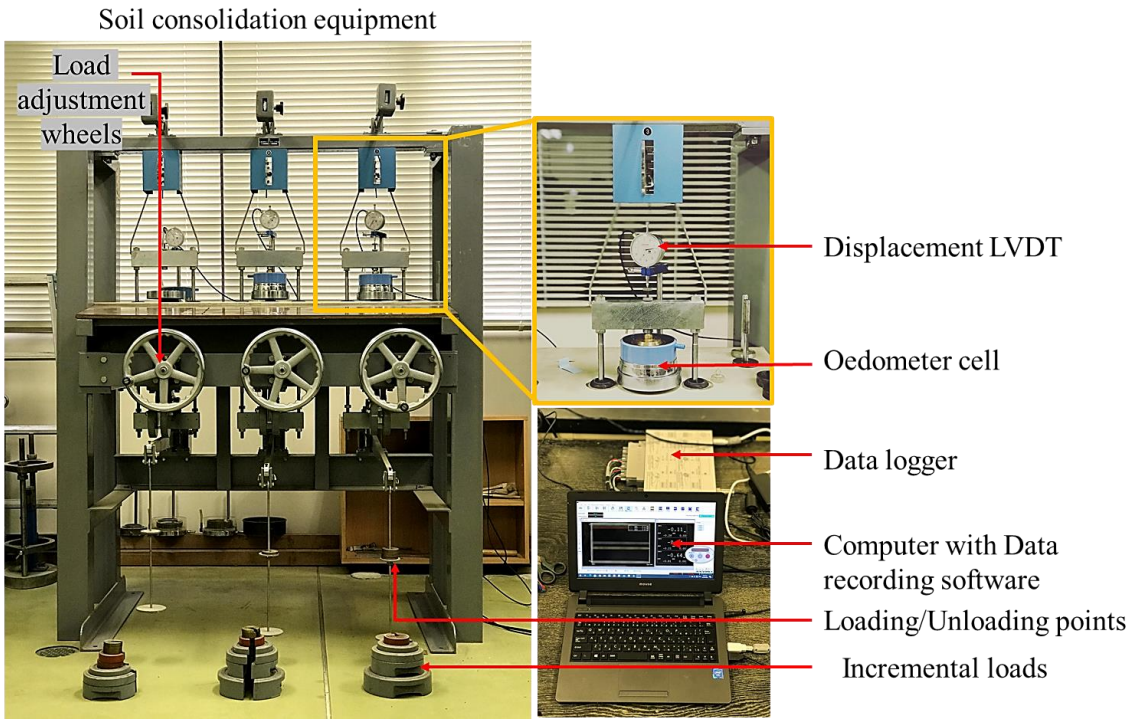

Figure 23 Soil consolidation testing equipment.

4.3.3 Triaxial Compression Test

Following the Japan Geotechnical Society 0520~0524 standards, consolidated drained (CD) triaxial tests were performed on cylindrical specimens measuring 5 cm (in diameter) and 12.5 cm in height. In a consolidated drained triaxial test, the sample is consolidated and sheared in compression slowly to allow pore pressures built up by the shearing to dissipate. The Consolidated Drained (CD) Triaxial Compression Test is a widely used laboratory technique for determining the mechanical properties of soils. It is handy for assessing the strength and deformation characteristics of cohesive soils, which can be prone to instability and failure under shear conditions. The CD triaxial compression test involves subjecting a cylindrical soil specimen to a series of axial and confining stresses in a specially designed apparatus known as a triaxial cell, as shown in Figure 24. The soil specimen is first compacted to a desired density and moisture content and then placed inside the triaxial cell, where a confining fluid surrounds it, typically water. The cell is then pressurized to create a confining stress around the specimen, which helps to simulate the in-situ stress conditions of the soil.

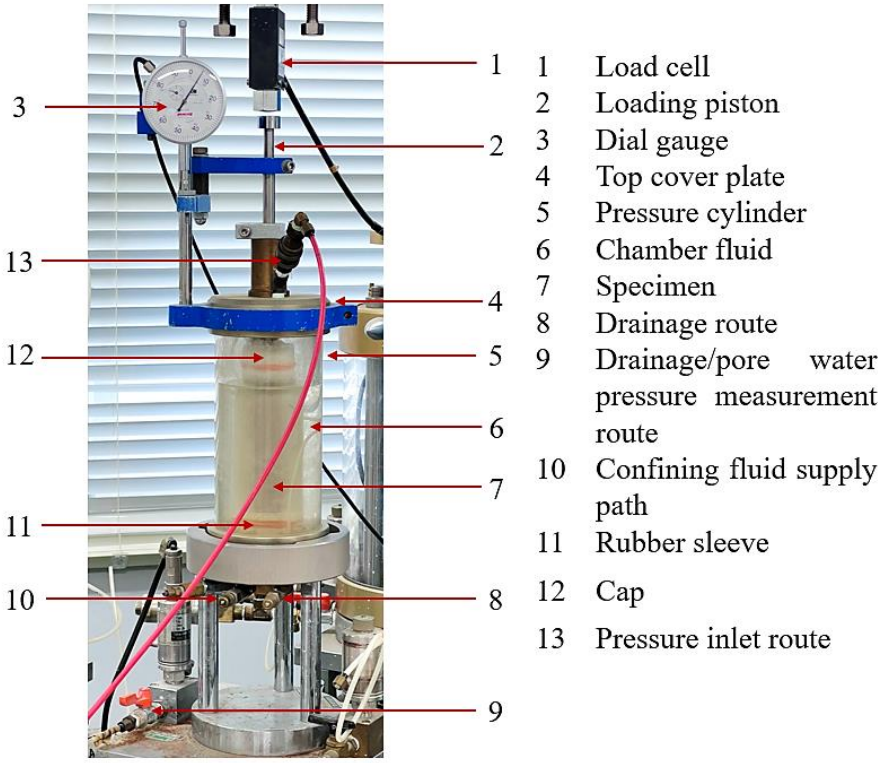

Figure 24 Triaxial testing apparatus.

4.3.3.1 Material Preparation and Testing Procedure

In this study, the specimens were prepared by compacting each blend in three layers inside a mold of 5 cm (in diameter) and 12.5 cm in height using a 1 kg rammer at a 30 cm falling height. All specimens were set at the optimum moisture content obtained from compaction tests and wet-cured for one day, seven days, and 28 days at a constant temperature of 25 degrees Celsius before testing. Each specimen was set up in the triaxial test pressure chamber and sealed with a rubber sleeve, as shown in Figure 24.

The consolidated drained triaxial tests experimental setup consisted of the following major components; (1) load cell to measure the axial load, (2) loading piston to apply the axial loading on top of the specimen, (3) dial gauge to measure the axial displacement, (5) pressure cylinder to contain the chamber fluid, (6) chamber fluid to apply the hydrostatic chamber pressure (σ_3), (9) drainage/pore water pressure measurement route, (10) confining fluid supply path and (13) air pressure inlet route.

This study's confining pressures were 50 kPa, 100 kPa, and 150 kPa. The drainage/pore water-pressure measurement route was left open to ensure a drained condition within the specimen.

Specimens were allowed to shear slowly enough at a rate of 0.5mm/minute so that the pore water pressure did not develop within the composite structure. During the experiment, values of deviatoric stresses and axial strains were recorded in a data logger. The experiment was stopped once the peak value of the deviatoric stress was attained and then reduced to two-thirds or at 10% axial strain.

4.3.4 Unconfined Compression Strength (UCS) Test

UCS Test is used in geotechnical engineering to determine the shear strength and compressibility of a soil sample. This test is often performed on undisturbed or remolded soil samples taken from the ground that are relatively soft or cohesive, such as clays or silts. In engineering practice, the unconfined compressive strength (UCS) test is the most commonly used and feasible technique to assess the strength of the optimum mix designs of stabilized and reinforced soil worldwide (Zhang et al., 2019).

4.3.4.1 Material Preparation and Testing Procedure

Following the specimen codes and specified combination schemes listed in Table 8, the UCS tests were done on cylindrical specimens with dimensions 5cm diameter and 12.5 cm height to examine the compressibility behavior of the mix ratios. The specimens were prepared using a cylindrical mold of similar dimensions and a rammer weighing 1kg at a falling height of 30cm. All specimens were set at the optimum moisture content obtained from compaction tests and wet-cured for one day, seven days, and 28 days at a constant temperature of 25 degrees Celsius before testing.

The test is typically performed in a laboratory setting, where a cylindrical soil sample is loaded axially until it fails. The specimens are not confined by any external confining pressure, hence the name "unconfined" compression test, as shown in Figure 25. The data sets obtained from each specimen were then analyzed in the stress-strain curve plots to evaluate the compressive stress (q_u)

and axial strain(ε) relationship and the modulus of deformation, E_{50}. The testing procedures followed the Japan Industrial Standards, JIS A 1216 (2010).

The major components of the UCS testing equipment include; a proving ring, a load dial gauge, a displacement dial gauge, pressurizing plates (top cap and fixed plate), and a compressor (with a wheel and moving plate). A detailed illustration is shown in Figure 25.

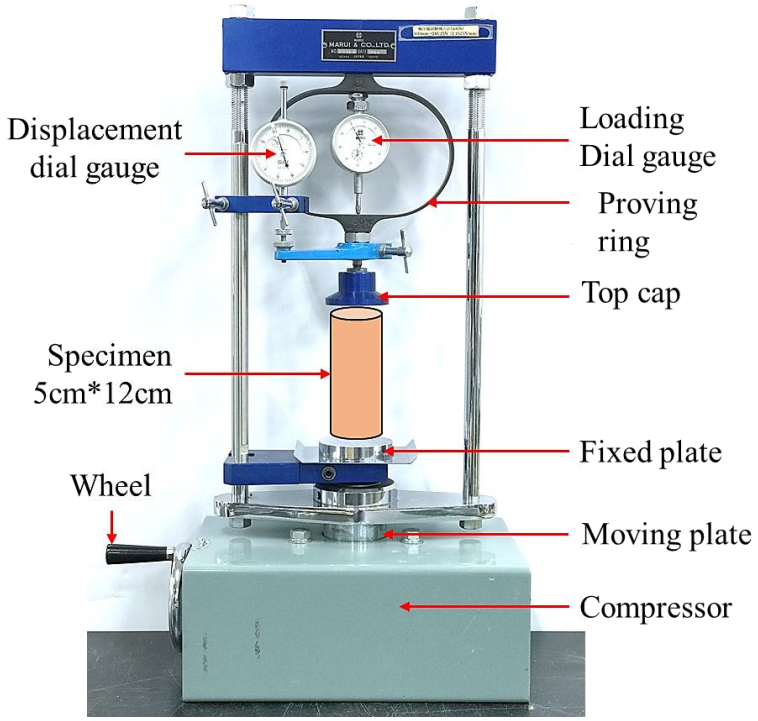

Figure 25 UCS testing equipment.

4.3.5 Summary of the Specimen Preparation Procedure for Triaxial and UCS Tests

The soil was sieved through the 2 mm sieve and allowed to air dry for two weeks before specimen preparation. The specified combinations were prepared by dry-mixing the air-dried soil with RHA (5%, 10%, and 15% dry weight of soil) and cement (3% dry weight of soil) to a homogeneous mix, as shown in Figure 26 (a).

In this study, RHA dosage was set to 5-15% due to the maximum utilization of the amorphous silica at low percentages. This RHA range also aided in providing data sets for a comprehensive parametric

analysis of the effects of varied dosages of RHA. On the other hand, minimum dosages of cement reduced cement usage and provided Ca+ ions in optimal proportions during pozzolanic reactions. Incorporating RHA as a cement reduction parameter agreed with the environmental conservation and carbon emission reduction goals explained in Chapters 1 and 2.

Next, water was added to the dry mix considering the w_{opt} and the maximum dry density of each specific combination evaluated from the compaction tests to initiate the chemical stabilization phase through hydration [Figure 26 (b)]. Basalt fiber (1% dry weight of soil) with filament lengths of 3 mm, 6 mm, and 12 mm were sprinkled on the top surface of the soil-RHA-Cement mixture to ensure random distribution and reduce fiber balling during the next phase of mixing as shown in Figure 26 (c). When fibrous materials such as basalt or other types of fibers are incorporated into the soil, they can become entangled and form balls or clumps. This balling effect can happen due to factors such as inadequate mixing, insufficient decomposition or breakdown of the fibers, or improper distribution of the fibers in the soil. To avoid this phenomenon, using minimal dosages is reasonable, hence the 1% used in this study.

The fiber content was set at 1% to avoid tangling or balling during the specimen preparation, affecting the blends' homogeneity. The manual mixing of all the materials guaranteed an even distribution of basalt fibers within the new composite material, as shown in Figure 26 (d).

Blend combinations were prepared at the maximum dry density (ρ_{dmax}) and -3% optimum moisture content (w_{opt}), after which three cylindrical specimens were prepared for each level of confining pressure [Figure 26 (e)] and tested after a moist-curing period of 1, 7, and 28 days. Preparing soil specimens at -3% w_{opt} can provide insights into the soil's compactability, stability, and strength characteristics under drier conditions. The detailed list of the specified combinations used in this study is shown in Table 8.

Figure 26 (a) Step 1: Dry mixing of Soil, RHA, and Cement in specified combinations.

Figure 26 (b) Step 2: Addition of water considering the w_{opt} of specified combinations.

Figure 26 (c) Step 3: Addition of varied basalt fiber filament lengths in specified combinations.

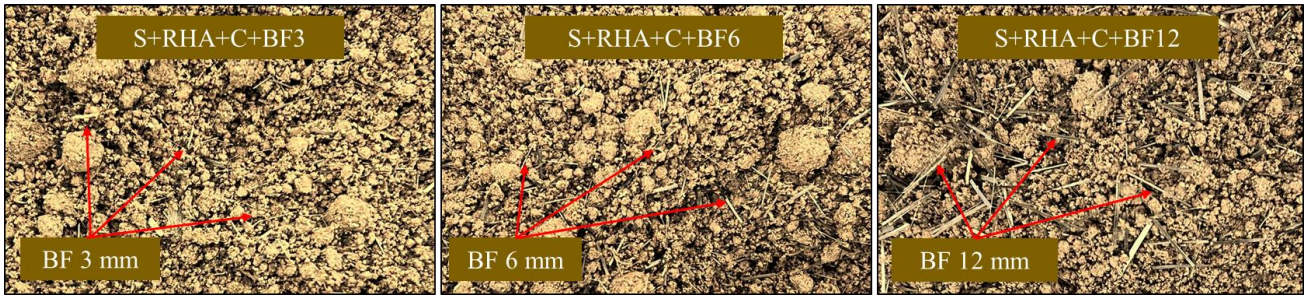

Figure 26 (d) Step 4: Manual mixing of the materials: To ensure the random orientation of the basalt fibers and to achieve a homogeneous mix.

Figure 26 (e) Step 5: Specimen preparation- 3 specimens per confining pressure for all specified triaxial and UCS tests combinations.
Figure 26 (a-e) Preparation of materials and specimen.

4.3.6 Soil Permeability Test: Constant Head Test

The soil constant head permeability test is a widely used laboratory test for determining the hydraulic conductivity, or permeability, of undisturbed and restructured soils. The test involves the determination of the flow rate of water through a soil specimen of a specific length and cross-sectional area under a constant head condition. The hydraulic conductivity, or permeability, is then calculated using Darcy's Law, which relates the flow rate, hydraulic head, and soil properties such as porosity and tortuosity. Hydraulic conductivity is a soil property used in soil classification systems, and it can help engineers predict the behavior of soils under different loading conditions. A detailed illustration of the constant head permeability testing equipment is shown in Figure 27.

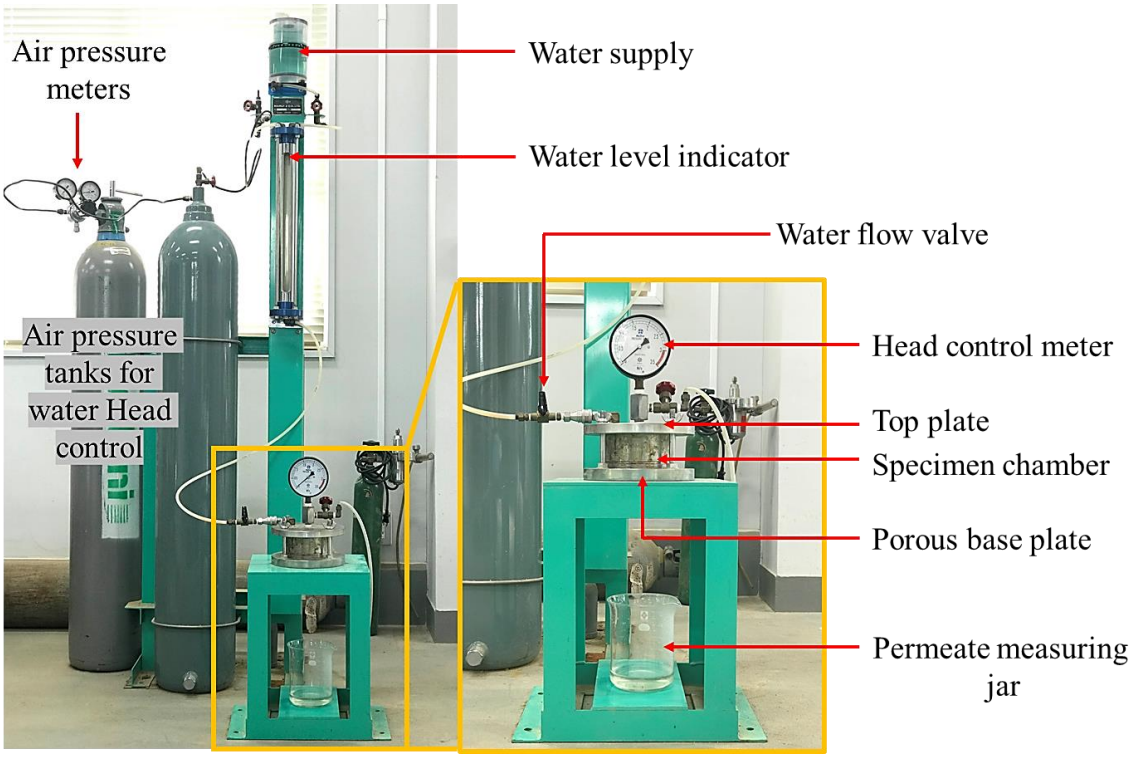

Figure 27 The constant head permeability testing equipment.

4.3.6.1 Material Preparation and Testing Procedure

In this study, a constant head permeability test was carried out to examine the coefficient of permeability, k, for all the specimens considering curing periods 1 day, 7 days, and 28 days. Each specimen was compacted in three layers in the compaction mold (10.4 cm diameter and 6.3cm height) at 20 blows per layer to maintain constant compaction energy. The specimens were wet-cured while retaining the water content at OMC, allowing enough hydration and pozzolanic activity. The constant water head was maintained at 45m, simulated by the air pressure of 0.45 MPa in the water chamber on top of the specimen. Water flowed through the specimen until it was saturated before taking the first reading. Four readings were taken by measuring the volume of percolated water and the corresponding time taken for flow. Afterward, the average k of each flow was used to evaluate the final permeability coefficient (k). The experimental procedures followed Japan Industrial Standards, JIS A 1218 (2010).

4.3.7 Scanning Electron Microscopy (SEM) Test

Scanning Electron Microscopy (SEM) is a powerful analytical tool used in materials science and engineering for investigating the microstructure and morphology of various materials. The technique involves scanning a focused electron beam over the sample surface and detecting the scattered electrons from the sample. By analyzing the patterns of electron scattering, SEM can provide high-resolution images of the sample's surface, revealing information about its topography, morphology, and chemical composition. Expansive soils undergo significant volume changes upon wetting or drying, leading to structural damage in foundations, roads, and other civil engineering structures. Therefore, stabilization and reinforcement techniques can be used to improve the mechanical properties of these soils and reduce their susceptibility to shrink-swell cycles. However, the effectiveness of these techniques depends on the microstructure and morphology of the soil.

SEM analysis can provide valuable insights into the microstructure of stabilized and fiber-reinforced expansive soils. For example, SEM images can reveal the distribution and orientation of fibers within the soil matrix and the interactions between the fibers and the soil particles. In addition, SEM can identify any changes in the morphology of the soil particles and the development of new phases or chemical bonds due to the stabilization or reinforcement process. A comprehensive SEM analysis was conducted across all specimen combination schemes to understand the microstructural developments concerning the projected strength developments with the curing period. A schematic representation of the scanning electron microscope used in this study is shown in Figure 28.

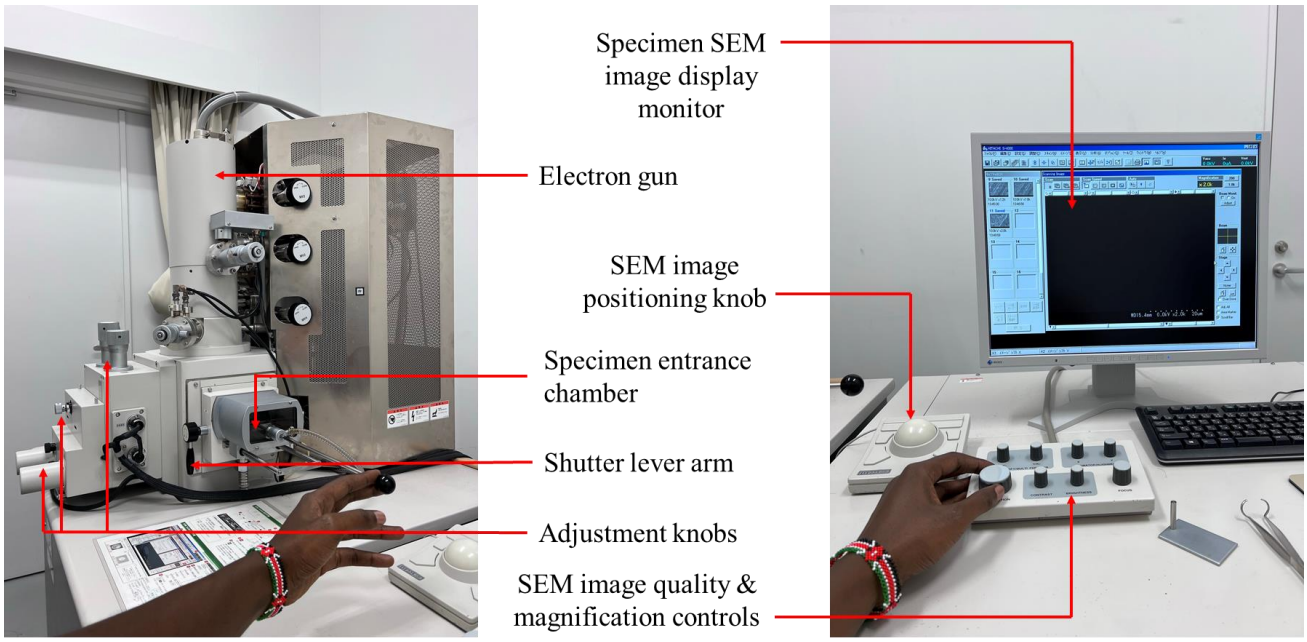

Figure 28 A schematic representation of the scanning electron microscope.

4.3.7.1 Specimen Preparation and Testing Procedure

In this investigation, the SEM images of the specific combination schemes were captured at magnifications ranging between x500 and x5000. The SEM test specimens were collected from consolidation, triaxial, and UCS test specimens. A small piece measuring 5mm by 5mm was cut out randomly from each combination and taped on the sample holding device. Next, the specimens were

gold-coated in an ion-based device before being set into the scanning electron microscope for further analysis, as will be discussed in the next section.

4.3.8 X-ray Powder Diffraction (XRD) Test

X-ray Powder Diffraction (XRD) is a popular technique for analyzing the crystalline structure of materials. XRD analysis involves passing a beam of X-rays through a sample and measuring the diffraction pattern produced by the interaction of the X-rays with the sample's crystalline structure. The diffraction pattern provides information about the crystal structure of the material, such as the lattice spacing and orientation of the crystal planes. XRD analysis can be used to identify the mineralogy of a sample and determine the changes in its crystalline structure due to external factors such as stabilizers or fibers.

Figure 29 presents a detailed illustration of the X-ray Powder Diffraction (XRD) Testing equipment, indicating the major components.

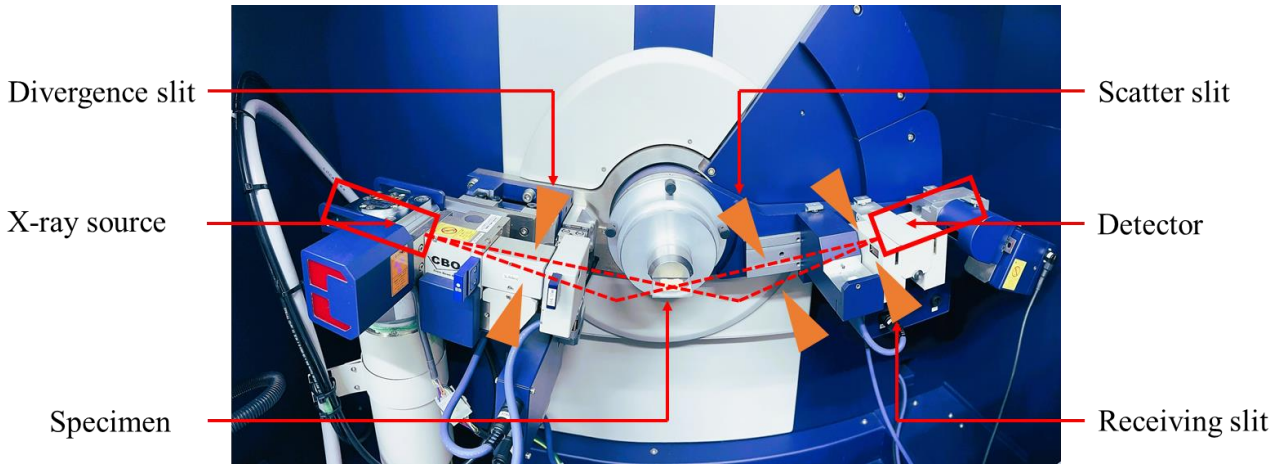

Figure 29 X-ray Powder Diffraction (XRD) testing equipment.

4.3.8.1 Specimen Preparation and Testing Procedure

The XRD test specimens were collected from consolidation, triaxial, and UCS test specimens after the end of the curing period. The representative samples were air-dried at 25 °C to avoid chemical decomposition from heat exposure. Once dry, the samples were crushed into a fine powder using a

mortar and pestle. Next, the powder was spread evenly on a glass sample plate, followed by making the sample surface smooth and fitting to the sample plate's reference plane. The extra powder was removed with ethanol, and the glass sample plate was inserted inside the specimen holder for testing.

CHAPTER 5 : RESULTS AND DISCUSSION

5.1 Compaction Characteristics Results

5.1.1 Effects of RHA, Cement, and Basalt Fiber on Compaction Characteristics

The geotechnical properties of soil, such as shear strength, bearing capacity, permeability, and consolidation, highly depend on the moisture content and the compaction density. The results of moisture content (w) and dry density (ρ) for soil and the soil blends in this study are shown in Figure 30, emphasizing the maximum values for the optimum moisture content (w_{opt}) and the maximum dry density (ρ_{dmax}) for all the specified combinations under study. Generally, the optimum water content increased with an increased percentage of RHA, while the maximum dry density reduced with increased RHA dosage.

Additionally, the compaction curves did not pass the saturation line (S_r), establishing the correctness of the relationships between w_{opt} and ρ_{dmax}. It was evident from Figure 30 (a) that the w_{opt} increased from 24% (soil only) to 27% and 28% after adding RHA and RHA-cement to the expansive soil, respectively. Besides, adding basalt fibers filaments to the soil, RHA, and cement composite had minimal effects on the w_{opt}. It was also observed that increasing basalt fiber filament lengths in the soil composite had minimal influence on ρ_{dmax} for all three blends. For instance, w_{opt} was maintained at 29% for all combinations while ρ_{dmax} varied slightly with values 1.35 g/cm^3 for specimen S:5R:3C:1BF3 and 1.37 g/cm^3 for both S: 5R:3C:1BF6 and S:5R:3C:1BF12.

A similar trend was also observed for the 10% and 15% RHA composites. However, the w_{opt} increased with the increase in RHA percentage from 5 to 15% while the ρ_{dmax} reduced within the same range [Figures 30 (b) and (c)]. For instance, increasing RHA dosage from 5 to 10 to 15% increased the w_{opt} from 27 to 29 to 33% while the ρ_{dmax} reduced from 1.41 to 1.34 to 1.25 g/cm^3. A summary of the w_{opt} and ρ_{dmax} relationship is illustrated in Table 9.

Table 9 Relationship between w_{opt} and ρ_{dmax}

Combination Code	w_{opt} (%)	ρ_{dmax} (g/cm^3)
S-Control	23.98	1.45
S:5R	27.03	1.43
S:5R:3C	28.51	1.42
S:5R:3C:1BF	29.51	1.37
S:10R	29.02	1.36
S:10R:3C	30.99	1.34
S:10R:3C:1BF	31.59	1.31
S:15R	33.66	1.30
S:15R:3C	34.14	1.26
S:15R:3C:1BF	35.61	1.25

The increase in w_{opt} was attributed to; the high-water absorption rate of RHA due to its porous structure (Zhang et al., 1996), the additional porosity due to fiber interconnectivity, and water requirements due to the heat of hydration brought about by the cement. Also, the addition of cement and RHA led to volumetric changes in the structure of the aggregates during flocculation, leading to a significant increase in the void ratio hence the rise in moisture content (Basha et al., 2005).

Further, the maximum dry density (ρ_{dmax}) decreased due to the low specific gravities of RHA and cement compared to the soil (Ali et al., 1992; Jha and Gill, 2006). A decrease in the maximum dry density compared to the control specimen indicated that low compaction energy is needed; hence an economical compaction cost can be realized (Muntohar and Hantoro, 2000).

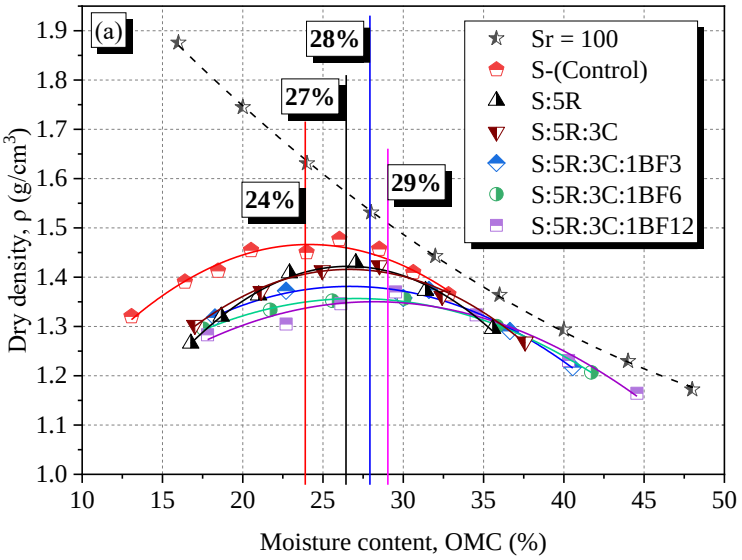

Figure 30 (a) Compaction curves for 5%RHA, 3%Cement and different lengths of Basalt Fibers (BF 3mm, BF 6mm and BF 12mm).

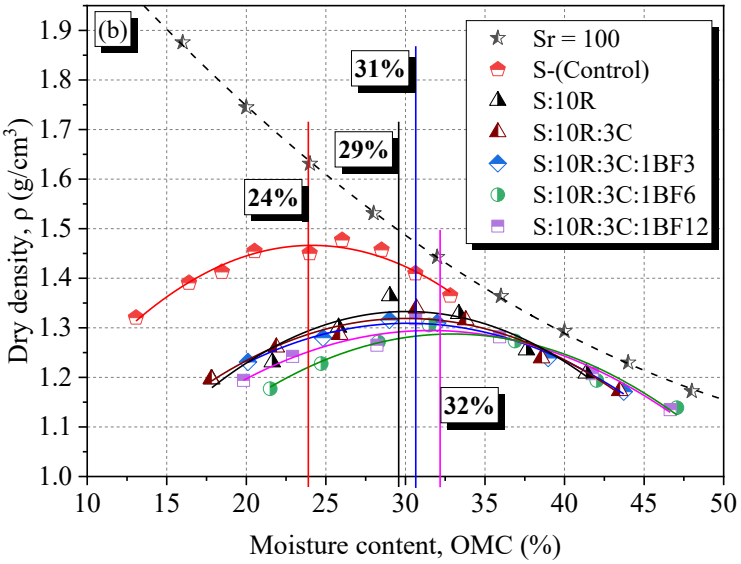

Figure 30 (b) Compaction curves for 10%RHA, 3%Cement and different lengths of Basalt Fibers (BF 3mm, BF 6mm and BF 12mm).

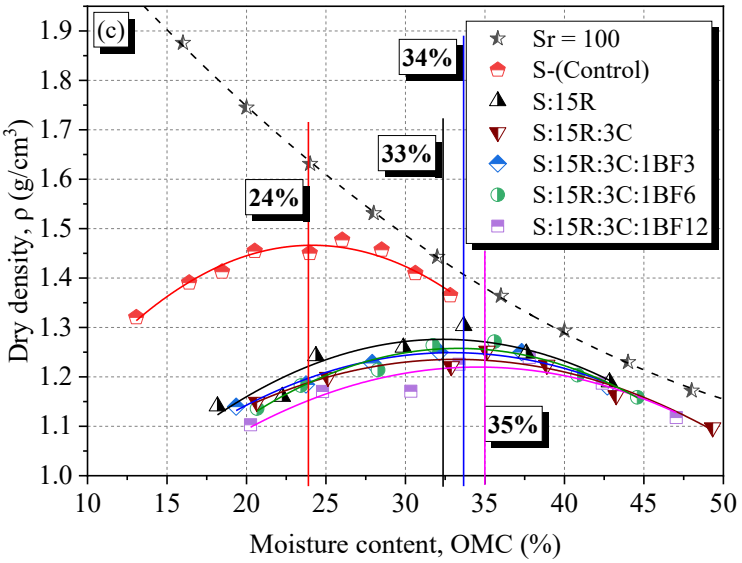

Figure 30 (c) Compaction curves for 15%RHA, 3%Cement and different lengths of Basalt Fibers (BF 3mm, BF 6mm and BF 12mm).

Figure 30 Compaction curves.

5.2 Consolidation Characteristics Results

In this section, the specimen states before and after consolidation were assessed. Subsequently, the influence of the additives on the one-dimensional consolidation coefficients and index properties was analyzed using the time-compression curves from the oedometer test. The curves were used to assess the yield stress (σ_y), Normalized compression curves, consolidation index(C_c), swelling index (C_s), and coefficient of consolidation (c_v). Followed by a series of equations applied to determine the coefficient of volume change (m_v) and the permeability coefficient (k) at pre-yield stress, yield stress, and post-yield stress phases. Furthermore, a correlation was analyzed between the one-dimensional consolidation coefficients with basalt fibers' length and the RHA-cement content. Microstructural analyses (SEM and XRD) quantified the structural modifications in the specimen upon consolidation, considering the soil composite structure, fiber reinforcement, and the porosity of the specimen combination schemes under study.

5.2.1 Consolidation Framework

In geotechnical engineering, chemically stabilized soils possess an artificial soil structure due to the hydration effect of cement and the pozzolanic reactions present (Horpibulsuk et al., 2004; Suebsuk et al., 2010; Du et al., 2014). Therefore, during the loading/reloading phase on such artificially structured soils, the compression index is low until the yield pressure (σ_y) is realized due to the resistances attributed to the soil structure. An ideal illustration of the consolidation behavior of soils is shown in Figure 31. Beyond this yield pressure (σ_y), compressibility is significantly increased due to the loss of soil structure, also known as destructuring (Kamruzzaman et al., 2009; Wang et al., 2013; Horpibulsuk et al., 2010). During destructuring, the additional void ratio (e_s) declines with the increasing effective vertical pressure(σ_v) due to the soil structure. Hence, with a further rise in σ_v, the compression curve of the artificially structured clay tends to meet the compression curve of

remolded/destructured clay, also known as the Intrinsic Compression Line (ICL) (Nagaraj et al., 1998; Burland, 1990).

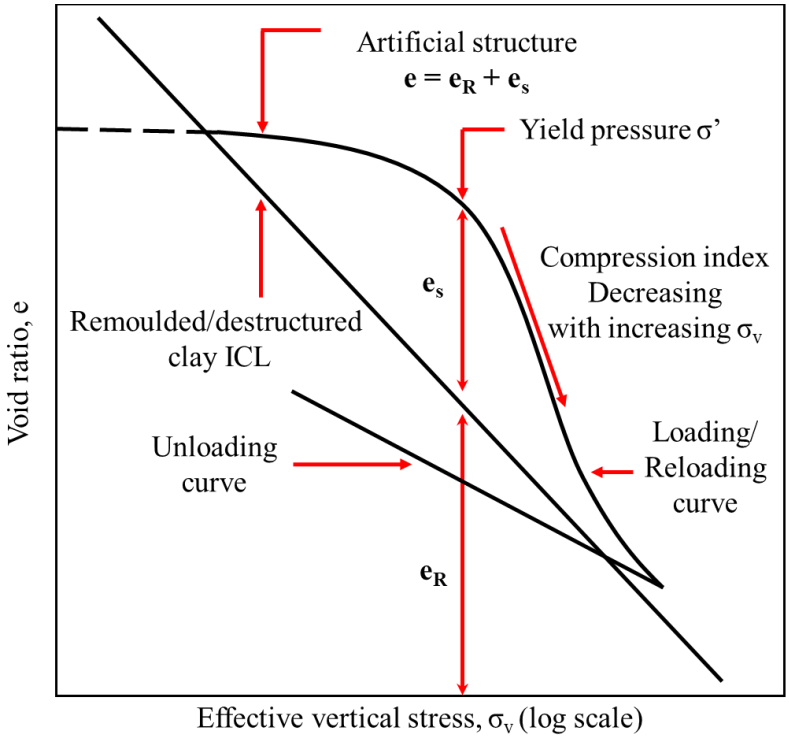

Figure 31 Consolidation behavior of soil. (modified from Du et al., 2014).

This variation in the void ratio can be expressed as:

$$e = e_R + e_s \quad (9)$$

Where e: represents the void ratio of the artificially structured soil, e_R: represents the void ratio of the remolded/destructured clay, and lastly, e_s: is the additional void ratio attributed to the soil structure destruction (Liu and Carter, 1999). Burland et al., 1998 suggested the ICL as a reference point for interpreting the responses of all artificially structured clays when the effective stresses were between 10kPa and 4000kPa in all testing conditions. The ICL was plotted in terms of void ratio (e) given by Equations 10 and 11 versus the log of the effective vertical pressure, log σ_v.

$$e = I_v C_c^* + e^*100 \quad (10)$$

$$I_v = 2.45 - 1.285 \log \sigma_v + 0.179 \log \sigma_v^3 \quad (11)$$

Where; C_c* is the intrinsic compression index defined by the difference between the void ratio of the remolded clay at 100kPa (e*100) and 1000kPa (e*1000) and I_v: the intrinsic void index. It was resolved that, for normally consolidated clay, the position of consolidation curves to the ICL line depended on the structural composition of the clay soil (Burland et al., 1998). In addition, Hong et al., 2010 found that when the stress levels were higher than the yield pressure of the remolded/reconstituted soil, the compression curves of remolded/ reconstituted clay normalized well with the ICL. The validity of this consolidation framework was illustrated in this study for the proposed reconstituted clay soil composite, as will be discussed in this Chapter.

5.2.2 Specimen Conditions Before and After Consolidation ($w_{initial}$, w_{final}, e, ρ_{wet} and S_r)

The initial condition of the stabilized soil specimen before consolidation is essential for selecting the appropriate consolidation pressure and duration. The soil's initial properties, such as moisture content, degree of compaction, and wet density, can significantly affect its response to consolidation. If these conditions are not accurately determined, it can result in erroneous test results, leading to incorrect conclusions about the soil's strength and stability. Figure 32 and Table 10 represent the specimen conditions and descriptive statistics of the specimen conditions, respectively. Equations 12, 13, 14, and 15 were used to calculate the initial (w_i) and final water content (w_f), void ratio (e), wet density (ρ_t), and saturation levels (S_{ro}) of the 16 specimen combinations.

$$w_i \text{ or } w_f = \frac{m_i - m_s}{m_s} \text{ x } 100 \quad (12)$$

$$e = \frac{H_i}{H_s} - 1 \; ; \; H_s = \frac{m_s}{\rho_s \pi D^2/4} \quad (13)$$

$$\rho_t = \frac{m_i}{(AH_i)} \; ; \; A = \pi D^2/4 \quad (14)$$

$$S_{ro} = \frac{w_o \rho_s}{e_o \rho_w} - 1 \quad (15)$$

Where; w_i: initial moisture content (%), w_f: final moisture content (%), m_i: initial specimen mass (g), m_s: specimen oven-dry mass (g), H_i: initial specimen height (cm), H_s: actual specimen height (cm), A: cross-sectional area of the specimen (cm^2), D: specimen diameter (cm), ρ_s: density of soil particles (g/cm^3), ρ_w: density of water (g/cm^3).

The initial states ($w_{initial}$ and ρ_{wet}) were evaluated in this study to justify the accuracy of the specimen preparation procedures. They can be used to validate the authenticity of the results.

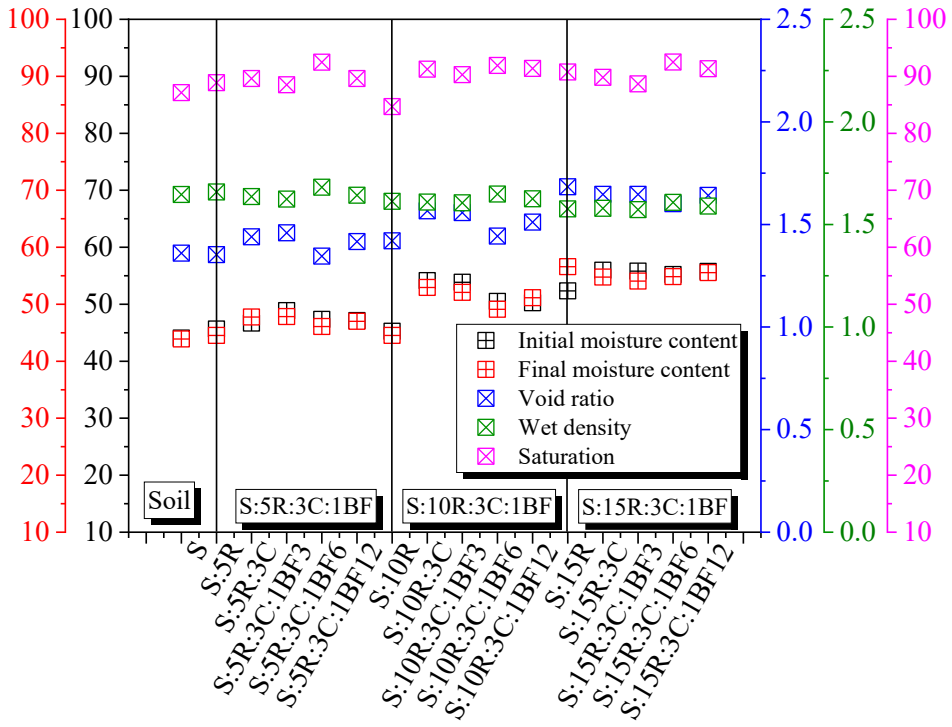

Figure 32 Specimen conditions before and after consolidation.

Table 10 Descriptive statistics of the specimen conditions in Figure 32

Item	Units	Total number of specimen	Mean	Standard deviation	Coefficient of variation	Minimum	Maximum
Initial Moisture content, w_i	%	16	50.8778	4.1284	0.0811	44.0532	55.8053

Final moisture content, w_f	%	16	50.1627	3.9918	0.0795	43.8949	55.5363
Void ratio, e		16	1.49832	0.1108	0.0740	1.34564	1.64647
Wet density	g/cm^3	16	1.62405	0.0320	0.0197	1.57189	1.68152
Saturation	%	16	90.3745	1.8417	0.0203	87.1351	92.4881

The mean saturation level of the prepared specimen was 90%, while the mean void ratio and wet density were 1.49 and 1.62 g/cm^3, respectively. The final conditions, such as the final moisture content and void ratio, can be compared with the initial conditions to determine the effectiveness of the stabilization process. Moreover, the final conditions can be used to estimate the long-term behavior of the stabilized soil, such as its settlement and creep properties, which are essential for designing structures that can withstand long-term loading and environmental effects. The void ratio, wet density, and saturation standard deviations were kept to minimum values of 0.11, 0.03, and 1.84, respectively, justifying close standardization in specimen conditions before testing. However, to achieve the standardized values, it was requisite to adjust the amount of water during specimen preparation to compensate for the high water affinity of RHA, as demonstrated by the compaction curves in a related study (Owino et al., 2022a). Hence the standard deviation values of 4.12 and 3.99 for initial and final moisture contents, respectively. It is also noteworthy that increasing the RHA content from 0% to 15% contributed to a slight increase in the void ratios of the specimen due to the porous morphology of the RHA particles (Chen et al., 2021).

5.2.3 Time-Compression Curves (t vs. Δh)

According to the theory of one-dimensional consolidation, soil undergoes a time-dependent displacement/deformation when acted upon by an external load. These deformations can lead to the draining of excess pore water pressure due to the gradual transition of the applied loads from the

pore water to the soil particles under steady pressure. The notable assumptions in this theory include; (1) soil is linearly elastic, (2) soil grains and water are incompressible, (3) the load is applied in the vertical direction only, (4) the drainage of the pore water is one-dimensional in the direction of the load, (5) the coefficient of consolidation, the coefficient of volume change and the permeability coefficients are constant, (6) the time lag of consolidation is dependent on the low permeability of expansive soils (Yuan-qiang et al., 2004; Terzaghi, 1943).

Based on this theory, the time-displacement plots of all 16 specimen combinations for the load increments in the present study are shown in Figure 33 (a)-(g). Figure 33 (a) shows no clear distinction between the primary and secondary consolidation phases at low compression pressures for basalt fiber unreinforced and reinforced specimens. However, as the consolidation pressures increased, a clear contrast between the primary and secondary consolidation phases in the time-displacement curves was evident, owing to the generated exponential curve forms (Figure 33 (b)-(g)).

At high consolidation pressures of 1256 kPa [(Figure 33 (g)], the soil particles are pushed closer together, reducing the void space or porosity between them. This reduction in porosity leads to a decrease in compressibility and an increase in the consolidation rate. As a result, the time compression curves shift to the left, indicating faster consolidation.

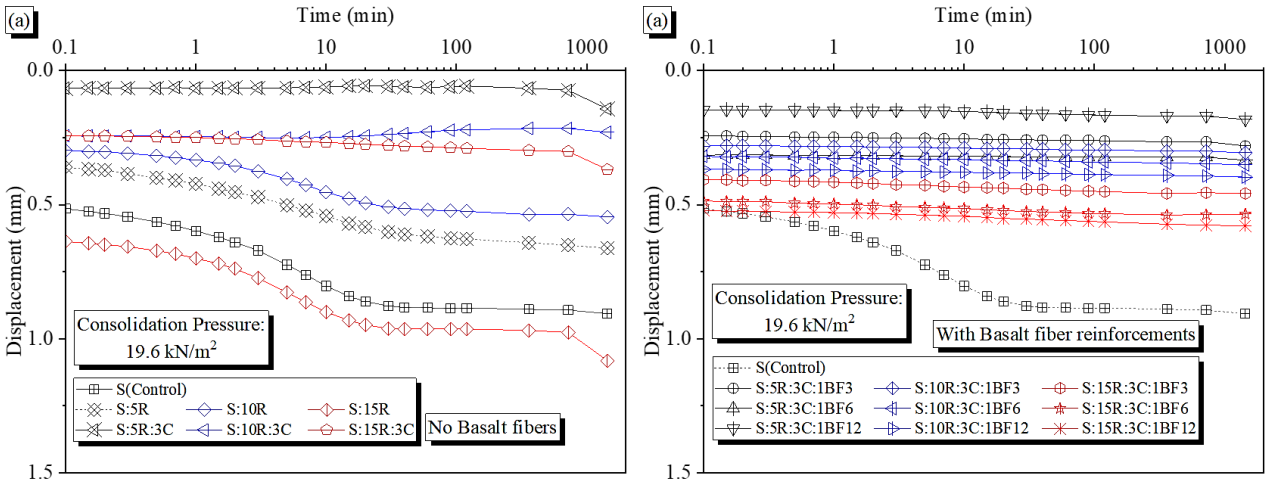

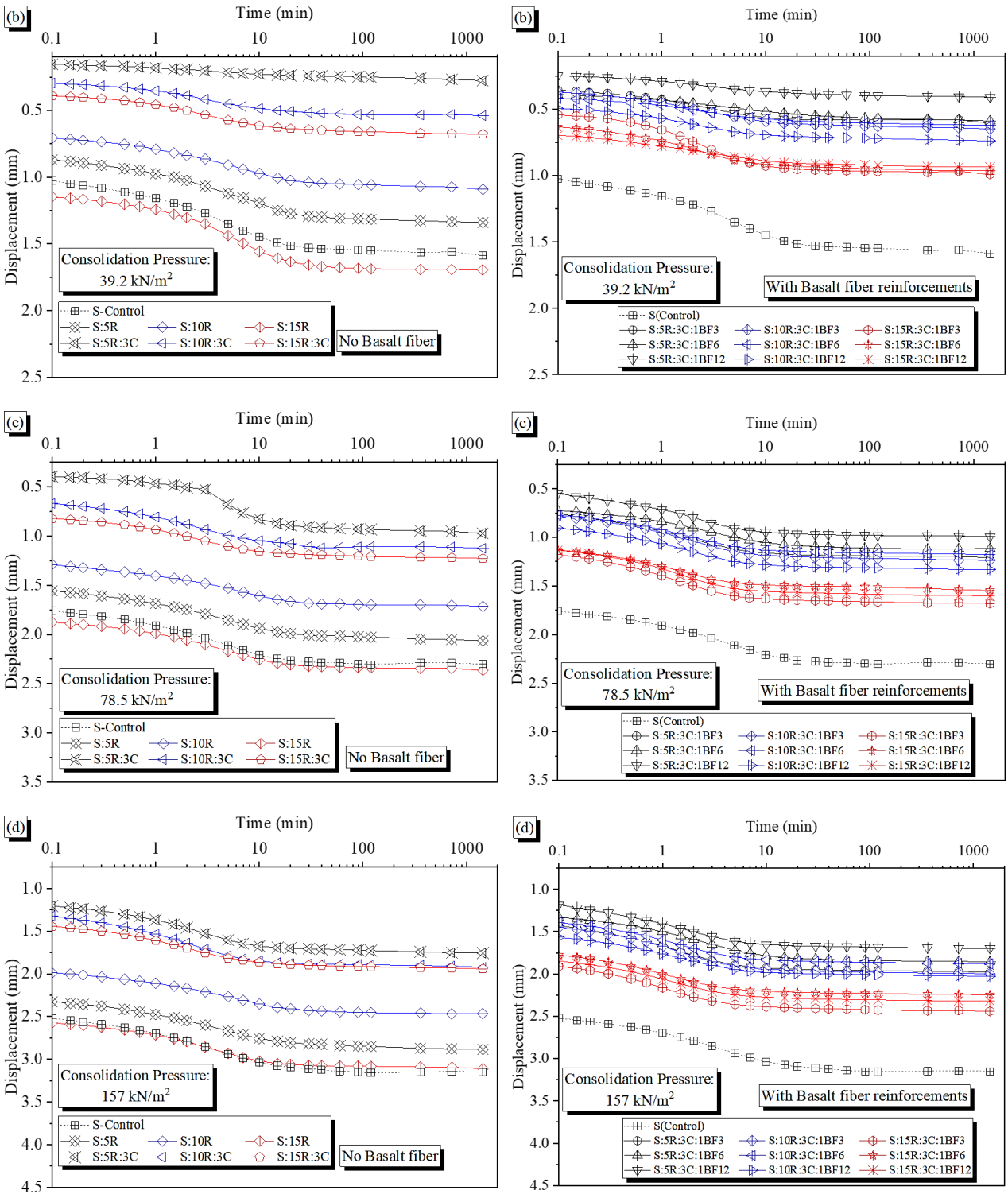

The increase in consolidation pressure also increases the soil's stiffness, as the particles are more tightly packed together. This increase in stiffness results in a steeper slope of the time compression curve, indicating that the soil requires more force to compress it to a given deformation.

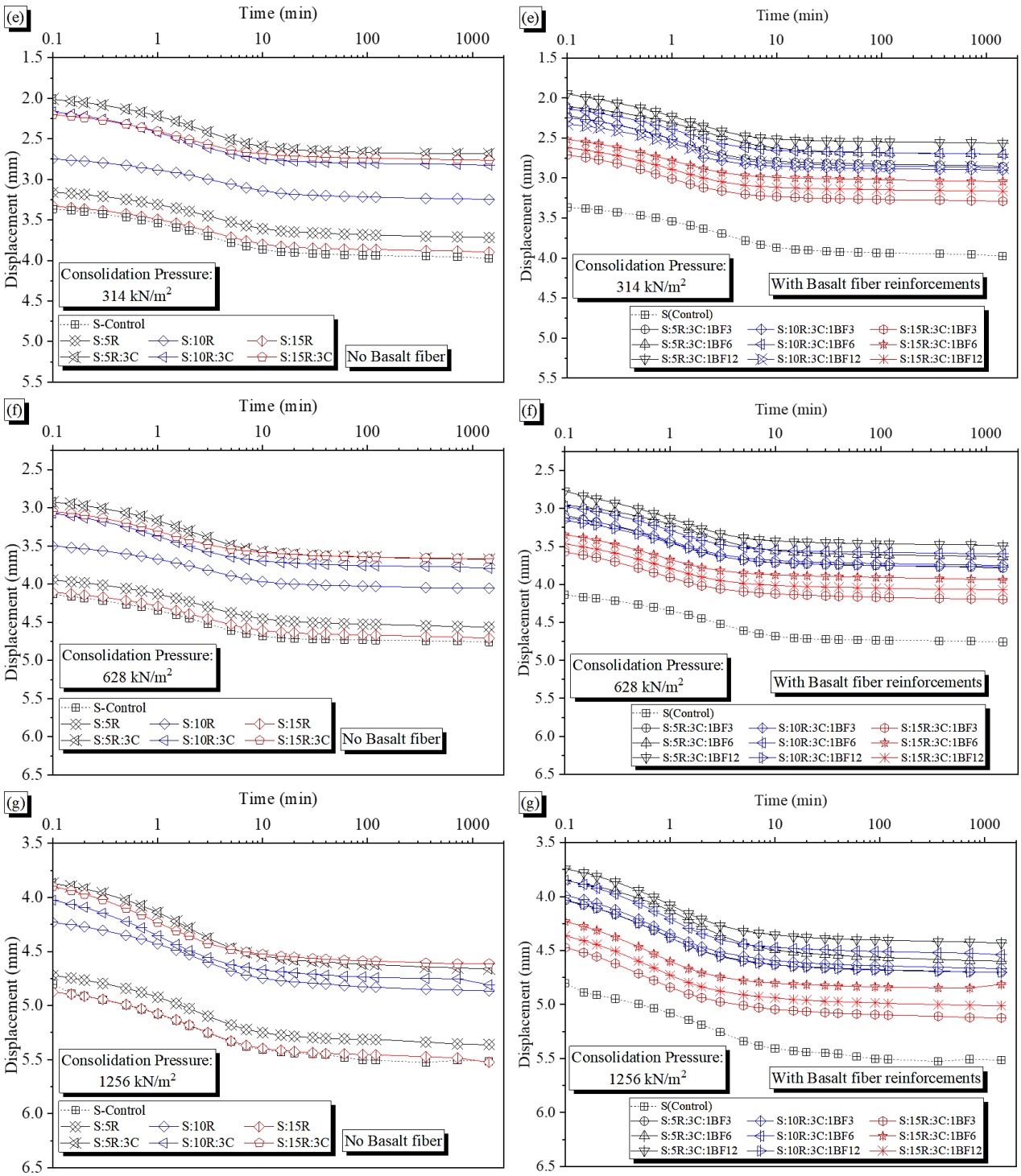

Figure 33 (a-g) Time-displacement curves.

From these plots, the time T_{50} required to reach 50% primary consolidation was evaluated by defining the 0% primary consolidation stage from the early portion of the curve and the 100% primary consolidation stage from the point of intersection between primary and secondary

consolidation segments using the logarithm of time method (Casagrande and Fadum, 1940). It was noteworthy that the time T_{50} was highly dependent on the RHA-cement content, as illustrated in Figure 34. Increasing the RHA content from 5% to 15% decreased the time required to achieve a certain degree of consolidation under the same effective stress. Similar results were also recorded by Jain and Puri (2013).

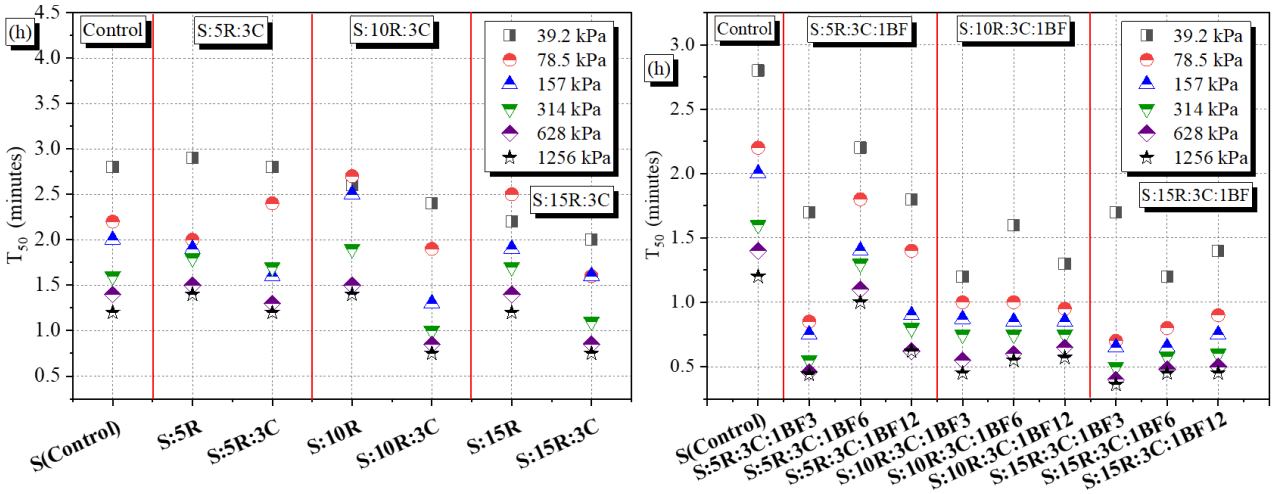

Figure 34 Relationship between T_{50} and specimen combinations schemes.

It was also apparent that for basalt fiber reinforced and RHA-Cement stabilized expansive soils; the T_{50} reduced significantly with increased consolidation pressure. This decrease prompted a uniform secondary consolidation phase, preventing structural failures from prolonged primary consolidation. Moreover, adding different lengths of basalt fibers significantly reduced the T_{50} values compared to the control specimen (S), constituting only soil.

5.2.4 Compression Curves (e vs. σ, σ_y)

One of the primary outputs of the Oedometer test is the compression curve. This curve represents the relationship between the applied stress and the resulting strain of the soil sample over time. The compression curve can be used to determine the compression index, which is a measure of the compressibility of the soil. The void ratio (e) versus effective vertical pressure (log σ_v) compression curves for the reconstituted soil specimens at 5, 10, and 15% RHA contents and those including 3%

cement are shown in Figure 35 (a), Figure 35 (b), and Figure 35 (c), respectively. The influence of varying the basalt fiber length from 3mm to 6mm to 12mm was also shown in each RHA content. In all the figures presented in this study, the symbol S denoted soil, *i*R specified a specimen with an RHA content of *i*%; *i*C showed cement content of *i*%, while BF*i* indicated a specimen with basalt fiber length *i*mm. It can be seen from Figures 35 (a), 35 (b), and 35 (c) that the compression curves of all S*i*R*i*CBF*i* reconstituted soil specimens lay above that of the corresponding soil specimen and showed a typical concave shape due to the effects of soil-structure (Hong et al., 2010; 2012). When the effective vertical pressure (σ_v) was lower than the yield pressure (σ_y), slight compressibility was realized due to the resistances initiated by the soil structure (Leroueil and Vaughan, 1990). After the yield pressure, the compressibility of the reconstituted and stabilized soils increased significantly due to the gradual collapse of the soil structure at higher effective vertical pressure levels.

Meanwhile, it was noteworthy that the relationship between the void ratios and the effective vertical pressure was highly dependent on the length of basalt fiber, RHA content, and cement content, with higher void ratios in the S:15R:3C:1BF specimens. Noticeably, the void ratio decreased as the effective vertical pressure increased for all instances. The yield pressure (σ_y) can be estimated from these plots using the Casagrande method (Casagrande, 1936).

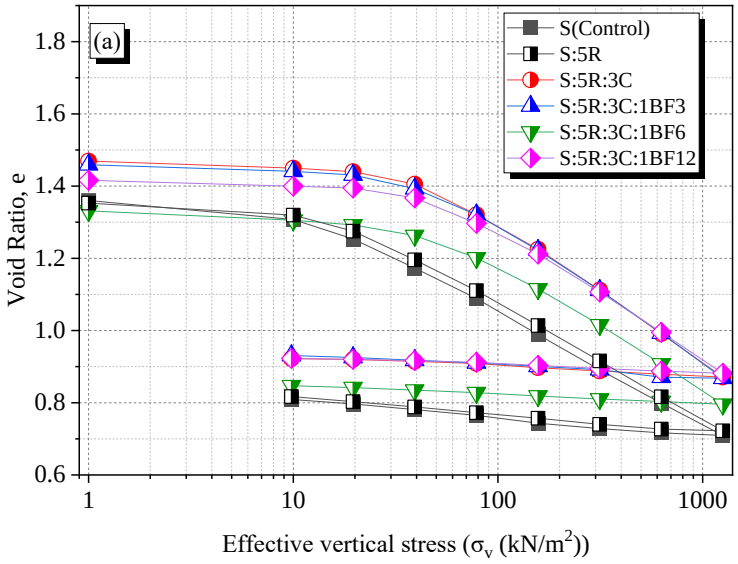

Figure 35 (a) Compression curves for S(Control), 5%RHA, 3%Cement and different lengths of Basalt Fibers (BF 3mm, BF 6mm and BF 12mm).

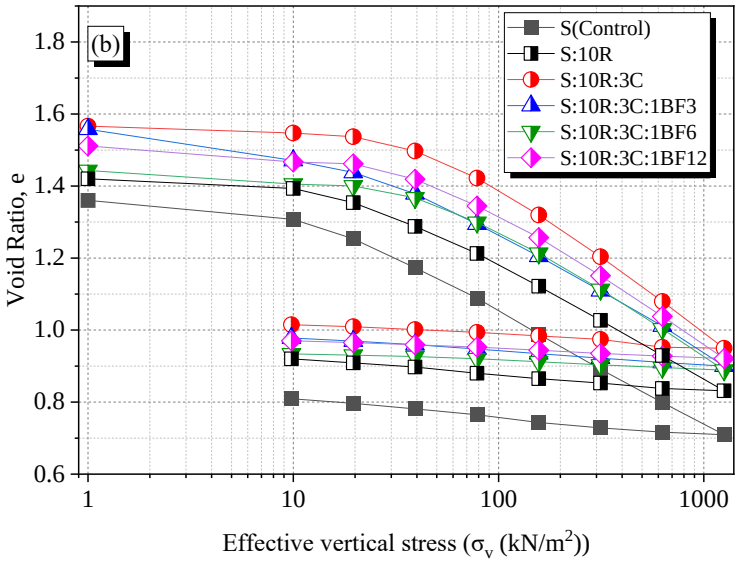

Figure 35 (b) Compression curves for S(Control), 10%RHA, 3%Cement and different lengths of Basalt Fibers (BF 3mm, BF 6mm and BF 12mm).

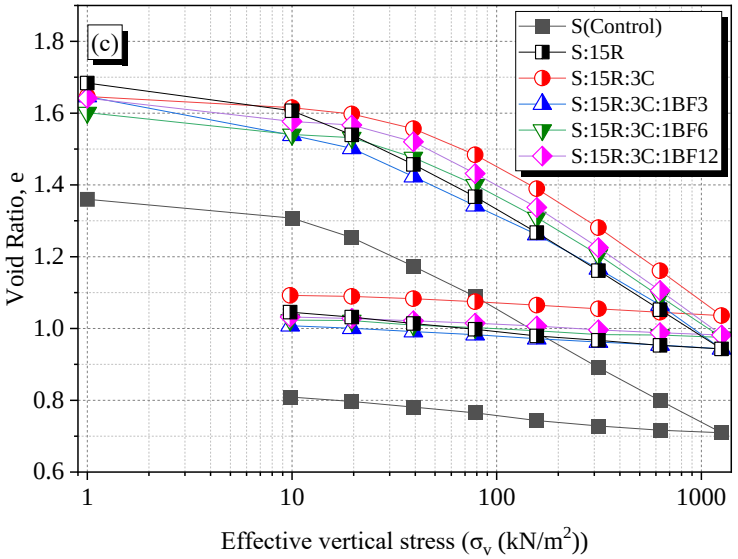

Figure 35 (c) Compression curves for S(Control), 15%RHA, 3%Cement and different lengths of Basalt Fibers (BF 3mm, BF 6mm and BF 12mm).

Figure 35 Compression curve for unreinforced and basalt fiber reinforced soil for **(a)** 5%RHA:3C specimen, **(b)** 10%RHA:3C specimen, and **(c)** 15%RHA:3C specimen

From the compression curves in Figure 35, the yield pressures (σ_y) for all the specimen combinations under study were evaluated and presented in Figure 36. The yield pressure is the pressure at which plastic deformation first occurs in the specified specimen. This σ_y can be determined from the oedometer test by identifying the point on the pressure-void ratio curve where the slope of the curve starts to decrease. Notably, the specimen containing 5%RHA attained the highest values of yield pressures, and the values were reduced with increasing RHA content. The Relationship between yield pressure (σ_y) and various lengths of basalt fiber is shown in Figure 37. It can be observed that

increasing the length of basalt fibers from 0mm to 12mm improved the yield pressure of the reconstituted soil composite for all the RHA-Cement mix ratios. The random fiber inclusion and the orientation of basalt fibers increased the specimen's stiffness hence improving the yield pressure (σ_y). From this phenomenon, it can be concluded that the random inclusion of high tensile strength fibers enhanced the mechanical interaction between the fibers and the surrounding reconstituted soil composite through an anchoring effect and was more significant as the length of basalt fibers increased from 0mm to 12 mm.

Furthermore, the increment in yield pressure was due to the resistance to compression pressures initiated by the pozzolanic reaction in the soil structure. For example, at low RHA contents of 5%, there was a significant improvement in reconstituted soil structure due to the complete utilization of RHA and cement during the pozzolanic reactions. This structural development and basalt fiber reinforcements formed a highly compact reconstituted soil structure. On the other hand, increasing the RHA content to 10% and 15% led to excess RHA within the reconstituted soil composite, producing a more compressible reinforced and stabilized soil composite structure.

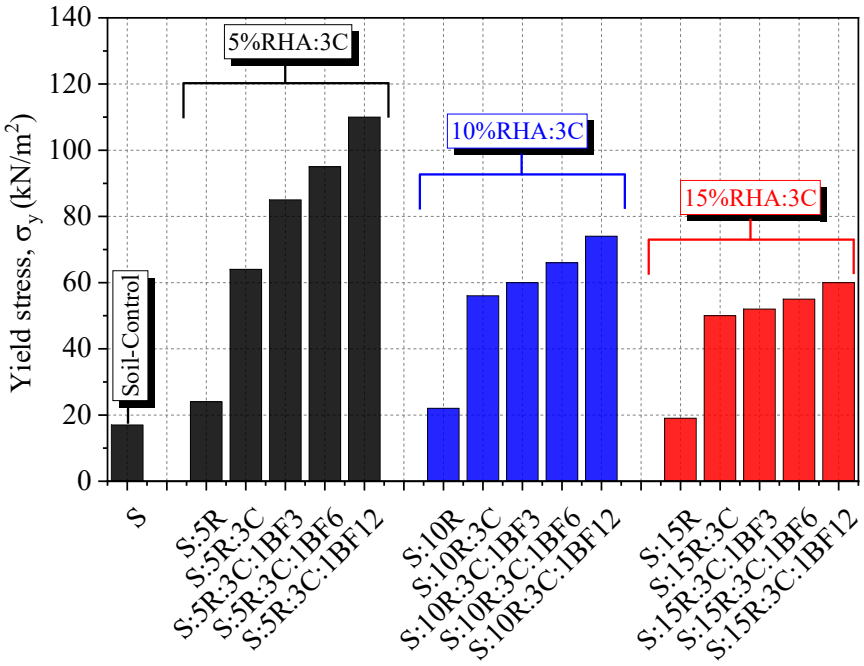

Figure 36 Relationship between yield pressure (σ_y) and specimen composition.

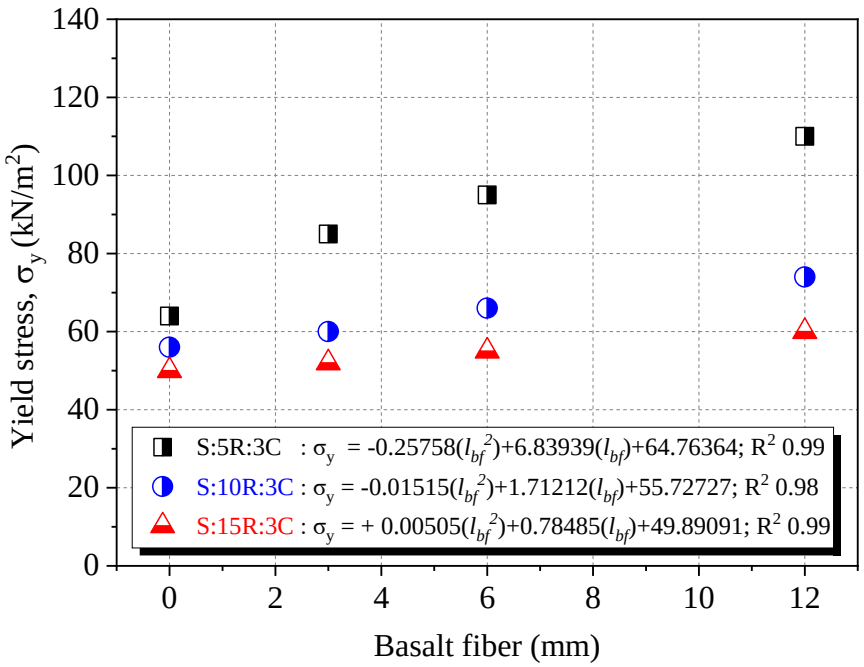

Figure 37 Relationship between yield pressure (σ_y) and basalt fiber length (l_{bf}).

5.2.5 Normalized Compression Curve (I_v vs. σ_v)

Burland (1990) introduced the normalizing void index (I_v) to correlate the compression curves of various remolded clay with the initial water contents ranging between 0.6 to 4.5 times the liquid limit. This correlation reported that the compression curves normalized well with the void index of reconstituted clays at initial water contents 1.0–1.5 times the liquid limits. Therefore, a unique line named the ICL was suggested to express the normalized compression curve in terms of the void index versus effective vertical pressures. The Intrinsic Compression Line (ICL) is a straight line that represents the compressibility characteristics of soil. It is obtained by plotting the normalized void ratio versus the logarithm of the normalized effective stress and then drawing a straight line through the compression data points. The intercept of the ICL with the vertical axis represents the natural void ratio (e_0), which is the void ratio of the soil when it is fully saturated and not subject to any external forces. The normalized compression curves of reconstituted soil composites for S, S:5R, S:5R:3C, S:5R:3C:1BF, and S:10R:3C:1BF specimens are shown in Figure 38 (a) and 38 (b), respectively, calculated using Equation 11.

Despite the discrepancy in stabilization extent and basalt fiber lengths in the specimens, the compression curves of the reconstituted soil composite normalized perfectly with the ICL after the yield pressure phase, as suggested by Hong et al., 2010. The perfect normalization illustrated the presence of significant bonding in the new stabilized soil composite (Bulrand et al., 1996). In addition, the higher effective vertical pressures (ranging from 100-1200kN/m^2) accelerated the rearrangement of the soil-RHA and soil-RHA-cement particles and the basalt fibers relative to each other, resulting in a compact reconstituted soil structure.

On the other hand, the normalized curves for S:15R:3C:BF6 and S:15R:3C:BF12 were positioned below the ICL at vertical pressures above 100kN/m^2 due to high RHA content in the reconstituted clay soil, as illustrated in Figure 38 (c). The inadequate pozzolanic reactions led to unsubstantial bonding between the specimen structure (caused by the accumulation of excess RHA in the specimen structure and basalt fiber interfacial contacts), leading to rapid destructuring in the soil at high loading pressures. Overall, the normalized compression curves (NCC), intrinsic compression curve (ICL), and intrinsic void ratio (I_v) are all essential tools for understanding the compressibility and densification behavior of soil, which can be helpful in geotechnical engineering applications such as foundation design and slope stability analysis.

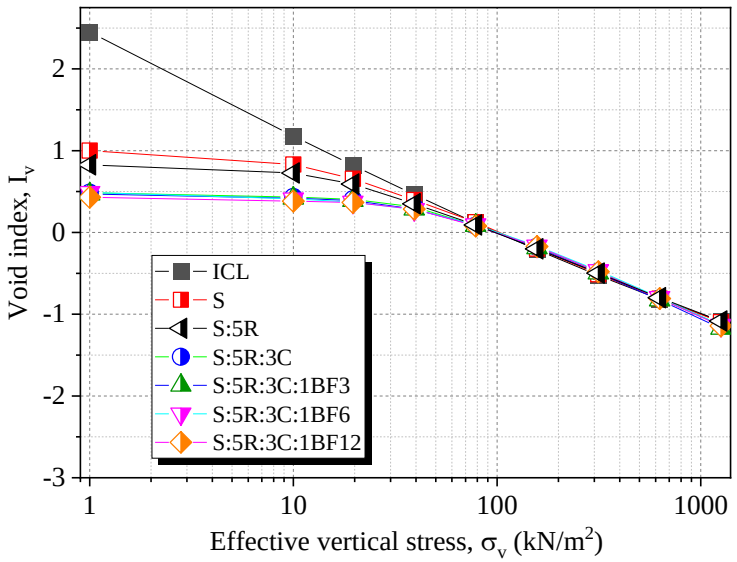

Figure 38 (a) Normalized compression curves for S(Control), 5%RHA, 3%Cement and different lengths of Basalt Fibers (BF 3mm, BF 6mm and BF 12mm) with reference to the ICL

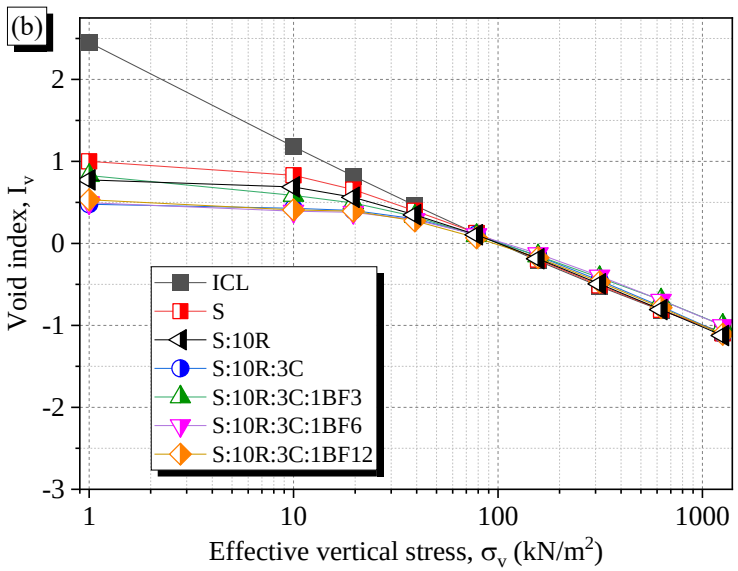

Figure 38 (b) Normalized compression curves for S(Control), 10%RHA, 3%Cement and different lengths of Basalt Fibers (BF 3mm, BF 6mm and BF 12mm) with reference to the ICL.

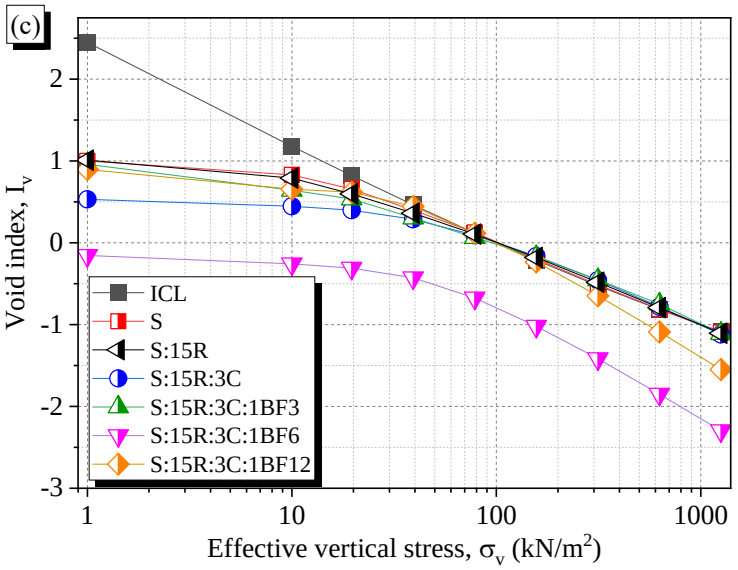

Figure 38 (c) Normalized compression curves for S(Control), 15%RHA, 3%Cement and different lengths of Basalt Fibers (BF 3mm, BF 6mm and BF 12mm) with reference to the ICL.

Figure 38 Normalized compression curves for unreinforced and basalt fiber reinforced soil for **(a)** 5%RHA:3C specimen, **(b)** 10%RHA:3C specimen, and **(c)** 15%RHA:3C specimen.

5.2.6 Compression Index, C_c

The compression index (C_c) is a fundamental parameter in determining the one-dimensional consolidation settlement of reconstituted clays. The greater the C_c value, the higher the chances of one-dimensional consolidation. The index was calculated from the normal consolidation phase (Loading phase) of the compression curves due to the elastic behavior of the soil. The compression index can be easily obtained by extending the straight-line portion of the normal consolidation region of the compression curves in Figures 35 (a), 35 (b), and 35 (c). Then, taking the difference in the

void ratio (e) divided by the change in effective vertical pressure (σ_v) in the log scale as shown in Equation 16.

$$C_c \text{or } C_s = \frac{e_a - e_b}{\log(\sigma_b^1 - \sigma_a^1} \quad (16)$$

In this study, the C_c value was influenced mainly by the lengths of the basalt fiber included in the reconstituted soil composite for a given soil-RHA-cement content, as shown in Figure 39. The specimen without basalt fibers showed C_c values ranging between 0.39 and 0.41 as the RHA content increased from 5% to 15%. Specifically, higher C_c values were recorded in the soil-RHA-Cement specimen, indicating high compressibility, meaning it will experience significant deformation under applied stress. In civil and geotechnical engineering practice predicting the deformation of soils with a high compression index can be challenging due to the considerable volume change that can occur under stress. This change can make it difficult to accurately estimate the amount of settlement that will occur under loading. Therefore additional reinforcements are necessary to enhance the compressibility of such cement-stabilized soils.

Adding basalt fiber into the reconstituted soil composite reduced the compression index values by approximately 16% to values between 0.329 - 0.351; 0.33-0.345; 0.35-0.37 for basalt fiber lengths 3mm, 6mm, 12mm, respectively. A comparable reduction in compression index values when fibers are supplemented into a soil composite was noted by Kar and Pradhan (2011). It is also apparent from Figure 39 that the degree of compression was dependent on the length of basalt fibers in the specimen. For example, an increase in basalt fiber length from 3mm to 6mm gives an insignificant rise in compression index compared to the notable development at 12mm. Moreover, it is noteworthy that compression index values are kept to an average value of 0.3 for the 5% RHA-3% cement specimen, and a nominal increase is achieved as the RHA content rises to 10% and 15%-3% cement. This nominal increase in the compression index was due to the mobilized rearrangement of the

particles in the reconstituted soil composite due to the additional porosity formed by the excess RHA in the soil-RHA-cement composite. Moreover, the relationship between the C_c and the length of basalt fiber was further evaluated using the curve fitting method and presented in equation forms, as shown in Figure 40.

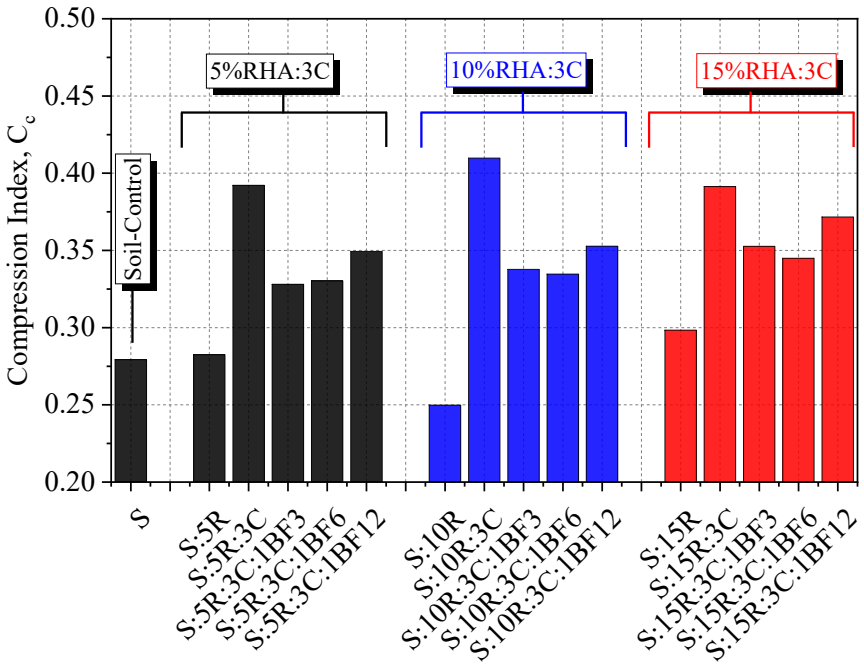

Figure 39 Relationship between compression index (C_c) and specimen composition.

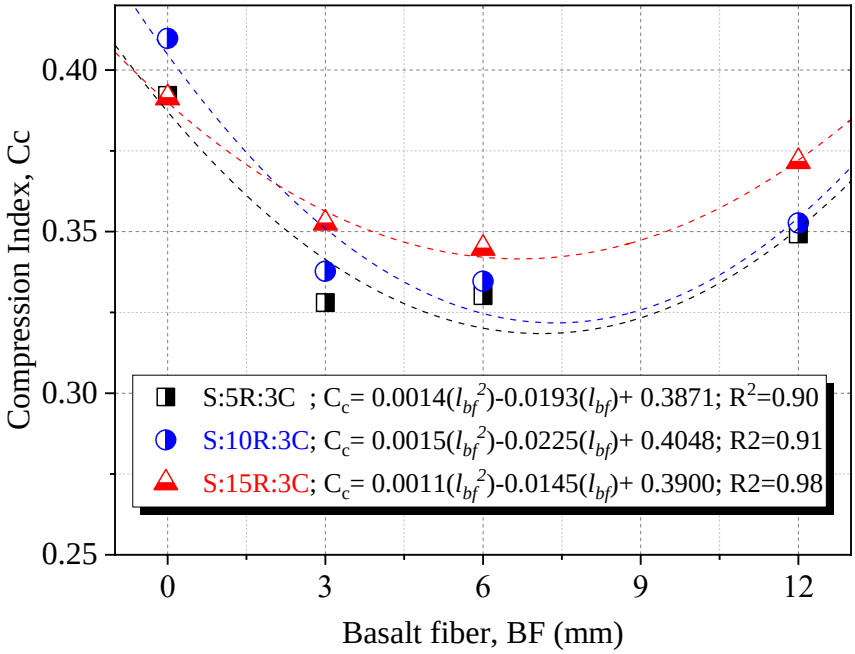

Figure 40 Compression index C_c versus length of basalt fibers.

5.2.7 Swelling Index, C_s

Expansive clay soils have great swelling potential due to the dominant clay minerals that change volume when moisture changes ensue. Using fibers to solve this swelling problem has recently gained research attention (Kar and Pradhan, 2011; Babu et al., 2008; Malekzadeh and Bilsel, 2012). In this study, the dimensional influence of basalt fiber to curb the swelling of reconstituted clay soils stabilized by RHA and minimal dosages of cement was presented as shown in Fig. 41 using Equation 16 and the unloading compression curves in Figures 35 (a), 35 (b), and 35 (c).

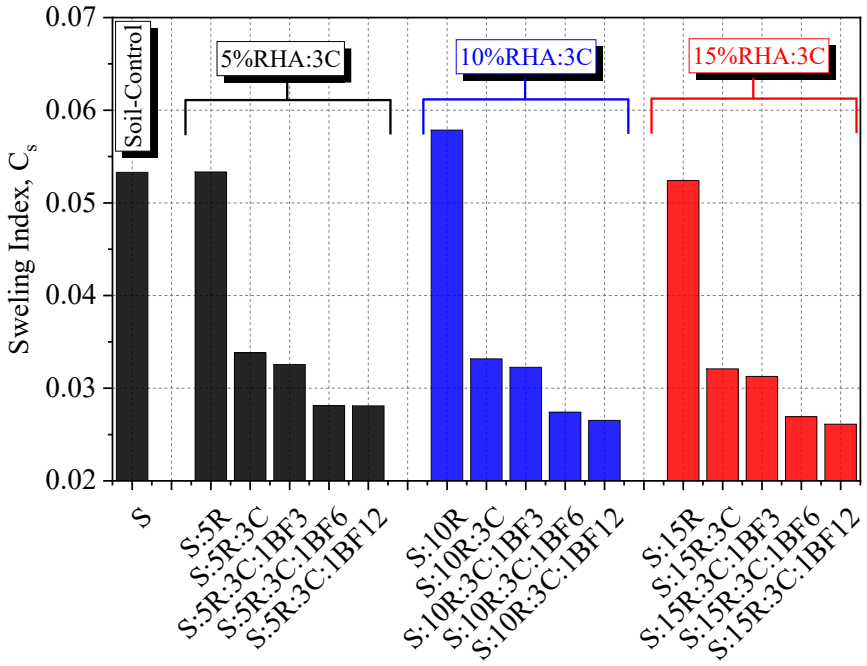

Figure 41 Relationship between swelling index (C_s) and specimen composition.

The reconstituted soil composite without basalt fibers depicted high swelling indexes due to the absence of particle anchorage mechanism brought about by the fiber reinforcements. Additionally, it was concluded that the high swelling indexes experienced by the S:RHA specimens (0.053 to 0.058) were mainly due to the high water affinity of the hollow RHA microstructure hence the rapid volume changes during the unloading phase. However, upon basalt fiber addition, the swelling index of the 5% RHA-3% cement reconstituted soil specimen reduced from 0.0339 (for BF3mm) to 0.028 (for BF12mm), and a similar trend was observed for 10% and 15% RHA specimens as illustrated in

Figure 41. Also, it was evident that longer fibers (BF12mm) substantially reduced the swelling index. For instance, reconstituted soil composites with 3mm basalt fibers had a swelling index of 0.0326, 0.0322, and 0.0312 for 5%, 10%, and 15% RHA, respectively. In comparison, reconstituted soil specimens with 12mm basalt fibers attained 0.028, 0.0265, and 0.0261 for 5%, 10%, and 15% RHA, respectively. The intensity of fiber interaction within the specimen arrested the interparticle movements hence the reduced swelling potential during the unloading phase compared to the specimen without fibers.

Furthermore, basalt fiber reinforcements' influence on the swell index was more significant at higher rice husk ash content. The high RHA contents mixed with nominal cement dosages produced a low-plastic material with a high water absorption rate. Hence, the swelling index decreased with increased rice husk ash content (Muntohar, 2002; Eberemu et al., 2016). Ultimately, the relationship between the C_s and the length of basalt fiber was evaluated using the curve fitting method and presented in equation forms, as shown in Figure 42, to help design engines predict the C_s projections for basalt fibers ranging between 0mm and 12mm.

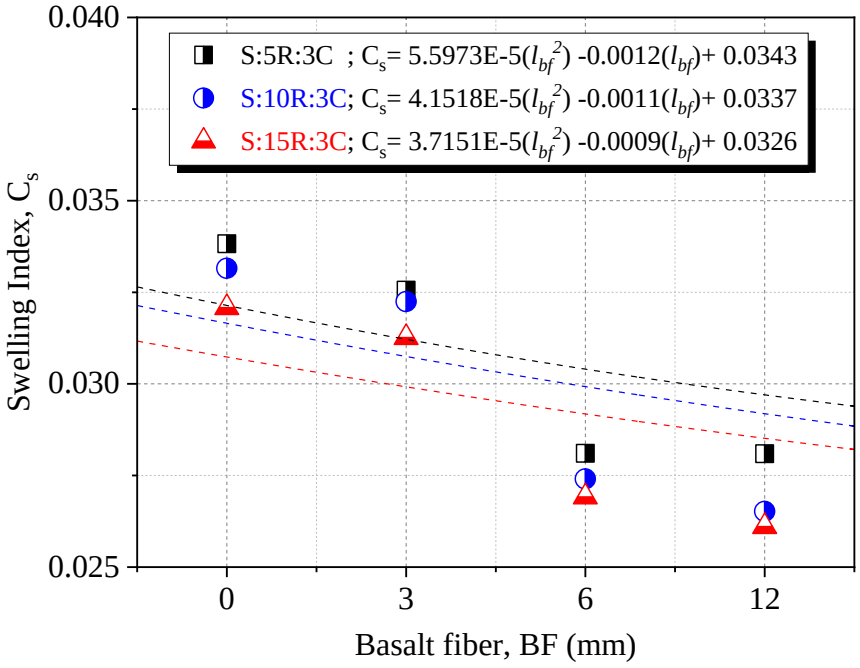

Figure 42 Swelling index C_c versus length of basalt fibers.

5.2.8 Assessment of Compression Curves (C_c vs. σ_y)

The compression curve can be assessed in terms of the compressive index (a measure of the compressibility of soil) and the yield pressure (defined as the pressure required to achieve a specific strain in the soil). The yield pressure is an essential parameter in the design of all engineering structures as it calculates the safe bearing capacity of soil and the required depth of foundations. The test results in this study demonstrate that the compressibility of clay soils reinforced with basalt fiber and stabilized with RHA and cement can be determined by three parameters: length of basalt fibers (l_{bf}), yield pressure (σ_y), and RHA-cement content (%). It is also evident that the compressibility rate is directly related to the degree of bonding as reflected by the yield pressure (σ_y) (Horpibulsuk et al., 2004; Du et al., 2014). This study attributed this bonding phenomenon to the pozzolanic reactions (between soil, RHA, and cement) and basalt fiber reinforcements. For example, considering the S:5R:3C:1BF12 specimen, the yield stresses increase to 110kN/m^2, reducing the compressive index from 0.392 to 0.35, as shown in Figure 43 (a). Also, a reduction in compression index as yield pressure increased was observed for S:10R:3C:1BF12 and S:15R:3C:1BF12 with values of 0.354 and 0.37, respectively. The curve fitting equations illustrating the relationship between the compressive index (C_c) and yield pressure (σ_y), based on the experimental data of clay soils reinforced with different lengths of basalt fibers (3mm to 12mm) and stabilized with RHA-cement mixtures, is therefore expressed as follows:

$$C_c = 0.00007\ \sigma_y^2 - 0.0147\ \sigma_y + 1.008;\ \text{for S:5R:3C:}i\text{BF composites} \quad (17)$$

$$C_c = 0.00066\ \sigma_y^2 - 0.0890\ \sigma_y + 3.301;\ \text{for S:10R:3C:}i\text{BF composites} \quad (18)$$

$$C_c = 0.00159\ \sigma_y^2 - 0.1768\ \sigma_y + 5.245;\ \text{for S:15R:3C:}i\text{BF composites} \quad (19)$$

Where: C_c is the compression index, and σ_y is the reconstituted soil composite yield pressure. The correlation coefficients (R^2) of the yield pressure versus the compression index showed high reliability of the test data, as illustrated in Figures 43 (a) [0.99], 43 (b) [0.86], and 43 (c) [0.94].

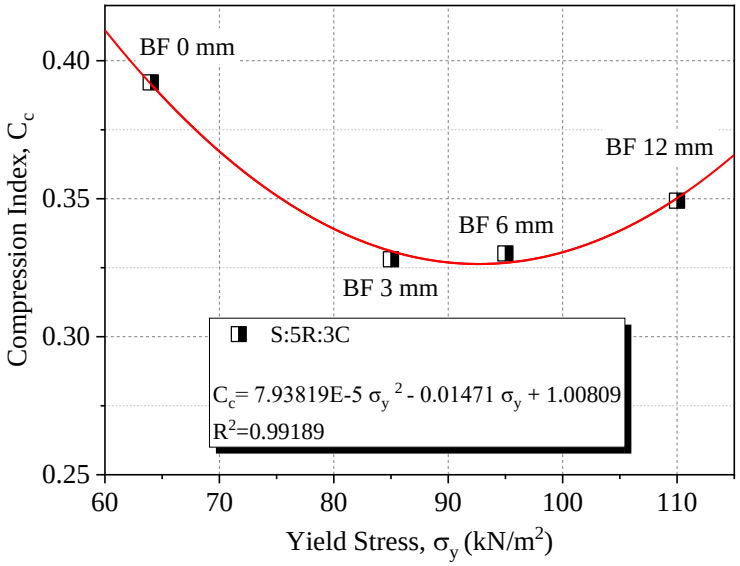

Figure 43 (a) Relationship between σ_y and C_c for 5%RHA:3C specimen with different lengths of Basalt Fibers (BF 3mm, BF 6mm and BF 12mm).

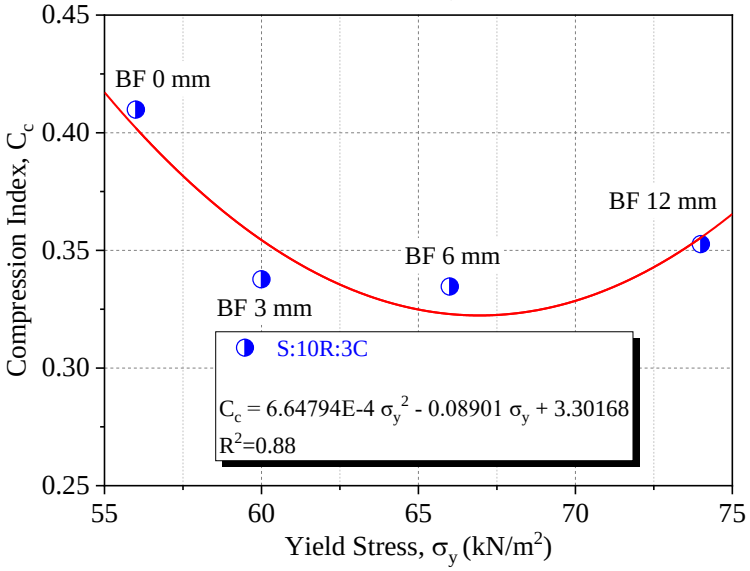

Figure 43 (b) Relationship between σ_y and C_c for 10%RHA:3C specimen with different lengths of Basalt Fibers (BF 3mm, BF 6mm and BF 12mm).

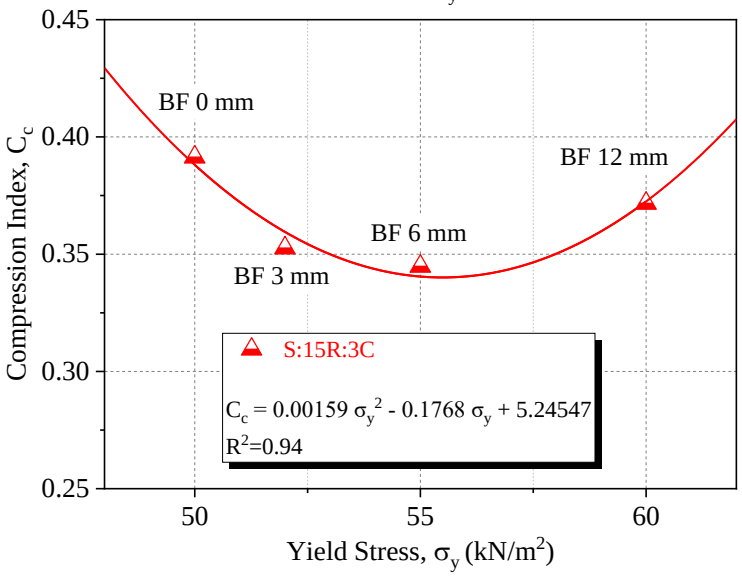

Figure 43 (c) Relationship between σ_y and C_c for 15%RHA:3C specimen with different lengths of Basalt Fibers (BF 3mm, BF 6mm and BF 12mm).

Figure 43 Relationship between σ_y and C_c.

5.2.9 Coefficient of Consolidation (c_v)

The coefficient of consolidation (c_v) measures the rate at which the soil consolidation process proceeds, a basic differential equation developed by Terzaghi (1943). A presentation of the c_v as a function of the average vertical consolidation pressure ($\bar{p}$) is shown in Figure 44 (a) and (b) for unreinforced and fiber-reinforced stabilized soil composites, respectively. The vertical axis (c_v) was on a logarithmic scale against the horizontal axis, plotted as the geometric mean average consolidation pressure ($\bar{p}$) (with values 14, 28, 55, 111, 222, 444, and 888 kPa) calculated by Equation 20. All the analytical equations followed the Japanese Industrial Standards 1217 and 1227.

$$\bar{p} = \sqrt{(p \cdot p')} \tag{20}$$

Where: p is the pressure increment, and p' is the consolidation pressure at the previous loading stage in kPa. The data points corresponding to 14 kPa were omitted in Figure 44 owing to the non-uniform vertical stress-time responses at low consolidation pressure. The c_v data points were defined by Equation 21 in cm^2/day for all the 16 oedometer tests.

$$c_v = 0.197 \left(\frac{\bar{H}}{2} \right)^2 \left(\frac{1440}{T_{50}} \right) \tag{21}$$

Where; c_v is the coefficient of consolidation in cm^2/day, $\bar{H}$ is the average height of the specimen, 0.197 is the value of the time coefficient at 50% consolidation, and 1440 is the unit conversion factor to cm^2/day. In RHA-only and RHA-cement stabilized soils, adding rice husk ash (RHA) and cement can significantly improve the strength and stiffness of the soil, as well as its compressibility and consolidation behavior. Additionally, the relationship between c_v and $\bar{p}$ for RHA-cement stabilized soils can vary depending on factors such as the RHA and cement content, the type of soil being stabilized, and the specific testing conditions used. In general, however, this study demonstrated that RHA-cement stabilized soils exhibited lower consolidation coefficients than the fiber-reinforced stabilized soils due to the increased strength and stiffness of the stabilized material, as shown in Figure 44 (a). In conclusion, the low c_v can result in faster consolidation times and reduced settlement,

which can benefit foundation design and construction applications. However, such chemically stabilized soils are prone to shrinkage and cracking under high loads hence the call for fiber reinforcements to solve infrastructure failure due to one-dimensional consolidation.

On the other hand, considering the basalt fiber reinforced specimens, the variation of c_v with $\bar{p}$ for the fiber-RHA-cement specimen showed a similar trend to that observed for the control specimen (soil only), as shown in Figure 44 (b). During the first loading phase, it was observed that the c_v increased as the $\bar{p}$ approached the yield stress. In contrast, afterward, the value remained approximately constant in the post-yield phase. The yield stress phase (50kPa to 110kPa) was evaluated from the void ratio (e) versus effective vertical pressure (log σ_v) compression curves for the reconstituted soil specimens, as discussed in Section 5.2.4. The observed approximate constant values of c_v revealed that creep effects should be carefully considered while working with basalt fiber reinforced and RHA-stabilized expansive soils. This trend agreed with the results Ferrari et al. (2016) observed while working on the one-dimensional consolidation of shales.

Additionally, the increasing c_v trend with $\bar{p}$ was attributed to the enhanced chemical and mechanical properties derived from RHA stabilization and basalt fiber reinforcements. Robinson and Allam (1998) and Sridharan and Nagaraj (2004) also recorded a similar trend of increasing c_v with consolidation pressure) when analyzing the role of mechanical and physio-chemical factors on the c_v trend with $\bar{p}$. It was also evident that the RHA content played a significant role in influencing the trend of the consolidation rate. For example, specimen S:5R:3C:1BF12, with 5% RHA content, produced the lowest c_v values compared to specimen S:15R:3C:1BF3 (15%RHA content), which had the highest c_v values. This increase in the c_v values at 15% RHA was due to the increased hydraulic conductivity associated with the porous structure of RHA and the additional voids created by random fiber intersections. A comparable increase in c_v value with increasing hydraulic

conductivity was also recorded by Yeo et al. (2005). It is also noteworthy that the RHA content influenced the c_v value depending on the degree of pozzolanic activity in the specimen. The complete utilization of RHA during pozzolanic reactions for specimens with 5% and 10% RHA developed their mechanical properties by improving the compressibility behavior hence the low c_v values. Moreover, as observed for all the specimens tested, the c_v value varied at the same $\bar{p}$ depending on the RHA content.

Furthermore, to correlate the coefficient of consolidation (c_v) with basalt fiber reinforcements, all c_v values were plotted against the lengths of basalt fibers, as shown in Figure 45 (a-c). In general, the length of basalt fibers significantly influenced the c_v value, as shown in the correlation plots. The reduction in c_v was more significant in the specimen containing 12mm basalt fibers, as shown in Figures 45 (a) and 45 (b), representing RHA compositions of 5% and 10%, respectively. For example, considering the maximum $\bar{p}$ of 888kPa, with the basalt fiber length increased from 3mm to 12mm, the c_v values for the 5%RHA specimen reduced from 321.02cm^2/d to 147cm^2/d. A similar reduction in the c_v with increasing basalt fiber length was further reported for the 10%RHA specimens with excerptions in the 15%RHA specimens at 12mm basalt fiber length, as revealed in Figure 45 (c). It can be concluded that the RHA content established a boundary condition at 10% RHA, beyond which a further increase in RHA content increased the c_v value with increasing fiber content. Also, it was evident that the coefficient of consolidation was dependent on average consolidation pressure during the loading stage, with an apparent inverse relationship.

Further, using the c_v versus length of basalt fiber plots, the curve-fitting correlation equations were evaluated and presented in Figures 45 (a-c). The equations can predict the c_v values at specific basalt fiber lengths and consolidation pressures for fiber lengths ranging from 3mm to 12mm. Nonetheless, the equations derived herein were based on the response of stabilized and fiber-reinforced expansive soil composites; hence additional study should be undertaken while working on other types of soils

under the same scope. It can be concluded that the longer basalt fibers provided sufficient reinforcements in the specimen by resisting excessive compression during the loading phase, resulting in a reduced consolidation rate.

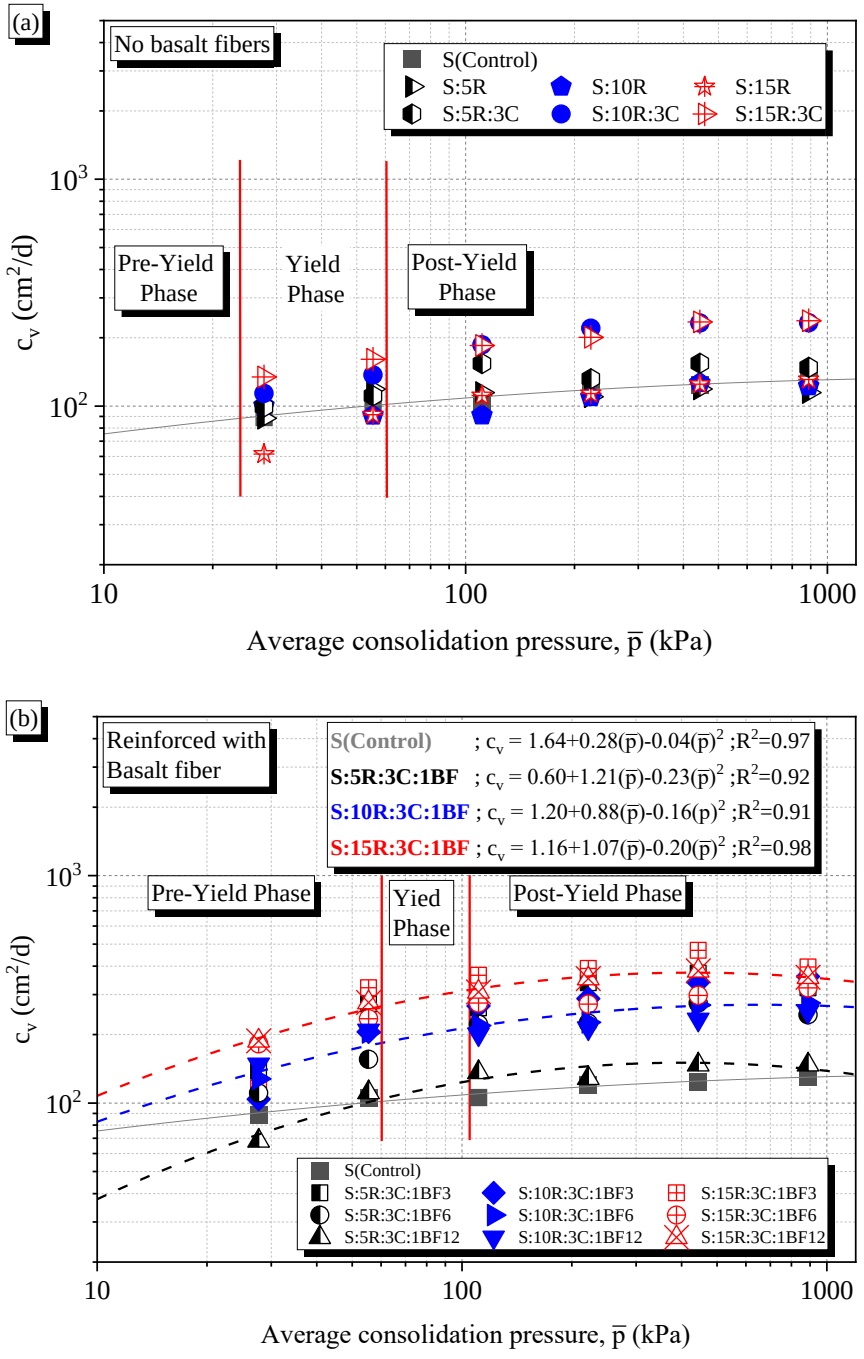

Figure 44 Relationship between c_v and $\bar{p}$ for **(a)** Unreinforced specimen; S, S:R, S:R:3C, **(b)** Basalt fiber reinforced specimen; S:R:3C:1BF.

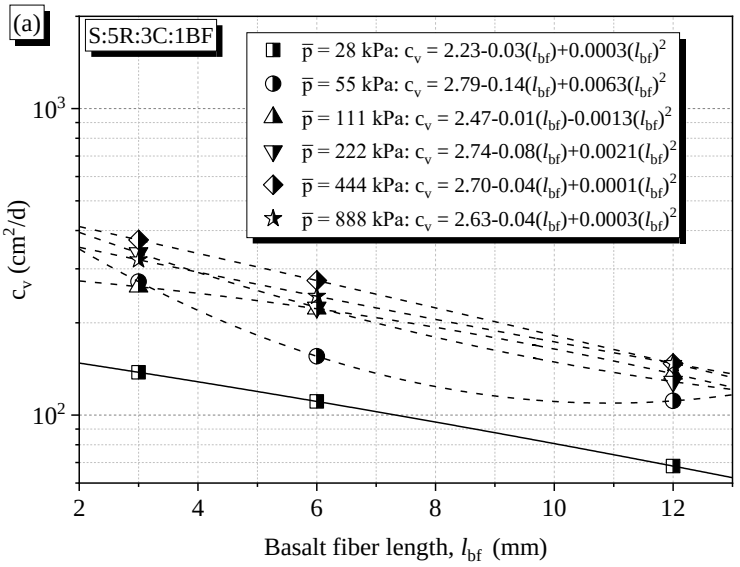

Figure 45 (a) Correlation between c_v and l_{bf} for 5%RHA:3C specimen reinforced with different lengths of Basalt Fibers (BF 3mm, BF 6mm and BF 12mm).

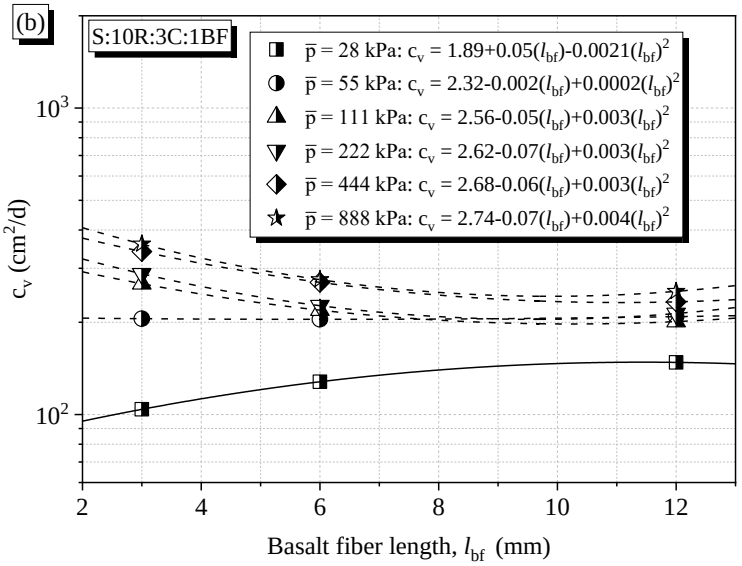

Figure 45 (b) Correlation between c_v and l_{bf} for 10%RHA:3C specimen reinforced with different lengths of Basalt Fibers (BF 3mm, BF 6mm and BF 12mm).

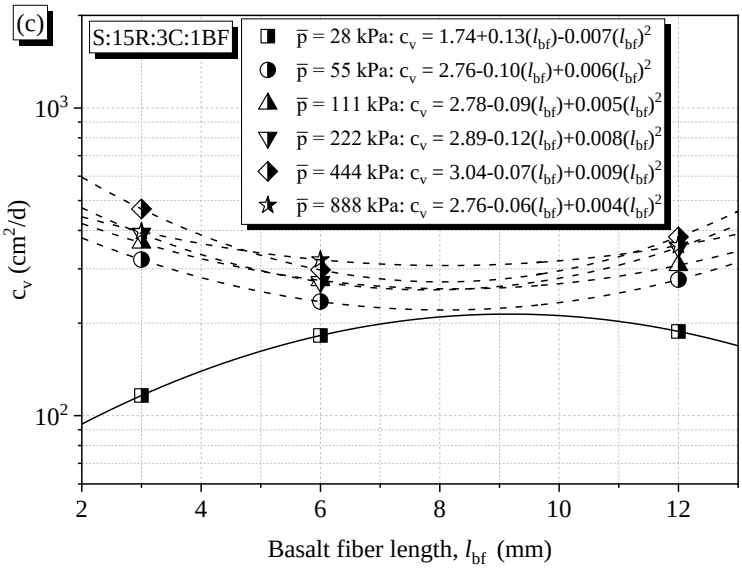

Figure 45 (c) Correlation between c_v and l_{bf} for 15%RHA:3C specimen reinforced with different lengths of Basalt Fibers (BF 3mm, BF 6mm and BF 12mm).

Figure 45 Correlation between c_v and l_{bf}.

5.2.10 Coefficient of Volume Change (m_v)

In the construction industry, foundation settlement is one of the safety considerations used in the geotechnical assessment of engineering structures. Excessive settlement can cause structural damage or significantly reduce the durability of the structure. Evaluating the coefficient of volume change (m_v) has been demonstrated to be a suitable parameter in calculating the consolidation settlement, providing essential measures to counter the projected soil settlement. The coefficient of volume change can be defined as the change in volume of a soil mass per unit of initial volume when subjected to an effective pressure increase. According to the Japan Industrial Standards 1217 and 1227, m_v is the ratio of the volume change of soil to the difference in the effective pressure and is calculated using Equation 22.

$$m_v = \frac{\Delta\varepsilon/100}{\Delta_p} \qquad (22)$$

Where; $\Delta\varepsilon$ is the compression strain generated at each loading stage [the ratio of the consolidation amount (ΔH) to average specimen height ($\bar{H}$)], and Δp is the consolidation pressure increment.

The variation of m_v at different compactive efforts for unreinforced specimens and those reinforced with different basalt fiber lengths and various RHA-Cement contents is shown in Figure 46 (a) and (b). The coefficient of volume change was higher at low consolidation pressures (14kPa) in both data sets due to the high swelling pressures in the expansive soil compared to the applied load. Eberemu et al. (2016) reported a similar response to low consolidation loads. In general, irrespective of the fiber reinforcement length, and RHA stabilization, the m_v value showed a reducing trend as the average consolidation pressure increased. This reduction was induced by the compressive forces rearranging and closely packing the composite materials, increasing the bonding forces and yield stress in the specimen, thereby reducing the m_v considerably. A relatable reduction in m_v with increasing pressure was also realized by Santagata et al. (2008).

Additionally, it was noteworthy that the m_v value was dependent on the specimen composition in the pre-yield and post-yield phases. For instance, in the pre-yield phase, considering the unreinforced specimens, S:5R:3C had the lowest m_v values of $4.31*10^{-4}$ m^2/kN compared to specimen S:15R with $2.67*10^{-3}$ m^2/kN. This difference was attributed to the difference in specimen structure, derived from the pozzolanic reactions between the specimen composition. Specimen S:15R lacked the cementitious properties derived from the absence of $Ca^{2+,}$ while S:5R:3C maximized the reactions to produce a stiff specimen microstructure, as will be discussed in section 5.2.11. in the post-yield phase, the m_v value reduced considerably with increasing average consolidation pressure, as shown in Figure 46 (a).

On the other hand, considering the basalt fiber reinforcement and RHA-cement content, specimen S:5R:3C:1BF3 showed the lowest m_v values of $1.20*10^{-4}$ m^2/kN compared to specimen S:15R:3C:1BF3 with $1.07*10^{-3}m^2/kN$ during the pre-yield phase(p=14 kPa), as shown in Figure 46 (b). This difference was probably due to the enhanced stiffness and resistance to compressive forces obtained from the complete pozzolanic reactions at 5%RHA than at 15%RHA. For example, at p=14 kPa, the fiber-reinforced specimen with 5%RHA portrayed a direct relationship, with the coefficient of volume change increasing from $1.20x10^{-4}$ m^2/kN to $1.41x10^{-4}$ m^2/kN to $2.19x10^{-4}$ m^2/kN for basalt fiber lengths 3mm, 6mm, and 12mm respectively. On the other hand, an inverse relationship was observed for higher RHA-cement contents. With 10%RHA attaining m_v values of $5.69x10^{-4}$ m^2/kN to $2.20x10^{-4}$ m^2/kN while 15%RHA produced $1.07x10^{-4}$ m^2/kN to $3.53x10^{-4}$ m^2/kN as the length of basalt fibers increased from 3mm to 12mm.

It was further concluded that RHA and basalt fiber reinforcements slightly increased the m_v with increasing compactive force across all specimens during the pre-yield phase. This slight increase was due to the additional displacements required to reduce the voids created by the porous RHA and the random distribution of basalt fibers. However, in the post-yield state, the ultimate compact

structure in the specimen provided resistance to compressive forces leading to a significant reduction in m_v with average consolidation pressure. Similar responses have also been observed by Xu et al. (2020), Eberemu (2011), Eberemu et al. (2016), and Laskar and Pal (2013).

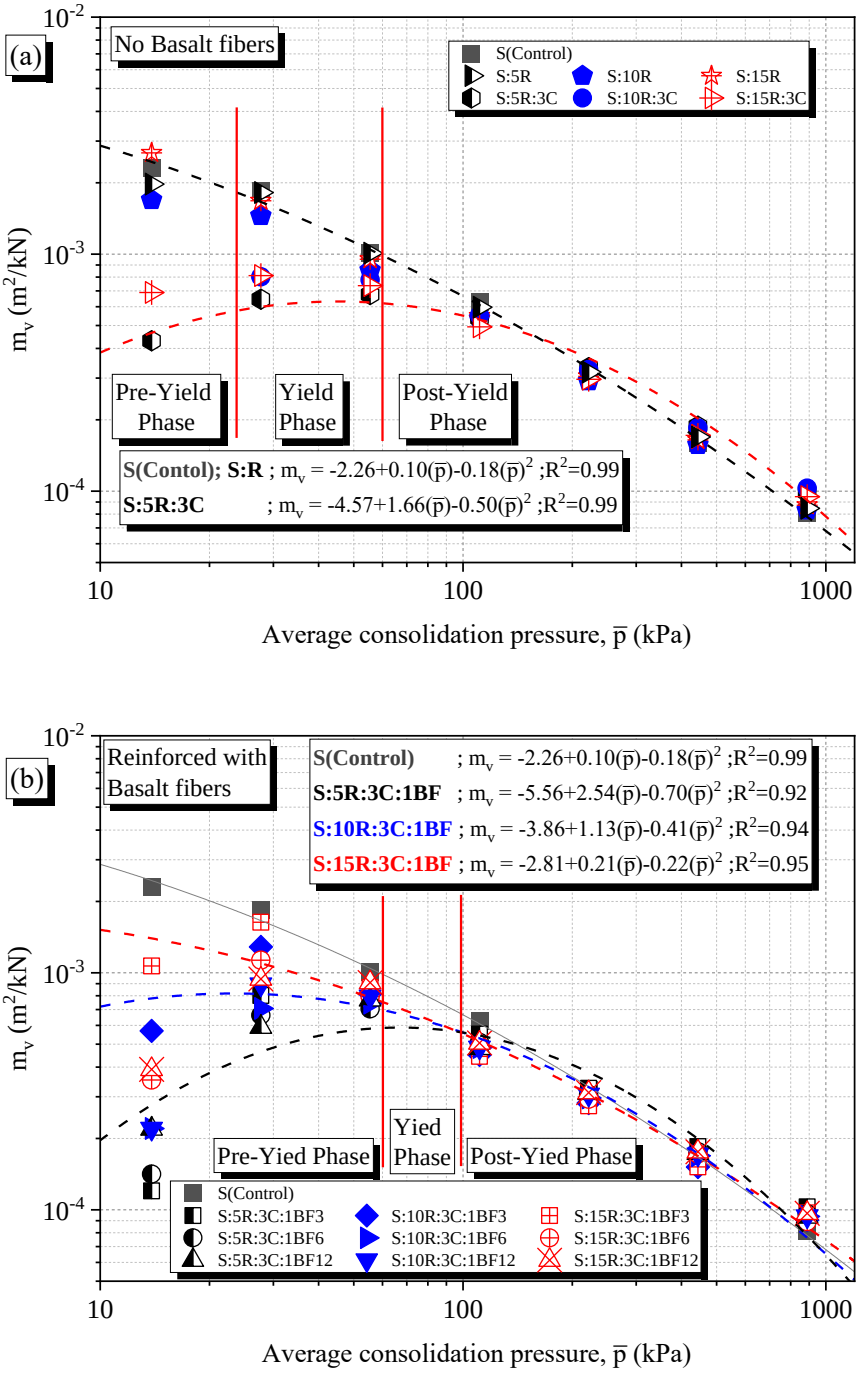

Figure 46 Relationship between m_v and $\bar{p}$ for **(a)** Unreinforced specimen; S, S:R, S:R:3C, **(b)** Basalt fiber reinforced specimen; S:R:3C:1BF.

Besides, a plot of m_v on the log scale against basalt fiber length (l_{bf}) was considered to correlate the relationship between the m_v and the length of basalt fiber, as illustrated in Figure 47 (a), (b), and (c) for specimens S:5R:3C:1BF, S:10R:3C:1BF, and S:15R:3C:1BF respectively. It was evident that increasing the length of basalt fibers in specimens had minimal effects on m_v with increasing consolidation pressures from 55 to 888 kPa. Generally, slightly higher m_v values were recorded for the specimens containing 15%RHA due to the extra volume changes initiated by the high void ratios. Additionally, from the m_v versus length of basalt fiber (l_{bf}) plots, the curve fitting correlation equations to predict m_v were evaluated and presented across all specimens.

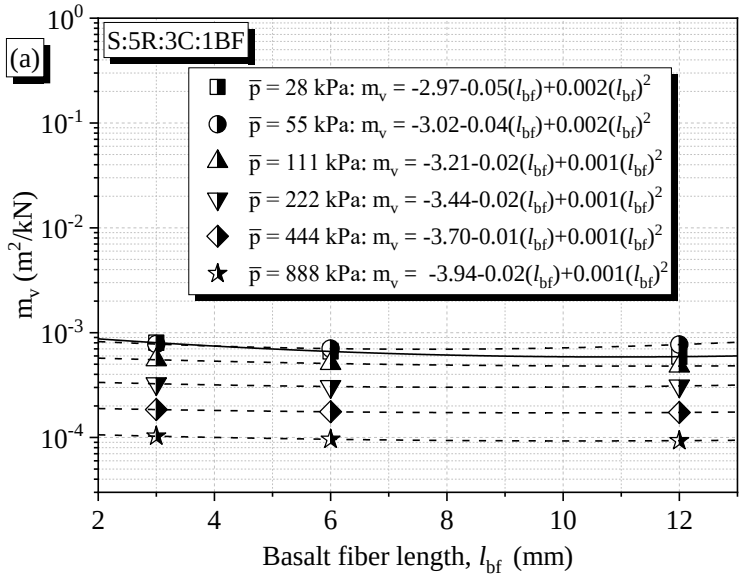

Figure 47 (a) Correlation between m_v and l_{bf} for 5%RHA:3C specimen reinforced with different lengths of Basalt Fibers (BF 3mm, BF 6mm and BF 12mm).

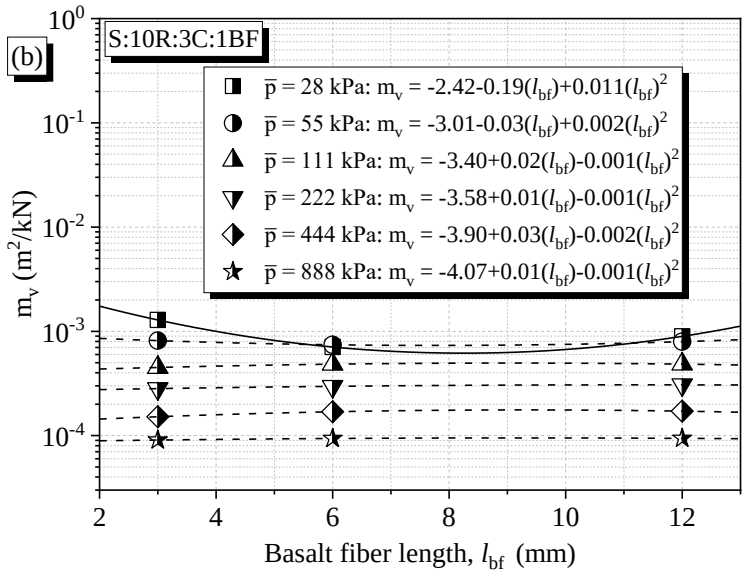

Figure 47 (b) Correlation between m_v and l_{bf} for 10%RHA:3C specimen reinforced with different lengths of Basalt Fibers (BF 3mm, BF 6mm and BF 12mm).

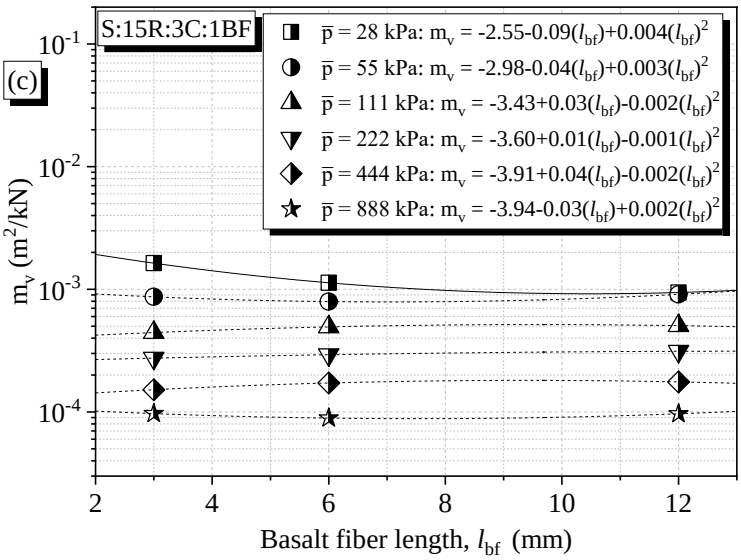

Figure 47 (c) Correlation between m_v and l_{bf} for 15%RHA:3C specimen reinforced with different lengths of Basalt Fibers (BF 3mm, BF 6mm and BF 12mm).

Figure 47 Correlation between m_v and l_{bf}.

These equations can predict the coefficient of volume change (m_v) if basalt fiber (l_{bf}) length and the average consolidation pressures are provided for fiber lengths ranging from 3mm to 12mm. Similar to the c_v equations in the previous section, the proposed equations were based on the response of stabilized and fiber-reinforced expansive soil composites.

5.2.11 Permeability Coefficient (k)

This section highlights the effects of basalt fiber length and RHA-cement contents on the permeability coefficient (k) of unreinforced and reinforced stabilized expansive soils undergoing one-dimensional consolidation. Permeability describes the rate at which water can move through the pores within a soil medium and has proven to be an essential parameter influencing soil consolidation and strength. Following the Japan Industrial Standards 1217 and 1227, the permeability coefficient can be calculated using Equation 23.

$$k = \frac{c_v m_v \gamma_w}{8.64 \times 10^8} \quad (23)$$

Where k is the permeability coefficient in m/s, c_v is the coefficient of consolidation, m_v is the coefficient of volume change, γ_w is the unit volume weight of water (9.81kN/m^3), and 8.64x10^8 is the conversion parameter of k to m/s. Figure 48 (a) and (b) compared the pressure dependence of the

unreinforced and reinforced stabilized expansive soil's permeability coefficient, respectively, considering the following factors; RHA content, RHA-cement content, length of basalt fibers, and the average consolidation pressure. It was found that the permeability coefficient varied in the order of 10^{-10} to 10^{-9} and was greatly influenced by the average consolidation pressure.

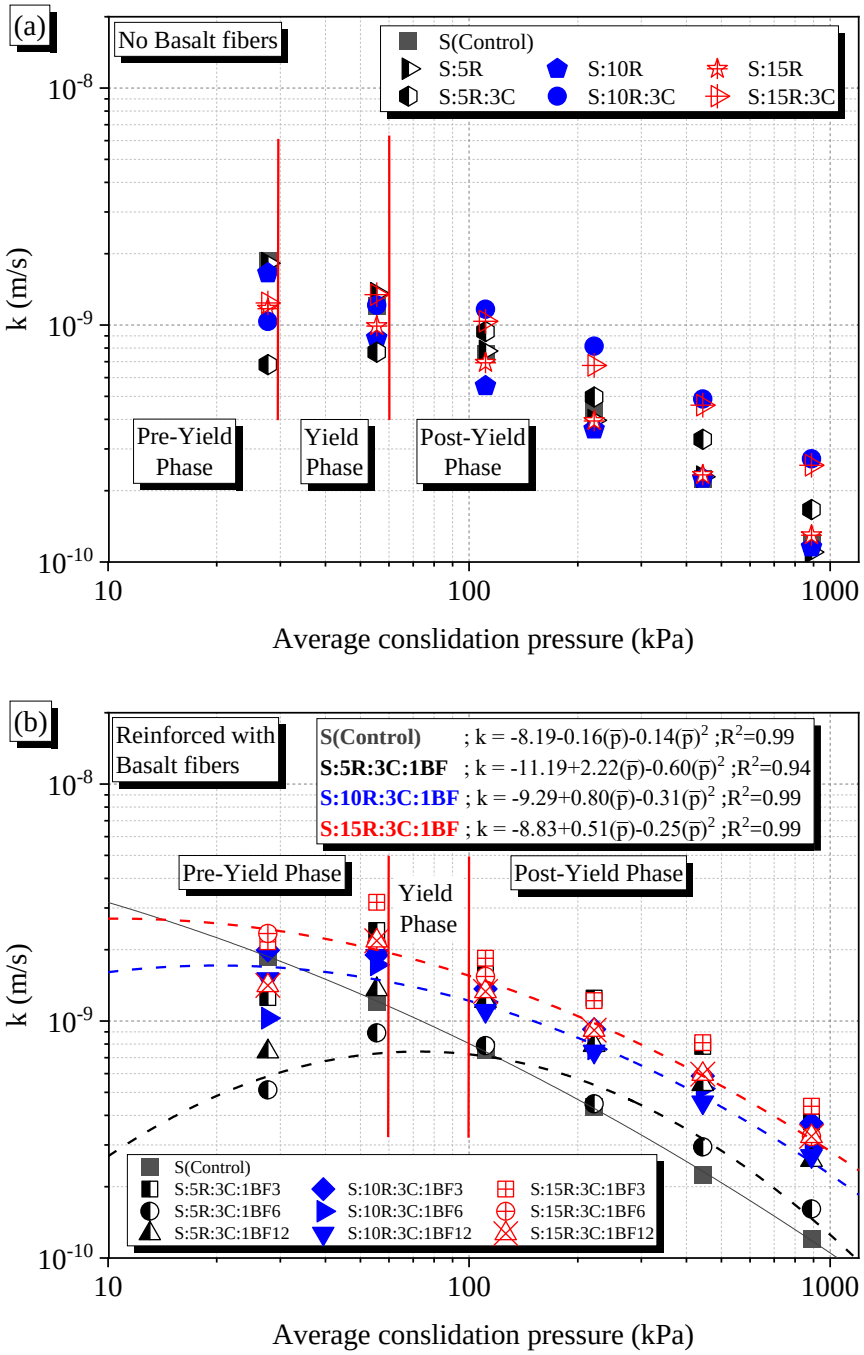

Figure 48 Relationship between k and $\bar{p}$ for **(a)** Unreinforced specimen; S, S:R, S:R:3C, **(b)** Basalt fiber reinforced specimen; S:R:3C:1BF.

Also, the value of k increased during the pre-yield phase and decreased significantly in the post-yield phase for all the reinforced specimens tested. However, the value of k in the observed trend depended on the specimen's RHA-cement content and basalt fiber length. For instance, the permeability coefficient increased with RHA content for all the individual average consolidation pressures, as shown in Figure 48 (b). This increase was due to the high porosity caused by the excess RHA particles and the voids networks created by basalt fibers in the composite specimen. Additionally, the pozzolanic compounds generated due to RHA and cement precipitation enhanced cementation at low RHA-cement contents hence the low k values at 5%RHA. A similar reduction in the permeability coefficient due to pozzolanic reaction has also been recorded by other studies, such as Onyelowe et al. (2021), Jamil et al. (2013), Gupta and Kumar (2017), and Nshimiyimana et al., (2018).

However, as the average consolidation pressure increased, the k value reduced to an almost constant value of order 10^{-10} for all the tested specimens due to the complete removal of the voids and sufficient rearrangement of soil-RHA-cement and fibers. This relationship between voids and permeability indicated that voids played the dominant role in affecting the permeability coefficient. Cheng et al. (2020) also observed a similar relationship while experimenting with the consolidation properties of reconstituted clay soils.

Supplementary to the analyses discussed, a correlation plot was considered regarding the influence of the basalt fiber length on the permeability coefficient, as shown in Figure 49 (a)-(c). In Figure 49 (a), representing basalt fiber reinforced specimen with 5%RHA and 3%cement, the permeability coefficient reduced with increasing fiber length up to 6mm. The declining trend of k with the length of basalt fiber for the 5%RHA-3C specimens can be attributed to the well-defined structural development due to cementation from adequate pozzolanic reaction and enhanced reinforcement. However, a further increase in the basalt fiber length to 12mm slightly increased the permeability due to the longer paths for water to drain more quickly through the specimen. The rise in permeability

coefficient with the length of fiber reinforcements was also observed by Abdi et al. (2008) while investigating the effects of fiber inclusion on the hydraulic conductivity in clay soils. In the case of 10%RHA-3C and 15%RHA-3C, shown in Fig. 8 (c) and Fig. (d), respectively, a very minimal reduction in the k value was recorded for all the average consolidation pressure increments. From these correlation plots, curve-fitting equations were formulated to assist design engineers in predicting the projected permeability coefficients for RHA-basalt fiber stabilized soils for a given average consolidation pressure and length of basalt fiber (3mm to 12mm).

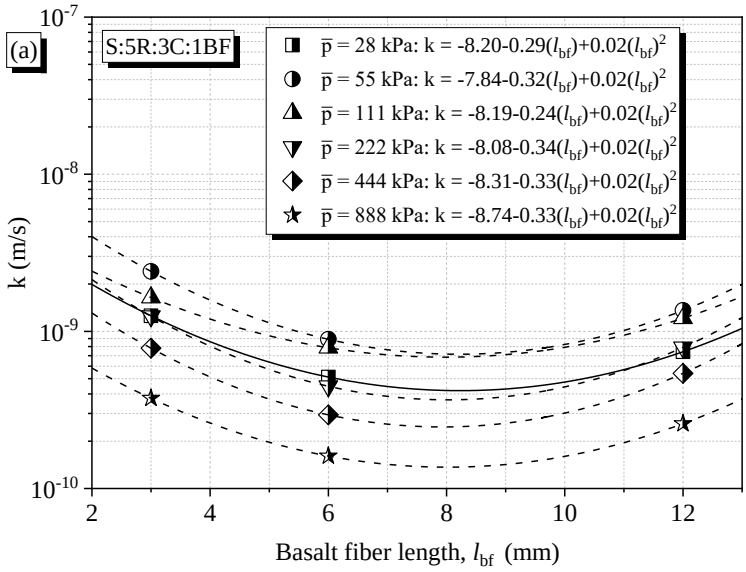

Figure 49 (a) Correlation between k and l_{bf} for 5%RHA:3C specimen reinforced with different lengths of Basalt Fibers (BF 3mm, BF 6mm and BF 12mm).

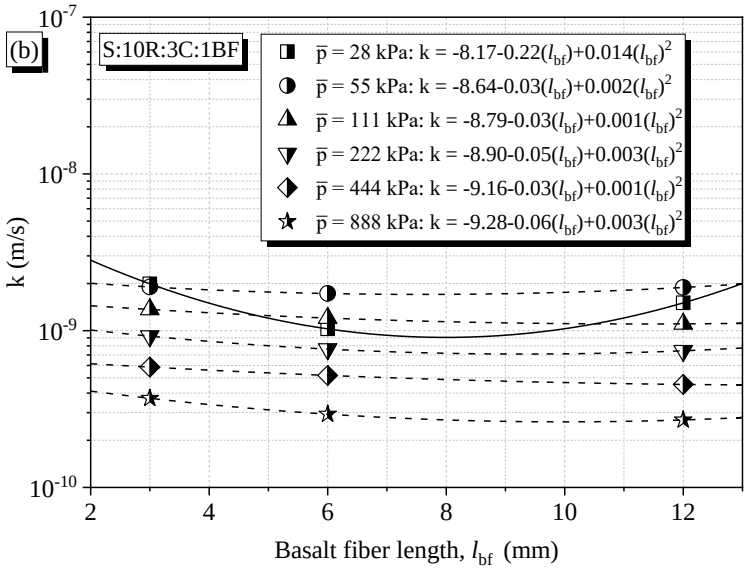

Figure 49 (b) Correlation between k and l_{bf} for 10%RHA:3C specimen reinforced with different lengths of Basalt Fibers (BF 3mm, BF 6mm and BF 12mm).

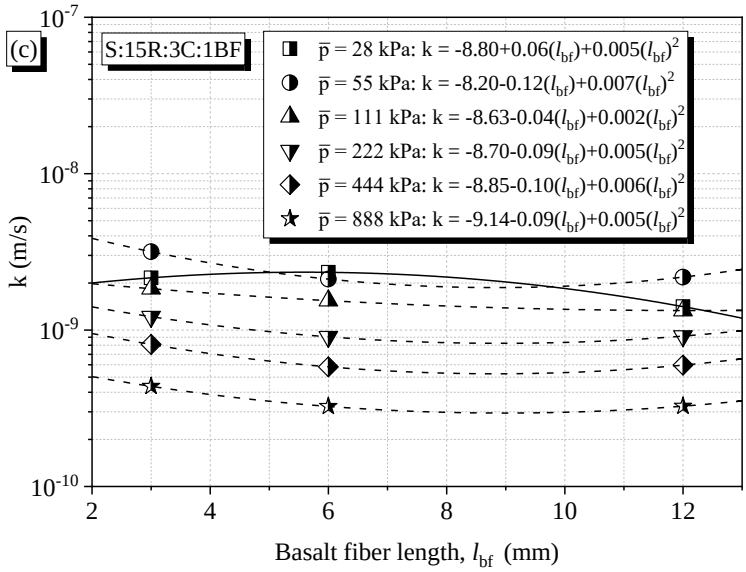

Figure 49 (c) Correlation between k and l_{bf} for 15%RHA:3C specimen reinforced with different lengths of Basalt Fibers (BF 3mm, BF 6mm and BF 12mm).

Figure 49 Correlation between k and l_{bf}.

5.2.12 Microstructural Analysis

The microstructural analysis is an essential tool for investigating the properties and behavior of construction materials. In this section, the microstructural analysis of soil stabilized with rice husk ash (RHA), cement, and reinforced with basalt fibers, using scanning electron microscopy (SEM) and X-ray diffraction (XRD), will be discussed. Upfront, the microstructural analysis on stabilized and reinforced soil samples was prepared and examined using SEM. SEM is a powerful technique that allows for the imaging of materials at high magnifications, providing detailed information about the surface morphology and microstructure of the material.

The effect of basalt fiber reinforcements and stabilization using RHA-cement mixtures on the consolidation coefficients of reconstituted expansive soils can be explained by capturing the microstructural development through a scanning electron microscope (SEM). SEM micrographs at a magnification of X500 and scale of 100 μm, showing the coupling effect of the basalt fibers with the compact cementitious composite soil-RHA-Cement matrix for the tested specimen combinations, are shown in Figures (50), (51), and (52). These SEM images represented the corresponding specimen states at the end of the consolidation process (Average consolidation pressure = 888kPa).

This section discussed a detailed analysis to justify the trends of the microstructure-dependent coefficients, such as the coefficient of consolidation (c_v) and the permeability coefficient (k), as discussed earlier.

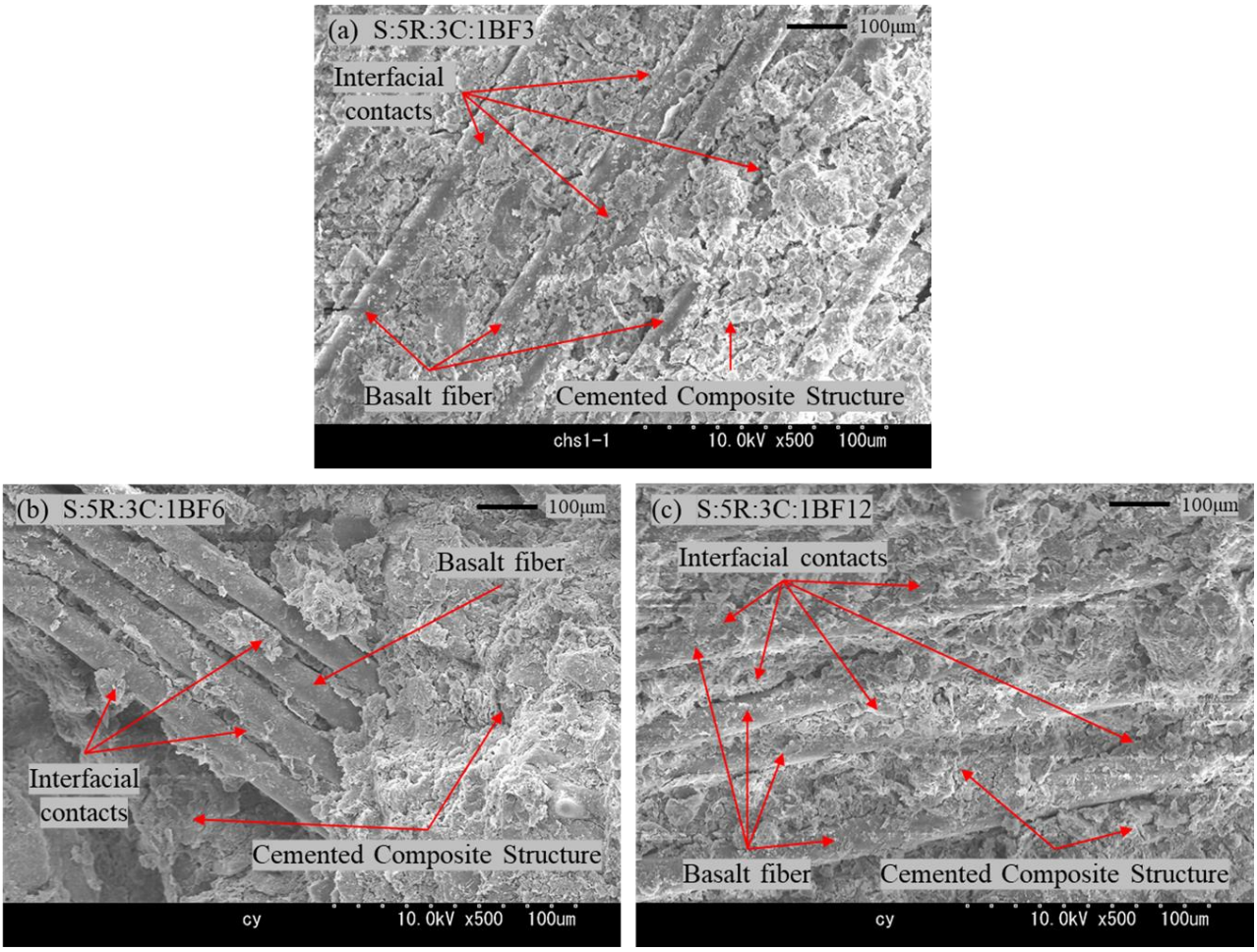

Figure 50 SEM imagery for 5%RHA-3%C composites **(a)** Specimen S:5R:3C:1BF3, **(b)** Specimen S:5R:3C:1BF6, **(c)** Specimen S:5R:3C:1BF12.

Figure 50 (a-c) represents the SEM imagery of the fiber-reinforced 5%RHA-3C composites. The mobilization of basalt fiber reinforcements was driven by the highly significant interfacial contacts developed during the physical connection between the cementitious soil matrix and the fiber surface. The interfacial contacts were more pronounced when the length of basalt fibers increased from 3mm to 12mm due to the increased fiber surface area and the interconnectivity arising from the intense fiber network. Additionally, a clear indication of a cemented compact structure was evident due to

the complete utilization of 5%RHA and cement during the pozzolanic reactions. The interfacial contacts resisted compressibility, reducing the coefficient of consolidation (c_v) for the 5%RHA composites, as shown in Figure 44. At the same time, the cementitious structure eliminated excess voids, hence the lower permeability coefficient values (k) for the 5%RHA-3%C composites, as presented in Figure 48. The tendency of fiber reinforcements to improve the bonding strength of expansive soil was also observed by Syed et al. (2020) when stabilizing expansive clays using geo-polymerization and fiber reinforcement.

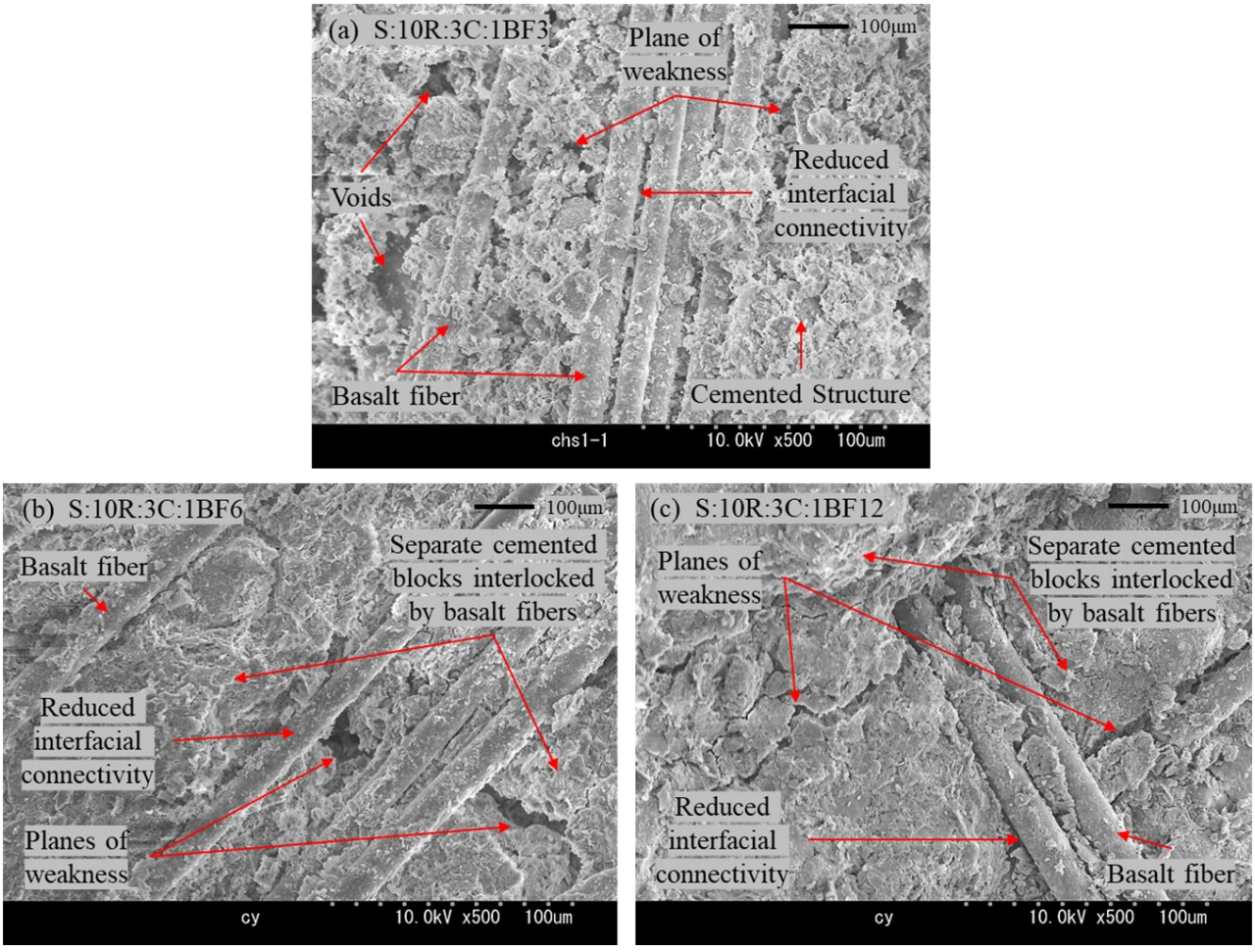

Figure 51 SEM imagery for 10%RHA-3%C composites **(a)** Specimen S:10R:3C:1BF3, **(b)** Specimen S:10R:3C:1BF6, **(c)** Specimen S:10R:3C:1BF12.

Contrarily, the rising trends of c_v and k for the fiber-reinforced specimen containing 10%RHA and 3%C were justified by the occurrence of planes of weakness and voids in the specimens, as displayed in Figure 51 (a-c). However, the discrete distributions of high tensile strength basalt fibers in the

specimen structure interlocked the separate cemented blocks, restricting further cracks during consolidation. The interlocking mechanism was more significant with increasing basalt fiber length from 3mm to 12mm. Additionally, the micro-structural bonding was slightly reduced for these composites due to the inadequate intensity of the interfacial contacts in the specimen structure compared to the 5%RHA-3C specimens.

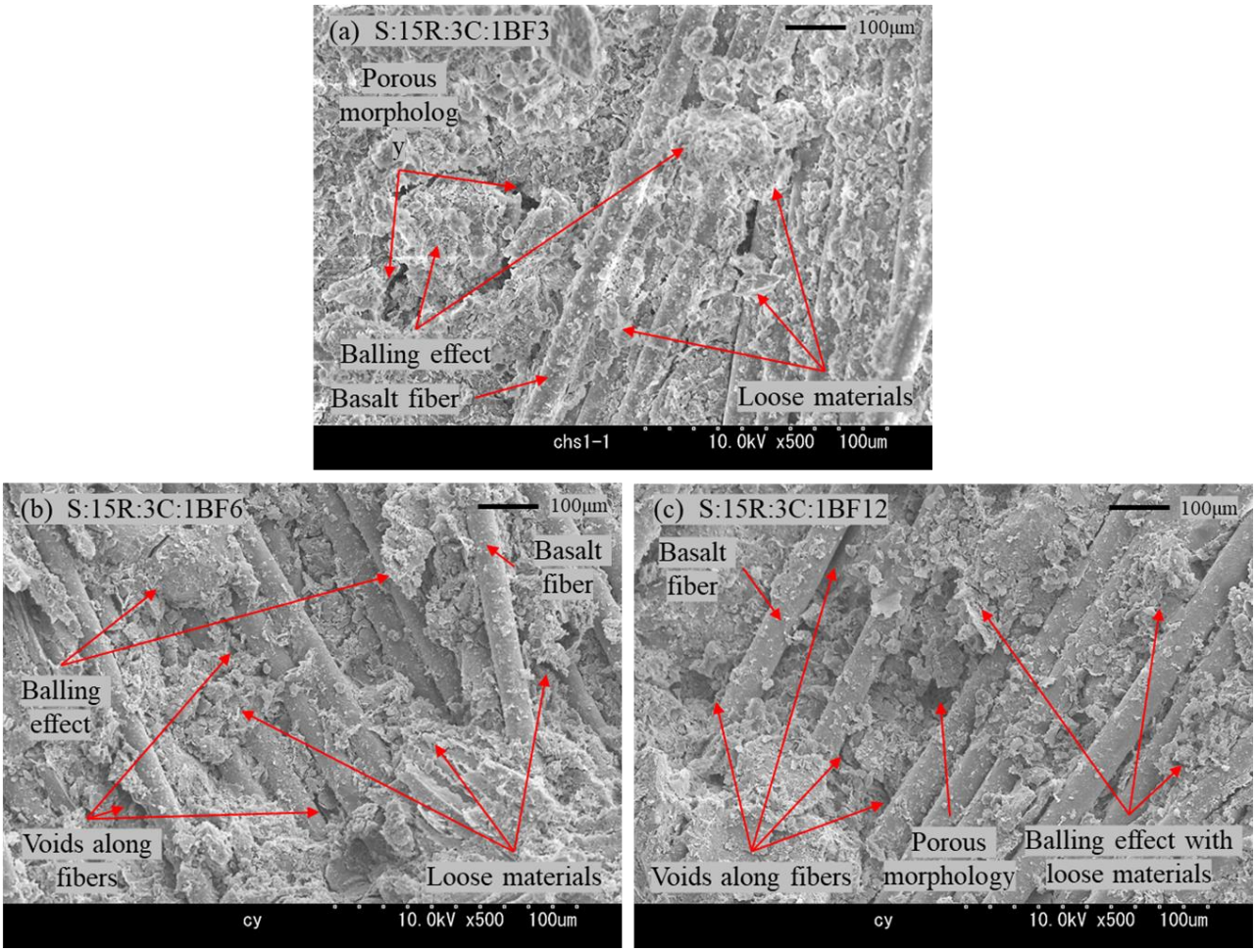

Figure 52 SEM imagery for 15%RHA-3%C composites **(a)** Specimen S:15R:3C:1BF3, **(b)** Specimen S:15R:3C:1BF6, **(c)** Specimen S:15R:3C:1BF12.

Considering the basalt fiber reinforced specimens containing 15%RHA-3%C shown in Figure 52 (a-c), it was noteworthy that the influences on c_v and k depended on the extent of interfacial contacts and the presence of loose materials, as will be discussed in this section. Up front, it was observed that the smooth basalt fiber surfaces indicated insufficient interfacial contacts between basalt fibers

and the soil-RHA-cement composite compared to the 5%RHA-3%C and 10%RHA-3%C composites. The reduced interfacial connectivity reduced the microstructural bonding, increasing the values of c_v and k considerably. Next, the confirmation of fine loose material in the SEM images indicated high compressibility when subjected to one-dimensional loading, increasing the value of c_v value as shown in Figure 44. Also, the developments of voids along the basalt fibers and pores within the specimen were more significant hence the increasing trends of k, as illustrated in Figure 48 for the 15%RHA-3%C composites.

Furthermore, the reduced pozzolanic activity at 15%RHA-3%C due to excess accumulation of RHA led to the balling of soil-RHA-cement particles around the basalt fibers hence the more notably porous structure. As a result, the void ratios increased, allowing room for considerable particle rearrangement during loading. This balling effect developed a highly compressible and porous specimen structure, increasing the c_v and k values.

In addition to SEM, XRD was used to analyze the stabilized and reinforced soil microstructure, as shown in Figure 53 (a-g). XRD is a technique that is used to identify the crystalline phases present in a material. The XRD analysis revealed the presence of several crystalline phases in the stabilized and reinforced soil, including calcium aluminosilicate hydrate bonds, hydrous calcium aluminum sorosilicate bonds, and quartz. The presence of calcium silicate hydrate bonds and calcium hydroxide indicated the formation of a cementitious matrix in the soil due to the addition of RHA and cement. On the other hand, the presence of quartz was likely due to the natural occurrence of this mineral in the soil and RHA. In Figure 53 (a), the XRD analysis of 5%RHA-3%Cement-1%BF reconstituted soil composites shows high peaks of Calcium Aluminohexasilicate Tetrahydrate $[(CaO)(Al_2O_3)(SiO_2)_6\ 4(H_2O)]$, Calcium Aluminum-Magnesium hexaSilicate heptaHydrate $[(CaO)(Al_2Mg_2O_{15})(SiO_2)_6\ 7(H_2O)]$, Gismondine $[CaAl_2Si_2O_{12}\cdot4(H_2O)]$ also known as CSH Gels. The presence of alumina in the CAHS gels significantly increased the stability of the reconstituted

soil composites hence improving yield pressures of up to 110kN/m^2 (for BF12mm) and developing the c_v and k as discussed in the previous section. Correspondingly, increasing the RHA contents to 10% and 15% led to the formation of CSH gel, but with fewer crystalline peaks compared to the 5%RHA specimens, as shown in Figure 53 (b) and 53 (c), respectively. The fragility of the 10% and 15% RHA composites are quantified by the reduced maximum yield pressures of 74kN/m^2 (for BF12mm) and 60kN/m^2 (for BF12mm), respectively.

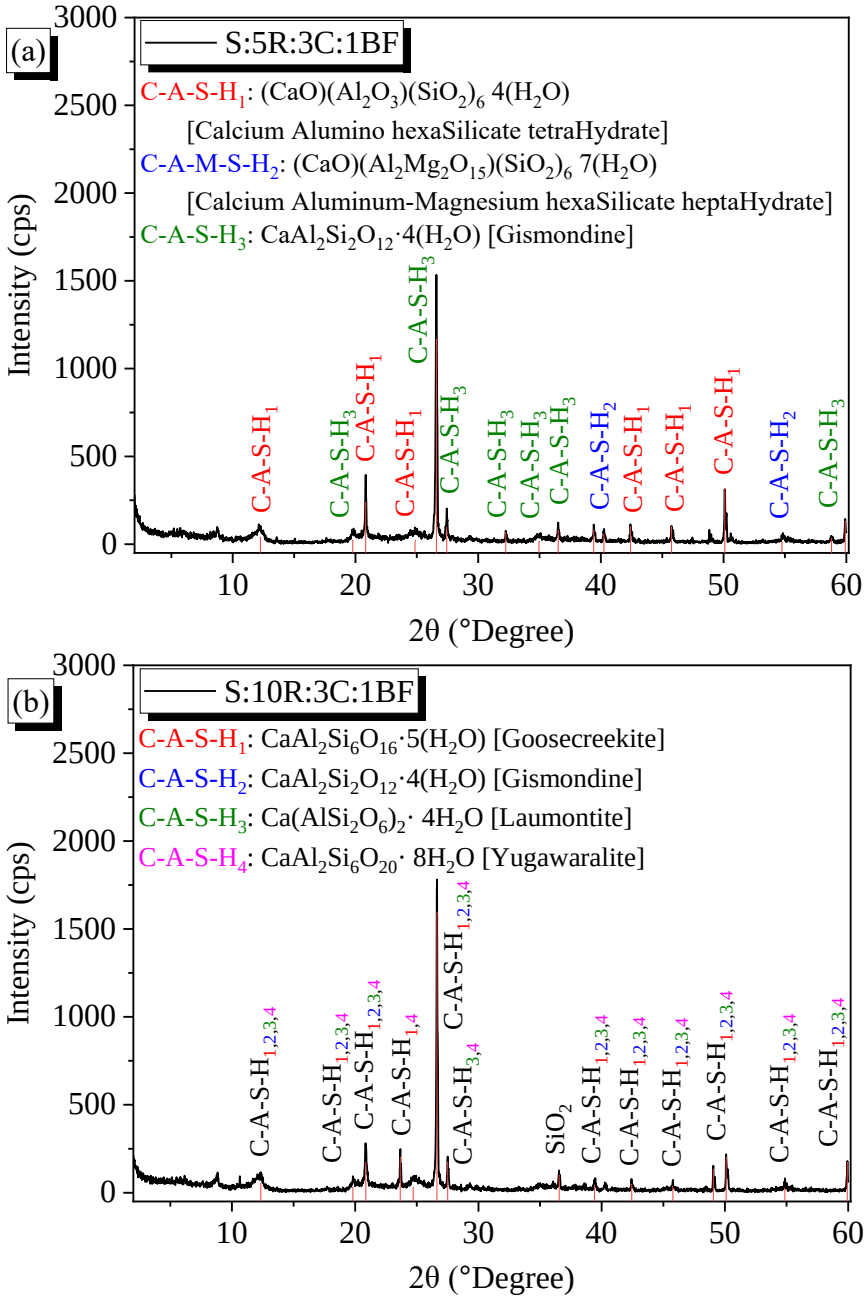

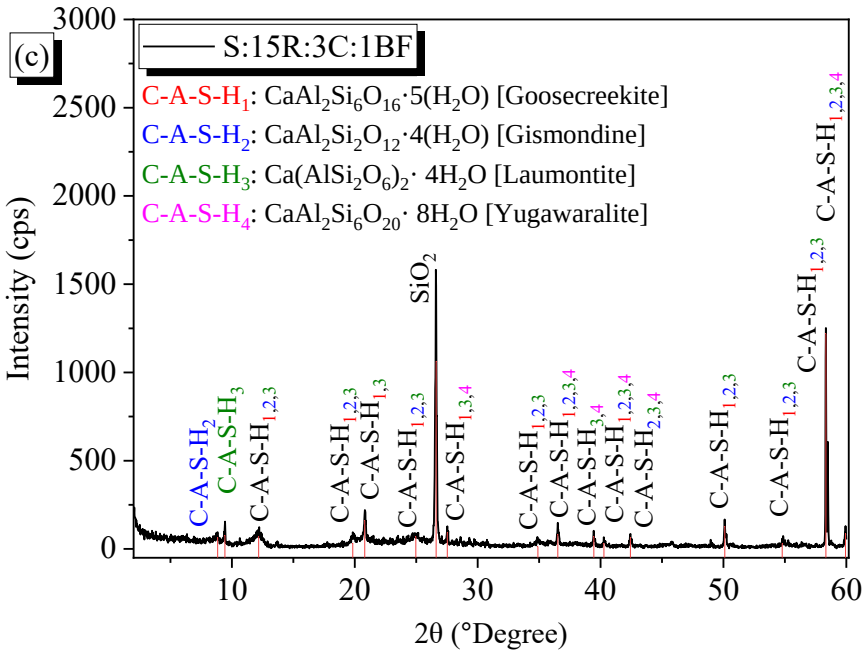

Figure 53 XRD analyses during consolidation **(a)** X-ray diffraction (XRD) analysis of the S:5R:3C:1BFspecimen after consolidation **(b)** X-ray diffraction (XRD) analysis of the S:10R:3C:1BFspecimen after consolidation **(c)** X-ray diffraction (XRD) analysis of the S:15R:3C:1BFspecimen after consolidation.

Additionally, at higher RHA contents (10% and 15%), the presence of SO_2 peaks indicated the presence of excess Si^{+2} ions in the stabilized and reinforced soil composite hence the reduced strength. However, with the addition of basalt fibers, the 10% and 15% RHA reconstituted soil composites showed improved characteristics in terms of yield pressure (σ_y), c_v, m_v, and k more than the control specimens (soil only).

5.3 Triaxial Compression Test Results

5.3.1 Stress-Strain Relationships (σ, ε)

Stress-strain relationships refer to the behavior of a material under stress, such as when it is subjected to external forces or loads. The stress-strain relationships of RHA-cement stabilized expansive soils with basalt fiber reinforcements were evaluated using consolidated drained (CD) triaxial compression tests. These tests provided valuable insights into the behavior of the modified soil under various loading conditions, allowing engineers to design structures that can withstand the effects of

expansive soils. By measuring the deformation and stress of the soil, the strength, stiffness, and ductility of the soil were accurately determined, providing a better understanding of its behavior under different loading conditions.The effects of basalt fiber filament length on the deviatoric stresses (Δσ) and axial strains (ε) acting within the specimens with curing periods are discussed in this section. A series of triaxial tests for confining pressures 50 kPa, 100 kPa, and 150 kPa were conducted, and the results were plotted after 1 day, 7 days, and 28 days of curing, as shown in Figures 54 to 65. For reference, the stress-strain relationship for the control specimen (soil only) was established in Figure 54. The control specimen graphs showed that the confining pressures had a minimal influence on the ultimate deviatoric stress (Δσ), with a small increment recorded after 28 days of curing. The low deviatoric stresses were due to the brittleness of the soil and the lack of proper bonding between the soil particles during shearing - a common phenomenon for highly cohesive soils (including clay and expansive soils).

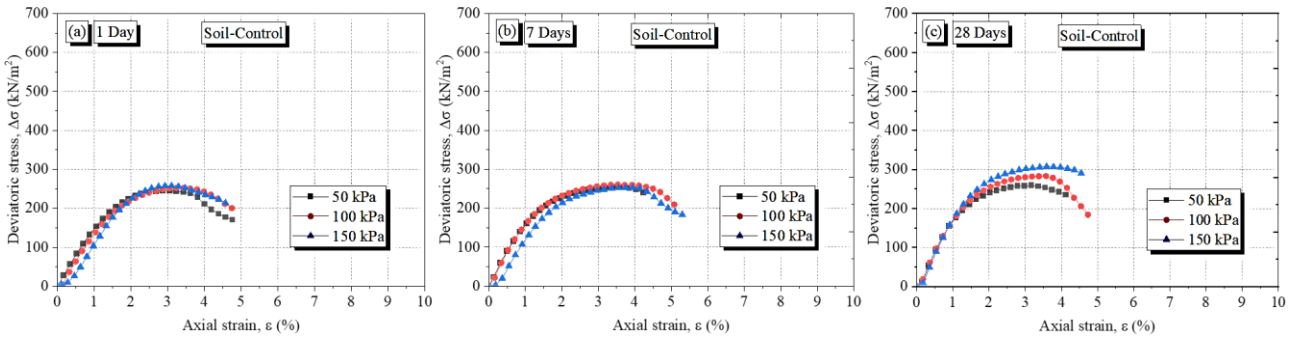

Figure 54 Stress-Strain relationship for soil only with curing period: **(a)** 1 day, **(b)** 7 days, and **(c)** 28 days.

However, with the addition of RHA and RHA: Cement to the expansive soil, there was a clear distinction between the deviatoric stresses (Δσ) with different confining pressures. The relationship between axial strain (ε) and the deviatoric stress (Δσ) for specimens containing 5%RHA and 5%RHA:3%cement has been illustrated in Figure 55 and Figure 56, respectively. In both instances, the deviatoric stresses (Δσ) increased with the curing period, with the cement composites recording the highest values at 150 kPa confining pressures compared to the control. However, it was

noteworthy that the addition of cement decreased the axial strains (ε) at maximum deviatoric stresses (Δσ) in the tested specimens. At the same time, a brittle nature was evident on the cement composites due to the sharp decrease in the deviatoric stress (Δσ) after the peak value was realized, as compared to the significant softening behavior on the 5%RHA specimens. A similar response was recorded for the 10%RHA and 15%RHA soil composites, as will be discussed in section 5.3.2. It was noted that the deviatoric stresses reduced with increased RHA content from 5% to 15% in both instances.

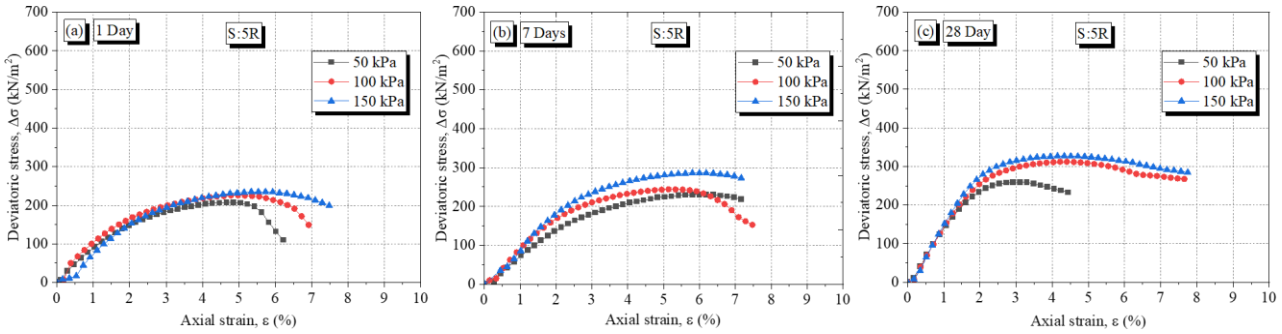

Figure 55 Stress-Strain relationship for soil:5%RHA with curing period: **(a)** 1 day, **(b)** 7 days, and **(c)** 28 days.

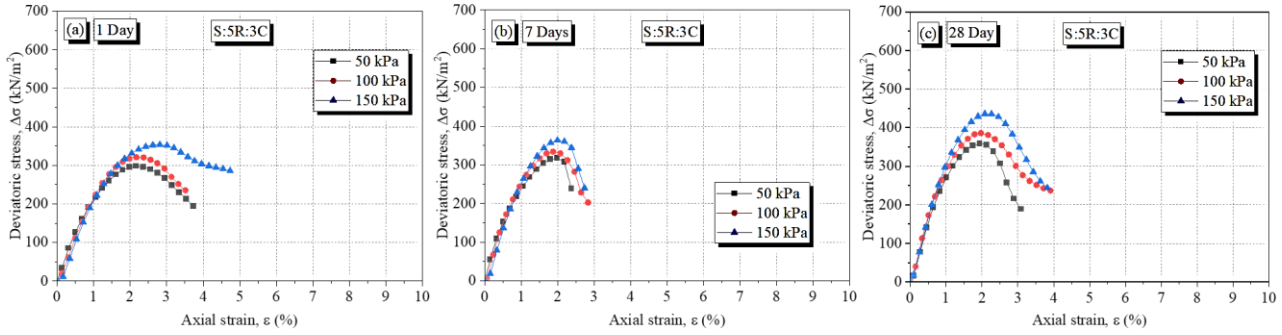

Figure 56 Stress-Strain relationship for soil:5%RHA:3C with curing period: **(a)** 1 day, **(b)** 7 days, and **(c)** 28 days.

Adding basalt fiber filament lengths into the soil-RHA-cement composite highly influenced the maximum deviatoric stress (Δσ) at failure compared to the unreinforced specimen described above. After 1 day of curing, the stress-strain relationships for specimens reinforced with basalt fiber 3 mm, 6 mm, and 12 mm were analyzed and plotted as illustrated in Figures 57, 58, and 59 for 5%RHA, 10%RHA and 15%RHA composites, respectively. The increase in deviatoric stress (Δσ) caused by the basalt fibers was consistent and increased with filament length for all the RHA contents. Also, it

was noteworthy that the deviatoric stresses (Δσ) increased with the confining pressure. Besides, varying the basalt fiber filament length from 3 mm to 12 mm increased the axial strain slightly, with a notable 1% increase in axial strain (ε) for the 12mm specimens at maximum deviatoric stress. However, deviatoric stresses in the soil decreased when RHA content was increased from 5% to 10% to 15% for all three sets of filament lengths. This response has been illustrated in detail in Figures 58 and 59 for 10%RHA and 15%RRHA, respectively.

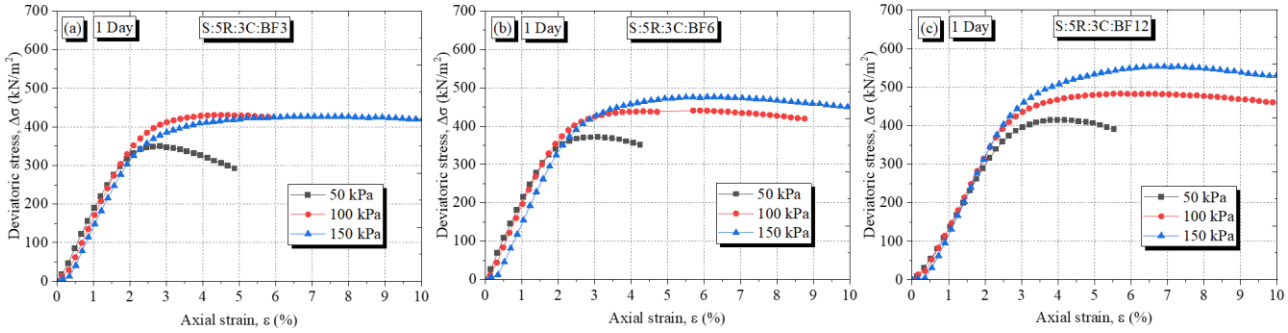

Figure 57 Stress-Strain relationship after 1 day of curing for 5%RHA-3%C specimen reinforced with **(a)** BF 3mm, **(b)** BF 6mm, and **(c)** BF 12mm.

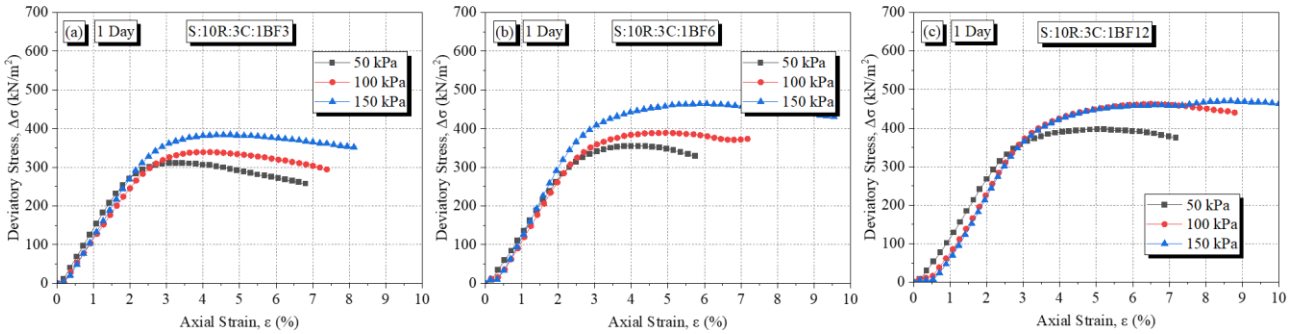

Figure 58 Stress-Strain relationship after 1 day of curing for 10%RHA-3%C specimen reinforced with **(a)** BF 3mm, **(b)** BF 6mm, and **(c)** BF 12mm.

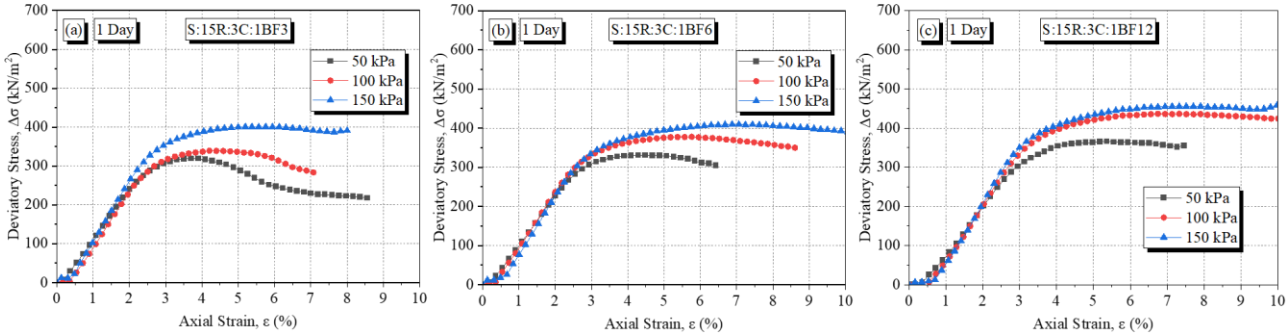

Figure 59 Stress-Strain relationship after 1 day of curing for 15%RHA-3%C specimen reinforced with **(a)** BF 3mm, **(b)** BF 6mm, and **(c)** BF 12mm.

The primary reason for this decrease in deviatoric stresses was the tendency of excess RHA to fill the voids in the soil matrix, which reduced the soil's porosity and density.

To further clarify the performance of different basalt fiber filament lengths, sets of specimens were moist-cured for 7 and 28 days, followed by testing to examine how the curing period influenced the shear characteristics, as shown in Figures 60 to 66. The results indicated a notable improvement in the deviatoric stresses (Δσ) compared to the 1-day curing results and the control specimen. This increase was due to the additional stiffness initiated by the fiber reinforcements and cementation from the pozzolanic reactions during curing. After 7 days, the deviatoric stresses (Δσ) with values 481.15 kN/m^2, 527.19 kN/m^2, and 557.39 kN/m^2 for 3 mm, 6 mm, and 12 mm filament length, respectively, were recorded for the fiber reinforced 5%RHA-3%C composites (Figure 60). The fiber-reinforced 10%RHA-3%C composites recorded deviatoric stresses (Δσ) with values 467.20 kN/m^2, 463.03 kN/m^2, and 507.44 kN/m^2 for 3 mm, 6 mm, and 12 mm filament length (Figure 61) while the 15%RHA-3%C composites recorded the lowest deviatoric stresses (Δσ) with values 431.55 kN/m^2, 431.59 kN/m^2, and 481.62 kN/m^2 for 3 mm, 6 mm, and 12 mm filament length(Figure 62). Despite the decrease in Δσ with increasing RHA content in the stabilized and reinforced soil composite, the attained values were still significantly higher than those of the control specimen (soil only).

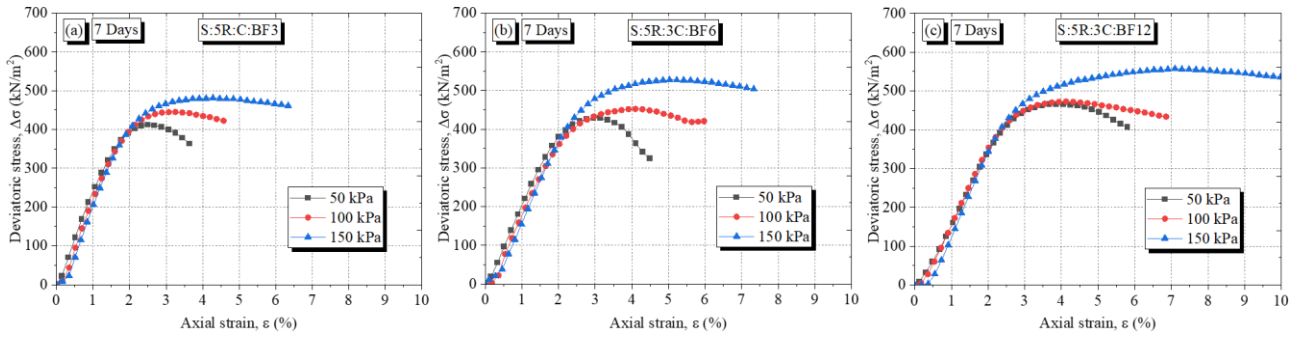

Figure 60 Stress-Strain relationship after 7 days of curing for 5%RHA-3%C specimen reinforced with **(a)** BF 3mm, **(b)** BF 6mm, and **(c)** BF 12mm.

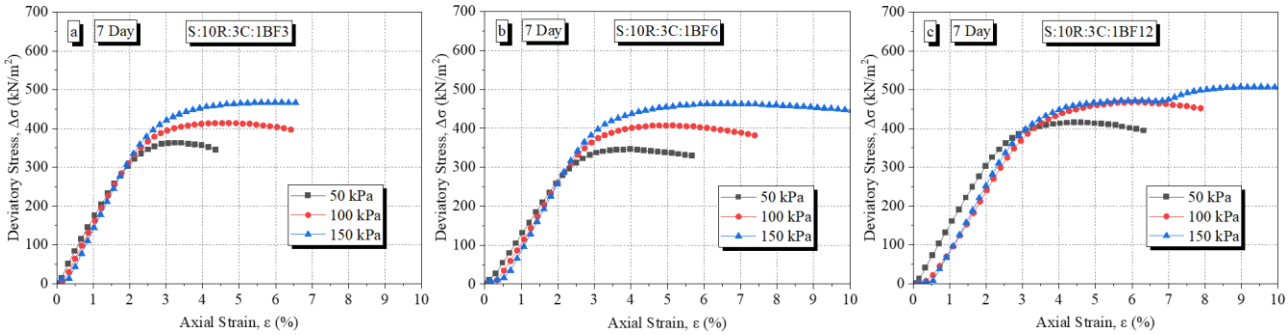

Figure 61 Stress-Strain relationship after 7 days of curing for 10%RHA-3%C specimen reinforced with **(a)** BF 3mm, **(b)** BF 6mm, and **(c)** BF 12mm.

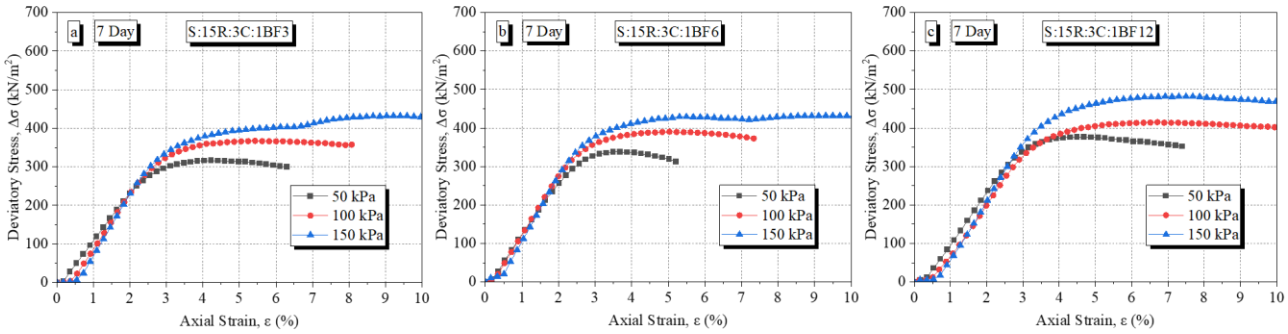

Figure 62 Stress-Strain relationship after 7 days of curing for 15%RHA-3%C specimen reinforced with **(a)** BF 3mm, **(b)** BF 6mm, and **(c)** BF 12mm.

The curing effect was more dominant after 28 days, where the record-high deviatoric stresses (Δσ) with values 537.33 kN/m^2, 569.91 kN/m^2, and 631.86 kN/m^2 for 3 mm, 6 mm, and 12 mm filament length, respectively, were recorded for the fiber reinforced 5%RHA-3%C composites, as shown in Figure 63. The fiber-reinforced 10%RHA-3%C composites recorded deviatoric stresses (Δσ) with values 490.55 kN/m^2, 509.65 kN/m^2, and 546.04 kN/m^2 for 3 mm, 6 mm, and 12 mm filament length (Figure 64) while the 15%RHA-3%C composites recorded the lowest deviatoric stresses (Δσ) with values 479.47 kN/m^2, 472.62 kN/m^2, and 490.03 kN/m^2 for 3 mm, 6 mm, and 12 mm filament length(Figure 65). Compared to the results after 7 days curing period, the decrease in Δσ with increasing RHA content in the stabilized and reinforced soil composite was still significantly higher than those of the control specimen (soil only). The maximized pozzolanic reactions after 28 days between soil particles, water, RHA, and cement, led to the formation of a strong and durable material hence the high deviatoric stresses.

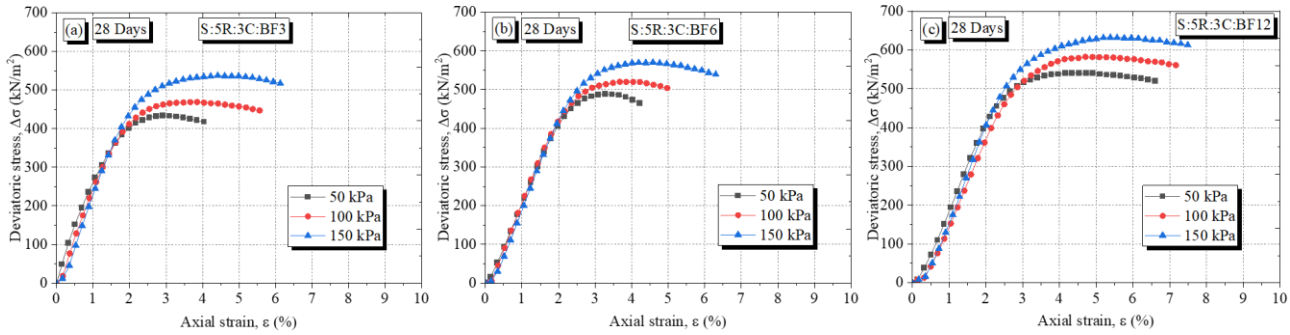

Figure 63 Stress-Strain relationship after 28 days of curing for 5%RHA-3%C specimen reinforced with **(a)** BF 3mm, **(b)** BF 6mm, and **(c)** BF 12mm.

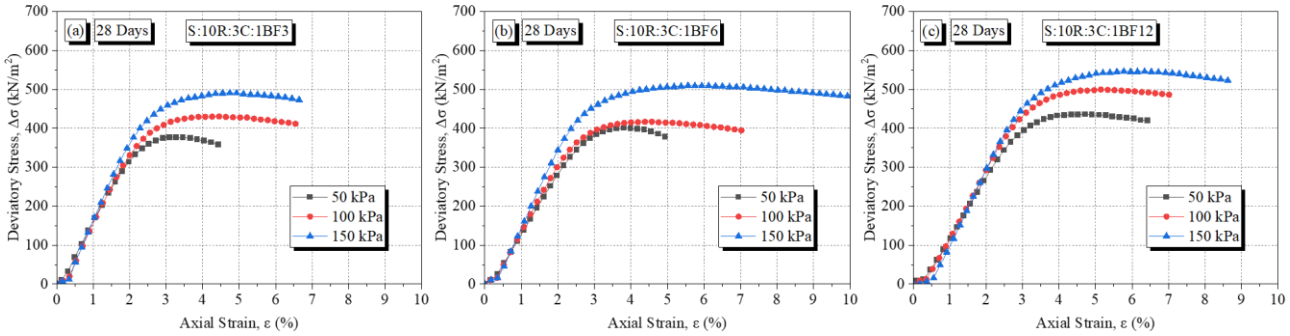

Figure 64 Stress-Strain relationship after 28 days of curing for 10%RHA-3%C specimen reinforced with **(a)** BF 3mm, **(b)** BF 6mm, and **(c)** BF 12mm.

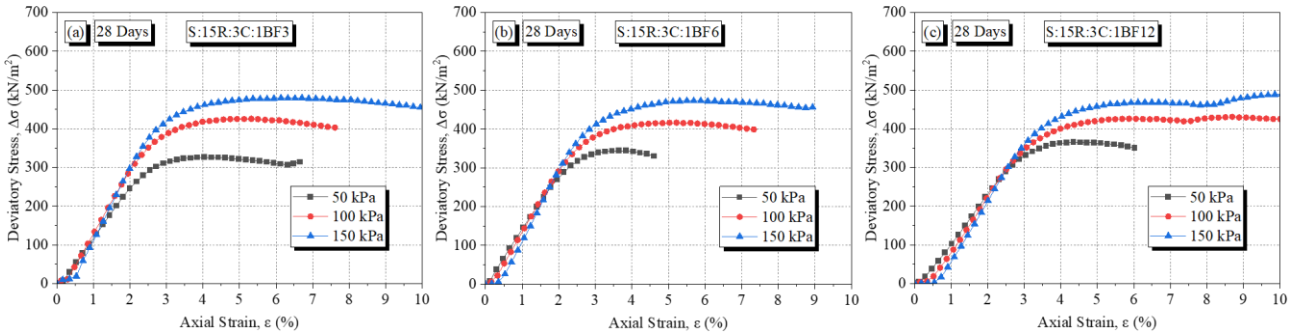

Figure 65 Stress-Strain relationship after 28 days of curing for 15%RHA-3%C specimen reinforced with **(a)** BF 3mm, **(b)** BF 6mm, and **(c)** BF 12mm.

These results concluded that the deviatoric stresses (Δσ) increased with the basalt fiber filament length and that significant improvement depended on the curing period allowed before testing. However, the developments in deviatoric stresses were mainly affected by the specimen composition; hence the reduced deviatoric stresses were recorded as the amount of RHA increased from 5% to 15%. On the other hand, adding longer basalt fiber filament lengths increased the value of axial strains (ε) required to achieve maximum deviatoric stresses in the specimens.

The interfacial forces between the fibers and the soil-RHA-cement composite were progressively mobilized at such high strain levels, reaching high levels of deviatoric stresses (Δσ) within the specimen (Consoli et al. 1999). Incorporating longer fiber filament lengths in the specimen enhanced the ductility, thus the ability to withstand maximum deviatoric stresses (Δσ) at high axial strains. Tang et al. (2007) and Consoli et al. (1999) showed a similar improvement in the ductility of fiber-reinforced soil composites. Additionally, the results depicted that a further increase in the strains after the peak deviatoric stress led to the loss of shear strength. However, the loss of shear strength followed a gradual projection due to the low elastoplastic deformations in the specimen along the failure plane. These deformations triggered the steady softening behavior. Consoli et al. (2007) and Heineck et al. (2005) also observed a similar gradual loss in shear strength at large shear strains while investigating the performance of fibers in sandy soil.

5.3.2 Specimens Failure Patterns

Furthermore, to understand the mechanical responses to shear for unreinforced and fiber-reinforced specimens, photo data showing the failure patterns for specimens tested after 28 days of moist curing were obtained, as illustrated in Figures 66 and 67 for unreinforced specimen and basalt fiber-reinforced specimens, respectively. The control specimen (soil only) and the unreinforced specimens experienced a simple shear with well-defined cracks forming along the failure plane, as shown in Figure 66. This cracking was due to the brittle nature of the soil once the maximum deviatoric stresses were achieved. However, adding basalt fibers arrested the formation of these cracks in the specimen, further enhancing ductility derived from the improved contact friction between basalt fibers and the soil-RHA-cement composite, as shown in Figure 67. Besides, there was a significant reduction in the visible vertical planes of weakness (cracks) as the filament lengths increased from 3 mm to 6 mm to 12 mm, thus depicting additional elasticity in the specimens. Similar results on the

effectiveness of fibers in arresting cracking in fiber-reinforced soil composites were also observed in other studies (Ghorbani and Salimzadehshooiili, 2019; Yadav et al., 2018).

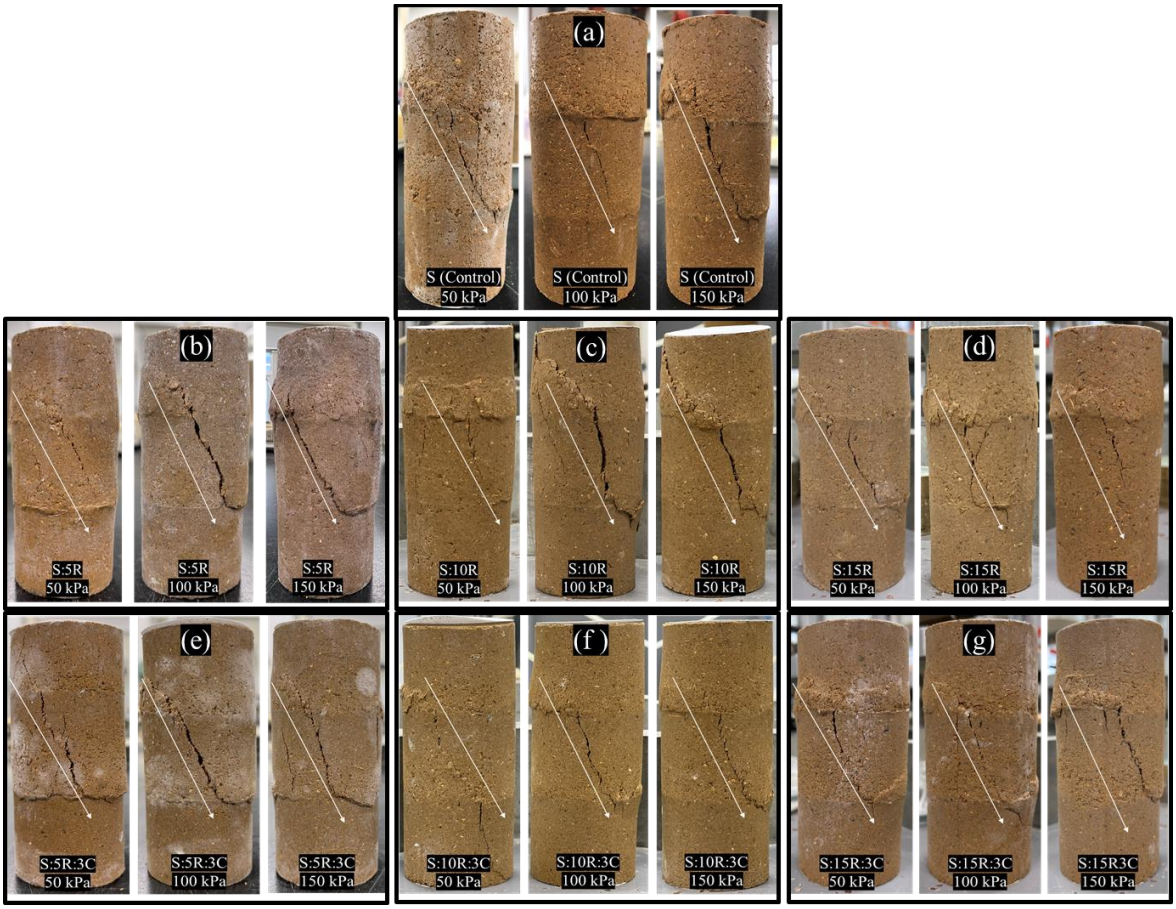

Figure 66 The failure planes of unreinforced specimens at 50, 100, and 150 kPa confining pressure.

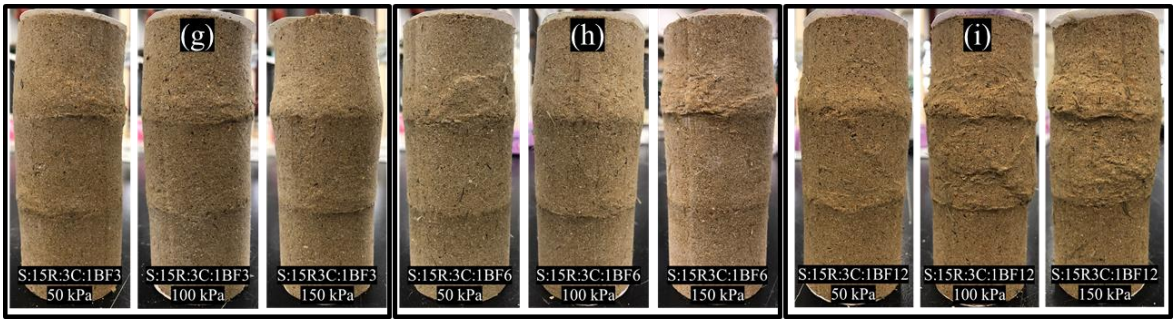

Figure 67 The failure planes of reinforced specimens at 50, 100, and 150 kPa confining pressure.

5.3.3 Shear Strength Parameters: Mohr-Coulomb failure theory

In this study, shear parameters of the stabilized expansive soil were quantified using the Mohr-Coulomb failure theory, presented in terms of the shear strength (τ) versus effective normal stress (σ). Considering specimens subjected to different stress conditions, simulating the in-situ stress variations with depth, the failure stress circles corresponding to the various stresses (50 kPa, 100 kPa, and 150 kPa) were represented by points A, B, and C, respectively, as illustrated in Figure 68. A tangent line to the Mohr semi-circles satisfied the general failure criterion, and values of cohesion in kN/m^2 and angle of internal friction in radians was evaluated from the straight-line equation to represent stress states at failure.

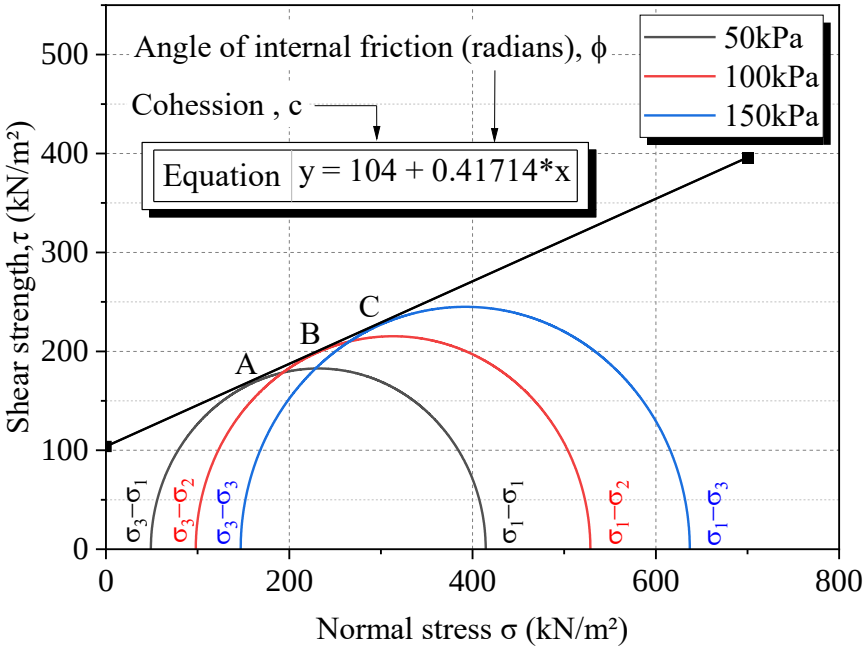

Figure 68 Stress circles at failure corresponding to different principal stresses..

Representative plots of the Mohr Columb stress circles for specimens tested after 28 days of curing were shown in Figures 69 to 71 for the unreinforced specimens (Control, S:5%, and S:5R:3C). Notably, the shear parameters, i.e., cohesion and angle of internal friction, increased considerably with the addition of RHA and RHA-Cement mixtures for the unreinforced specimens. Also, significant developments were observed as the curing period increased from 1 day to 28 days for all data sets (Control, S:5%, and S:5R:3C)

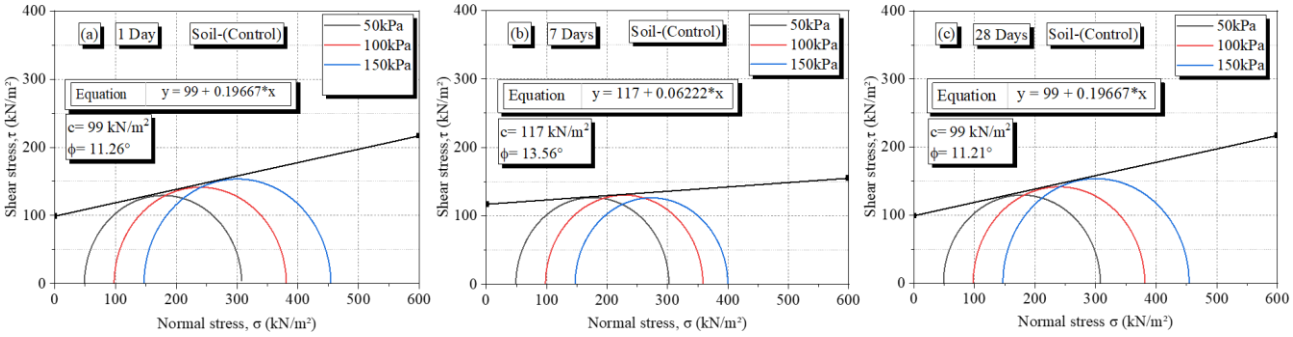

Figure 69 Mohr Columb stress circles for the soil-(Control) specimens: **(a)** after 1 day of curing, **(b)** after 7 days of curing, **(c)** after 28 days of curing.

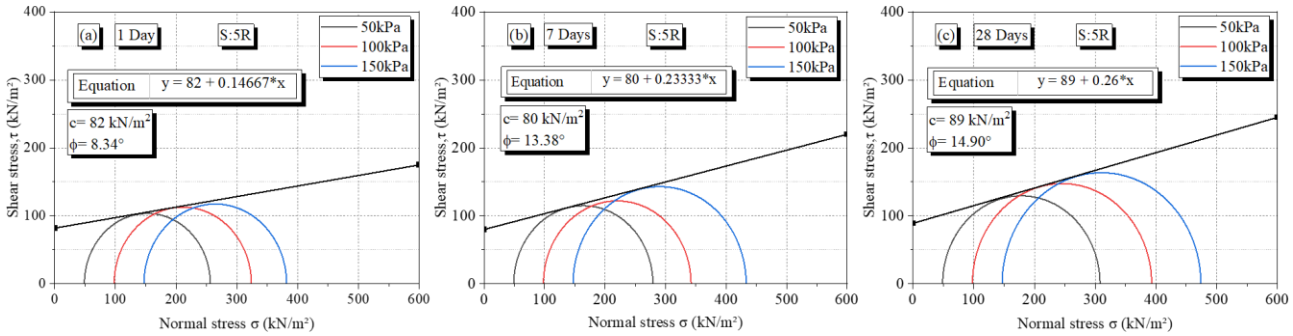

Figure 70 Mohr Columb stress circles for the S:5RHA specimens: **(a)** after 1 day of curing, **(b)** after 7 days of curing, **(c)** after 28 days of curing.

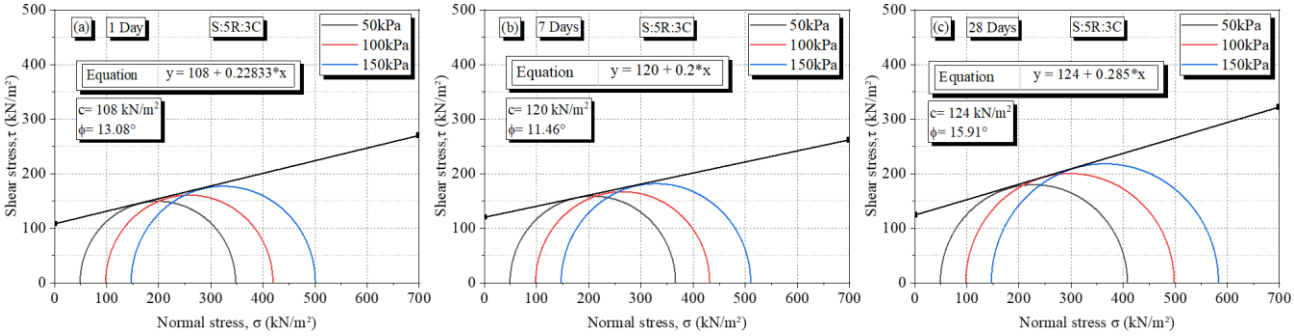

Figure 71 Mohr Columb stress circles for the S:5RHA:3C specimens: **(a)** after 1 day of curing, **(b)** after 7 days of curing, **(c)** after 28 days of curing.

Figures 72 to 80 presented the Mohr Columb stress circles for the reinforced specimens. The development in shear parameters was dictated by the curing period, basalt fiber length, and the specimen structural composition (Soil:RHA:Cement).

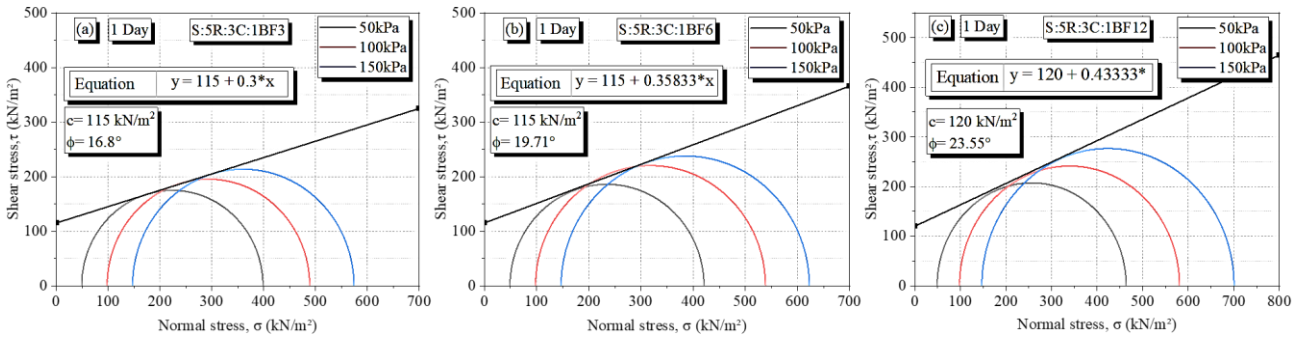

Figure 72 Mohr Columb stress circles for the 5RHA:3C fiber reinforced specimens after 1 day of curing **(a)** S:5R:3C:1BF3 **(b)** S:5R:3C:1BF6 **(c)** S:5R:3C:1BF12.

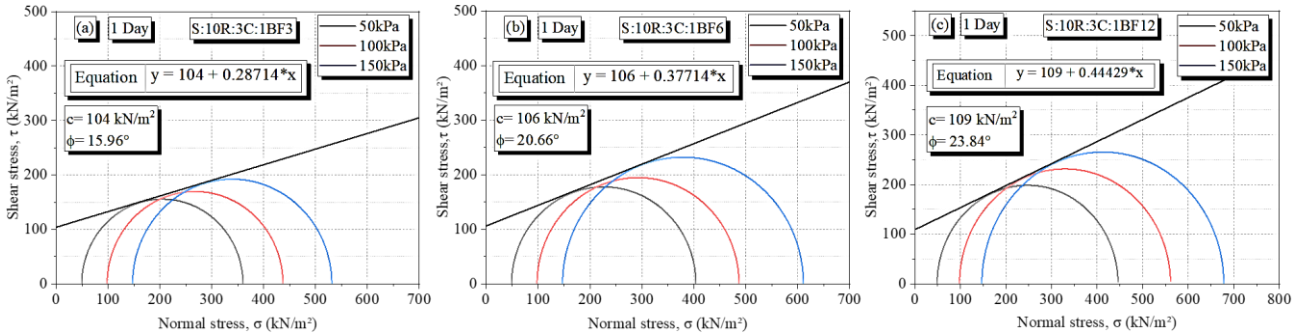

Figure 73 Mohr Columb stress circles for the 10RHA:3C fiber reinforced specimens after 1 day of curing **(a)** S:5R:3C:1BF3 **(b)** S:5R:3C:1BF6 **(c)** S:5R:3C:1BF12.

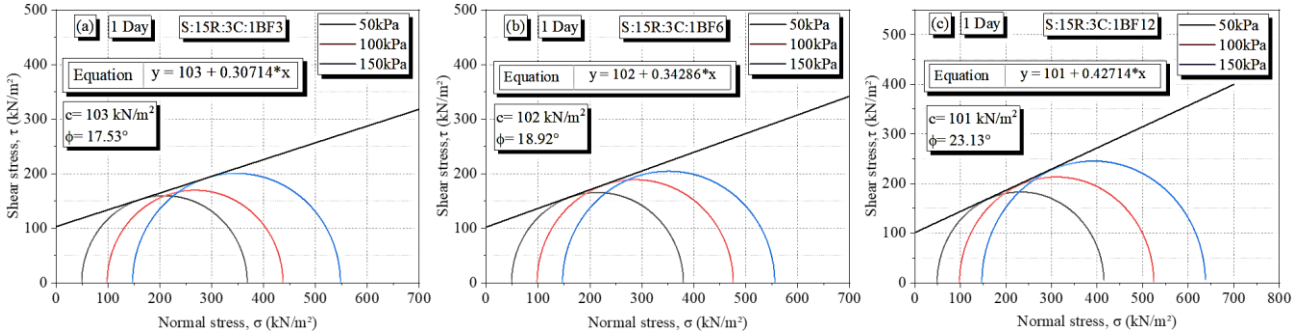

Figure 74 Mohr Columb stress circles for the 15RHA:3C fiber reinforced specimens after 1 day of curing **(a)** S:5R:3C:1BF3 **(b)** S:5R:3C:1BF6 **(c)** S:5R:3C:1BF12.

Fibers added to the soil increased the ultimate tensile strength and resistance to cracking and deformation. This increase, in turn, led to a shift in the Mohr-Coulomb failure envelope toward higher values of shear strength (c and ϕ), as shown by the stress circles in the graph (Figure 72-80).

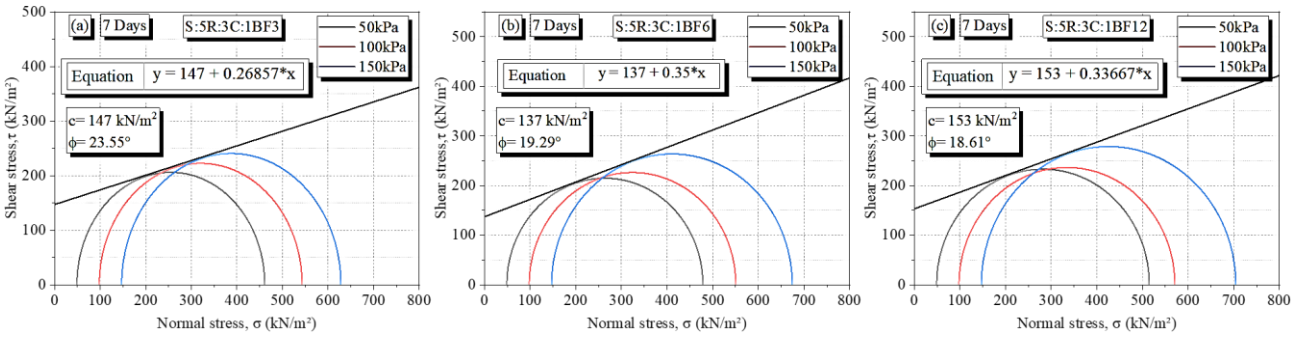

Figure 75 Mohr Columb stress circles for the 5RHA:3C fiber reinforced specimens after 7 days of curing **(a)** S:5R:3C:1BF3 **(b)** S:5R:3C:1BF6 **(c)** S:5R:3C:1BF12.

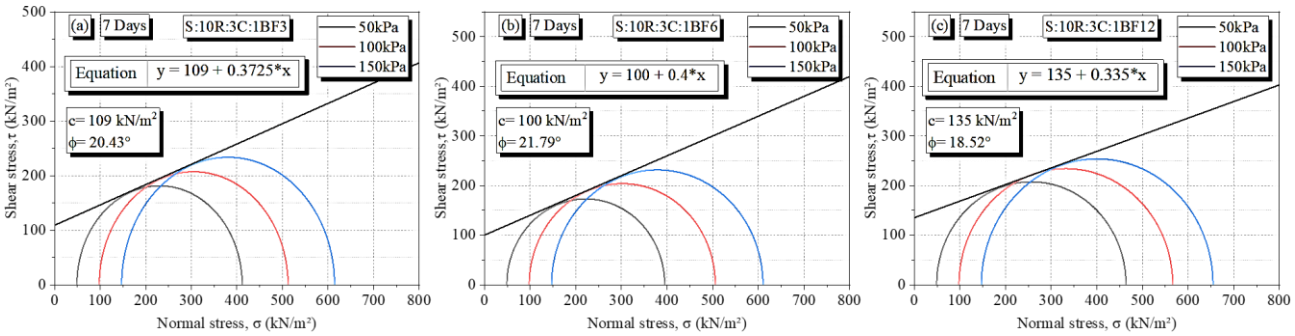

Figure 76 Mohr Columb stress circles for the 10RHA:3C fiber reinforced specimens after 7 days of curing **(a)** S:5R:3C:1BF3 **(b)** S:5R:3C:1BF6 **(c)** S:5R:3C:1BF12.

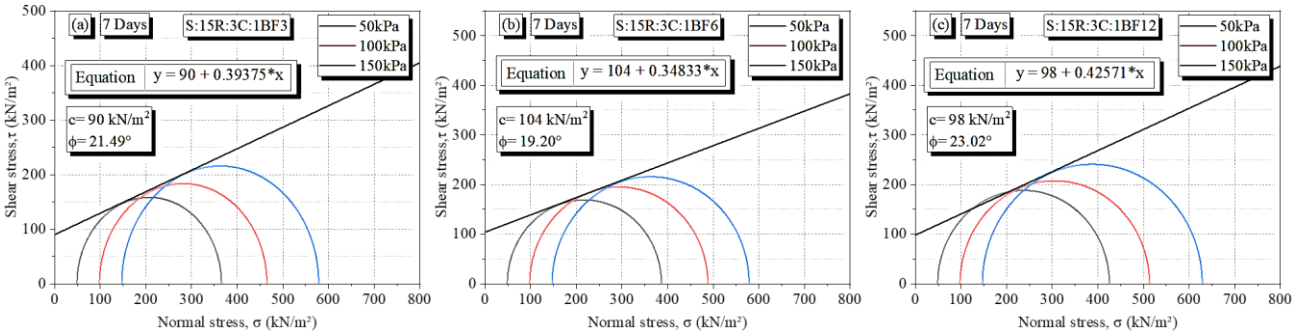

Figure 77 Mohr Columb stress circles for the 15RHA:3C fiber reinforced specimens after 7 days of curing **(a)** S:5R:3C:1BF3 **(b)** S:5R:3C:1BF6 **(c)** S:5R:3C:1BF12.

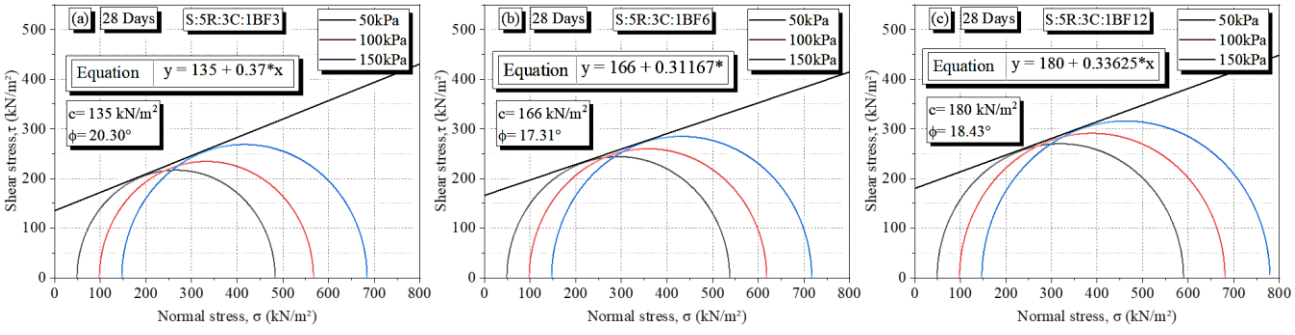

Figure 78 Mohr Columb stress circles for the 5RHA:3C fiber reinforced specimens after 28 days of curing **(a)** S:5R:3C:1BF3 **(b)** S:5R:3C:1BF6 **(c)** S:5R:3C:1BF12.

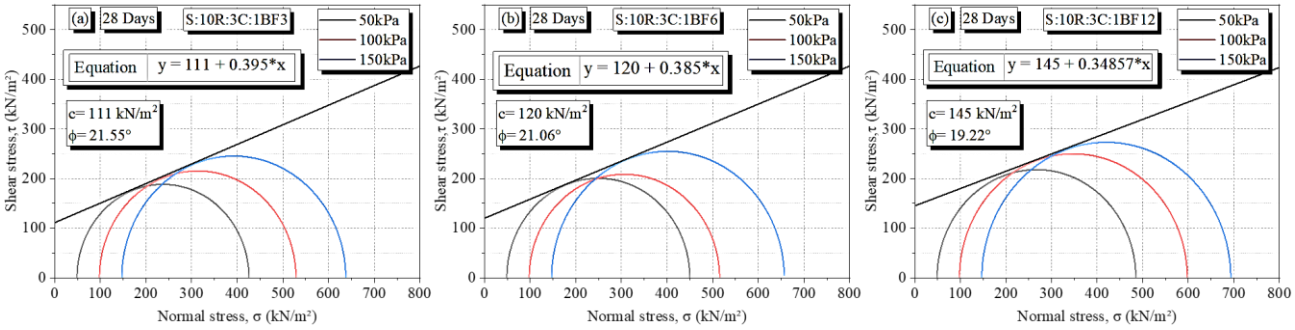

Figure 79 Mohr Columb stress circles for the 10RHA:3C fiber reinforced specimens after 28 days of curing **(a)** S:5R:3C:1BF3 **(b)** S:5R:3C:1BF6 **(c)** S:5R:3C:1BF12.

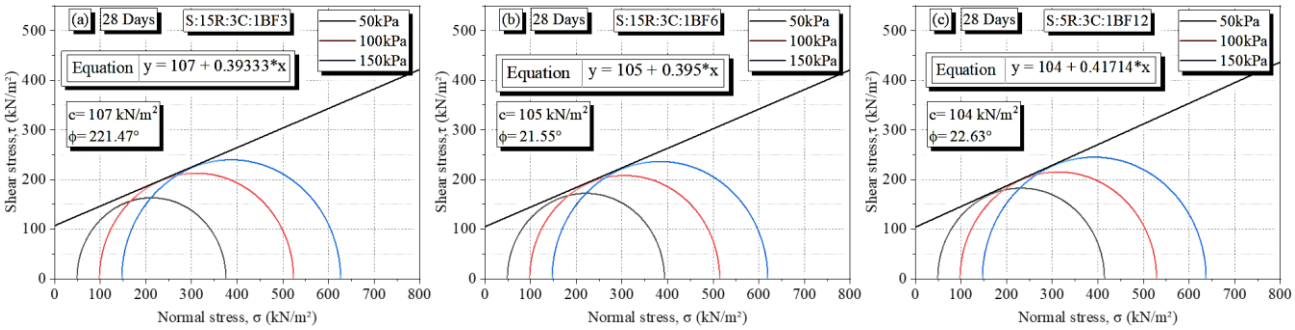

Figure 80 Mohr Columb stress circles for the 15RHA:3C fiber reinforced specimens after 28 days of curing **(a)** S:5R:3C:1BF3 **(b)** S:5R:3C:1BF6 **(c)** S:5R:3C:1BF12.

In Figure 81, a correlation of the cohesion values for the unreinforced and fiber-reinforced composites with the curing period was analyzed. From Figure 81 (a), the S:5R specimens recorded the lowest cohesive strengths due to the limited calcium ions leading to weaker cementitious bonds in the composite matrix. A similar trend was observed for the S:10R [Figure 81(b)] and S:15R [Figure 81 (c)]. Conversely, the cohesion of the control specimen increased after 7 days of curing. Then it reduced considerably after 28 days of curing due to the degradation of the soil particle bonds. However, upon adding a nominal dosage of cement, a steady increase in the cohesive strength was noted for the S:5R:3C specimen, with c increasing from 108 kN/m^2 to 120 kN/m^2 and ultimately to 124 kN/m^2 for 1 day, 7 days, and 28 days respectively. A similar trend was observed for the S:10R:3C [Figure 81(b)] and S:15R:3C [Figure 81 (c)], with a reduction in the cohesive strength to 107 kN/m^2 and 104 kN/m^2, respectively, as the amount of RHA in the composite matrix increased from 5% RHA to 10%RHA and ultimately to 15%RHA.

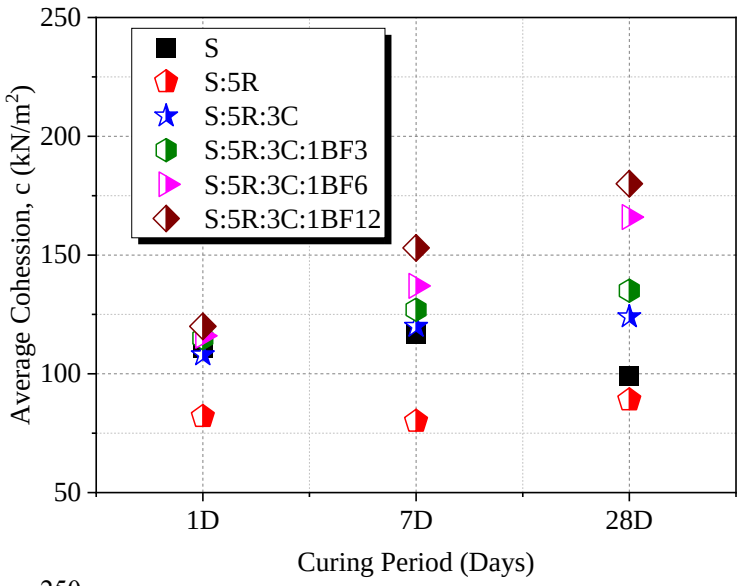

Figure 81 (a) Cohesive strength of 5%RHA:3C specimen reinforced with different lengths of Basalt Fibers (BF 3mm, BF 6mm and BF 12mm).

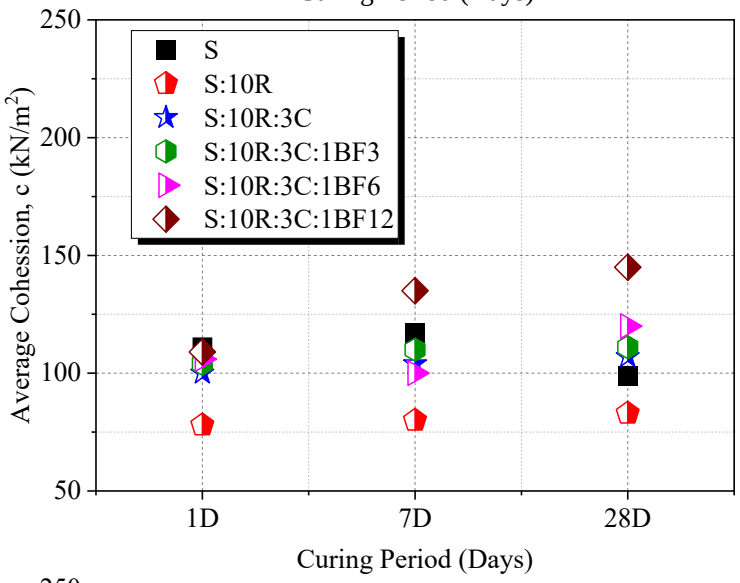

Figure 81 (b) Cohesive strength of 10%RHA:3C specimen reinforced with different lengths of Basalt Fibers (BF 3mm, BF 6mm and BF 12mm).

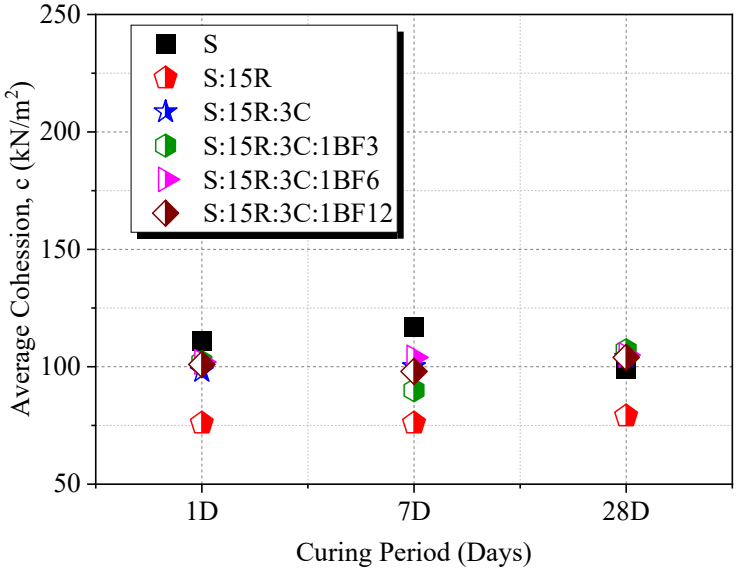

Figure 81 (c) Cohesive strength of 15%RHA:3C specimen reinforced with different lengths of Basalt Fibers (BF 3mm, BF 6mm and BF 12mm).

Figure 81 Cohesive strength with curing period.

On the other hand, basalt fiber addition into the chemically stabilized specimen significantly improved the cohesion at each curing stage. However, the increasing cohesion value depended on the basalt fiber filament length present in the specimens. For instance, the specimens containing 12 mm basalt fiber filaments attained the highest cohesion of 180 kN/m^2 after 28 days of curing compared to the 166 kN/m^2 and 135 kN/m^2 obtained from the 6 mm and 3 mm specimens, respectively. It can be concluded that longer basalt fiber filament lengths strengthened the reinforcement effects by efficiently distributing the loads to adjacent fibers, enabling the stabilized specimen to act as a dense structure through fiber interactions. Using shorter fibers (6 mm and 3 mm) lowered the cohesion due to the reduced fiber contact areas hence a less dense network in the specimen. This phenomenon was observed by other researchers (Nguyen and Fatahi, 2016).

Additionally, as the RHA content increased from 5% to 15%, the cohesive strength of the stabilized and reinforced soil decreased. The reduction in the cohesive strength of RHA-stabilized soil with increased RHA content was attributed to the following factors: (i) adding RHA increased the soil's porosity, reducing its density and strength, filling the gaps between the soil particles and creating additional spaces that reduced particle-to-particle contact, (ii) the addition of RHA altered the particle size distribution of the soil, which led to a weaker soil structure. The particle size distribution was a critical factor in determining the soil's strength and stability, and any changes to this distribution significantly affect the soil's engineering properties. However, it was noteworthy that adding basalt fiber reinforcements into the 10%RHA specimens significantly improved the cohesive strength compared to the control specimen. For instance, the maximum cohesive strength of 145 kN/m^2 was attained by adding 12 mm basalt fibers for specimen combination S:10R:3C:1BF12.

To address the reduction in cohesive strength of RHA-stabilized soil with increased RHA content, it is crucial to balance the RHA content to achieve the desired level of soil stabilization without compromising the soil's cohesive strength. Testing and analyzing the stabilized soil under varying

RHA contents can help identify the optimal RHA content for a particular application. Moreover, it is essential to ensure that the soil is given sufficient curing time to reach its maximum strength, regardless of the RHA content.

It was also recognized that the angle of internal friction of the fiber-reinforced specimen improved compared to the unreinforced soil, as shown in Figure 82. The angle of internal friction is a measure of the resistance of soil to shear deformation. The increase in the angle of internal friction of RHA stabilized, and basalt fiber reinforced soil as the length of basalt fibers increases from 3 mm to 12 mm can be attributed to several factors. Firstly, adding the soil stabilizing agents (RHA and cement) enabled large clusters to form and, in turn, increased the grain-to-grain contact during shearing. Secondly, adding basalt fibers to the stabilized soil composite improved the physical interaction between the soil clusters by anchoring them together to form a denser structural framework that enhanced frictional resistances during shearing. Thirdly, longer basalt fibers had a greater surface area per unit volume than shorter fibers creating more surface area for the RHA-cement composite to bond with, resulting in a stronger bond between the RHA, cement, and the basalt fibers. The increased bonding strength helped reinforce the soil and its resistance to shear deformation. However, slight variations were recorded as the RHA content increased from 5% to 15% due to the corresponding modifications in the specimen structure during the curing period. Fourthly, longer basalt fibers bridged larger gaps between soil particles, creating a more robust network of interlocking fibers within the soil, distributing the stress more evenly throughout the soil and preventing localized failure. Finally, longer basalt fibers also acted as a physical barrier, preventing the movement of soil particles and reducing the potential for shear deformation. This effect was more pronounced at longer fiber lengths, as the fibers spanned considerable distances between particles. A clear representation of the influence generated by RHA content, basalt fiber length, minimal cement dosage, and curing period has been illustrated in Figure 82.

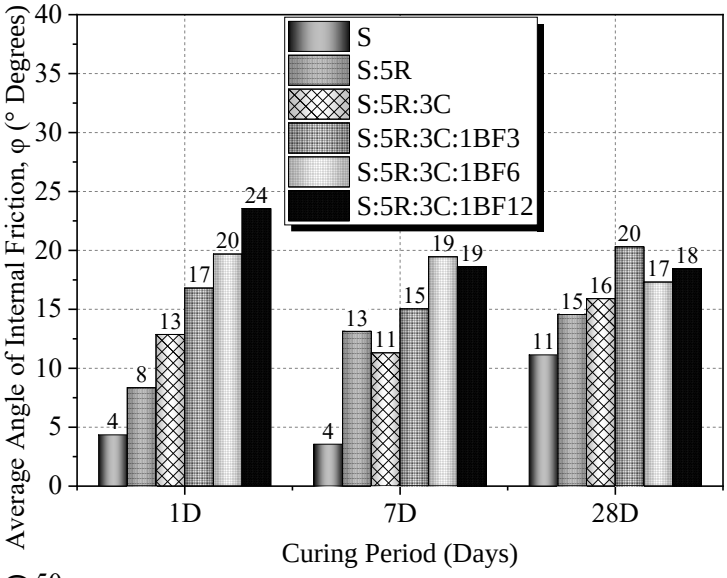

Figure 82 (a) Angle of internal friction of 5%RHA:3C specimen reinforced with different lengths of Basalt Fibers (BF 3mm, BF 6mm and BF 12mm).

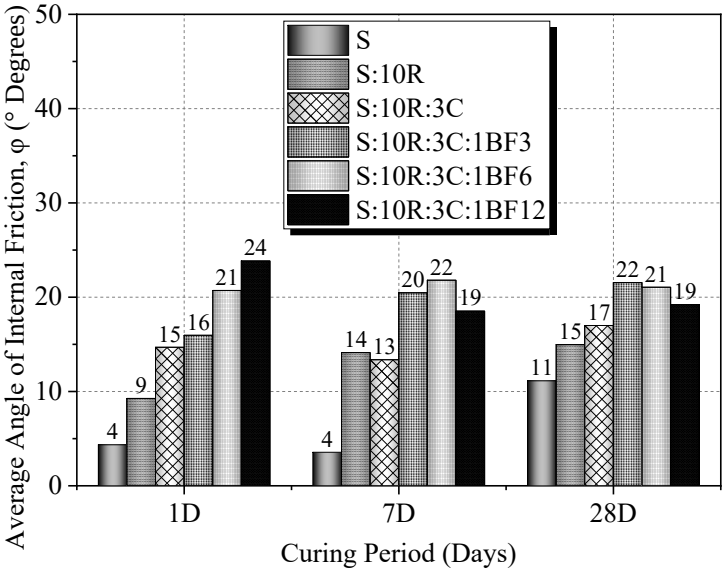

Figure 82 (b) Angle of internal friction of 10%RHA:3C specimen reinforced with different lengths of Basalt Fibers (BF 3mm, BF 6mm and BF 12mm).

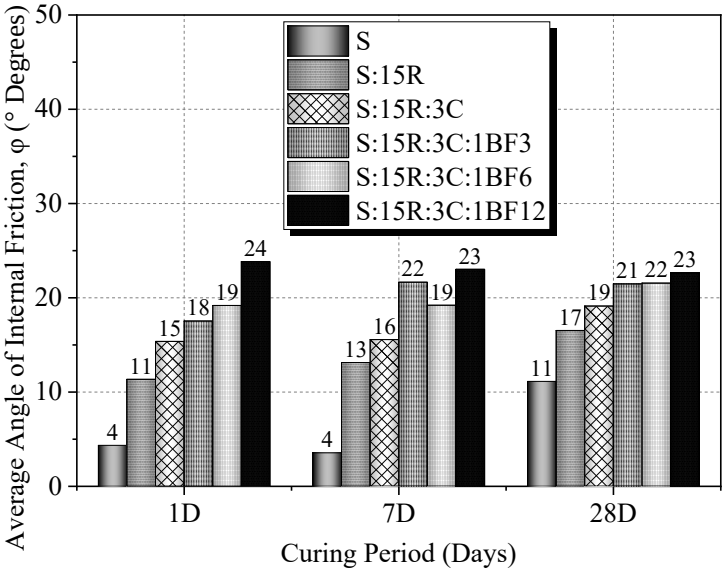

Figure 82 (c) Angle of internal friction of 5%RHA:3C specimen reinforced with different lengths of Basalt Fibers (BF 3mm, BF 6mm and BF 12mm).

Figure 82 The angle of internal friction with the curing period.

Further, to uphold the significance of this research, a comparison between the shear strength parameters of this study with other relevant studies was established, considering different types of fibers and stabilization methods. Comparing our findings with other relevant findings done before is an essential aspect of research because it provides a context for our study and enables us to evaluate the novelty and significance of our results. By comparing our findings with prior research, we can identify areas of agreement and disagreement and assess the consistency and generalizability of our results. Notably, the new composite containing 5%RHA, 3% cement, and 12 mm basalt fibers attained the highest cohesion values compared to the composites reinforced with sisal (Wu et al., 2014), jute (Yixian et al., 2016), and polypropylene fibers (Cai et al., 2006) and the unreinforced composites containing RHA (Nahar et al., 2021) and cement (Ghadakpour et al., 2020) [Figure 83 (a)]. For example, Najmun et al. showed that stabilizing expansive soils with 5% RHA attained a maximum cohesive strength value of 85 kN/m^2. In another relevant study, Ghadakpour et al. (2020) showed that adding nominal cement dosages (2%) increased the cohesive strength to 100 kN/m^2 (Cai et al., 2006). However, in this study, adding 12mm basalt fibers to such composites significantly increased cohesive strength to 180 kN/m^2 with percentage increases of 112% and 80% compared to the 5%RHA and 3% cement composites, respectively.

Additionally, changes in fiber type showed an increase in cohesive strength by up to 44%, 58%, and 8% for the jute fiber, sisal fiber, and polypropylene fiber, respectively, compared to the cohesive strength of 12 mm basalt fiber reinforced composites. On the other hand, in Figure 83 (b), the variation in the angle of internal friction was less significant for the fiber-reinforced composites. Jute fiber and sisal fiber showed an average ϕ of 25.8%, indicating a 545% increase compared to the ϕ of the control specimen (S-Control). This study recorded a 350% increase in ϕ, indicating significant developments in ϕ compared to the control specimen (S-Control). However, studies by Najmun et

al. (2121), Cai et al. (2006), and Ghadakpour et al. (2020) showed slightly higher ϕ values due to the higher percentages of sand content in the clayey soil used in their study.

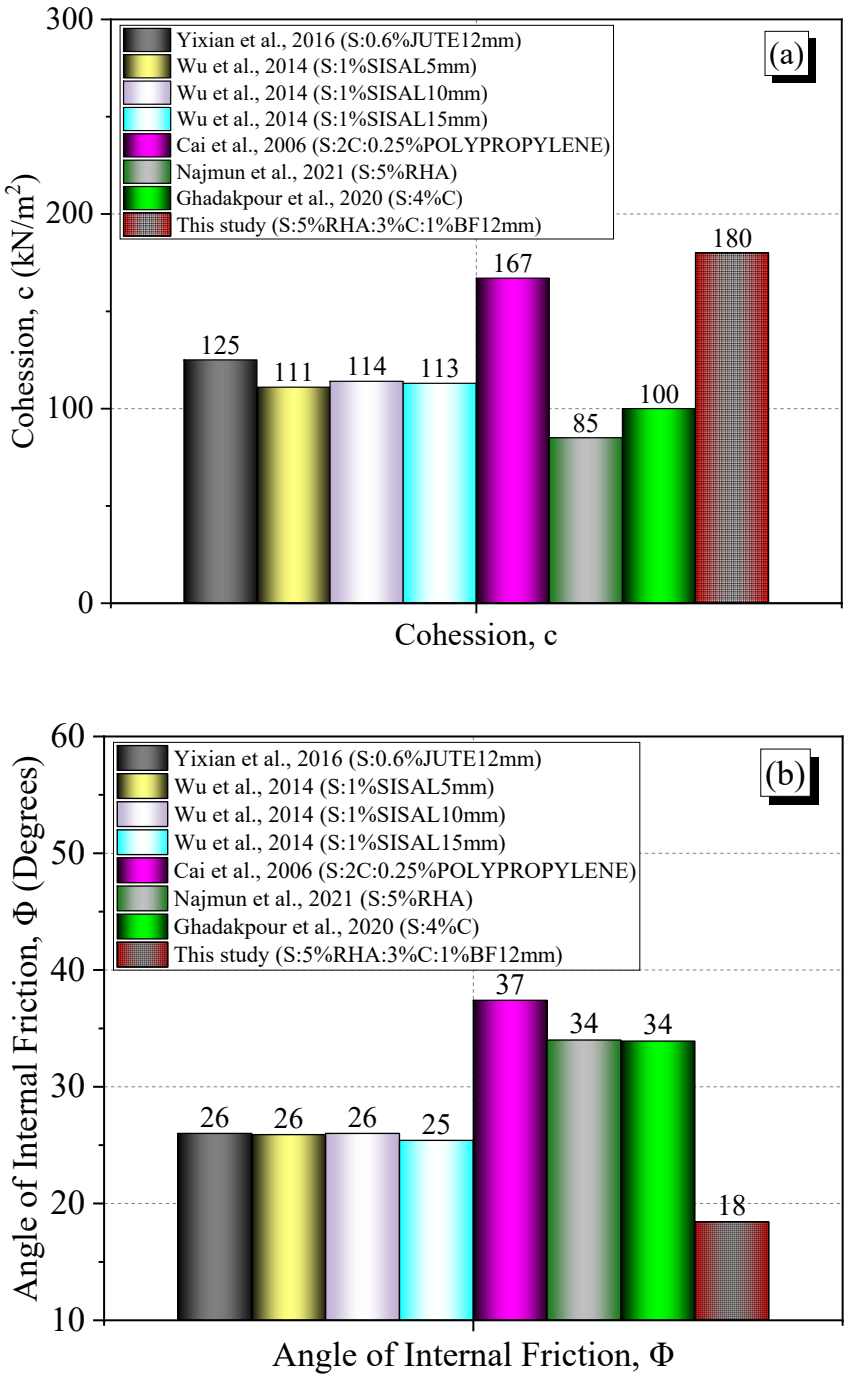

Figure 83 A comparison between shear strength parameters with relevant studies **(a)** Cohesion **(b)** Angle of internal friction.

5.4 Unconfined Compression Strength Results

5.4.1 Stress-Strain Relationships (σ, ε)

This section shows the relationship between compressive stress (q_u) and axial strain (ε) for RHA percentages (5%, 10%, and 15%), 3% cement, and basalt fiber lengths (3mm, 6mm, and 12mm). In Figure 84 (a), the maximum compressive stresses, q_u, were achieved with 5% RHA specimen at lower axial strains, ε, compared to the control. In Figures 84 (b) and 84 (c), adding RHA to 10% and 15% reduced the compressive stresses with a slight increase in the axial strain for all basalt fiber lengths. Basha et al. (2005) and Rao et al. (2011) also observed a similar trend in axial strain versus RHA. Compressive stress reduction can be attributed to the reduced cementitious properties due to excess RHA, hence less bonding of soil particles and basalt fibers, leading to increased axial displacements. Nevertheless, all 10% RHA and 15% RHA specimens produced significant stress-bearing capacity compared to the control specimen.

Correspondingly, curing period was considered for 1 day, 7 days, and 28 days as shown in Figure 85. A slight improvement in q_u was observed from the graph for all the specimens after 7 days of curing. For example, specimen S:5R:3C:1BF12 had an unconfined compressive strength (UCS) of 292 kN/m^2 after one day, and the value increased to 318 kN/m^2 at 7 days of curing. After 28 days of curing, there was a significant increase in the UCS value for S:5R:3C:1BF3, S:5R:3C:1BF6, and S:5R:3C:1BF12 specimens with values 438 kN/m^2, 453 kN/m^2 and 463 kN/m^2 respectively. The soil matrix also gained strength with an increase in the length of basalt fibers which enhanced the bonding of soil particles by anchoring them together. The highest compressive strengths considering basalt fiber length were obtained from S:5R:3C:1BF12 (463 kN/m^2), S:10R:3C:1BF12 (362 kN/m^2), S:15R:3C:1BF12 (297 kN/m^2) compared to the control specimens'147 kN/m^2. The UCS increased due to the basalt fiber reinforcements, as seen in this study, and chemical reaction in the soil matrix, leading to silica gel formation (Kumar et al., 2006).

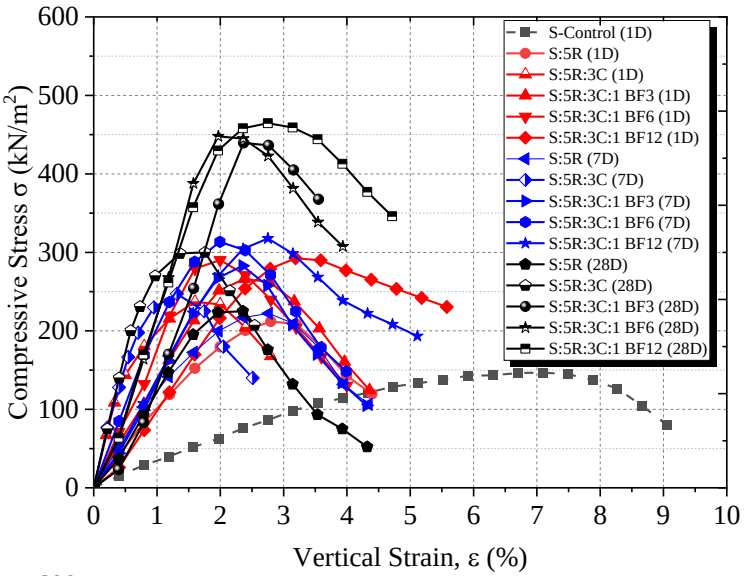

Figure 84 (a) Stress-strain relationship of 5%RHA specimen reinforced with different lengths of Basalt Fibers (BF 3mm, BF 6mm and BF 12mm) with curing period.

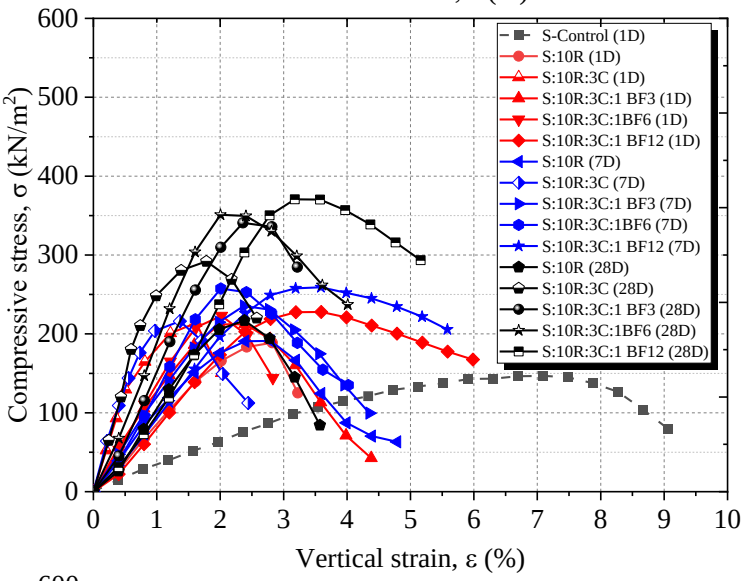

Figure 84 (b) Stress-strain relationship of 10%RHA specimen reinforced with different lengths of Basalt Fibers (BF 3mm, BF 6mm and BF 12mm) with curing period.

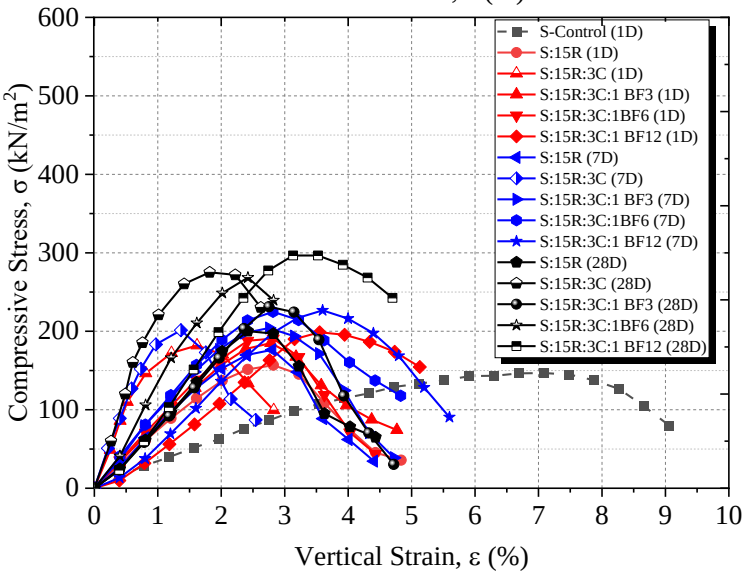

Figure 84 (c) Stress-strain relationship of 15%RHA specimen reinforced with different lengths of Basalt Fibers (BF 3mm, BF 6mm and BF 12mm) with curing period.

Figure 84 UCS test stress-strain relationships.

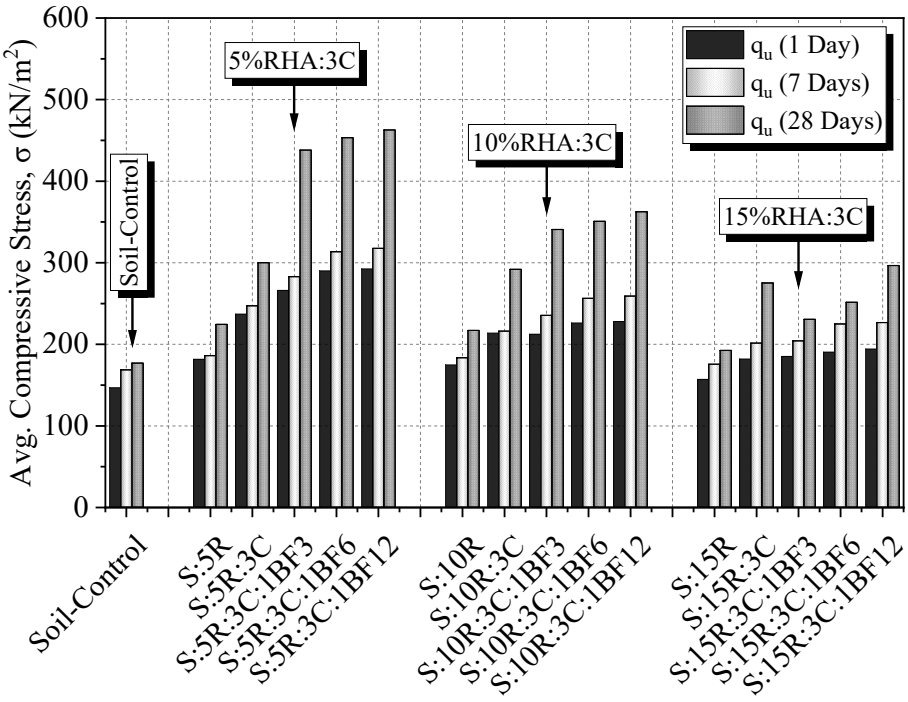

Figure 85 Variation of UCS test compressive stress (q_u) with curing period.

Das (2021) classified the quality of subgrade based on UCS value, with hard sub-base having UCS values greater than 380kN/m^2. From this study, S:5R:3C:1BF12 produced a compressive strength of 463 kN/m^2 and can be used as subgrade material for construction works.

5.4.2 Specimen Failure Patterns

In addition, to comprehend the mechanical reactions to shear in unreinforced and fiber-reinforced specimens, photographs of the failure patterns in specimens tested after 28 days of moist curing were taken. These images, depicted in Figure 86, show the failure patterns for the unreinforced specimen and the basalt fiber-reinforced specimens, respectively. Figure 86 summarises the failure planes for the control specimen (S) and the unreinforced and the basalt fiber-reinforced specimen. Upon maximum compression load, the unreinforced specimens experienced a simple shear failure with a diagonal failure plane on the upper layers. On the other hand, the fiber-reinforced specimen showed some resistance to failure due to the multiple failure planes evident on the specimen surface upon maximum load. It was observed that cracks occurred in the vertical plane for the control specimen

at a strain of 7%. However, adding basalt fibers reduced this strain value considerably to less than 3% for the stabilized and reinforced specimen. This reduction in axial strain is shown in Figure 87 for 5%, 10%, and 15% RHA soil composites.

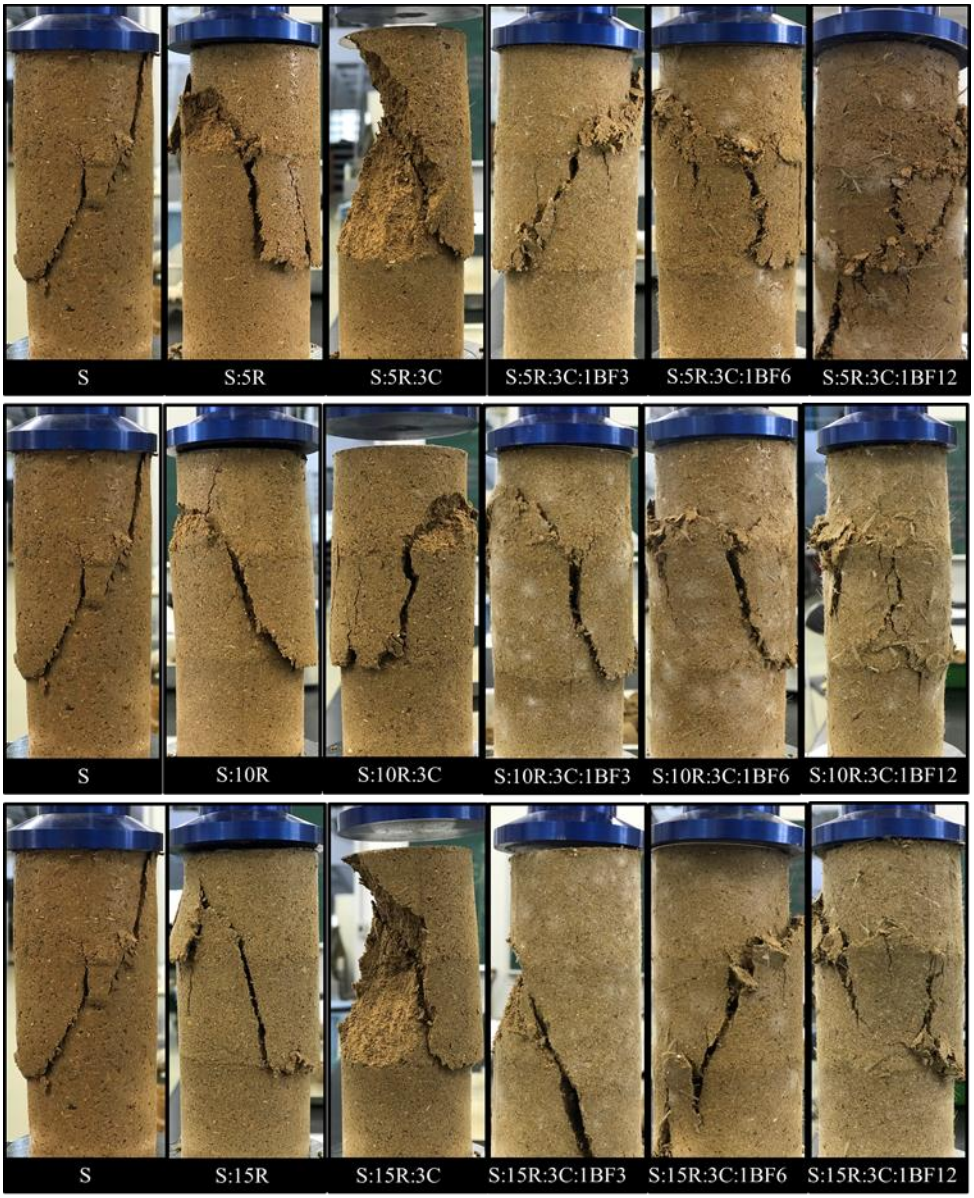

Figure 86 UCS test specimen failure patterns.

Amongst the basalt fiber specimen, 12mm long fibers had a 1% increase in axial strain compared to BF 3mm and BF 6mm. The increase was due to the slight extra deformations during compression, which were required to tension the randomly placed long 12mm basalt fibers in the specimen

structure before the reinforcing benefits were realized. Lawton et al. (1993) reported a relatable increase in strain value using multi-oriented geosynthetics. The axial strains reduced slightly after 28 days of curing, signifying shear strength and stiffness development in the soil specimen.

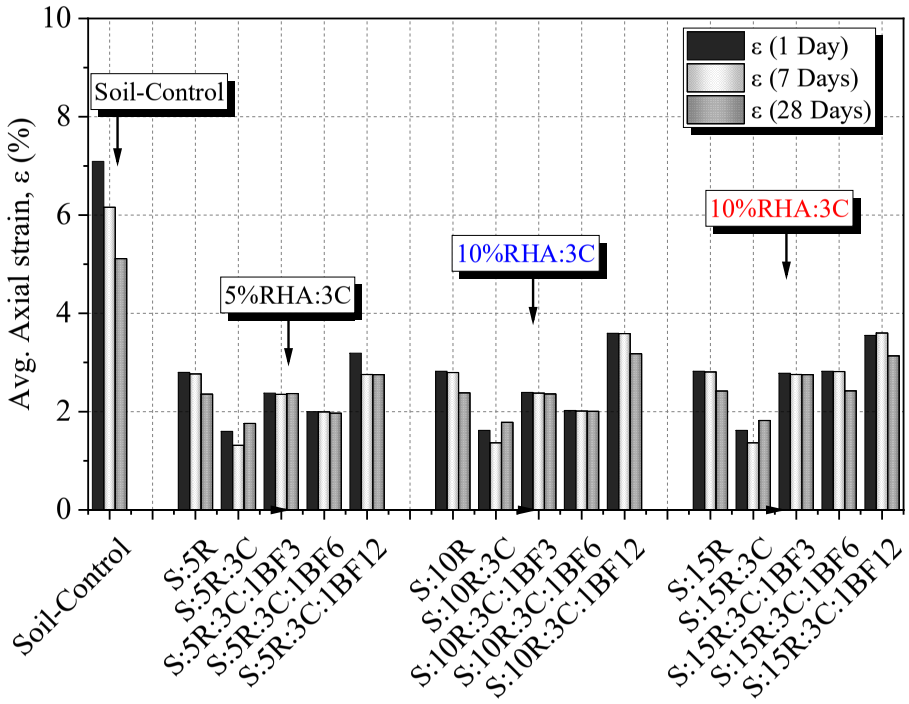

Figure 87 Variation in axial strain with curing period.

5.4.3 Modulus of Deformation (E_{50})

For better clarification on the field use of the results, Figure 88 shows the relationship between the modulus of deformation, E_{50}, and the curing period. The modulus of deformation, also known as the secant modulus or tangent modulus, is a measure of a material's stiffness or resistance to deformation under an applied load. E_{50} refers explicitly to the modulus of deformation at 50% of the ultimate tensile strength of a material. It is calculated by dividing the stress at 50% of the maximum tensile strength by the corresponding strain. The resulting value represents the material's stiffness in the linear region of the stress-strain curve.

The modulus of deformation is an important mechanical property used in the design and analysis of composite materials, as it helps to predict how a material will behave under loading conditions. This

study observed a significant increase in E_{50} after 28 days of curing, with 5% mix ratios giving the highest values. For mix ratios, 5R, S:5R:3C:1BF3, S:5R:3C:1BF6, S:5R:3C:1BF12, the modulus of deformations were 16MPa, 20Mpa, 26MPa, and 29MPa, respectively, which were much higher compared to control specimen (3MPa). Specimen S:5R:3C:1BF12 gave the maximum E_{50} due to the high compressive stress of 463 kN/m^2 and additional reinforcing effect after the tensioning of the longer fibers compared to the fiber lengths of 3mm and 6mm. The dimensional configurations of the basalt fibers and the random distribution of the 12mm fibers reinforced a larger area in the composite soil structure than the shorter 3mm and 6mm upon full tensioning during compression, giving the highest E_{50} values, as illustrated in detail in Figure 88.

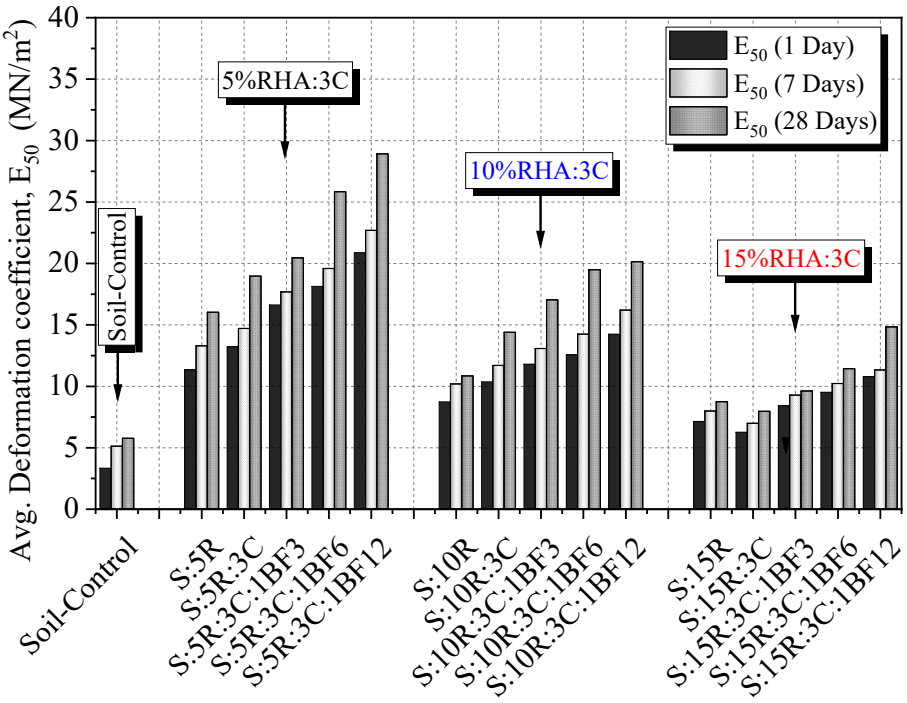

Figure 88 Variation of modulus of deformation (E_{50}) with curing period.

5.5 Validation of Shear Strength Developments

The test results discussed above (Triaxial and UCS tests) demonstrated that the shear developments in the stabilized specimens were mainly due to the reinforcement extent on the cemented composite structure: influenced by the basalt fiber filament length and pozzolanic activity. This study validated these phenomena through SEM and XRD analyses.

5.5.1 Microstructural Analysis using SEM Imagery

The SEM images of RHA-Cement and basalt fiber reinforced stabilized soil may reveal the reinforcement fibers' distribution, orientation, and morphology within the soil matrix. The images show the bonding interface between the fibers and the soil matrix, as well as any defects or flaws that could affect the mechanical properties of the composite material. Additionally, SEM images can provide information about the pore structure, porosity, and grain size of the soil matrix, which can influence the composite material's strength, stiffness, and durability.

This study conducted a microstructural examination to show the structural modification of the soil-only specimen, followed by analyzing the ultimate composite structure after adding RHA and cement. It was evident that micro-crack formation was a common phenomenon in the unreinforced specimens, as shown in Figure 89, Figure 90, and Figure 91 for S-Control, S:5R, and S:5R:3C blends, respectively. In the control specimen (S-Control) [Figure 89 (a), 89 (b)], the porous morphology (micro-pores) alongside the micro-cracks indicated a higher potential for shear failure during loading due to the increased planes of weakness in the sample at 7 days and 28 days of curing. However, for the S:5R [Figure 90 (a), 90 (b)], a reduction in micro-cracks formation and the development of cemented composite structure after 28 days of curing validated the increase in the cohesion values, as shown in Section 5.3 and the UCS values in Section 5.4.

Furthermore, adding nominal dosages of cement enhanced the degree of cementation in the composite structure with the curing period, reducing micro-pores and micro-cracks development, as shown in [Figure 91 (a), 91 (b)]. This phenomenon led to a steady increase in cohesion compared to the S-control and S:5R specimens, as indicated earlier. It was also justifiable through SEM imagery that the cement underwent a chemical reaction with water during the curing period, forming hydration products that bound the soil particles together. As a result, the degree of cementation increased, improving the composite material's mechanical properties.

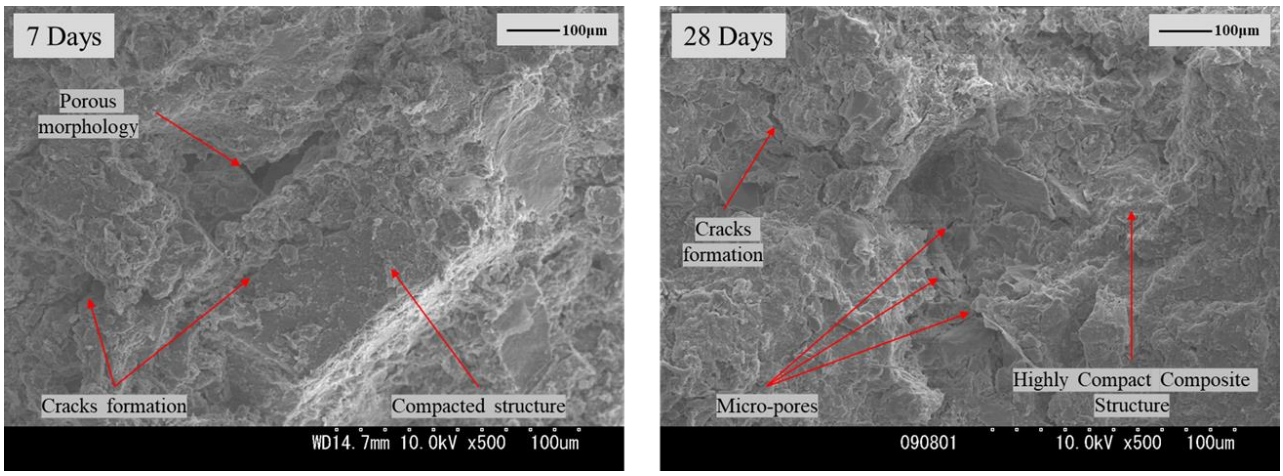

Figure 89 SEM image for S-Control specimen after **(a)** 7 days curing at x500 **(b)** 28 days curing at x500.

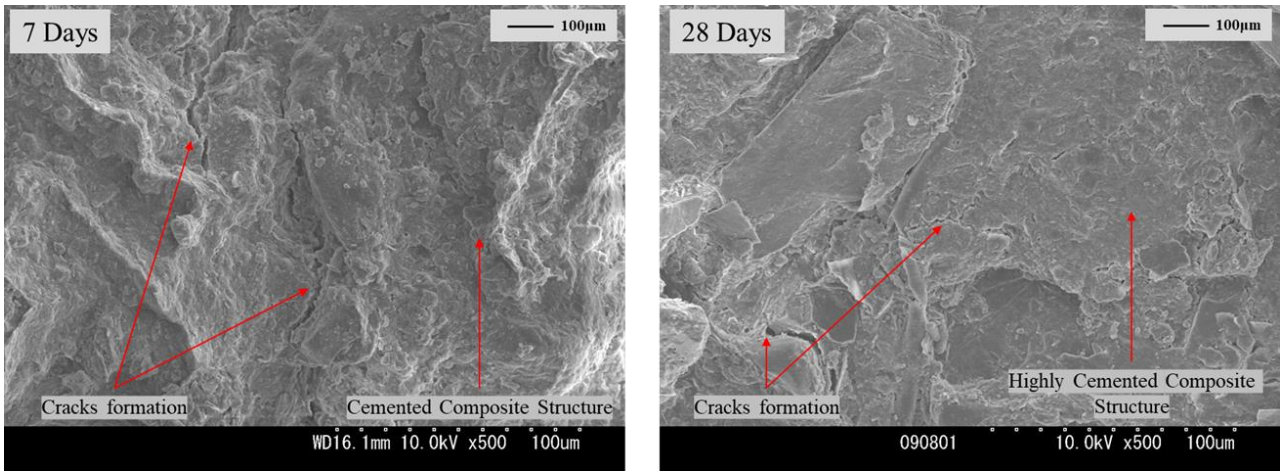

Figure 90 SEM image for S:5R specimen after **(a)** 7 days curing at x500 **(b)** 28 days curing at x500.

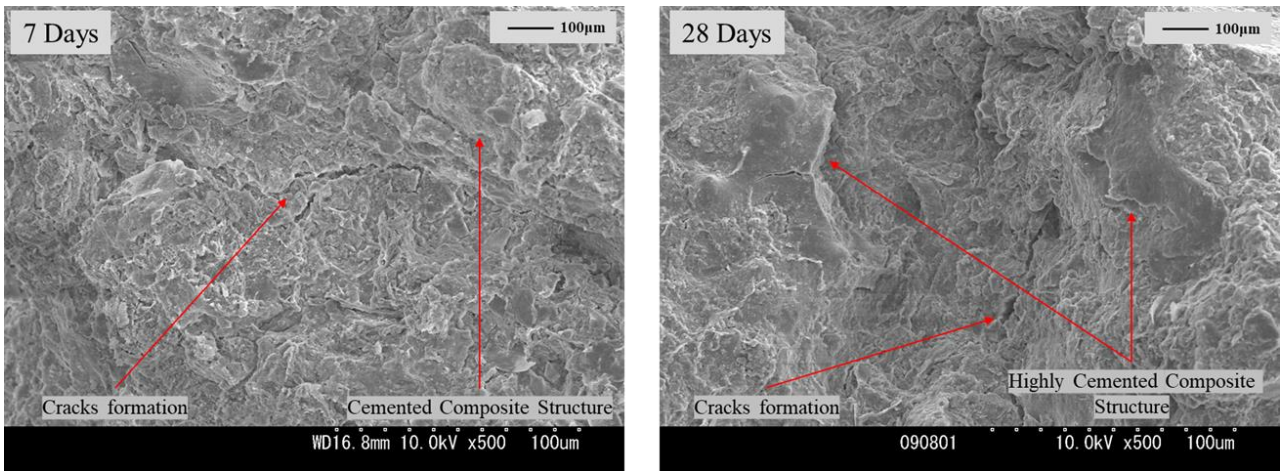

Figure 91 SEM image for S:R:3C specimen after **(a)** 7 days curing at x500 **(b)** 28 days curing at x500.

Moreover, the interactions between the basalt fiber filaments and the cemented composite structure on shear development were verified. The SEM images of the high-strength specimen (S:5R:3C:1BF12) after drained shearing at 150 kN/m^2 confining pressure are presented in Figures 92 (a) and 92 (b). It was observed that after 7 days of curing, separate cemented blocks were interlocked together by loosely packed basalt fiber filaments. Further, after 28 days of curing, the interfacial contacts between basalt fiber filaments and the surrounding composite materials increased significantly, improving the bonding degree within the composite structure. As a result, the basalt fiber filaments bridged the gaps between the separate cemented blocks enabling them to withstand higher degrees of stress during the shearing process. This bridging mechanism was a factor of basalt fiber filament length (from 3 mm to 12 mm) and the degree of cementation within the specified specimen composition, as indicated in the progressive increase in the cohesion and angle of internal friction values in Section 5.3 and the UCS values in Section 5.4.

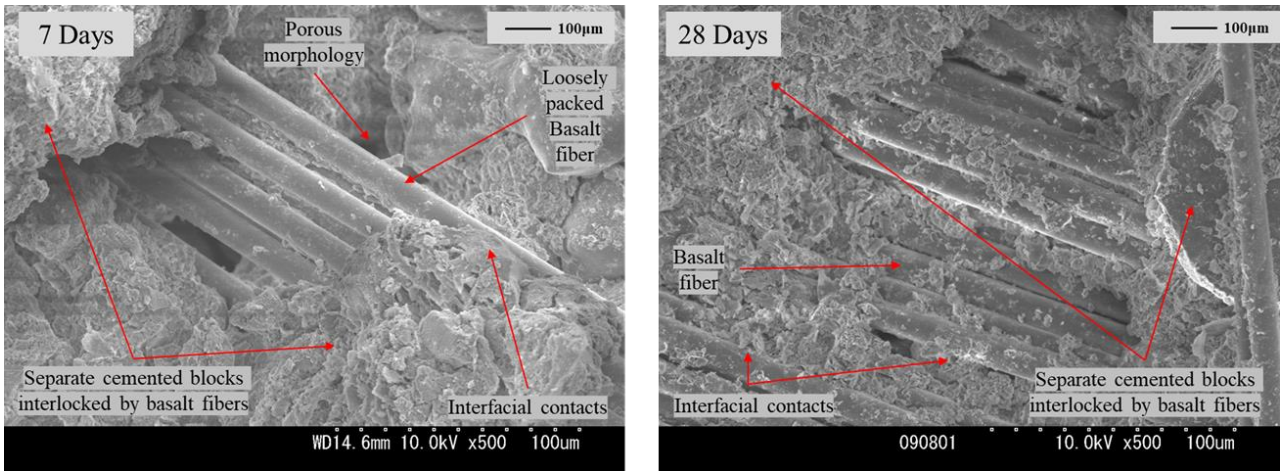

Figure 92 SEM image for S:R:3C:1BF specimen after **(a)** 7 days curing at x500 **(b)** 28 days curing at x500.

5.5.2 Microstructural Analysis using XRD

Through XRD analyses of the control specimen (Soil only), SiO_2 (silicon dioxide) crystalline peaks were prevalent, typically present in amorphous (non-crystalline) form, as well as in various crystalline phases. The most common crystalline form of SiO_2 in soils is quartz, which has a well-

defined crystal structure and can be readily detected by X-ray diffraction (XRD)—also, we noticed a few peaks of amorphous CASH bonds in the soil during curing. However, the dominance of unreacted silica content justified the low shear developments in the unstabilized soil, as shown in Figures 93 (a) and 93 (b), representing 7 days and 28 days of curing, respectively.

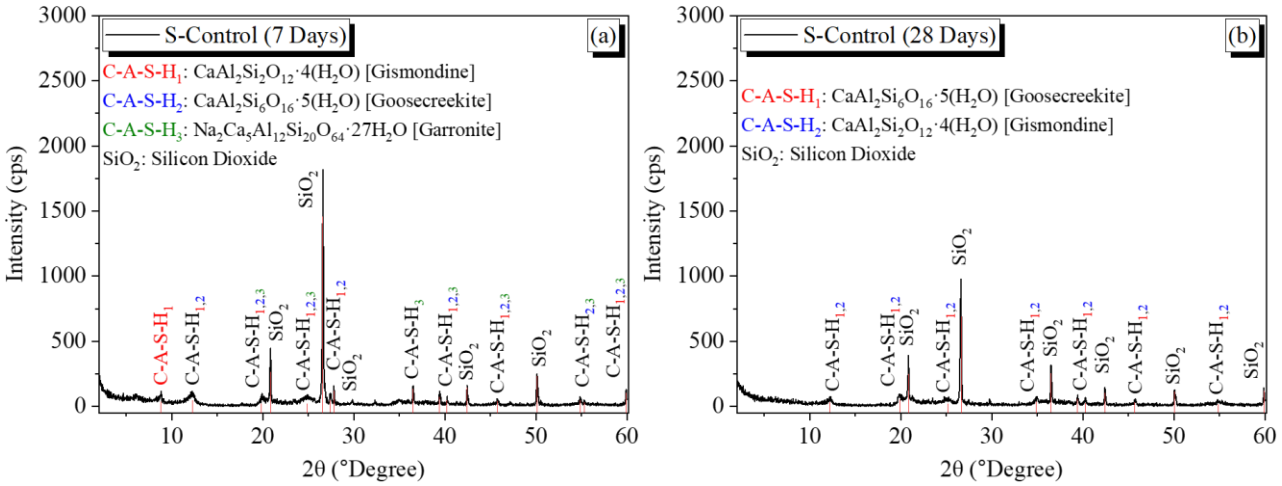

Figure 93 XRD analysis of the S-Control specimen after **(a)** 7 days of curing **(b)** 28 days of curing.

Moreover, the XRD analysis of the RHA-treated composites revealed the dominance of hydrous calcium aluminum sorosilicates (C-A-S) after 7 days of curing [Figure 94 (a)], while additional prevalent C-A-S-H bonds were observed after 28 days of curing [Figure 94 (b)], signifying the developments in shear strength compared to the control specimen. The development of hydrate silicate chains (CASH) in soil stabilized with RHA is likely a result of these cementitious reactions during the curing period (28 days). Hydrate silicate chains are a type of cementitious compound that can form when silica-rich materials like RHA react with calcium hydroxide in the presence of water. Even though no cement was used in these specimens, significant amounts of calcium silicate hydrate (C-A-S-H) bonds formed because RHA and soil contained silica and other calcium minerals like calcium oxide (CaO) that reacted in the presence of water to form C-A-S-H. However, increasing the RHA content to 15% showed crystalline SO_2 peaks indicating the presence of unreacted silica in the composite soil structure hence the deteriorating shear strength at higher RHA contents.

Figures 95 and 96 represent the X-ray diffraction (XRD) analysis for 10%RHA and 15%RHA composites, respectively.

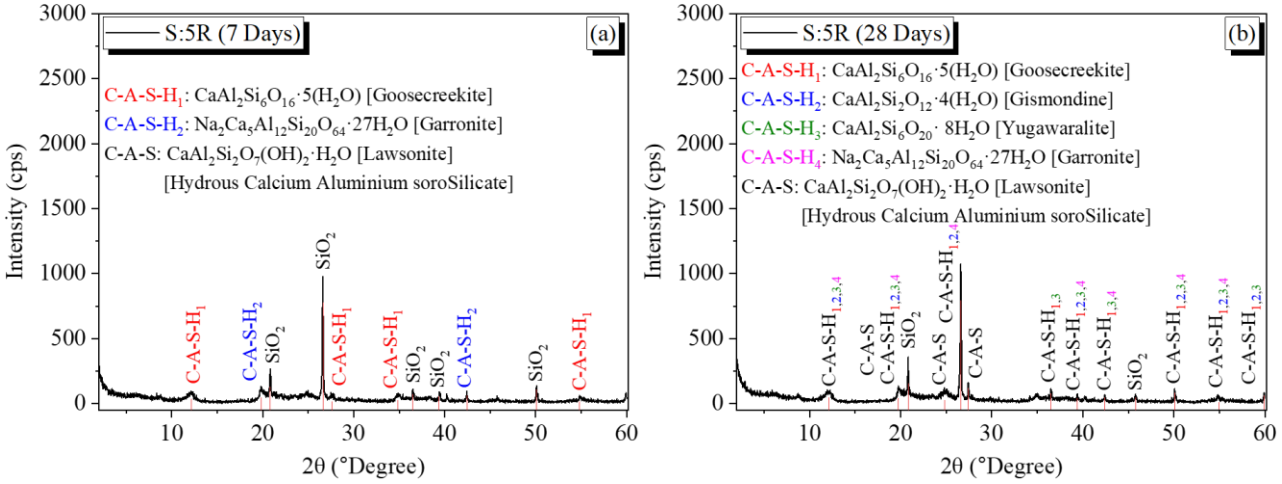

Figure 94 XRD analysis of the S:5R specimen after **(a)** 7 days of curing **(b)** 28 days of curing.

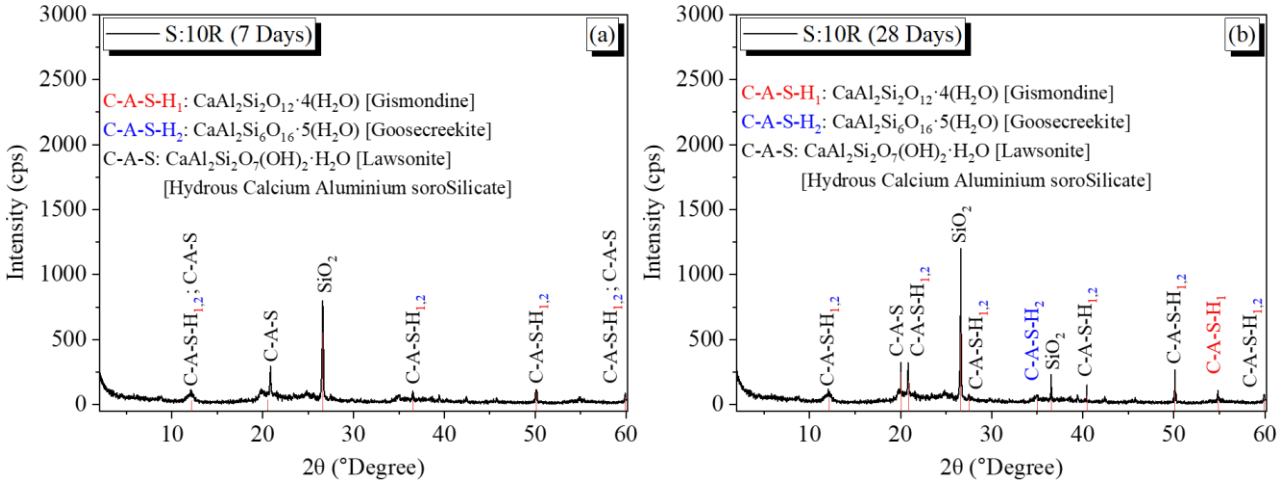

Figure 95 XRD analysis of the S:10R specimen after **(a)** 7 days of curing **(b)** 28 days of curing.

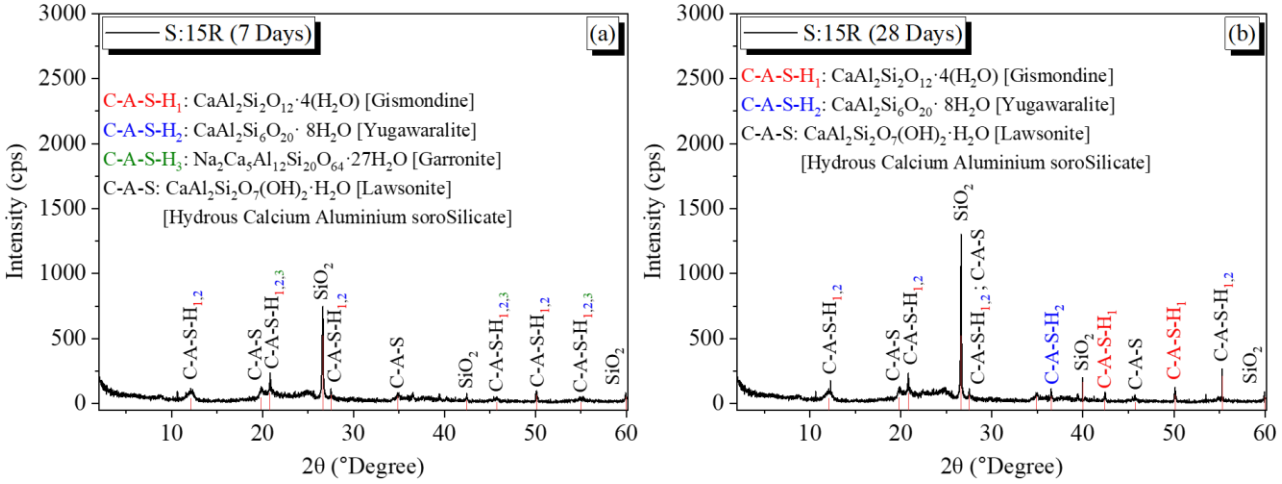

Figure 96 XRD analysis of the S:15R specimen after **(a)** 7 days of curing **(b)** 28 days of curing.

Considering the Soil-RHA-Cement combinations, crystalline peaks of Calcium AluminoSilicate Hydrates (C-S-H), a product of the pozzolanic reactions between soil, cement, and amorphous silica found in RHA, were observed. In literature, during the process of C-A-S-H formation, higher chances of the uptake of other minerals present in the soil, RHA, and cement, such as Magnesium (Mg) and Aluminum (Al) compounds, were observed in the past (Bonen and Cohen, 1992; Gollop and Taylor, 1992; Santhanam et al., 2002). This study also observed that during the early stages of curing (7 days), when the pH was still low, the emerging C-A-S-H bonds got decalcified on the surface of the specimen into amorphous silica, which reacted with Mg in the soil composite and yielded traces of Magnesium Silicate Hydrates (M-S-H). This decalcification process led to the formation of Calcium Aluminum-Magnesium Silicate Heptahydrate (C-A-M-S-H $[(CaO)(Al_2Mg_2O_{15})(SiO_2)_6\ 7(H_2O)]$ in the specimens, which slightly reduced the effectiveness of the C-A-S-H in stabilizing the soil composite, as shown in Figure 97 (a).

However, after 28 days of curing, it was observed that there was no further uptake of Mg ions; instead, continued uptake of Aluminum ions in C-A-S-H gel was evident. Aluminum ions uptake occurred both in the surface, interlayer, and in the silicate chains, leading to the formation of stronger C-A-S-H gel bonds known as Calcium Alumino Hexasilicate Tetrahydrate $[(CaO)(Al_2O_3)(SiO_2)6\ 4(H_2O)]$ as shown in Figure 97 (b). This Al uptake at higher pH values were also recorded in other relevant studies (Bach et al., 2013; L'Hôpital et al., 2015; Lothenbach and Nonat, 2015; Richardson et al., 2008; Richardson, 2008). The Mg concentrations were reduced due to the increased specimen pH above 10, leading to a much lower aqueous magnesium concentration than calcium, thereby enhancing the formation of stronger C-A-S-H bonds in all the specimens (Bernard et al., 2017; Lothenbach et al., 2015). Consequently, the interaction between the tensioned basalt fiber filament lengths and the stronger C-A-S-H bonds validated and dictated the rate of development in shear strength with the curing period. In Figures 98 and 99, representing 10%RHA and 15%RHA

composites, respectively, the slight reduction in the C-A-S-H peaks led to decreased shear strength, as discussed in Sections 5.3 and 5.4.

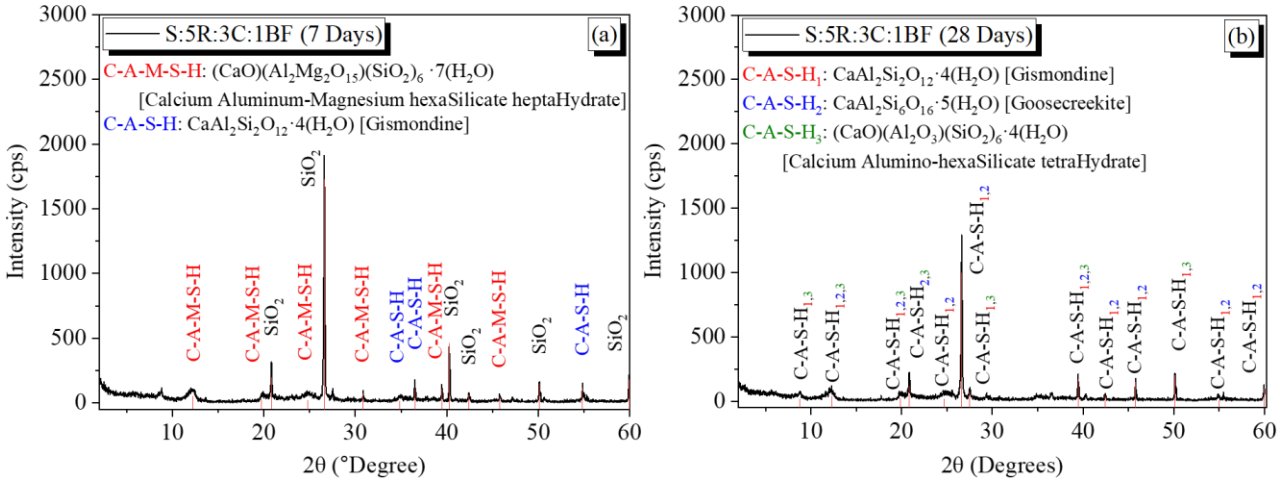

Figure 97 XRD analysis of the S:5R:3C specimen after **(a)** 7 days of curing **(b)** 28 days of curing.

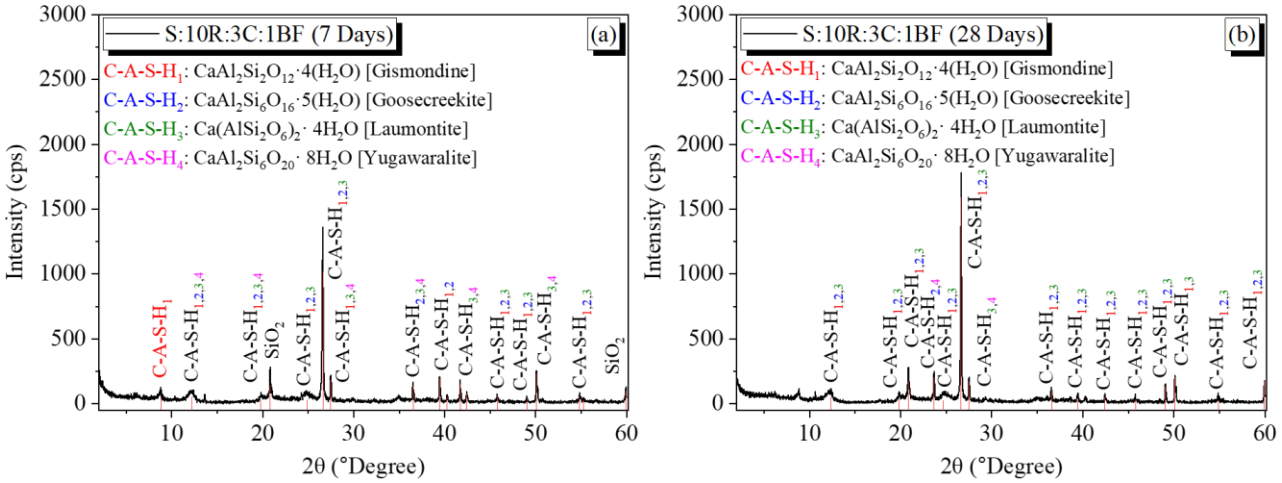

Figure 98 XRD analysis of the S:10R:3C specimen after **(a)** 7 days of curing **(b)** 28 days of curing.

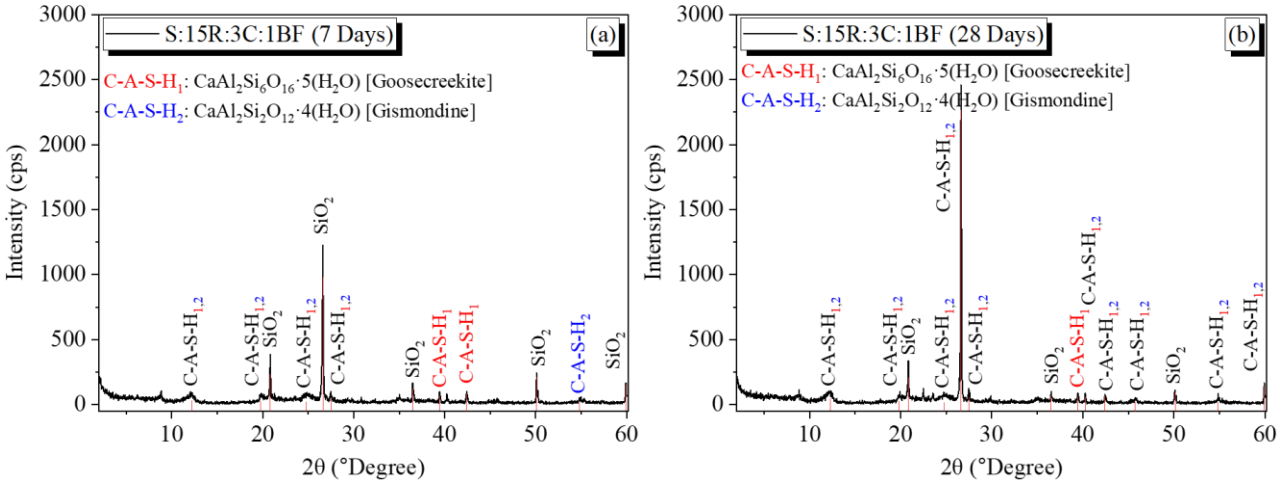

Figure 99 XRD analysis of the S:15R:3C specimen after **(a)** 7 days of curing **(b)** 28 days of curing.

5.6 Permeability Tests Results

5.6.1 Coefficient of Permeability (k)

The permeability test examined the water flow rate through the soil medium and was expressed as the permeability coefficient (k). This water flow rate significantly impacted soils' physical properties regarding subgrade or fill material drainage. In this study, the soil had a very low permeability of $7.1x10^{-6}$ cm/s, which was not considered suitable for subgrade or shallow foundation use. However, adding basalt fibers into the soil increased k to 10^{-5} cm/s for all 5% to 10%RHA specimens and 10^{-4} cm/s for 15%RHA specimens, as shown in Figure 100. Notably, from 1 day to 7 days of curing, k increased due to the rapid flocculation of particles in the specimens (Hossain and Sakai, 2008; Wong, 2008; Owino at al., 2022b) that led to the formation of larger voids in addition to the gaps created by basalt fibers. Flocculation is the process by which soil particles agglomerate and settle due to stabilizers, increasing the pore size and reducing the soil's ability to resist water flow. The rapid flocculation of particles in the specimens was observed due to the pozzolanic reaction of RHA and cement with the soil, which led to the formation of larger clusters of cementitious compounds. However, at 28 days of curing, the appearance of these cementitious compounds increased the binding between the soil particles, resulting in reduced pore sizes and hence the low k values.

Adding basalt fibers to the RHA, RHA-Cement stabilized soil further enhanced the flocculation process due to the mechanical interlocking between the fibers and soil particles, which increased the strength of the specimens. However, longer fibers introduced longer drainage routes in the specimen structure hence the slight increase in the k value with basalt fiber length. It was also evident that k declined at 28 days of curing due to the cementation effect that enhanced the binding of the particles in the specimen (Liu et al., 2017; Mendonça et al., 2021; Mollamahmutoglu, M. and Avcı, 2018). The cementation effect occurred due to the hydration of cementitious compounds formed during the pozzolanic reaction between soil, RHA, and cement.

The hydration of these compounds resulted in the formation of cementitious products, further enhancing the particles' binding in the specimen. The decline in the permeability coefficient of the specimens at 28 days of curing indicated that the specimens were becoming less porous, which is a desirable property for soil stabilization. The slight reduction in permeability upon complete hydration of the cementitious structure at 28 days meant that water infiltration into the soil was moderately restricted, which could prevent erosion and improve the stability of the soil. Therefore, using RHA and nominal dosages of cement as a stabilizer in combination with basalt fibers can be an effective method for soil stabilization in construction projects.

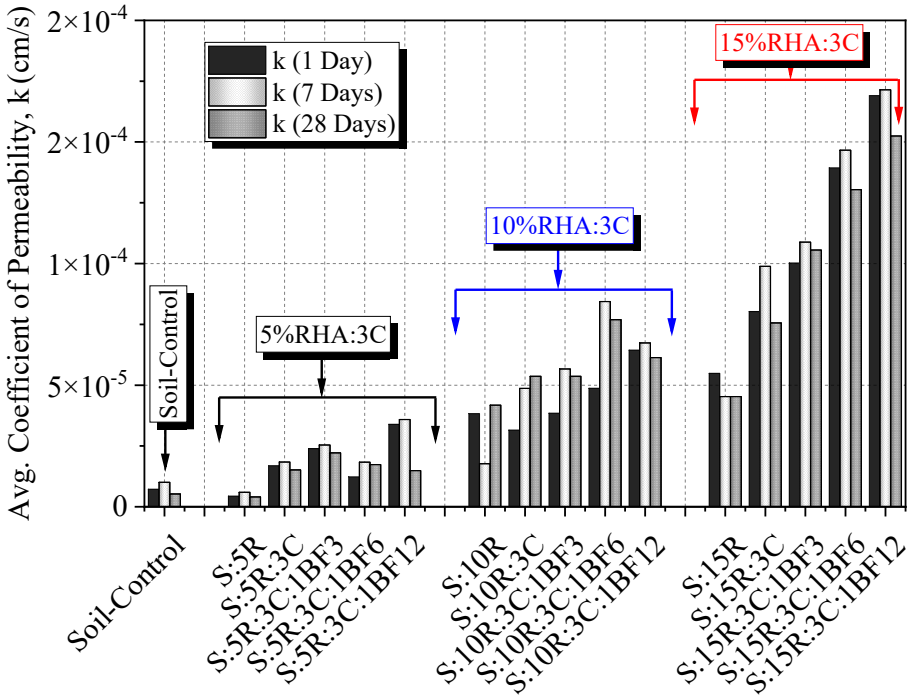

Figure 100 Variation of the permeability coefficient with specimen composition and curing period.

Another property that was of great importance in soil stabilization was void ratio (e). The void ratio (e) is the ratio of the volume of voids to the volume of solids in a soil sample. It is an important parameter because it determines the soil's permeability, compressibility, and shear strength. This study investigated the effect of specimen composition and curing time on the void ratio of basalt fiber-reinforced RHA-cement stabilized soil. It was found that the void ratio of most of the specimens

decreased after 28 days of curing. This decrease was attributed to the formation of cementitious compounds that increased the binding between the soil particles, resulting in reduced pore sizes and decreased void ratio. This reduction phenomenon justified the permeability coefficient (k) trends described in Figure 100. A detailed illustration of the variation in the void ratio(e) with specimen composition and curing period is shown in Figure 101.

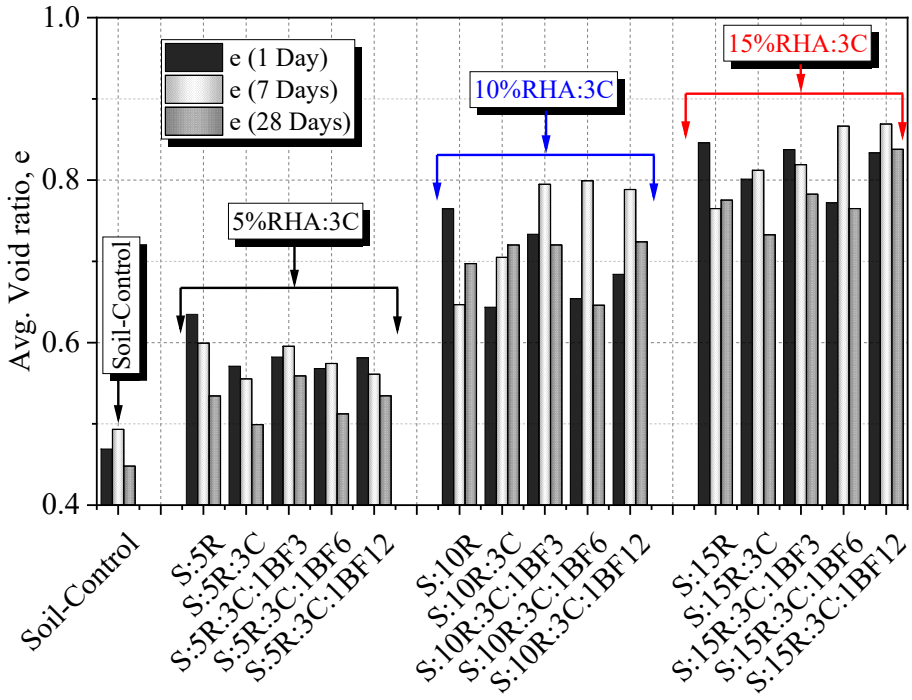

Figure 101 Variation of the void ratio (e) with specimen composition and curing period.

5.6.2 Microstructural Analysis

Soil permeability coefficient and void ratio are essential for understanding compacted soil behavior. The permeability coefficient refers to the ability of soil to allow fluids to flow through it, while the void ratio measures the amount of void space within the soil mass. These properties are affected by a range of factors, including compaction, curing period, and soil cohesiveness. The analysis found that the compacted S-control specimen structure showed a reduction in void ratio and permeability coefficient with an increase in curing period, from 1 day to 7 days to 28 days. This significant observation indicated that the compacted soil became more cohesive over time. Also, the increased

cohesiveness resulting from the curing process caused the soil particles to become more tightly packed and interlocked. As a result, the void space within the soil mass decreased, and the soil became less porous. The SEM microstructural analysis confirmed that the compacted soil mass was indeed less porous and more tightly packed, with the curing period increasing to 28 days, as shown in Figure 102. As a result of this compaction during curing, the permeability coefficient and the void ratio decreased. Moreover, the reduction in the void ratio and permeability coefficient of compacted soil with an increase in the curing period can be attributed to the chemical reactions within the soil during the curing process. The formation of mineral crystals, cementitious compounds, and the precipitation of soil minerals resulted in a more cohesive soil mass with fewer void spaces. Therefore, understanding these chemical reactions is essential for engineers using such soils.

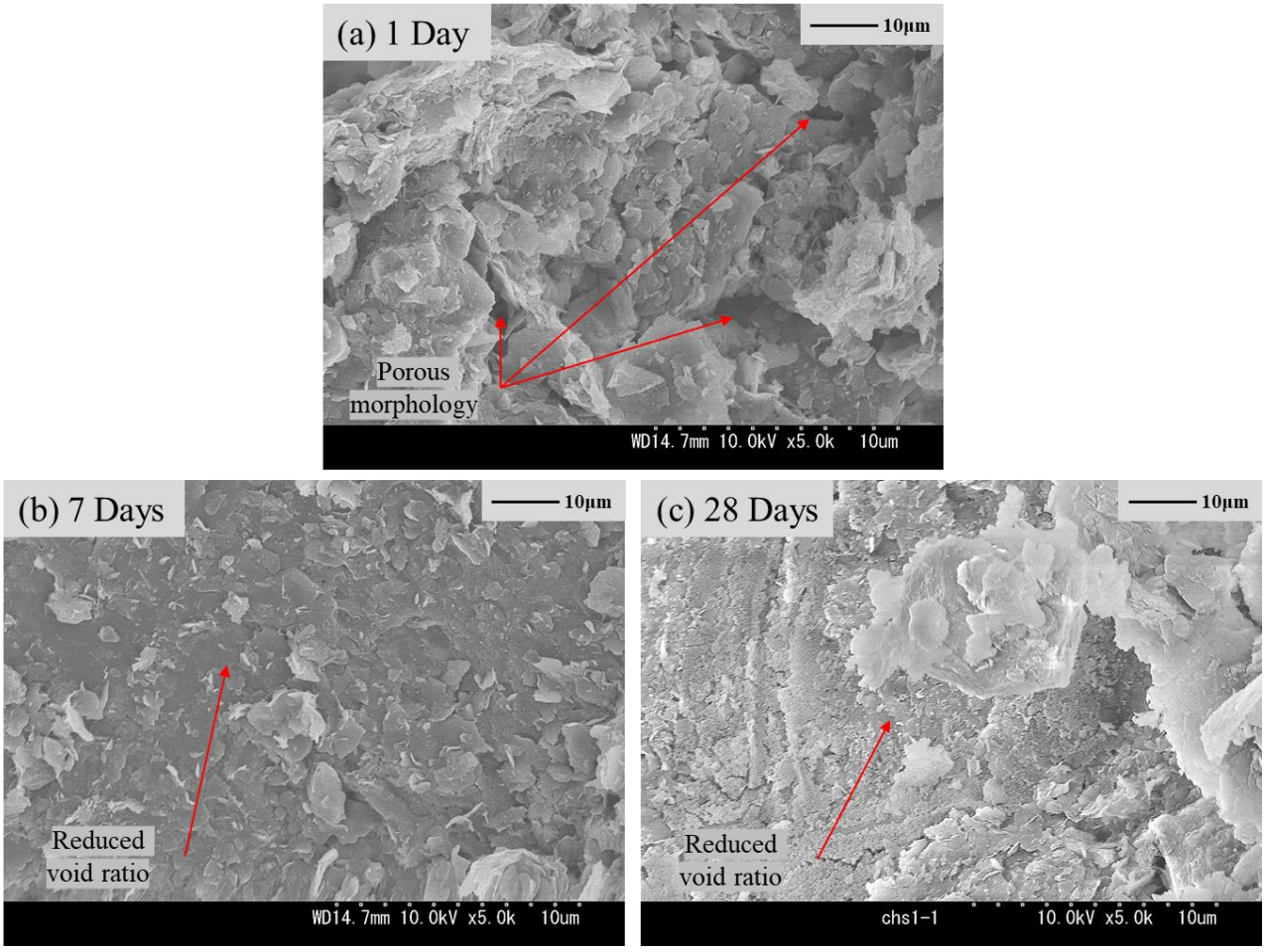

Figure 102 SEM imagery for S-Control specimens **(a)** 1 day of curing, **(b)** 7 days of curing, **(c)** 28 days of curing.

Next, the SEM microstructural analysis examined the permeability coefficient and the void ratio of soils stabilized with 5% RHA and 3% cement (Figure 103). The results showed a slight increase in void ratio and permeability coefficient after seven days of curing due to flocculation. Flocculation is when the soil particles are brought together to form larger aggregates. The increased porous morphology in the specimen structure validated the slight increase in void ratio and permeability coefficient. However, after 28 days of curing, there was a considerable reduction in the void ratio and permeability coefficient due to the compact cemented specimen structure (pozzolanic activity between soil, RHA, and cement) observed in the SEM images. The compact cemented composite microstructure decreased the porosity and permeability of the soil, which was reflected in the reduction of the void ratio and permeability coefficient, as indicated in Section 5.6.1.

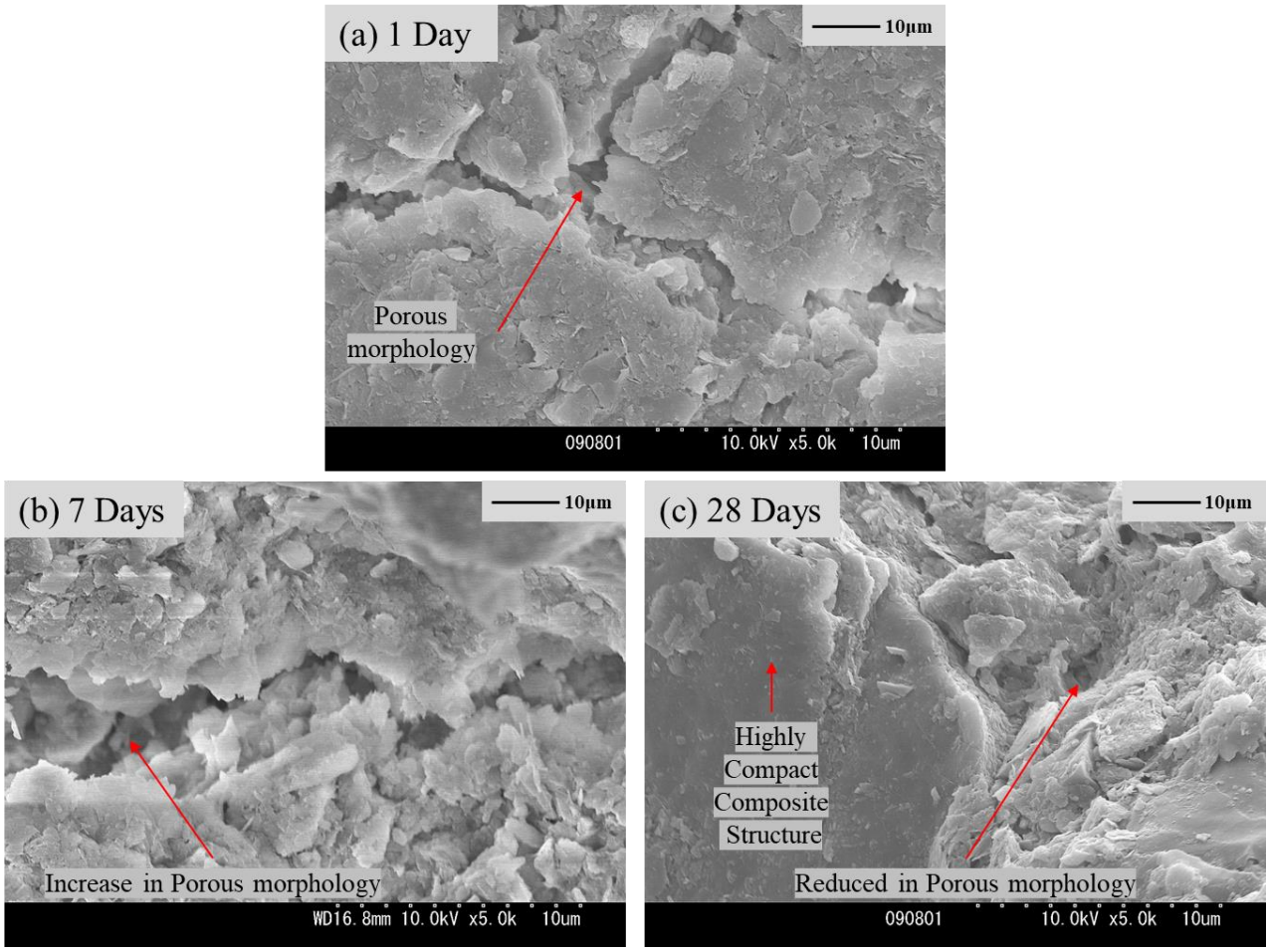

Figure 103 SEM imagery for S:5RHA:3C specimens **(a)** 1 day of curing, **(b)** 7 days of curing, **(c)** 28 days of curing.

In soil stabilization, the use of multiple stabilizing agents in combination can have a significant impact on the properties of the stabilized soil. In this context, increasing the RHA content to 10% while maintaining the cement content at 3% was investigated, as shown in Figure 104. The results showed that the specimens with 10% RHA and 3% cement had a slightly higher void ratio and permeability coefficient than the 5% RHA and 3% cement specimens, but the trend remained the same at 7 days and 28 days of curing. This slight increase in the void ratio and permeability coefficient can be attributed to the porosity of the excess RHA particles. However, it is essential to note that increasing the RHA content beyond a specific limit can negatively impact the stabilized soil's properties. Excessive RHA can result in a decrease in compressive strength and can also lead to the formation of weaker bonds between the soil particles.

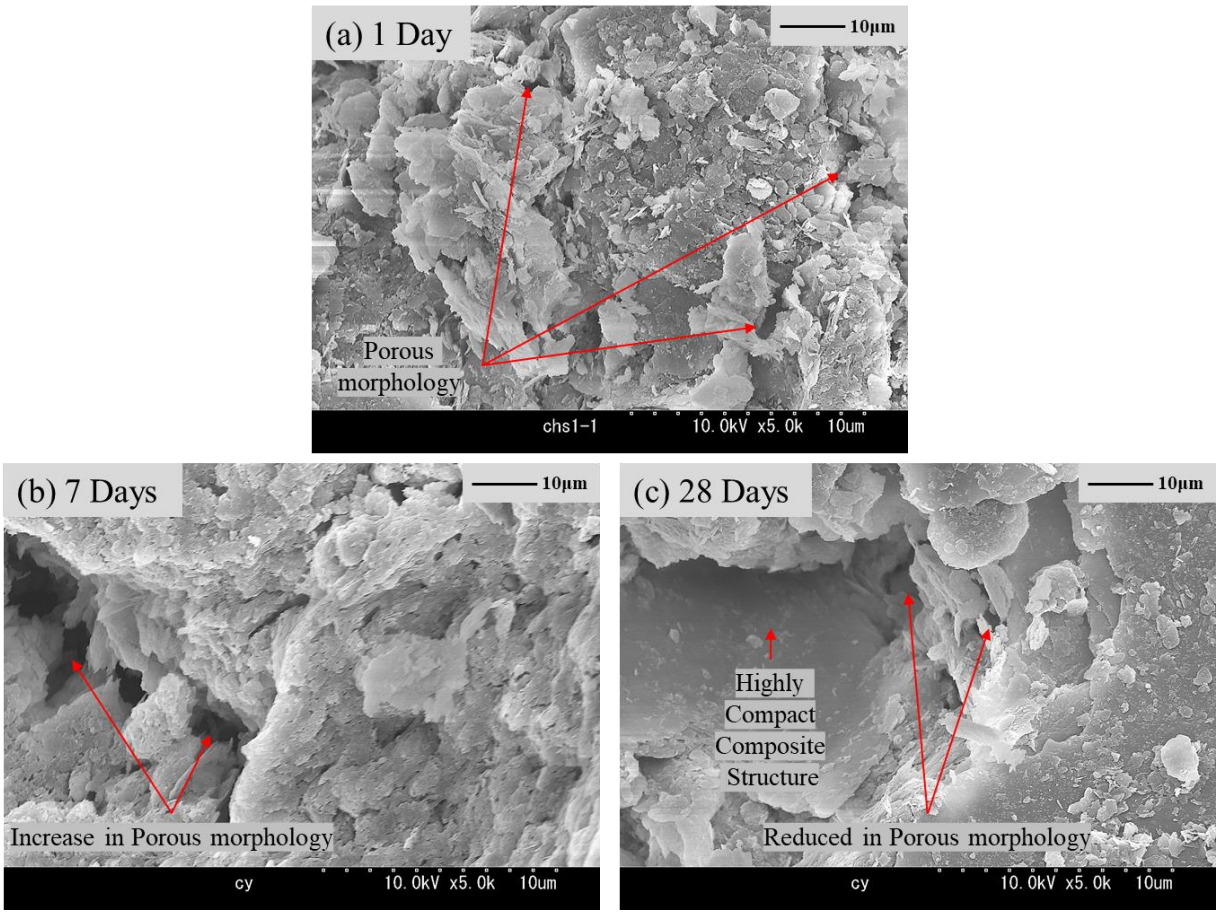

Figure 104 SEM imagery for S:10RHA:3C specimens **(a)** 1 day of curing, **(b)** 7 days of curing, **(c)** 28 days of curing.

Ultimately, the study results showed that the specimens with 15% RHA and 3% cement had the highest void ratio and permeability coefficient compared to the 5% RHA and 3% cement and 10% RHA and 3% cement specimens, as shown in Figure 105. This void ratio and permeability coefficient increase was attributed to the excess RHA in the specimen structure. Excess RHA led to the accumulation of more fine materials in the specimen structure, resulting in the dominance of loose materials, as shown in Figures 105 (b) and (c), as the curing period increased from 1 day to 28 days. This dominance of loose material was due to the inability of the excess porous RHA to be used during the pozzolanic reactions, resulting in a higher void ratio and permeability coefficient. Therefore, it is crucial to determine the optimum content of RHA and cement for a particular soil type to achieve the desired engineering properties.

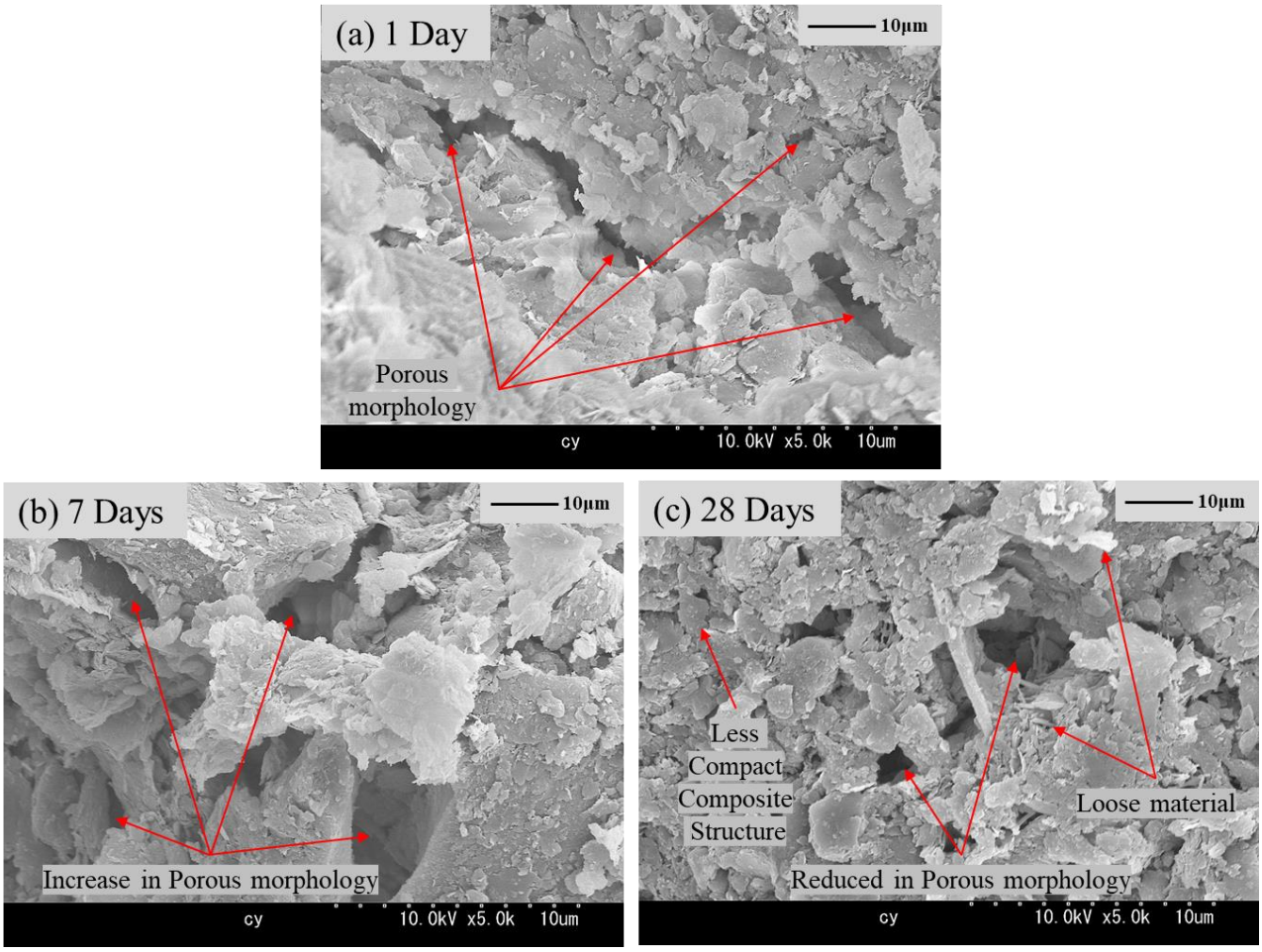

Figure 105 SEM imagery for S:15RHA:3C specimens **(a)** 1 day of curing, **(b)** 7 days of curing, **(c)** 28 days of curing.

Considering the basalt fiber reinforced specimens, it was noteworthy that for all the RHA-cement contents, the permeability coefficient and the void ratio increased with increased basalt fiber length, as shown in Section 5.6.1. Additionally, after 28 days of curing, the values of k and e reduced as the fiber reinforcement effect and presence of different degrees of cementation preceded according to the specified specimen composition. After 7 days of curing, it was observed that all the basalt fiber stabilized specimens depicted conspicuous drainage channels along the basalt fibers, increasing the porosity. Additionally, insignificant interfacial bonds between the fibers and the cemented soil composite, as shown in Figure 106 (a), led to a weaker structural bond.

However, at 28 days of curing, the reductions in the k and e values were justified by the increased bonding intensity in the basalt fiber reinforced specimens, indicated by the significant decrease in the drainage channels and the robust interfacial bonds, as shown in Figure 106 (b). It can be concluded that for the fiber-reinforced stabilized combinations, the variations in k and e were controlled by the following factors; (i) basalt fiber length, (ii) the amount of RHA-cement mixtures in the specimen structure, and (iii) the curing period.

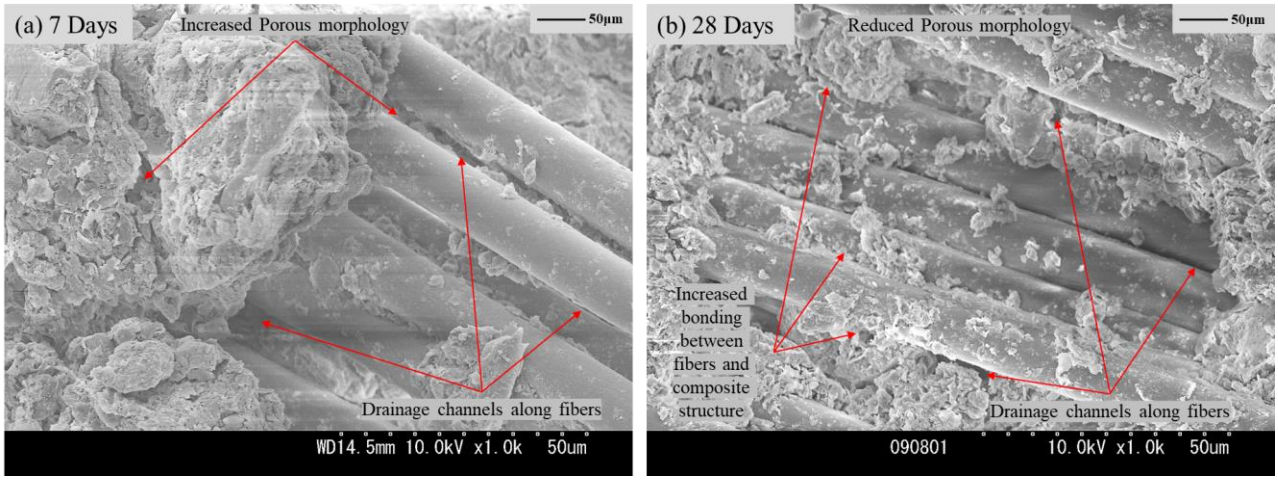

Figure 106 SEM imagery showing the effects of basalt fiber reinforcements on the trends of k and e **(a)** 7 days of curing, **(b)** 28 days of curing.

CHAPTER 6 SIGNIFICANCE AND APPLICATIONS OF THE CURRENT RESEARCH

6.1 Significance of the Current Research: A Kenya Case Study

Some of the driving factors that make this research significant include:

(i) Vast Deposits of Very Clayey to Clayey Soils in Kenya; The soil is the most critical material in the construction industry. In many parts of Kenya, expansive clay soils are prevalent and unsuitable for construction due to their poor geotechnical properties, as shown in Figure 107. As a result, engineers have been challenged to develop sustainable stabilization techniques to improve the quality of these soils. This chapter will examine the significance of current research on stabilizing weak expansive clay soils using Rice Husk Ash (RHA), minimal dosages of cement, and basalt fibers based on the current situation in Kenya.

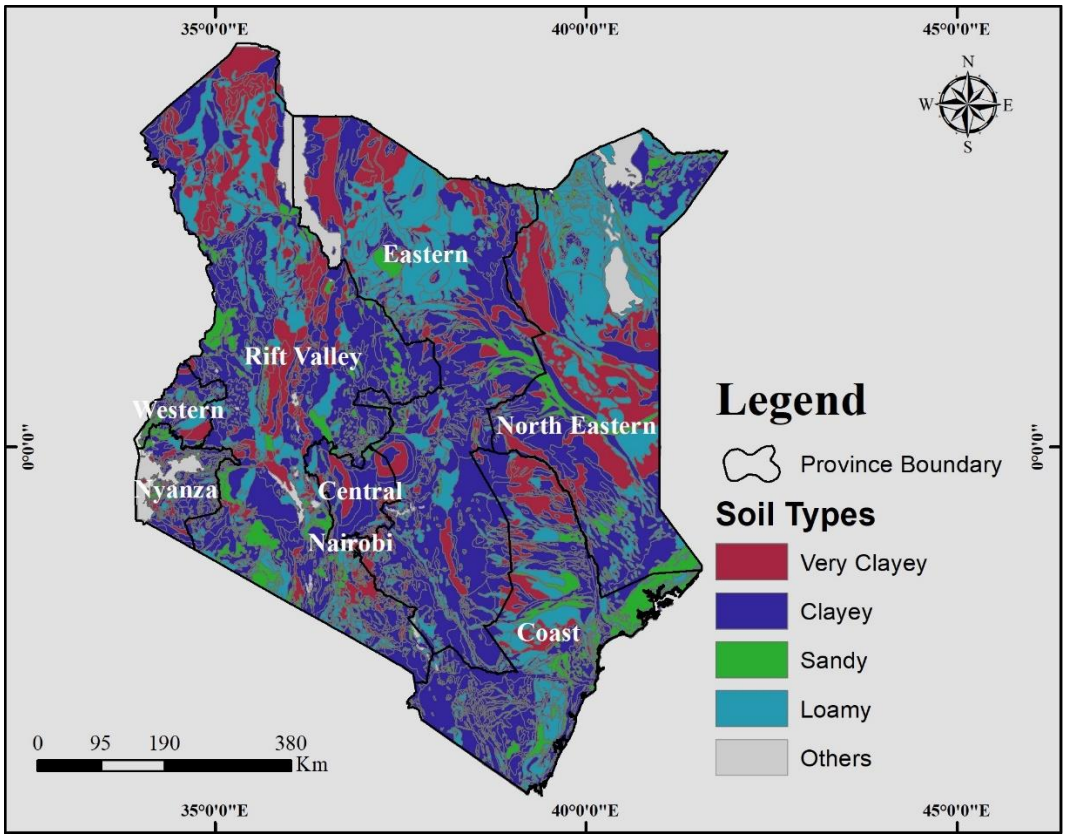

Figure 107 The dominant soil types in Kenya.

(ii) Vast Deposits of Basalt Rocks in Kenya; Considering the vast deposits of basalt rocks in Kenya, as shown in Figure 108, the relevance and potential use of basalt fibers to reinforce such soils is a viable option compared to the available fibers used today. Additionally, the depletion of the limestone deposits (a natural mineral deposit)[Figure 108] and the negative environmental impacts from its mining and cement manufacture calls for sustainable means of soil stabilization based on the sustainable development goals (SDG9).

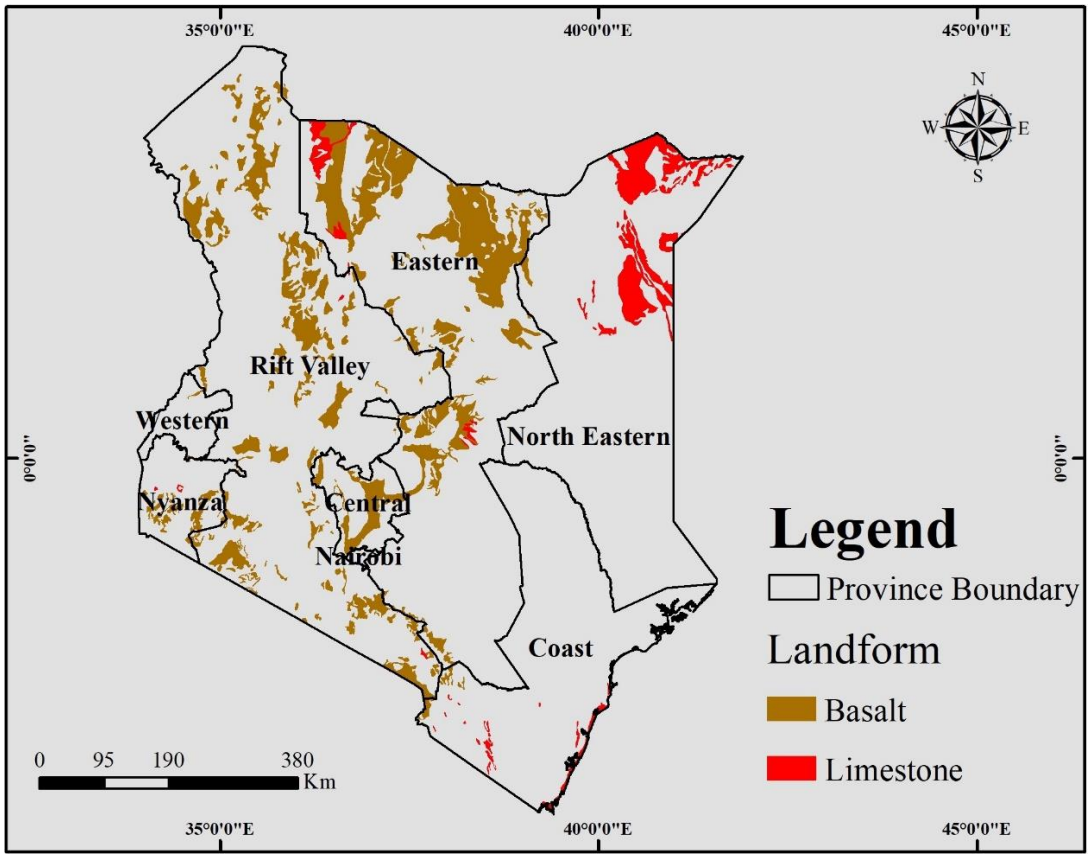

Figure 108 The deposits of basalt rocks and limestone.

(iii) Rice Production Expected to Increase by 50%; Rice is one of the most important staple foods in the world, providing essential nutrition to billions of people. The production and consumption of rice are expected to increase significantly in the coming years, particularly in regions such as Africa, where rice has become an increasingly important food crop. Figure 109 shows some of Africa's dominant rice-producing countries as of 2022.

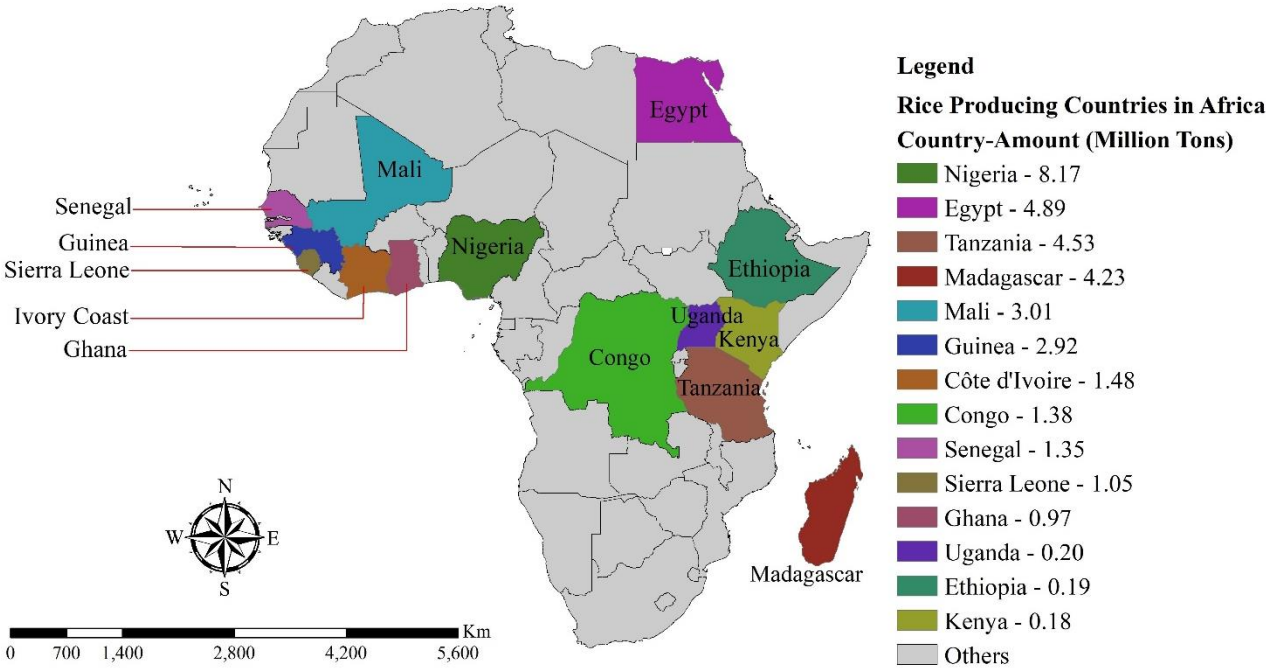

Figure 109 Some of the rice-producing countries in Africa.

With this increase in production, the amount of rice husks generated as a byproduct of the milling process is also expected to rise significantly. According to Seck et al. (2013), rice consumption is expected to increase by 130% in 2035 compared to 2010, with production rates projected to increase by 50%. This increase will make rice husks available in abundance, boosting the potential implications of obtaining RHA and using it in sustainable soil stabilization. The abundance of rice husks and the potential for sustainable soil stabilization using renewable resources such as RHA and basalt fibers offer significant economic and environmental benefits. Furthermore, using alternative stabilizers could significantly reduce the environmental footprint of construction projects while being more cost-effective and sustainable.

(iv) Rice Husks Disposal Challenges in Kenya; This is a sustainability aspect following SDG9. Rice husks are the outermost layer of the rice grain, which are removed during the milling process. Although they have many potential uses, including as a source of energy and raw material for various industries, the disposal of rice husks is still a significant challenge in many regions. One of the main

challenges of rice husk disposal is the high volume of waste generated. Disposing of such a large volume of waste can be challenging and expensive, especially in areas with limited infrastructure and resources like developing countries. For example, Figure 110 shows the disposal problem outside the Mwea Irrigation Scheme Rice Milling factory in central Kenya.

Figure 110 RHA disposal challenge outside the Mwea Irrigation Scheme Rice Milling factory in Kenya.

Another challenge is the environmental impact of rice husk disposal. Burning rice husks, a common disposal method, can result in air pollution and release greenhouse gases. In addition, improper disposal of rice husks can lead to water pollution and other environmental problems. Furthermore, rice husk disposal can also have economic implications. For example, if rice husks are not disposed of properly, they can become a breeding ground for pests and diseases, damaging crops and impacting agricultural productivity. Therefore, finding innovative and sustainable ways to dispose of rice husks is critical to reducing environmental problems and supporting sustainable development. In the context of the driving factors **(i)** to **(iv)**, this research will be highly significant in providing sustainable stabilization solutions to constructing durable and safe facilities on the vast areas covered in expansive soils. The current study investigated the effectiveness of using RHA, minimal dosages of cement, and basalt fibers in stabilizing weak expansive clay soils. Where laboratory tests to

evaluate the geotechnical properties of the stabilized soil, such as the consolidation behavior, triaxial compression, unconfined compressive strength, and permeability tests on a wide array of specified combinations, were conducted and evaluated. The results showed that adding RHA-cement mixture and basalt fibers to the soil improved its geotechnical properties significantly, as elaborated in Chapter 5. Moreover, improved workability and reduced soil shrinkage and swelling potential were also observed. The minimal dosage of cement used in the study reduced the stabilization cost while still achieving the desired geotechnical properties by reducing the amount of cement usage.

Based on these results, the current research is significant in several ways; (i) It provides engineers with a sustainable and cost-effective alternative to cement in the stabilization of expansive soils, (ii) RHA is an abundant and low-cost waste material that can be obtained from rice mills, making it an environmentally friendly alternative to cement, (iii) the use of minimal dosages of cement reduces the overall cost of stabilization while still achieving the desired results. Making the technique affordable for small-scale projects, such as rural road construction, where resources are limited, and (iv) Finally, the research is significant because it addresses a major challenge facing the construction industry in Kenya. Expansive soils are prevalent in many parts of the country, and their stabilization is crucial for constructing durable and safe structures. The current research provides engineers with a sustainable and cost-effective technique for stabilizing these soils, improving infrastructure and economic growth.

Therefore, it is recommended that engineers and researchers in the construction industry embrace this technique and conduct further research to optimize the stabilization process and develop appropriate design guidelines. The government should also promote sustainable stabilization techniques in infrastructure development to ensure the construction of safe and durable structures. Ultimately, the significance of the current research cannot be overstated, as it has the potential to improve the quality of construction and infrastructure in Kenya and beyond.

6.2 Application in Civil and Geotechnical Engineering

Soil stabilization is an essential aspect of construction aimed at enhancing soil strength and durability. With the increase in the demand for sustainable building materials, there has been a growing interest in the use of recyclable aggregates and natural fibers in ground improvement. This has led to the development of sustainable soil stabilization alternatives that can be used for various applications, including;

6.2.1 Road Construction:

One of the primary applications of stabilized and reinforced soils is road construction. Stabilized soils can enhance the strength and durability of the subbase and subgrade, reducing the likelihood of pavement distress, rutting, and other forms of pavement deterioration. Using stabilized soils can reduce the amount of conventional construction materials required for the subbase and subgrade, resulting in significant cost savings. Additionally, stabilized soils can be used to improve the load-bearing capacity of the subbase and subgrade, which can allow for heavier machinery to be accommodated on the road.

6.2.2 Embankment Fills:

Another application of stabilized soils is in embankment fills. Embankment fills are commonly used to construct dams, highways, railways, and other transportation infrastructure projects. Stabilized soils can reinforce embankment fills, reducing the likelihood of soil settlement, slope instability, and other forms of embankment failure. Using stabilized soils can increase the overall stability and strength of the embankment fill, which can result in a safer and more reliable engineering infrastructure.

6.2.3 Landfill Liners:

Stabilized soils can also be used as landfill liners. Landfill liners are critical components of modern waste management systems, as they help to prevent the release of harmful contaminants into the

environment. By using stabilized soils as landfill liners, it is possible to enhance the strength and durability of the liner, which can reduce the likelihood of liner failure and contamination. Additionally, stabilized soils can be used to improve the overall performance of the landfill liner, which can result in a more effective waste management system.

6.2.4 Slope stabilization:

Slope stabilization is another application of stabilized soils. Slope instability is a common problem in many construction projects, particularly in areas with steep slopes or unstable soils. Using stabilized soils makes it possible to reinforce the slope and improve its stability, thereby reducing the likelihood of slope failure, landslides, and other forms of slope instability. Additionally, sustainably stabilized soils can reduce the overall cost of slope stabilization projects, as they require readily available materials that can be found in abundance (for example, RHA) compared to conventional slope stabilization techniques.

6.2.5 Foundation materials:

Stabilized soils can also be used as foundation materials. Foundation materials are critical components of building construction projects, as they provide the necessary support for the building. Using stabilized soils as foundation materials can enhance the foundation's strength and durability, thereby reducing the likelihood of foundation settlement, cracking, and other forms of foundation failure. Additionally, stabilized and reinforced soils can reduce the overall cost of foundation construction projects.

6.2.6 Retaining walls:

Finally, stabilized soils can be used in the construction of retaining walls. Retaining walls are commonly used in the construction of infrastructure projects, such as highways and railways, as well as in commercial and residential construction projects. Using stabilized soils can enhance the

strength and durability of the retaining wall, thereby reducing the likelihood of retaining wall failure, slope instability, and other forms of retaining wall damage.

In conclusion, RHA-stabilized and fiber-reinforced soils offer a sustainable and cost-effective solution for various construction applications. The use of natural fibers and recyclable aggregates in soil stabilization has the potential to significantly reduce the environmental impact of construction activities while also providing a viable alternative to conventional construction materials. With continued research and development, it is likely that the use of stabilized and reinforced soils will become increasingly common in the construction industry, helping to pave the way for a more sustainable and resilient built environment based on the Sustainable Development Goals (SDG9).

CHAPTER 7 : CONCLUSIONS AND RECOMMENDATIONS

7.1 Conclusions Based on the Consolidation Behaviour

This study presented an experimental analysis based on a series of oedometer tests to investigate the dimensional influence of basalt fiber reinforcements on the consolidation behavior of RHA-cement stabilized soils. The dimensional effects of basalt fibers and the RHA-cement content on the consolidation yield pressure(σ_y), compression index (C_c), and swelling index (C_s) at the pre-and post-yield state were discussed. The concept of the intrinsic compression line was adopted to assess the compression curves of the unreinforced and the fiber-reinforced soil composite. Additionally, the correlation between the one-dimensional consolidation coefficients with the length of basalt fiber and RHA-cement content in fiber-reinforced RHA-treated expansive soils was examined. An effort was made to explain more rationally the influence basalt fiber length and RHA-cement content have on the coefficient of consolidation (c_v), coefficient of volume change (m_v), and permeability coefficient (k), drawing further justifications through SEM imagery and XRD analyses. The following conclusions can be made:

i. Increasing the length of basalt fiber in the reconstituted clay soil composite improved the consolidation yield pressure (σ_y). This increase in yield pressure was also dependent on the RHA-cement content in the reconstituted soil structure. This behavior suggested that the composition of soil structure mainly governed the degree of yield pressure. The reconstituted clay soil composite with 12mm basalt fibers, 5%RHA content (RHA), and 3% cement had a highly cemented and reinforced structure hence the high σ_y of 110kN/m^2 as confirmed in the SEM and XRD analysis.

ii. Adding basalt fiber to RHA-cement-stabilized soils significantly reduced the compression index (C_c). This study observed a 16% reduction compared to the control specimen. As the length of basalt fiber increased from 3mm to 6 mm, there was a 0.6% increase in the compression index,

and at 12 mm, the C_c increased by 6% but was still lower than the C_c of the control specimens. This response illustrated that basalt fibers improved the compressive index, improving consolidation yield stress, σ_y.

iii. The swell index for basalt fiber-reinforced RHA-cement stabilized soils decreased with fiber length and RHA content increment. The reduction in the swelling index indicated improved stability of the reinforced soil composite.

iv. The curve-fitting empirical relationships between C_c and σ_y were proposed. These equations can be used for compressibility analysis in soils reinforced with basalt fibers ranging from 0-12mm to estimate the projected compression index if the yield pressure and the length of basalt fibers ranging between 0 mm to 12 mm are known.

v. Increasing the length of basalt fibers for each RHA content reduced the coefficient of consolidation (c_v). This reduction was more significant for fiber-reinforced specimens constituting 5%RHA and 10%RHA, with 54.21% and 30% reduction percentages at the end of consolidation. This response indicated that the degree of consolidation depended on the specimen composition and the degree of reinforcement.

vi. The coefficient of volume change (m_v) was greatly influenced by the average consolidation pressure rather than the specimen composition (fiber length and RHA-cement content). However, at low consolidation pressures during the pre-yield stage, fiber-RHA-cement reinforced specimens depicted lower volume changes than the control specimen. Also, a slight increase of m_v with average consolidation pressure was evident compared to the control specimen.

vii. The permeability coefficient (k) of the fiber-reinforced specimen with 5%RHA-3%C reduced with increasing fiber length, whereas, in the case of 10%RHA-3C and 15%RHA-3C, a very minimal reduction in the k value was recorded with increased fiber length.

viii. The curve fitting equations shown in Chapter 5 proposed the analytical equations for evaluating c_v, m_v, and k for basalt fiber lengths ranging between 0 mm and 12 mm, RHA content between 5%-15%, 3% cement, and consolidation pressure stage. However, it should be noted that the equations derived herein were based on the response of stabilized and basalt fiber-reinforced expansive soil composites; hence additional study should be undertaken while working on other types of soils.

ix. The SEM imagery showed that the random distribution of basalt fibers in the stabilized composite enhanced the reinforcing network within the specimens. Increasing the basalt fiber length from 3mm to 12mm provided a more robust reinforcing phenomenon in the stabilized composite, thereby controlling the interfacial strength. This strength enhancement contributed significantly to the trend of the consolidation coefficients.

x. This study concluded that a reconstituted clay soil composite with 1% 12mm basalt fibers, 5% RHA, and 3% cement considerably improved consolidation behavior. This composite had an enhanced yield pressure of 110kN/m^2, compression index of 0.349, and swelling index of 0.0281. Additionally, the relationships discussed demonstrated that reinforcing expansive soils with 12mm basalt fibers, 5%RHA, and 3%cement gave superior qualities to the other mix combinations. Specimen S:5R:3C:1BF12, with 5% RHA content, produced the lowest c_v values compared to other specimens. Also, 5%RHA-3C specimens revealed a well-defined structural development due to cementation from adequate pozzolanic reaction and enhanced reinforcement, as depicted in the SEM images. The slight increase in the k value at BF 12 mm enhanced the hydraulic conductivity of the stabilized soil compared to the other mix combinations, indicating improved drainage conditions. The slow rate at which the soil consolidation process proceeds for this combination (i.e., low c_v values) makes it superior to other mix combinations in this study.

xi. The experimental and analytical methodologies presented in this paper are thus believed to be of great significance for quantifying and interpreting one-dimensional consolidation coefficients and their correlation to fiber reinforcement and RHA-cement stabilization techniques. Also, the correlation equation provided in this study can be used as design charts regarding the consolidation and settlement trends of basalt fiber-RHA-cement stabilized expansive soils.

7.2 Conclusions on the Shear Behaviour: Triaxial Compression Tests

In this study, a series of consolidated drained (CD) triaxial tests were carried out on soil composites reinforced with high-strength basalt fiber filaments (filament lengths 3, 6, and 12 mm) and chemically stabilized with RHA-cement mixtures (5%-15%RHA, and 3% cement), considering curing periods 1 day, 7 days, and 28 days. The experimental results, including the compaction test, stress-strain relationship, and ultimate shear strengths, were reported. The microstructure interaction and chemical composition were also analyzed using SEM and XRD. The following conclusions can be drawn:

i. The combined effects of basalt fiber reinforcements and cementation decreased the maximum dry density (ρ_{dmax}) while maintaining the optimum moisture content (w_{opt}), ensuring economical compaction cost. However, maximum dry density (ρ_{dmax}) reduced across all tested specimen combinations with increasing RHa content. The optimum moisture content (w_{opt}) increased with increasing RHA content due to the high water affinity of the RHA porous microstructure.

ii. During shearing, the improved frictional resistances from fiber reinforcements and cementation in the specimens increased the initial deviatoric stress for the 5%RHa composites to a maximum value of 631.86 kN/m^2, followed by a gradual softening behavior before failure. This development in the deviatoric stresses during loading led to significant growth in shear strength with cohesion and an angle of internal friction reaching maximum values of 180 kN/m^2 and 18.43

degrees, respectively, for specimens having 12 mm filament lengths (S:5R:3C:1BF12) after a curing period of 28 days.

iii. The experimental results showed that fiber filament length dictated the effectiveness of basalt fibers as a potential ground improvement material. The interaction between the longer fibers (12mm) and the specimen's cementitious bonds significantly improved the ultimate shear strength compared to the shorter fibers (6 mm and 3 mm). In addition, the 12 mm basalt fiber filaments greatly affected the specimen ductility at peak stresses than the 6 mm and 3 mm filaments. The 12 mm basalt fiber reinforcing mechanism through interfacial contacts within the new stabilized soil composite containing 5%RHA and 3% cement (S:5R:3C:1BF12) was validated as the optimum filament length and the best combination in choosing the new construction material for use as a base course during ground improvement. However, this conclusion is based on the filament range between 3mm and 12 mm. Further studies are necessary to evaluate the boundary limits considering basalt fiber dosage and filament length.

iv. SEM analysis showed a compact soil composite structure consisting of clusters of cemented materials (soil:RHA:Cement) anchored with basalt fiber filaments, validating the noteworthy developments in shear strength. Moreover, high levels of dominant Calcium AluminoHexasilicate TetraHydrate chains were recorded through XRD analysis.

v. As observed, the experimental results in this study were in good agreement with the related studies on reinforced soil composites. Thus, incorporating basalt fibers, RHA, and nominal dosages of cement into weak soils is a practical approach to solving geotechnical engineering challenges during ground improvement.

7.3 Conclusions on the Bearing Capacity: UCS Tests and Permeability Tests

Unconfined compressive strength tests and permeability tests on soil composites with basalt fibers (lengths 3mm, 6mm, and 12mm), cement (3% of the dry weight of soil), and rice husk ash (5%, 10%,

and 15% of the dry weight of soil) were carried out. The influence of these stabilization aggregates was demonstrated by stress-strain curves and associated geotechnical properties presented in graphical form to aid future designs and relevant construction applications. The effects of basalt fiber as a potential reinforcing material to RHA-treated soils for ground stabilization were investigated in this paper. The following conclusions can be drawn from the results and discussions in Chapter 5.

i. Unconfined compressive strength of compressible clay having 5% rice husk ash increased with the addition of basalt fibers from BF3mm to BF6mm to BF12mm. An increase in UCS value was also evident for 10% and 15% RHA which had UCS values higher than the control specimen but lower than the 5% RHA specimen.

ii. Basalt fibers (BF) and the cementitious soil mass improved compressibility and permeability. Notably, the dimensional considerations of the basalt fiber significantly influenced the compressive strength, with the 12mm fibers specimen, S:5R:3C:1BF12, showing the top q_u of 463 (kN/m^2) and E_{50} of 29(MN/m^2) after 28 days of curing at 25°C.

iii. It was also justifiable through SEM imagery and XRD analyses that the cement underwent a chemical reaction with water during the curing period, forming hydration products (C-A-S-H gels) that bound the soil particles together. As a result, the degree of cementation increased, improving the composite material's mechanical properties. These reactions were more robust on the 5%RHA and 12mm basalt fiber specimen hence the high bearing capacities shown in conclusion number (ii).

iv. The soil-only specimen had a very low permeability of $7.1x10^{-6}$ cm/s, which was not considered suitable for subgrade or shallow foundation use. However, adding basalt fibers into the soil increased k to 10^{-5} cm/s for all 5% to 10%RHA specimens and 10^{-4} cm/s for 15%RHA specimens enhancing the hydraulic conductivity across all the specimens tested in this investigation.

v. In general, including randomly oriented Basalt fiber into the soil, combined with the rapidly hardening C-A-S-H Gel, improved the geotechnical engineering behavior of the new material and can be proposed for use as a subgrade material for roads, pavements, and as fill material in foundation designs.

CHAPTER 8 FUTURE RESEARCH

In the last decade, geotechnical engineers have been driven by a sustainability approach when choosing construction materials, leading to the tendency to use natural fiber reinforcement techniques and new stabilization methods in ground improvement applications, as presented in this study. This approach is essential and can significantly impact the built environment, economy, and natural environment. Based on the extensive analysis in this study and the previous studies, some critical research gaps have been identified, and the future research prospects are listed as follows;

i. It is apparent that experimental laboratory results alone are insufficient to establish the general applicability of the data sets obtained in practical engineering practice. Therefore, a tailored constitutive model based on the experimental results and a theoretical approach using the hypoplastic model has been proposed as future research work to supplement the current study.

ii. Future work on narrowing down the specific applicability of the new composite material in engineering practice can be formulated using the simulation results on the practical applications obtained from item no. 1.

iii. An evaluation of the associated environmental impacts of the current study is necessary through the Life Cycle Assessment (LCA) methodology, considering the relevance of basalt fiber reinforcements and sustainable chemical stabilization processes for soils against conventional alternatives. LCA can be used to determine and classify the probable environmental impacts associated with all the stages of life of the final new composite material (Walubita et al., 2022; Polo-Mendoza et al., 2022a, 2022b). For example, assessment of the new material from raw material extraction, processing, distribution, use, recycling, and final disposal of the used materials depending on the engineering application proposed in item no. 2.

CHAPTER 9 : REFERENCES

Abdi, M.R., Parsapazhouh, A. and Arjmand, M., 2008. Effects of Random Fiber Inclusion on Consolidation, Hydraulic Conductivity, Swelling, Shrinkage Limit and Desiccation Cracking of Clays. Int. J. Civ. Eng. 6 (4), pp.284-292.

Adshead, D., Thacker, S., Fuldauer, L.I. and Hall, J.W., 2019. Delivering on the Sustainable Development Goals through long-term infrastructure planning. Global Environmental Change, 59, pp.101975. https://doi.org/10.1016/j.gloenvcha.2019.101975

Afrin, H., 2017. A review on different types soil stabilization techniques. International Journal of Transportation Engineering and Technology, 3(2), pp.19-24. https://doi.org/10.11648/j.ijtet.20170302.12

Ahmad, F., Bateni, F. and Azmi, M., 2010. Performance evaluation of silty sand reinforced with fibres. Geotextiles and geomembranes, 28(1), pp.93-99. https://doi.org/10.1016/j.geotexmem.2009.09.017

Akan, M.Ö.A., Dhavale, D.G. and Sarkis, J., 2017. Greenhouse gas emissions in the construction industry: An analysis and evaluation of a concrete supply chain. Journal of Cleaner Production, 167, pp.1195-1207. https://doi.org/10.1016/j.jclepro.2017.07.225

Alhassan, M., 2008. Permeability of Lateritic Soil Treated with Lime and Rice Husk Ash. Assumption University (AU) Journal of Technology, Bangkok, Thailand, vol. 12(2), pp.115–120.

Alhassan, M., 2008. Potentials of rice husk ash for soil stabilization. Assumption Univ. Journal of Technology, Bangkok, Thailand, 11: pp246-50.

Ali, F.H., Adnan, A. and Choy, C.K., 1992. Geotechnical properties of a chemically stabilized soil from Malaysia with rice husk ash as an additive. Geotechnical & Geological Engineering, 10, pp.117-134.

Ali, F.H., Adnan, A. and Choy, C.K., 1992. Geotechnical properties of a chemically stabilized soil from Malaysia with rice husk ash as an additive. Geotechnical & Geological Engineering, 10, pp.117-134. https://doi.org/10.1007/BF00881147

Alnmr, A., Ray, R.P. and Alsirawan, R., 2023. A State-of-the-Art Review and Numerical Study of Reinforced Expansive Soil with Granular Anchor Piles and Helical Piles. Sustainability, 15(3), p.2802. https://doi.org/10.3390/su15032802

Al-Rawas, A.A. and Goosen, M.F. eds., 2006. Expansive soils: recent advances in characterization and treatment.

Amu, O.O., Ogunniyi, S.A. and Oladeji, O.O., 2011. Geotechnical properties of lateritic soil stabilized with sugarcane straw ash. American journal of Scientific and industrial Research, 2(2), pp.323-331.

Amu, O.O., Owokade, O.S. and Shitan, O.I., 2011. Potentials of coconut shell and husk ash on the geotechnical properties of lateritic soil for road works. International Journal of Engineering and Technology, 3(2), pp.87-94.

Andavan, S. and Pagadala, V.K., 2020. A study on soil stabilization by addition of fly ash and lime. Materials Today: Proceedings, 22, pp.1125-1129. https://doi.org/10.1016/j.matpr.2019.11.323

Anggraini, V., Asadi, A., Huat, B.B. and Nahazanan, H., 2015. Effects of coir fibers on tensile and compressive strength of lime treated soft soil. Measurement, 59, pp.372-381. https://doi.org/10.1016/j.measurement.2014.09.059

Aprianti, E., Shafigh, P., Bahri, S. and Farahani, J.N., 2015. Supplementary cementitious materials origin from agricultural wastes–A review. Construction and Building Materials, 74, pp.176-187. https://doi.org/10.1016/j.conbuildmat.2014.10.010

Asgari, M.R., Baghebanzadeh Dezfuli, A. and Bayat, M., 2015. Experimental study on stabilization of a low plasticity clayey soil with cement/lime. Arabian Journal of Geosciences, 8, pp.1439-1452. https://doi.org/10.1007/s12517-013-1173-1

Ateş, A., 2016. Mechanical properties of sandy soils reinforced with cement and randomly distributed glass fibers (G.R.C.). Composites Part B: Engineering, 96, pp.295-304. https://doi.org/10.1016/j.compositesb.2016.04.049

Attah, I.C., Etim, R.K. and Usanga, I.N., 2021, March. Potentials of cement kiln dust and rice husk ash blend on strength of tropical soil for sustainable road construction material. In I.O.P. Conference Series: Materials Science and Engineering (Vol. 1036, No. 1, p. 012072). I.O.P. Publishing. http://dx.doi.org/10.1088/1757-899X/1036/1/012072

Bahar, R., Benazzoug, M. and Kenai, S., 2004. Performance of compacted cement-stabilised soil. Cement and concrete composites, 26(7), pp.811-820.https://doi.org/10.1016/j.cemconcomp.2004.01.003

Bahri, S., Mahmud, H.B. and Shafigh, P., 2018. Effect of utilizing unground and ground normal and black rice husk ash on the mechanical and durability properties of high-strength concrete. Sādhanā, 43, pp.1-12. https://doi.org/10.1007/s12046-018-0795-0

Basack, S., Goswami, G., Khabbaz, H., Karakouzian, M., Baruah, P. and Kalita, N., 2021. A comparative study on soil stabilization relevant to transport infrastructure using bagasse ash and

stone dust and cost effectiveness. Civil Engineering Journal (Iran) 7(11) pp.1947-63. http://dx.doi.org/10.28991/cej-2021-03091771

Basha, E.A., Hashim, R., Mahmud, H.B. and Muntohar, A.S., 2005. Stabilization of residual soil with rice husk ash and cement. Construction and building materials, 19(6), pp.448-453. https://doi.org/10.1016/j.conbuildmat.2004.08.001

Bennett, B., Visintin, P. and Xie, T., 2022. Global warming potential of recycled aggregate concrete with supplementary cementitious materials. J. Build. Eng. 52, pp.104394. https://doi.org/10.1016/j.jobe.2022.104394

Bhuvaneswari, S., Thyagaraj, T., Robinson, R.G. and Gandhi, S.R., 2010, December. Alternative technique to induce faster lime stabilization reaction in deeper expansive strata. In Proceedings of Indian Geotechnical Conference–2010, GEOtrendz, December 16–18, Mumbai, India (pp. 609-612).

Bie, R.S., Song, X.F., Liu, Q.Q., Ji, X.Y. and Chen, P., 2015. Studies on effects of burning conditions and rice husk ash (RHA) blending amount on the mechanical behavior of cement. Cement and Concrete Composites, 55, pp.162-168. https://doi.org/10.1016/j.cemconcomp.2014.09.008

Biswal, D.R., Sahoo, U.C. and Dash, S.R., 2019. Durability and shrinkage studies of cement stabilsed granular lateritic soils. International Journal of Pavement Engineering, 20(12), pp.1451-1462. https://doi.org/10.1080/10298436.2018.1433830

Biswas, A. and Krishna, A.M., 2017. Geocell-reinforced foundation systems: a critical review. International Journal of Geosynthetics and Ground Engineering, 3, pp.1-18. https://doi.org/10.1007/s40891-017-0093-7

Blankendaal, T., Schuur, P. and Voordijk, H., 2014. Reducing the environmental impact of concrete and asphalt: a scenario approach. J. Cleaner Prod. 66, pp.27-36. https://doi.org/10.1016/j.jclepro.2013.10.012

Bonen, D. and Cohen, M.D., 1992. Magnesium sulfate attack on portland cement paste-I. Microstructural analysis. Cement and concrete research, 22(1), pp.169-180. https://doi.org/10.1016/0008-8846(92)90147-N

Bordoloi, S., Garg, A. and Sekharan, S., 2017. A review of physio-biochemical properties of natural fibers and their application in soil reinforcement. Advances in Civil Engineering Materials, 6(1), pp.323-359.

Botero, E., Ossa, A., Sherwell, G. and Ovando-Shelley, E., 2015. Stress–strain behavior of a silty soil reinforced with polyethylene terephthalate (PET). Geotextiles and Geomembranes, 43(4), pp.363-369. https://doi.org/10.1016/j.geotexmem.2015.04.003

Bouhicha M., Aouissi F., and Kenai S., 2005. Performance of composite soil reinforced with barley straw Cement and Concrete Composites, 27 (5), pp. 617-621 https://doi.org/10.1016/j.cemconcomp.2004.09.013

Brooks, R.M., 2009. Soil stabilization with flyash and rice husk ash. International journal of research and reviews in applied sciences, 1(3), pp.209-217.

Bulrand, J., Standing, J.R., Mair, R.J., Linney, L.F. and Jardine, F.M., 1996. A collaborative research programme on subsidence damage to buildings: Prediction, protection and repair. In Geotechnical aspects of underground construction in soft ground (pp. 773-778).

Burland, J.B., 1990. On the compressibility and shear strength of natural clays. Géotechnique, 40(3), pp.329-378. http://dx.doi.org/10.1680/geot.1990.40.3.329

Bushra, I. and Robinson, R.G., 2009. Consolidation behaviour of a cement stabilised marine soil. In Proceedings of International Geotechnical Conference (pp. 431-434).

Cai, Y., Shi, B., Ng, C.W. and Tang, C.S., 2006. Effect of polypropylene fibre and lime admixture on engineering properties of clayey soil. Engineering geology, 87(3-4), pp.230-240. https://doi.org/10.1016/j.enggeo.2006.07.007

Casagrande, A., 1936. The determination of the pre-consolidation load and its practical significance. In Proc. 1st Int. Conf. Soil Mech., pp. 3-60

Casagrande, A., and R.E. Fadum, 1940. Notes on Soil Testing for Engineering Purposes," Harvard University Graduate School Engineering Publication, (8), Massachusetts.

Changizi, F. and Haddad, A., 2015. Strength properties of soft clay treated with mixture of nano-SiO2 and recycled polyester fiber. Journal of rock mechanics and Geotechnical Engineering, 7(4), pp.367-378. https://doi.org/10.1016/j.jrmge.2015.03.013

Chauhan, M.S., Mittal, S. and Mohanty, B., 2008. Performance evaluation of silty sand subgrade reinforced with fly ash and fibre. Geotextiles and geomembranes, 26(5), pp.429-435. https://doi.org/10.1016/j.geotexmem.2008.02.001

Chen, M., Shen, S.L., Arulrajah, A., Wu, H.N., Hou, D.W. and Xu, Y.S., 2015. Laboratory evaluation on the effectiveness of polypropylene fibers on the strength of fiber-reinforced and cement-stabilized Shanghai soft clay. Geotextiles and Geomembranes, 43(6), pp.515-523. https://doi.org/10.1016/j.geotexmem.2015.05.004

Chen, R., Congress, S.S.C., Cai, G., Duan, W. and Liu, S., 2021. Sustainable utilization of biomass waste-rice husk ash as a new solidified material of soil in geotechnical engineering: A review. Construction and Building Materials, 292, p.123219. https://doi.org/10.1016/j.conbuildmat.2021.123219

Chen, R., Congress, S.S.C., Cai, G., Duan, W. and Liu, S., 2021. Sustainable utilization of biomass waste-rice husk ash as a new solidified material of soil in geotechnical engineering: A review. Construction and Building Materials, 292, pp.123219. https://doi.org/10.1016/j.conbuildmat.2021.123219

Chenarboni, H.A., Lajevardi, S.H., MolaAbasi, H. and Zeighami, E., 2021. The effect of zeolite and cement stabilization on the mechanical behavior of expansive soils. Construction and Building Materials, 272, p.121630. https://doi.org/10.1016/j.conbuildmat.2020.121630

Cheng, G., Zhu, H.H., Wen, Y.N., Shi, B. and Gao, L., 2020. Experimental investigation of consolidation properties of nano-bentonite mixed clayey soil. Sustainability, 12(2), pp.459. https://doi.org/10.3390/su12020459

Chindaprasirt, P. and Rukzon, S., 2008. Strength, porosity and corrosion resistance of ternary blend Portland cement, rice husk ash and fly ash mortar. Construction and Building Materials, 22(8), pp.1601-1606. https://doi.org/10.1016/j.conbuildmat.2007.06.010

Chindaprasirt, P., Kanchanda, P., Sathonsaowaphak, A. and Cao, H.T., 2007. Sulfate resistance of blended cements containing fly ash and rice husk ash. Construction and Building Materials, 21(6), pp.1356-1361. https://doi.org/10.1016/j.conbuildmat.2005.10.005

Chouksey, A., Dev, N. and Kumari, S., 2019. Review paper on utilization potential of rice husk ash as supplementary cementitious material. In Sustainable Construction and Building Materials: Select Proceedings of ICSCBM 2018 (pp. 673-684). Springer Singapore. https://doi.org/10.1007/978-981-13-3317-0_60

Consoli, N.C., Casagrande, M.D.T. and Coop, M.R., 2007a. Performance of a fibre-reinforced sand at large shear strains. Géotechnique, 57(9), pp.751-756. https://doi.org/10.1680/geot.2007.57.9.751

Consoli, N.C., Heineck, K.S., Casagrande, M.D.T. and Coop, M.R., 2007b. Shear strength behavior of fiber-reinforced sand considering triaxial tests under distinct stress paths. Journal of geotechnical and geoenvironmental engineering, 133(11), pp.1466-1469. https://doi.org/10.1061/(ASCE)1090-0241(2007)133:11(1466)

Consoli, N.C., Prietto, P.D.M. and Ulbrich, L.A., 1999. The behaviour of a fibre-reinforced cemented soil. Proceedings of the Institution of Civil Engineers-Ground Improvement, 3(1), pp.21-30. https://doi.org/10.1680/gi.1999.030103

Consoli, N.C., Vendruscolo, M.A. and Prietto, P.D.M., 2003. Behavior of plate load tests on soil layers improved with cement and fiber. Journal of geotechnical and geoenvironmental engineering, 129(1), pp.96-101. https://doi.org/10.1061/(ASCE)1090-0241(2003)129:1(96)

Cristelo, N., Cunha, V.M., Dias, M., Gomes, A.T., Miranda, T. and Araújo, N., 2015. Influence of discrete fibre reinforcement on the uniaxial compression response and seismic wave velocity of a cement-stabilised sandy-clay. Geotextiles and Geomembranes, 43(1), pp.1-13. https://doi.org/10.1016/j.geotexmem.2014.11.007

Cristelo, N., Glendinning, S., Fernandes, L. and Pinto, A.T., 2013. Effects of alkaline-activated fly ash and Portland cement on soft soil stabilisation. Acta Geotechnica, 8, pp.395-405. https://doi.org/10.1007/s11440-012-0200-9

Cuisinier, O., Le Borgne, T., Deneele, D. and Masrouri, F., 2011. Quantification of the effects of nitrates, phosphates and chlorides on soil stabilization with lime and cement. Eng. Geol. 117(3-4), pp.229-235. https://doi.org/10.1016/j.enggeo.2010.11.002

Das, S. and Pal, S.K., 2012. Consolidation Characteristics of Silty-Clay Soil Mixed with Class F Indian Fly Ash. In Indian Geotechnical Conference, December, pp. 13-45.

de Jesús Arrieta Baldovino, J., dos Santos Izzo, R., Rose, J.L. and Avanci, M.A., 2020. Geopolymers based on recycled glass powder for soil stabilization. Geotechnical and Geological Engineering, 38(4), pp.4013-4031. https://doi.org/10.1007/s10706-020-01274-w

de Lima, T.E., de Azevedo, A.R., Marvila, M.T., Candido, V.S., Fediuk, R. and Monteiro, S.N., 2022. Potential of using Amazon natural fibers to reinforce cementitious composites: a review. Polymers, 14(3), pp.647. https://doi.org/10.3390/polym14030647

De Sensale, G.R., 2010. Effect of rice-husk ash on durability of cementitious materials. Cement and Concrete Composites, 32(9), pp.718-725. https://doi.org/10.1016/j.cemconcomp.2010.07.008

de Sensale, G.R., Ribeiro, A.B. and Gonçalves, A., 2008. Effects of R.H.A. on autogenous shrinkage of Portland cement pastes. Cement and Concrete Composites, 30(10), pp.892-897. https://doi.org/10.1016/j.cemconcomp.2008.06.014

Demirbaş, A., 2002. Fuel characteristics of olive husk and walnut, hazelnut, sunflower, and almond shells. Energy Sources, 24(3), pp.215-221. https://doi.org/10.1080/009083102317243601

Dhand, V., Mittal, G., Rhee, K.Y., Park, S.J. and Hui, D., 2015. A short review on basalt fiber reinforced polymer composites. Composites Part B: Engineering, 73, pp.166-180. https://doi.org/10.1016/j.compositesb.2014.12.011

Dhar, S. and Hussain, M., 2019. The strength behaviour of lime-stabilised plastic fibre-reinforced clayey soil. Road Materials and Pavement Design, 20(8), pp.1757-1778. https://doi.org/10.1080/14680629.2018.1468803

Divya, P.V., Viswanadham, B.V.S. and Gourc, J.P., 2014. Evaluation of tensile strength-strain characteristics of fiber-reinforced soil through laboratory tests. Journal of Materials in civil Engineering, 26(1), pp.14-23. https://doi.org/10.1061/(ASCE)MT.1943-5533.0000772

Du, Y.J., Horpibulsuk, S., Wei, M.L., Suksiripattanapong, C. and Liu, M.D., 2014. Modeling compression behavior of cement-treated zinc-contaminated clayey soils. Soils and Foundations, 54(5), pp.1018-1026. http://dx.doi.org/10.1016/j.sandf.2014.09.007

Duan, W., Cai, G., Liu, S., Yuan, J. and Puppala, A.J., 2019. Assessment of ground improvement by vibro-compaction method for liquefiable deposits from in-situ testing data. International Journal of Civil Engineering, 17, pp.723-735. https://doi.org/10.1007/s40999-018-0348-2

Eberemu, A.O. and Sada, H., 2013. Compressibility characteristics of compacted black cotton soil treated with rice husk ash. Nigerian J. Technol. 32(3), 507-521.

Eberemu, A.O., 2011. Consolidation properties of compacted lateritic soil treated with rice husk ash. Geomaterials, 1(3), pp.70. https://doi.org/10.4236/gm.2011.13011

Eberemu, A.O., Omajali, D.I. and Abdulhamid, Z., 2016. Effect of compactive effort and curing period on the compressibility characteristics of tropical black clay treated with rice husk ash. Geotechnical and Geological Engineering, 34, pp.313-322. https://doi.org/10.1007/s10706-015-9946-9

Fakhrabadi, A., Ghadakpour, M., Choobbasti, A.J. and Kutanaei, S.S., 2021. Evaluating the durability, microstructure and mechanical properties of a clayey-sandy soil stabilized with copper slag-based geopolymer against wetting-drying cycles. Bulletin of Engineering Geology and the Environment, 80, pp.5031-5051. https://doi.org/10.1007/s10064-021-02228-z

Fatahi, B., Fatahi, B., Le, T.M. and Khabbaz, H., 2013. Small-strain properties of soft clay treated with fibre and cement. Geosynthetics International, 20(4), pp.286-300. https://doi.org/10.1680/gein.13.00018

Fatahi, B., Khabbaz, H. and Fatahi, B., 2012. Mechanical characteristics of soft clay treated with fibre and cement. Geosynthetics International, 19(3), pp.252-262. https://doi.org/10.1680/gein.12.00012

Fentaw, M., Alemayehu, E. and Geremew, A., 2021. Experimental study of stabilization of expansive soil using the mixture of marble dust, rice husk ash and cement for sub-grade road construction: A case study of Woldia town. Journal of Civil Engineering, Science and Technology, 12(2), pp.141-159. https://doi.org/10.33736/jcest.3977.2021

Ferrari, A., Favero, V. and Laloui, L., 2016. One-dimensional compression and consolidation of shales. International Journal of Rock Mechanics and Mining Sciences, 88, pp.286-300. https://doi.org/10.1016/j.ijrmms.2016.07.030

Firoozi, A.A. and Baghini, M.S., 2017. AA Firoozi and CG Olgun, Fundamentals of soil stabilization,". International Journal of Geo-Engineering, 8(26). https://doi.org/10.1186/s40703-017-0064-9

Firoozi, A.A., Taha, M.R., Firoozi, A.A. and Khan, T.A., 2014. Assessment of nano-zeolite on soil properties. Aust. J. Basic. Appl. Sci. 8(19), pp.292-295.

Food and Agriculture Organization Corporate Statistical Database FAOSTAT. (2020). Statistical Database of the Food and agricultural organization of the United nation. http://faostat3.fao.org.

Formoso, C.T., Soibelman, L., De Cesare, C. and Isatto, E.L., 2002. Material waste in building industry: main causes and prevention. Journal of construction engineering and management, 128(4), pp.316-325.

G. Sarkar, M.R. Islam, DM Alamgir, D.M. Rokonuzzaman, Interpretation of Rice Husk Ash on Geotechnical Properties of Cohesive Soil, Global J.Res. in Eng.: Civ Struct. Eng. 12(2-A) (2012).

Galán-Marín, C., Rivera-Gómez, C. and Petric, J., 2010. Clay-based composite stabilized with natural polymer and fibre. Construction and Building Materials, 24(8), pp.1462-1468. https://doi.org/10.1016/j.conbuildmat.2010.01.008

Ganesan, K., Rajagopal, K. and Thangavel, K., 2008. Rice husk ash blended cement: Assessment of optimal level of replacement for strength and permeability properties of concrete. Construction and building materials, 22(8), pp.1675-1683. https://doi.org/10.1016/j.conbuildmat.2007.06.011

Gaw, B., Zamora, S., Albano, L.D. and Tao, M., 2011. Soil reinforcement with natural fibers for low-income housing communities. Partial fulfillment of the requirement for the Degree of Bachelor of Science: Worcester Polytechnic Institute. Project number: LDA-1006.

General, A., 2015. Transforming our world: The 2030 agenda for sustainable development. General Assembly. https://undocs.org/A/RES/70/1

Ghadir, P. and Ranjbar, N., 2018. Clayey soil stabilization using geopolymer and Portland cement. Constr. Build. Mater. 188, pp. 361-371. https://doi.org/10.1016/j.conbuildmat.2018.07.207

Ghorbani, A. and Salimzadehshooiili, M., 2018. Evaluation of strength behaviour of cement-RHA stabilized and polypropylene fiber reinforced clay-sand mixtures. Civil Eng J, 4, pp.2628-41. http://dx.doi.org/10.28991/cej-03091187

Ghorbani, A. and Salimzadehshooiili, M., 2019. Dynamic characterization of sand stabilized with cement and RHA and reinforced with polypropylene fiber. Journal of Materials in Civil Engineering, 31(7), pp.04019095. https://doi.org/10.1061/(ASCE)MT.1943-5533.0002727

Ghorbani, A., Salimzadehshooiili, M., Medzvieckas, J. and Kliukas, R., 2018. Strength characteristics of cement-rice husk ash stabilised sand-clay mixture reinforced with polypropylene fibers. The Baltic Journal of Road and Bridge Engineering, 13(4), pp.447-474. https://doi.org/10.7250/bjrbe.2018-13.428

Givi, A.N., Rashid, S.A., Aziz, F.N.A. and Salleh, M.A.M., 2010. Assessment of the effects of rice husk ash particle size on strength, water permeability and workability of binary blended concrete. Construction and Building Materials, 24(11), pp.2145-2150. https://doi.org/10.1016/j.conbuildmat.2010.04.045

Gollop, R.S. and Taylor, H.F.W., 1992. Microstructural and microanalytical studies of sulfate attack. I. Ordinary Portland cement paste. Cement and Concrete Research, 22(6), pp.1027-1038. https://doi.org/10.1016/0008-8846(92)90033-R

Gowthaman, S., Nakashima, K. and Kawasaki, S., 2018. A state-of-the-art review on soil reinforcement technology using natural plant fiber materials: Past findings, present trends and future directions. Materials, 11(4), p.553. https://doi.org/10.3390/ma11040553

Grist, E.R., Paine, K.A., Heath, A., Norman, J. and Pinder, H., 2013. Compressive strength development of binary and ternary lime–pozzolan mortars. Materials & Design (1980-2015), 52, pp.514-523. https://doi.org/10.1016/j.matdes.2013.05.006

Guney, Y., Sari, D., Cetin, M. and Tuncan, M., 2007. Impact of cyclic wetting–drying on swelling behavior of lime-stabilized soil. Building and environment, 42(2), pp.681-688. https://doi.org/10.1016/j.buildenv.2005.10.035

Guo, R., Wang, J., Bing, L., Tong, D., Ciais, P., Davis, S.J., Andrew, R.M., Xi, F. and Liu, Z., 2021. Global CO_2 uptake by cement from 1930 to 2019. Earth System Science Data, 13(4), pp.1791-1805. https://doi.org/10.5194/essd-13-1791-2021

Gupta, D. and Kumar, A., 2016. Strength characterization of cement stabilized and fiber reinforced clay–pond ash mixes. International Journal of Geosynthetics and Ground Engineering, 2, pp.1-11. https://doi.org/10.1007/s40891-016-0069-z

Gupta, D. and Kumar, A., 2017. Performance evaluation of cement-stabilized pond ash-rice husk ash-clay mixture as a highway construction material. Journal of Rock Mechanics and Geotechnical Engineering, 9(1), pp.159-169. https://doi.org/10.1016/j.jrmge.2016.05.010

Hadipramana, J., Samad, A.A.A., Ahmad Mujahid, A.Z., Mohammad, N. and Riza, F.V., 2013. Effect of uncontrolled burning rice husk ash in foamed concrete. In Advanced Materials Research (Vol. 626, pp. 769-775). Trans Tech Publications Ltd. https://doi.org/10.4028/www.scientific.net/AMR.626.769

Hák, T., Janoušková, S. and Moldan, B., 2016. Sustainable Development Goals: A need for relevant indicators. Ecological indicators, 60, pp.565-573. https://doi.org/10.1016/j.ecolind.2015.08.003

Heineck, K.S., Coop, M.R. and Consoli, N.C., 2005. Effect of microreinforcement of soils from very small to large shear strains. Journal of geotechnical and geoenvironmental engineering, 131(8), pp.1024-1033. https://doi.org/10.1061/(ASCE)1090-0241(2005)131:8(1024)

Hejazi, S.M., Sheikhzadeh, M., Abtahi, S.M. and Zadhoush, A., 2012. A simple review of soil reinforcement by using natural and synthetic fibers. Construction and building materials, 30, pp.100-116. https://doi.org/10.1016/j.conbuildmat.2011.11.045

Hong, Z.S., Yin, J. and Cui, Y.J., 2010. Compression behaviour of reconstituted soils at high initial water contents. Géotechnique, 60(9), pp.691-700. http://dx.doi.org/10.1680/geot.09.P.059

Hong, Z.S., Zeng, L.L., Cui, Y.J., Cai, Y.Q. and Lin, C., 2012. Compression behaviour of natural and reconstituted clays. Géotechnique, 62(4), pp.291-301. http://dx.doi.org/10.1680/geot.10.P.046

Horpibulsuk, S., Bergado, D.T. and Lorenzo, G.A., 2004. Compressibility of cement-admixed clays at high water content. Geotechnique, 54(2), pp.151-154.

Horpibulsuk, S., Liu, M.D., Liyanapathirana, D.S. and Suebsuk, J., 2010. Behaviour of cemented clay simulated via the theoretical framework of the Structured Cam Clay model. Computers and Geotechnics, 37(1-2), pp.1-9. http://dx.doi.org/10.1016/j.compgeo.2009.06.007

Horpibulsuk, S., Miura, N. and Bergado, D.T., 2004. Undrained shear behavior of cement admixed clay at high water content. Journal of geotechnical and geoenvironmental engineering, 130(10), pp.1096-1105. http://dx.doi.org/10.1061/(asce)1090-0241(2004)130:10(1096)

Hossain, M.Z. and Awal, A.A., 2011. Flexural response of hybrid carbon fiber thin cement composites. Construction and Building Materials, 25(2), pp.670-677. https://doi.org/10.1016/j.conbuildmat.2010.07.022

Hossain, M.Z. and Sakai, T., 2008. The effectiveness of nominal dosage of ordinary cement on strength and permeability of clayey soil. Journal of the Japanese Society of Soil Physics, 110, pp.25-35. https://doi.org/10.34467/jssoilphysics.110.0_25

Hu, H. and Liu, Y., 2010. High modulus, high tenacity yarns. In Technical textile yarns (pp. 329-386). Woodhead Publishing. https://doi.org/10.1533/9781845699475.2.329

Hussain, J., Khan, A. and Zhou, K., 2020. The impact of natural resource depletion on energy use and CO2 emission in Belt & Road Initiative countries: A cross-country analysis. Energy, 199, pp.117409. https://doi.org/10.1016/j.energy.2020.117409

Igwe, O. and Adepehin, E.J., 2017. Alternative approach to clay stabilization using granite and dolerite dusts. Geotechnical and Geological Engineering, 35(4), pp.1657-1664. https://doi.org/10.1007/s10706-017-0200-5

J.N. Jha, K.S. Gill, 2006. Effect of rice husk ash on lime stabilization of soil. J. Inst. Eng. (India), Part CV, Civil Engineering Division 87 (2006)33-39.

Jain, A. and Puri, N., 2013. Consolidation characteristics of highly plastic clay stabilized with rice husk ash. Int. J. of Soft Comput. Eng. (IJSCE). 2, pp.413-418.

Jalal, F.E., Xu, Y., Jamhiri, B. and Memon, S.A., 2020. On the recent trends in expansive soil stabilization using calcium-based stabilizer materials (C.S.M.s): a comprehensive review. Advances in Materials Science and Engineering, 2020, pp.1-23. https://doi.org/10.1155/2020/1510969

James, J. and Pandian, P.K., 2016. Industrial wastes as auxiliary additives to cement/lime stabilization of soils. Adv. Civ. Eng. pp.1267391, 17 pages. https://doi.org/10.1155/2016/1267391

Jamil, M., Kaish, A.B.M.A., Raman, S.N. and Zain, M.F.M., 2013. Pozzolanic contribution of rice husk ash in cementitious system. Construction and Building Materials, 47, pp.588-593. https://doi.org/10.1016/j.conbuildmat.2013.05.088

Jamsawang, P., Suansomjeen, T., Sukontasukkul, P., Jongpradist, P. and Bergado, D.T., 2018. Comparative flexural performance of compacted cement-fiber-sand. Geotextiles and Geomembranes, 46(4), pp.414-425. https://doi.org/10.1016/j.geotexmem.2018.03.008

Jaya, R.P., Nor, M.A.A.M., Ahmad, Z.A. and Amin, Z.M., 2013. Properties of mortar containing rice husk ash at different temperature and exposed to aggressive environment. In Advanced Materials Research (Vol. 620, pp. 87-93). Trans Tech Publications Ltd. https://doi.org/10.4028/www.scientific.net/AMR.620.87

JCK Corporation, 2022. Basalt Fiber Materials, Products and Development. バサルト繊維素材、製品、開発は JCK 株式会社へ, Accessed 31 August 2022. http://www.j-c-k.co.jp/shohin.html. https://drive.google.com/file/d/1qxw-ZF47EmhUFIJB3IIy6ndejN6pK1D9/view

JGS 0524~0524, 2001. Method for consolidated-drained triaxial compression test on soils, Jpn. Geotech. Soc. Dositsu Shiken Hou Dositsu Kogakkai: (2001)233-43. [In Japanese].

JIS A 1204, 2010. Sieve and hydrometer. Soil particle size analysis test. Japanese Industrial Standard, Guidance and Basic - Soil Test, The Jpn. Geotech. Soc. (in Japanese) (2010), pp.27.

JIS A 1205, 2010. Soil Liquid Limit and Plastic Limit tests. Japanese Industrial Standard, Guidance and Basic - Soil Test, The Jpn. Geotech. Soc. (in Japanese) (2010), pp.39.

JIS A 1210, 2010. Test method for soil compaction using a rammer. Japanese Industrial Standard, Guidance and Basic - Soil Test, The Jpn. Geotech. Soc. (in Japanese) (2010)71-78.

JIS A 1216, 2010. Method for unconfined compression test of soils. Japanese Industrial Standard, Guidance and Basic - Soil Test, The Jpn. Geotech. Soc. (in Japanese) 151-158.

JIS A 1217, 2010. Test method for soil consolidation test. Japanese Industrial Standard, Guidance and Basic - Soil Test, The Jpn. Geotech. Soc. (in Japanese) (2010), pp.215-227.

JIS A 1218, 2010. Permeability test of soils. Japanese Industrial Standard, Guidance and Basic - Soil Test, The Jpn. Geotech. Soc. (in Japanese) 91-102.

JIS A 1227, 2010. Test method for soil consolidation test. Japanese Industrial Standard, Guidance and Basic - Soil Test, The Jpn. Geotech. Soc. (in Japanese) (2010), pp.215-227.

Kamruzzaman, A.H., Chew, S.H. and Lee, F.H., 2009. Structuration and destructuration behavior of cement-treated Singapore marine clay. Journal of geotechnical and geoenvironmental engineering, 135(4), pp.573-589. http://dx.doi.org/10.1061/(asce)1090-0241(2009)135:4(573)

Kar, R. and Pradhan, P., 2011. Strength and compressibility characteristics of randomly distributed fiber-reinforced soil. International Journal of Geotechnical Engineering, 5(2), pp.235-243. https://doi.org/10.3328/IJGE.2011.05.02.235-243

Karatai, T.R., Kaluli, J.W., Kabubo, C. and Thiong'o, G., 2017. Soil stabilization using rice husk ash and natural lime as an alternative to cutting and filling in road construction. Journal of Construction Engineering and Management, 143(5), p.04016127.

Kaur, I., 2016. Effects of Rice Husk Ash–Cement Mixtures on Stabilization of Clayey Soils. International Journal of Computer Applications, 975, p.8887.

Kazemain, S. and Barghchi, M., 2012. Review of soft soils stabilization by grouting and. Scientific Research and Essays, 7(24), pp.2104-2111. https://doi.org/10.5897/SRE11.1186

Khalid, N., Mukri, M., Kamarudin, F. and Arshad, M.F., 2012. Clay soil stabilized using waste paper sludge ash (WPSA) mixtures. Electronic Journal of Geotechnical Engineering, 17(1), pp.1215-1225.

Khassaf, S.I., Jasim, A.T. and Mahdi, F.K., 2014. Investigation the properties of concrete containing rice husk ash to reduction the seepage in canals. International Journal of Scientific Technology Research, 3(4), pp.348-354.

Khazaei, J. and Moayedi, H., 2019. Soft expansive soil improvement by eco-friendly waste and quick lime. Arabian Journal for Science and Engineering, 44(10), pp.8337-8346.https://doi.org/10.1007/s13369-017-2590-3

Khemissa, M. and Mahamedi, A., 2014. Cement and lime mixture stabilization of an expansive overconsolidated clay. Applied Clay Science, 95, pp.104-110. https://doi.org/10.1016/j.clay.2014.03.017

Kitazume, M. and Terashi, M., 2013. The deep mixing method. C.R.C. press.

Kuhnt, G., 1993. Behavior and fate of surfactants in soil. Environmental Toxicology and Chemistry: An International Journal, 12(10), pp.1813-1820.

Kumar, A. and Gupta, D., 2016. Behavior of cement-stabilized fiber-reinforced pond ash, rice husk ash–soil mixtures. Geotextiles and Geomembranes, 44(3), pp.466-474. https://doi.org/10.1016/j.geotexmem.2015.07.010

Kumar, A., Walia, B.S. and Mohan, J., 2006. Compressive strength of fiber reinforced highly compressible clay. Construction and building materials, 20(10), pp.1063-1068. https://doi.org/10.1016/j.conbuildmat.2005.02.027

Kumari, N. and Mohan, C., 2021. Basics of clay minerals and their characteristic properties. Clay Clay Miner, 24, pp.1-29.

Laskar, A. and Pal, S.K., 2013. Effects of waste plastic fibres on compaction and consolidation behavior of reinforced soil. EJGE, 18, pp.1547-1558.

Lawton, E.C., Khire, M.V. and Fox, N.S., 1993. Reinforcement of soils by multioriented geosynthetic inclusions. Journal of Geotechnical Engineering, 119(2), pp.257-275.

Leroueil, S., Vaughan, P. R., 1990. The general and congruent effects of structure in natural soils and weak rocks, Géotech. (40) (3), pp.467-488

Li, J., Tang, C., Wang, D., Pei, X. and Shi, B., 2014. Effect of discrete fibre reinforcement on soil tensile strength. Journal of Rock Mechanics and Geotechnical Engineering, 6(2), pp.133-137. https://doi.org/10.1016/j.jrmge.2014.01.003

Lima, D.C. and Bueno, B.S., 1996. The mechanical response of soil-lime mixtures reinforced with short synthetic fiber. In Proc., 3rd Int. Symp. on Environ. Geotechnol. 1 (1996)868-877).

Little, D.N., 1992. Comparison of in-situ resilient moduli of aggregate base courses with and without low percentages of lime stabilization. ASTM International.

Little, D.N., 1995. Stabilization of pavement subgrades and base courses with lime. Kendall Hunt Publishing Company, Austin, Tex, USA

Little, D.N., Males, E.H., Prusinski, J.R. and Stewart, B., 2000. Cementitious stabilization. Transportation in the new millennium, Transportation Research Board, pp. 1–7, 2000. http://pubsindex.trb.org/view.aspx?id=639997

Liu, J., Qi, X., Zhang, D., Feng, Q., Wang, Y. and Kanungo, D.P., 2017. Study on the permeability characteristics of polyurethane soil stabilizer reinforced sand. Advances in Materials Science and Engineering, 2017. https://doi.org/10.1155/2017/5240186

Liu, J., Wang, T. and Tian, Y., 2010. Experimental study of the dynamic properties of cement-and lime-modified clay soils subjected to freeze–thaw cycles. Cold Regions Science and Technology, 61(1), pp.29-33. https://doi.org/10.1016/j.coldregions.2010.01.002

Liu, M.D. and Carter, J.P., 1999. Virgin compression of structured soils. Géotechnique, 49(1), pp.43-57. https://doi.org/10.1680/geot.1999.49.1.43

Liu, Y., Liu, X. and Liu, Z., 2022. Effects of climate change on paddy expansion and potential adaption strategies for sustainable agriculture development across Northeast China. Applied Geography, 141, p.102667. https://doi.org/10.1016/j.apgeog.2022.102667

Lorenzo, G.A. and Bergado, D.T., 2006. Fundamental characteristics of cement-admixed clay in deep mixing. Journal of materials in civil engineering, 18(2), pp.161-174. https://doi.org/10.1061/(ASCE)0899-1561(2006)18:2(161)

M.Y Fattah, F.H Rahil, K.Y.H. Al-Soudan, Improvement of clayey soil characteristics using Rice Husk Ash, J. Civ. Eng. and Urban. JCEU, ISSN-2252-0430, 3(1) (2013) 12-18.

Malekzadeh, M. and Bilsel, H., 2012. Swell and compressibility of fiber reinforced expansive soils. International journal of advanced Technology in civil engineering, 1(2), pp.42-45.

Malekzadeh, M., Lovisa, J. and Sivakugan, N., 2016. An overview of electrokinetic consolidation of soils. Geotechnical and Geological Engineering, 34, pp.759-776. https://doi.org/10.1007/s10706-016-0002-1

Malhotra V.M., Mehta P.K. 2004. Pozzolanic and cementitious materials. CRC Press, Boca Raton, FL, USA

Mallela, J., Quintus, H.V. and Smith, K., 2004. Consideration of lime-stabilized layers in mechanistic-empirical pavement design. The National Lime Association, 200(1), pp.1-40.

Marandi, S.M., Bagheripour, M.H., Rahgozar, R., and Zare H., 2008. Strength and ductility of randomly distributed palm fibers reinforced silty-sand soils. American Journal of Applied Sciences, 5(3), pp.209-220.

Mayooran, S., Ragavan, S. and Sathiparan, N., 2017. Comparative study on open air burnt low-and high-carbon rice husk ash as partial cement replacement in cement block production. Journal of Building Engineering, 13, pp.137-145. https://doi.org/10.1016/j.jobe.2017.07.011

Meena, S.K., Sahu, R. and Ayothiraman, R., 2021. Utilization of waste wheat straw fibers for improving the strength characteristics of clay. Journal of Natural Fibers, 18(10), pp.1404-1418. https://doi.org/10.1080/15440478.2019.1691116

Mendonça, A., Morais, P.V., Pires, A.C., Chung, A.P. and Oliveira, P.J.V., 2021. Reducing soil permeability using bacteria-produced biopolymer. Applied Sciences, 11(16), p.7278. https://doi.org/10.3390/app11167278

Metelková, Z., Boháč, J., Přikryl, R. and Sedlářová, I., 2012. Maturation of loess treated with variable lime admixture: Pore space textural evolution and related phase changes. Applied clay science, 61, pp.37-43. https://doi.org/10.1016/j.clay.2012.03.008

Mironova, M.V. and Ilyin, S.O., 2018. Effect of silica and clay minerals on rheology of heavy crude oil emulsions. Fuel, 232, pp.290-298. https://doi.org/10.1016/j.fuel.2018.05.164

Mishra, B., 2016. A study on ground improvement techniques and its applications. International Journal of Innovative Research in Science, Engineering and Technology, 5(1), pp.72-86.

Mishra, P., Shukla, S. and Mittal, A., 2022. Stabilization of subgrade with expansive soil using agricultural and industrial by-products: A review. Materials Today: Proceedings. https://doi.org/10.1016/j.matpr.2022.04.397

Mo, K.H., Alengaram, U.J., Jumaat, M.Z., Yap, S.P. and Lee, S.C., 2016. Green concrete partially comprised of farming waste residues: a review. J. Cleaner Prod. 117, pp.122-138. https://doi.org/10.1016/j.jclepro.2016.01.022

Mohammad, N., Moghal, A.A.B., Rasheed, R.M. and Almajed, A., 2022. Critical review on the efficacy of electrokinetic techniques in geotechnical and geoenvironmental applications. Arabian Journal of Geosciences, 15(8), p.781. https://doi.org/10.1007/s12517-022-10037-1

Mollamahmutoglu, M. and Avcı, E., 2018. Engineering properties of slag-based superfine cement-stabilized clayey soil. ACI Materials Journal, 115(4), pp.541-548.

Mosavat, N., Oh, E. and Chai, G., 2012. A review of electrokinetic treatment technique for improving the engineering characteristics of low permeable problematic soils. GEOMATE Journal, 2(4), pp.266-272. https://geomatejournal.com/geomate/article/view/1465

Mostafiz, R.B., Friedland, C.J., Rohli, R.V., Bushra, N. and Held, C.L., 2021. Property risk assessment for expansive soils in Louisiana. Frontiers in Built Environment, 7, p.754761. https://doi.org/10.3389/fbuil.2021.754761

Muñoz, Y.O., dos Santos Izzo, R.L., de Almeida, J.L., Baldovino, J.A. and Rose, J.L., 2021. The role of rice husk ash, cement and polypropylene fibers on the mechanical behavior of a soil from Guabirotuba formation. Transportation Geotechnics, 31, p.100673. https://doi.org/10.1016/j.trgeo.2021.100673

Muntohar, A.S. and Hantoro, G., 2000. Influence of rice husk ash and lime on engineering properties of a clayey subgrade. Electronic Journal of Geotechnical Engineering, 5(2000), pp.1-13.

Muntohar, A.S., 2002. Utilization of uncontrolled burnt rice husk ash in soil improvement. Civil Engineering Dimension, 4(2), pp.100-105. https://doi.org/10.9744/ced.4.2.pp.%20100-105

Muntohar, A.S., 2004, October. Uses of RHA to enhanced lime-stabilized clay soil. In International Conference of Geotechnical Engineering, University of Sharjah, United Arab Emirate (pp. 356-357).

Nagaraj, T.S., Pandian, N.S. and Narasimha Raju, P.S.R., 1998. Compressibility behaviour of soft cemented soils. Geotechnique, 48(2), pp.281-287. https://doi.org/10.1680/geot.1998.48.2.281

Nahar, N., Hossain, Z. and Tamaki, N., 2021. Optimum utilization of rice husk ash waste for ground improvement. Int. Agric. Eng. J, 30, pp.1-10.

Nahar, N., Owino, A.O., Khan, S.K., Hossain, Z. and Tamaki, N., 2021. Effects of controlled burn rice husk ash on geotechnical properties of the soil. Journal of Agricultural Engineering, 52(4). https://doi.org/10.4081/jae.2021.1216

Nath, B.D., Molla, M., Ali, K. and Sarkar, G., 2017. Study on strength behavior of organic soil stabilized with fly ash. International scholarly research notices, 2017. https://doi.org/10.1155/2017/5786541

Nazari, Z., Tabarsa, A. and Latifi, N., 2021. Effect of compaction delay on the strength and consolidation properties of cement-stabilized subgrade soil. Transportation Geotechnics, 27, p.100495. https://doi.org/10.1016/j.trgeo.2020.100495

Nehdi, M., Duquette, J. and El Damatty, A., 2003. Performance of rice husk ash produced using a new technology as a mineral admixture in concrete. Cement and concrete research, 33(8), pp.1203-1210. https://doi.org/10.1016/S0008-8846(03)00038-3

Nelson, E.J., Chao, K.C., Nelson, J.D. and Overton, D.D., 2017. Lessons learned from foundation and slab failures on expansive soils. Journal of Performance of Constructed Facilities, 31(3), pp.D4016007. https://doi.org/10.1061/(ASCE)CF.1943-5509.0000958

Nguyen, D.T. and Phan, V.T.A., 2021. Engineering properties of soil stabilized with cement and fly ash for sustainable road construction. International Journal of Engineering, 34(12), pp.2665-2671. https://doi.org/10.5829/IJE.2021.34.12C.12

Nguyen, L. and Fatahi, B., 2016. Behaviour of clay treated with cement & fibre while capturing cementation degradation and fibre failure–C3F Model. International Journal of Plasticity, 81, pp.168-195. http://dx.doi.org/10.1016/j.ijplas.2016.01.015

Njock, P.G.A., Chen, J., Modoni, G., Arulrajah, A. and Kim, Y.H., 2018. A review of jet grouting practice and development. Arabian Journal of Geosciences, 11, pp.1-31. https://doi.org/10.1007/s12517-018-3809-7

Noor, M.J.M.M., Aziz, A.A. and Suhadi, R.U.R., 1993. Effects of cement-rice husk ash mixtures on compaction, strength, and durability of Melaka Series lateritic soil. Prof. J. Inst. Surveyors Malaysia, 28, pp.61-7.

Novikau, R. and Lujaniene, G., 2022. Adsorption behaviour of pollutants: Heavy metals, radionuclides, organic pollutants, on clays and their minerals (raw, modified and treated): A

review. Journal of Environmental Management, 309, p.114685. https://doi.org/10.1016/j.jenvman.2022.114685

Nshimiyimana, P., Miraucourt, D., Messan, A. and Courard, L., 2018. Calcium carbide residue and rice husk ash for improving the compressive strength of compressed earth blocks. MRS Advances, 3(34-35), pp.2009-2014. https://doi.org/10.1557/adv.2018.147

Obuzor, G.N., Kinuthia, J.M. and Robinson, R.B., 2012. Soil stabilisation with lime-activated-GGBS—A mitigation to flooding effects on road structural layers/embankments constructed on floodplains. Engineering Geology, 151, pp.112-119. https://doi.org/10.1016/j.enggeo.2012.09.010

Olugbenga, A.M.U., Adetayo, O., Faluyi, F. and Akinyele, E., 2021. Experimental study of improving the properties of lime-stabilized structural lateritic soil for highway structural works using groundnut shell ash. Walailak Journal of Science and Technology (WJST), 18(9), pp.9475-17. https://doi.org/10.48048/wjst.2021.9475

Onyelowe, K., Alaneme, G., Igboayaka, C., Orji, F., Ugwuanyi, H., Van, D.B. and Van, M.N., 2019. Scheffe optimization of swelling, California bearing ratio, compressive strength, and durability potentials of quarry dust stabilized soft clay soil. Materials Science for Energy Technologies, 2(1), pp.67-77. https://doi.org/10.1016/j.mset.2018.10.005

Onyelowe, K.C., Onyia, M.E., Bui Van, D., Baykara, H. and Ugwu, H.U., 2021. Pozzolanic reaction in clayey soils for stabilization purposes: a classical overview of sustainable transport geotechnics. Advances in Materials Science and Engineering, 2021, pp.1-7. https://doi.org/10.1007/s41204-021-00123-2

Otunyo, A.W. and Chukuigwe, C.C., 2018. Investigation of the impact of palm bunch ash on the stabilization of poor lateritic soil. Nigerian Journal of Technology, 37(3), pp.600-604. https://doi.org/10.4314/njt.v37i3.6

Ouhadi, V.R., Yong, R.N., Amiri, M. and Ouhadi, M.H., 2014. Pozzolanic consolidation of stabilized soft clays. Applied Clay Science, 95, pp.111-118. https://doi.org/10.1016/j.clay.2014.03.020

Owino, A.O., Nahar, N., Hossain, Z. and Tamaki, N., 2022a. Dimensional influence of basalt fiber reinforcements on the consolidation behaviour of rice husk ash stabilized soils. Construction and Building Materials, 339, p.127686. https://doi.org/10.1016/j.conbuildmat.2022.127686

Owino, A.O., Nahar, N., Hossain, Z. and Tamaki, N., 2022b. Effects of basalt fibres on strength and permeability of rice husk ash-treated expansive soils. Journal of Agricultural Engineering, 53(1). https://doi.org/10.4081/jae.2022.1315

Pallanza, A., To, P. and Matheson, M., 2023. Lime stabilised road batters: A laboratory simulation of site flood conditions using a customised erosion apparatus and sample digitisation. Transportation Geotechnics, 40, p.100975. https://doi.org/10.1016/j.trgeo.2023.100975

Panda, A.P. and Rao, S.N., 1998. Undrained strength characteristics of an artificially cemented marine clay. Marine georesources & geotechnology, 16(4), pp.335-353. https://doi.org/10.1080/10641199809379976

Park, S.S., 2009. Effect of fiber reinforcement and distribution on unconfined compressive strength of fiber-reinforced cemented sand. Geotextiles and Geomembranes, 27(2), pp.162-166. https://doi.org/10.1016/j.geotexmem.2008.09.001

Patel, Y.J. and Shah, N., 2018. Enhancement of the properties of ground granulated blast furnace slag based self compacting geopolymer concrete by incorporating rice husk ash. Construction and Building Materials, 171, pp.654-662. https://doi.org/10.1016/j.conbuildmat.2018.03.166

Pode, R., 2016. Potential applications of rice husk ash waste from rice husk biomass power plant. Renewable and Sustainable Energy Reviews, 53, pp.1468-1485. https://doi.org/10.1016/j.rser.2015.09.051

Polo-Mendoza, R., Martinez-Arguelles, G. and Peñabaena-Niebles, R., 2022a. A multi-objective optimization based on genetic algorithms for the sustainable design of Warm Mix Asphalt (WMA). International Journal of Pavement Engineering, pp.1-21. https://doi.org/10.1080/10298436.2022.2074417

Polo-Mendoza, R., Penabaena-Niebles, R., Giustozzi, F. and Martinez-Arguelles, G., 2022. Eco-friendly design of Warm mix asphalt (WMA) with recycled concrete aggregate (RCA): A case study from a developing country. Construction and Building Materials, 326, p.126890. https://doi.org/10.1016/j.conbuildmat.2022.126890

Porbaha, A., Shibuya, S. and Kishida, T., 2000. State of the art in deep mixing technology. Part III: geomaterial characterization. Proceedings of the Institution of Civil Engineers-Ground Improvement, 4(3), pp.91-110. https://doi.org/10.1680/grim.2000.4.3.91

Poudyal, L. and Adhikari, K., 2021. Environmental sustainability in cement industry: An integrated approach for green and economical cement production. Resources, Environment and Sustainability, 4, pp.100024. https://doi.org/10.1016/j.resenv.2021.100024

Prusinski, J.R. and Bhattacharja, S., 1999. Effectiveness of Portland cement and lime in stabilizing clay soils. Transp. Res. Rec. 1652(1), pp.215-227. https://doi.org/10.3141/1652-28

Puppala, A.J., 2021. Performance evaluation of infrastructure on problematic expansive soils: Characterization challenges, innovative stabilization designs, and monitoring methods. Journal of Geotechnical and Geoenvironmental Engineering, 147(8), p.04021053. https://doi.org/10.1061/(ASCE)GT.1943-5606.0002518

Puppala, A.J., Congress, S.S. and Banerjee, A., 2019. Research advancements in expansive soil characterization, stabilization and geoinfrastructure monitoring. In Frontiers in geotechnical engineering (pp. 15-29). Singapore: Springer Singapore. https://doi.org/10.1061/(ASCE)GT.1943-5606.0002518

R. D. Koteswara, P. R. T. Pranav, M. Anusha, Stabilization of Expansive Soil with Rice Husk Ash, Lime, and Gypsum –An Experimental Study, Int. J. of Eng. Sci. Tech., (3) (11) (2011) 8076 – 8085.

Rabab'ah, S., Al Hattamleh, O., Aldeeky, H. and Alfoul, B.A., 2021. Effect of glass fiber on the properties of expansive soil and its utilization as subgrade reinforcement in pavement applications. Case Studies in Construction Materials, 14, p.e00485. https://doi.org/10.1016/j.cscm.2020.e00485

Rahman, M.A., 1986. The potentials of some stabilizers for the use of lateritic soil in construction. Building and Environment, 21(1), pp.57-61. https://doi.org/10.1016/0360-1323(86)90008-9

Rahman, M.A., 1987. Effects of cement-rice husk ash mixtures on geotechnical properties of lateritic soils. Soils and Foundations, 27(2), pp.61-65. https://doi.org/10.3208/sandf1972.27.2_61

Rajasekaran, G., 2005. Sulphate attack and ettringite formation in the lime and cement stabilized marine clays. ocean engineering, 32(8-9), pp.1133-1159. https://doi.org/10.1016/j.oceaneng.2004.08.012

Ramezanianpour, A.A., Mahdikhani, M. and Ahmadibeni, G.H., 2009. The effect of rice husk ash on mechanical properties and durability of sustainable concretes.

Rao, D.K., Pranav, P.R.T. and Anusha, M., 2011. Stabilization of expansive soil with rice husk ash, lime and gypsum–an experimental study. International Journal of Engineering Science and Technology, 3(11), pp.8076-8085.

Rao, S.M. and Shivananda, P., 2005. Role of curing temperature in progress of lime-soil reactions. Geotechnical & Geological Engineering, 23, pp.79-85. https://doi.org/10.1007/s10706-003-3157-5

Robinson, R.G. and Allam, M.M., 1998. Effect of clay mineralogy on coefficient of consolidation. Clays and clay minerals, 46, pp.596-600.

Rogelj, J., Shindell, D., Jiang, K., Fifita, S., Forster, P., Ginzburg, V., Handa, C., Kheshgi, H., Kobayashi, S., Kriegler, E., Mundaca, L., Séférian, R. and Vilariño, M. V., 2018. Mitigation Pathways Compatible with 1.5°C in the Context of Sustainable Development, available at: https://www.ipcc.ch/site/assets/uploads/sites/2/2019/02/SR15_Chapter2_Low_Res.pdf (last access: April 24 2023).

Rogers, C.D. and Glendinning, S., 2000. Lime requirement for stabilization. Transportation research record, 1721(1), pp.9-18. https://doi.org/10.3141/1721-02

Rozainee, M., Ngo, S.P., Salema, A.A. and Tan, K.G., 2008. Fluidized bed combustion of rice husk to produce amorphous siliceous ash. Energy for Sustainable Development, 12(1), pp.33-42. https://doi.org/10.1016/S0973-0826(08)60417-2

Salas, A., Delvasto, S., de Gutierrez, R.M. and Lange, D., 2009. Comparison of two processes for treating rice husk ash for use in high performance concrete. Cement and concrete research, 39(9), pp.773-778. https://doi.org/10.1016/j.cemconres.2009.05.006

Santhanam, M., Cohen, M.D. and Olek, J., 2003. Mechanism of sulfate attack: a fresh look: Part 2. Proposed mechanisms. Cement and concrete research, 33(3), pp.341-346. https://doi.org/10.1016/S0008-8846(02)00724-X

Santos, T., Almeida, J., Silvestre, J.D. and Faria, P., 2021. Life cycle assessment of mortars: A review on technical potential and drawbacks. Construction and Building Materials, 288, p.123069.

Saraswathy, V. and Song, H.W., 2007. Corrosion performance of rice husk ash blended concrete. Construction and building materials, 21(8), pp.1779-1784. https://doi.org/10.1016/j.conbuildmat.2006.05.037

Sebesta, S., 2005. Use of microcracking to reduce shrinkage cracking in cement-treated bases. Transportation research record, 1936(1), pp.2-11. https://doi.org/10.1177/0361198105193600101

Sefene, S.S., 2021. Determination of effective wood ash proportion for black cotton soil improvement. Geotechnical and Geological Engineering, 39(1), pp.617-625. https://doi.org/10.1007/s10706-020-01508-x

Sharma, M., Samanta, M. and Sarkar, S., 2019. Soil nailing: an effective slope stabilization technique. Landslides: Theory, practice and modelling, pp.173-199.

Sharma, V., Vinayak, H.K. and Marwaha, B.M., 2015. Enhancing compressive strength of soil using natural fibers. Construction and Building Materials, 93, pp.943-949. https://doi.org/10.1016/j.conbuildmat.2015.05.065

Sim, J. and Park, C., 2005. Characteristics of basalt fiber as a strengthening material for concrete structures. Composites Part B: Engineering, 36(6-7), pp.504-512. https://doi.org/10.1016/j.compositesb.2005.02.002

Singh, D. and Kumar, A., 2017. Geo-environmental application of municipal solid waste incinerator ash stabilized with cement. Journal of rock mechanics and Geotechnical Engineering, 9(2), pp.370-375. https://doi.org/10.1016/j.jrmge.2016.11.008

Singh, M., Sharma, R. and Abhishek, A., 2017. Soil stabilization using industrial waste (wheat husk and sugarcane straw ash). Int. J. Res. Eng. Technol, 4, pp.589-596.

Sivakumar Babu, G.L., Vasudevan, A.K. and Sayida, M.K., 2008. Use of coir fibers for improving the engineering properties of expansive soils. Journal of Natural Fibers, 5(1), pp.61-75. https://doi.org/10.1080/15440470801901522

Solanki, P. and Zaman, M., 2012. Microstructural and mineralogical characterization of clay stabilized using calcium-based stabilizers. In Scanning electron microscopy. IntechOpen. https://doi.org/10.5772/34176

Soleimani Kutanaei, S. and Janalizadeh Choobbasti, A., 2017. Effects of nanosilica particles and randomly distributed fibers on the ultrasonic pulse velocity and mechanical properties of cemented sand. Journal of Materials in Civil Engineering, 29(3), p.04016230. https://doi.org/10.1061/(ASCE)MT.1943-5533.0001761

Spence, R. and Mulligan, H., 1995. Sustainable development and the construction industry. Habitat International, 19(3), pp.279-292. https://doi.org/10.1016/0197-3975(94)00071-9

Sridharan, A. and Nagaraj, H.B., 2004. Coefficient of consolidation and its correlation with index properties of remolded soils. Geotech. Test. J. 27(5), 469-474.

Suebsuk, J., Horpibulsuk, S. and Liu, M.D., 2010. Modified Structured Cam Clay: A generalised critical state model for destructured, naturally structured and artificially structured clays. Computers and Geotechnics, 37(7-8), pp.956-968. http://dx.doi.org/10.1016/j.compgeo.2010.08.002

Suriya, P., Naveenkumar, K., Raj, E.M., Prabakaran, M. and Kumar, R.V., 2020, September. Analyzing the shear strength of clay soil by stone column aided with geosynthetics and waste

plastics. In A.I.P. Conference Proceedings (Vol. 2271, No. 1, p. 030017). A.I.P. Publishing L.L.C. https://doi.org/10.1063/5.0024748

Syed, M., GuhaRay, A., Agarwal, S. and Kar, A., 2020. Stabilization of expansive clays by combined effects of geopolymerization and fiber reinforcement. Journal of The Institution of Engineers (India): Series A, 101, pp.163-178. https://doi.org/10.1007/s40030-019-00418-3

Taha, M.M., Feng, C.P. and Ahmed, S.H., 2021. Modification of mechanical properties of expansive soil from north China by using rice husk ash. Materials, 14(11), pp.2789. https://doi.org/10.3390/ma14112789

Taher, Z.J., Scalia IV, J. and Bareither, C.A., 2020. Comparative assessment of expansive soil stabilization by commercially available polymers. Transportation Geotechnics, 24, p.100387. https://doi.org/10.1016/j.trgeo.2020.100387

Tang, C., Shi, B., Gao, W., Chen, F. and Cai, Y., 2007. Strength and mechanical behavior of short polypropylene fiber reinforced and cement stabilized clayey soil. Geotextiles and Geomembranes, 25(3), pp.194-202. https://doi.org/10.1016/j.geotexmem.2006.11.002

Terzaghi K., 1943. Theoretical Soil Mechanics[M]. New York, N Y: John Wiley and Sons Inc.

Thomas, B.S. and Gupta, R.C., 2015. Long term behaviour of cement concrete containing discarded tire rubber. Journal of Cleaner Production, 102, pp.78-87. https://doi.org/10.1016/j.jclepro.2015.04.072

Toé Casagrande, M.D., Coop, M.R. and Consoli, N.C., 2006. Behavior of a fiber-reinforced bentonite at large shear displacements. Journal of Geotechnical and Geoenvironmental Engineering, 132(11), pp.1505-1508. https://doi.org/10.1061/(ASCE)1090-0241(2006)132:11(1505)

Tom, J., 2012, June. Rice by product set to increase by husks. [Blog post]. Retrieved from http://tominmwea.blogspot.com/2012/06/rice-byproduct-set-to-increase-by-husks.html

Ureña, C., Azañón, J.M., Caro, J.M., Irigaray, C., Corpas, F., Ramírez, A., Rivas, F., Salazar, L.M. and Mochón, I., 2012. Use of Biomass Ash as a stabilization agent for expansive marly soils (SE Spain). EGU General Assembly, 2012.

Vakili, A.H., Salimi, M., Lu, Y., Shamsi, M. and Nazari, Z., 2022. Strength and post-freeze-thaw behavior of a marl soil modified by lignosulfonate and polypropylene fiber: An environmentally friendly approach. Construction and Building Materials, 332, p.127364. https://doi.org/10.1016/j.conbuildmat.2022.127364

Van Oss, H.G. and Padovani, A.C., 2002. Cement manufacture and the environment: part I: chemistry and technology. Journal of Industrial Ecology, 6(1), pp.89-105. https://doi.org/10.1162/108819802320971650

Venkatanarayanan, H.K. and Rangaraju, P.R., 2013. Material characterization studies on low-and high-carbon rice husk ash and their performance in portland cement mixtures. Advances in Civil Engineering Materials, 2(1), pp.266-287. https://doi.org/10.1520/acem20120056

Venkatanarayanan, H.K. and Rangaraju, P.R., 2015. Effect of grinding of low-carbon rice husk ash on the microstructure and performance properties of blended cement concrete. Cement and concrete composites, 55, pp.348-363. https://doi.org/10.1016/j.cemconcomp.2014.09.021

Veritasium, 2023. The Science of Thinking: Explaining concrete while getting buried in it [Video]. YouTube (Accessed April 28). https://www.youtube.com/watch?v=rWVAzS5duAs&t=1179s&ab_channel=Veritasium

Walubita, L.F., Martinez-Arguelles, G., Polo-Mendoza, R., Ick-Lee, S. and Fuentes, L., 2022. Comparative Environmental Assessment of Rigid, Flexible, and Perpetual Pavements: A Case Study of Texas. Sustainability, 14(16), p.9983. https://doi.org/10.3390/su14169983

Wang Y., Guo P., Ren W., Yuan B., Yuan H., Zhao Y., Shan S., and Cao P., 2017. Laboratory investigation of strength characteristics of expansive soil treated with jute fibre reinforcement International Journal of Geomechanics, 17 (11) https://doi.org/10.1061/(ASCE)GM.1943-5622.0000998

Wang, D., Abriak, N.E. and Zentar, R., 2013. Strength and deformation properties of Dunkirk marine sediments solidified with cement, lime and fly ash. Engineering Geology, 166, pp.90-99. http://dx.doi.org/10.1016/j.enggeo.2013.09.007

Wang, H.S., Tang, C.S., Gu, K., Shi, B. and Inyang, H.I., 2020. Mechanical behavior of fiber-reinforced, chemically stabilized dredged sludge. Bulletin of Engineering Geology and the Environment, 79, pp.629-643. https://doi.org/10.1007/s10064-019-01580-5

Wang, L., 2002. Cementitious stabilization of soils in the presence of sulfate. Louisiana State University and Agricultural & Mechanical College.

Wang, Q., Maezono, T., Chen, Q., Apaer, P., Wang, Y., Gui, L., Niida, D., Mitsumura, N., Domon, M., Fujiwara, I. and Yamaguchi, N., 2011. Basic study on combustion characteristics of waste rice husk and emission behavior from a new-type air vortex current combustor. uiae t bl Chem sr uti able Chem sr Sustainable Chemistry, pp.199.

Wang, Y.X., Guo, P.P., Ren, W.X., Yuan, B.X., Yuan, H.P., Zhao, Y.L., Shan, S.B. and Cao, P., 2017. Laboratory investigation on strength characteristics of expansive soil treated with jute fiber reinforcement. International Journal of Geomechanics, 17(11), p.04017101. https://doi.org/10.1061/(ASCE)GM.1943-5622.0000998

Wattez, T., Patapy, C., Frouin, L., Waligora, J. and Cyr, M., 2021. Interactions between alkali-activated ground granulated blastfurnace slag and organic matter in soil stabilization/solidification. Transportation Geotechnics, 26, p.100412. https://doi.org/10.1016/j.trgeo.2020.100412

Wong, L.S., Hashim, R. and Ali, F.H., 2008. Strength and permeability of stabilized peat soil. Journal of Applied Sciences, 8(21), pp.3986-3990.

Wu, Y., Li, Y. and Niu, B., 2014. Assessment of the mechanical properties of sisal fiber-reinforced silty clay using triaxial shear tests. The Scientific World Journal, 2014. https://doi.org/10.1155/2014/436231

Xu, D.S., Huang, M. and Zhou, Y., 2020. One-dimensional compression behavior of calcareous sand and marine clay mixtures. International Journal of Geomechanics, 20(9), p.04020137. https://doi.org/10.1061/(ASCE)GM.1943-5622.0001763

Xu, W., Lo, T.Y., Wang, W., Ouyang, D., Wang, P. and Xing, F., 2016. Pozzolanic reactivity of silica fume and ground rice husk ash as reactive silica in a cementitious system: A comparative study. Materials, 9(3), pp.146. https://doi.org/10.3390/ma9030146

Yadav, A.K., Gaurav, K., Kishor, R. and Suman, S.K., 2017. Stabilization of alluvial soil for subgrade using rice husk ash, sugarcane bagasse ash and cow dung ash for rural roads. International Journal of Pavement Research and Technology, 10(3), pp.254-261. https://doi.org/10.1016/j.ijprt.2017.02.001

Yadav, J.S., Tiwari, S.K. and Shekhwat, P., 2018. Strength behaviour of clayey soil mixed with pond ash, cement and randomly distributed fibres. Transportation Infrastructure Geotechnology, 5, pp.191-209. https://doi.org/10.1007/s40515-018-0056-z

Yeo, S.S., Shackelford, C.D. and Evans, J.C., 2005. Consolidation and hydraulic conductivity of nine model soil-bentonite backfills. Journal of Geotechnical and Geoenvironmental Engineering, 131(10), pp.1189-1198. https://doi.org/10.1061/(ASCE)1090-0241(2005)131:10(1189)

Yi, Y., Gu, L. and Liu, S., 2015. Microstructural and mechanical properties of marine soft clay stabilized by lime-activated ground granulated blast furnace slag. Appl. Clay Sci. 103, pp.71-76. https://doi.org/10.1016/j.clay.2014.11.005

Yin, J.H., 2001. Stress-strain-strength characteristics of soft Hong Kong marine deposits without or with cement treatment. Lowland Technology International, 3(1, June), pp.1-13. https://cot.unhas.ac.id/journals/index.php/ialt_lti/article/view/285

Yixian, W., Panpan, G., Shengbiao, S., Haiping, Y. and Binxiang, Y., 2016. Study on strength influence mechanism of fiber-reinforced expansive soil using jute. Geotechnical and Geological Engineering, 34, pp.1079-1088. https://doi.org/10.1007/s10706-016-0028-4

Yong, R.N. and Ouhadi, V.R., 2007. Experimental study on instability of bases on natural and lime/cement-stabilized clayey soils. Applied clay science, 35(3-4), pp.238-249. https://doi.org/10.1016/j.clay.2006.08.009

Yoobanpot, N. and Jamsawang, P., 2014. Effect of cement replacement by rice husk ash on soft soil stabilization. Agriculture and Natural Resources, 48(2), pp.323-332.

Yu, Q., Sawayama, K., Sugita, S., Shoya, M. and Isojima, Y., 1999. The reaction between rice husk ash and Ca (OH) 2 solution and the nature of its product. Cement and concrete research, 29(1), pp.37-43. https://doi.org/10.1016/S0008-8846(98)00172-0

Yuan-qiang, C., Xu, L. and Shi-ming, W., 2004. One-dimensional consolidation of layered soils with impeded boundaries under time-dependent loadings. Applied Mathematics and Mechanics, 25, pp.937-944. https://doi.org/10.1007/BF02438802

Zain, M.F.M., Islam, M.N., Mahmud, F. and Jamil, M., 2011. Production of rice husk ash for use in concrete as a supplementary cementitious material. Construction and building materials, 25(2), pp.798-805. https://doi.org/10.1016/j.conbuildmat.2010.07.003

Zhang, M.H., Lastra, R. and Malhotra, V.M., 1996. Rice-husk ash paste and concrete: some aspects of hydration and the microstructure of the interfacial zone between the aggregate and paste. Cement and concrete Research, 26(6), pp.963-977. https://doi.org/10.1016/0008-8846(96)00061-0

Zhang, R., Arrigoni, A. and Panesar, D.K., 2021. Could reactive MgO cement be a green solution? The effect of CO2 mineralization and manufacturing route on the potential global warming impact. Cem. Concr. Compos. 124, pp.104263. https://doi.org/10.1016/j.cemconcomp.2021.104263

Zhang, Y., Korkiala-Tanttu, L.K. and Borén, M., 2019. Assessment for sustainable use of quarry fines as pavement construction materials: part II-stabilization and characterization of quarry fine materials. Materials, 12(15), p.2450. https://doi.org/10.3390/ma12152450

Zhang, Z., Liu, S., Yang, F., Weng, Y. and Qian, S., 2021. Sustainable high strength, high ductility engineered cementitious composites (E.C.C.) with substitution of cement by rice husk ash. Journal of Cleaner Production, 317, p.128379. https://doi.org/10.1016/j.jclepro.2021.128379

Zheng, C., Zhao, D., Chen, C., Song, Z. and Zheng, S., 2013. Quantitative test technology study on the mesoscopic strength parameters of the mineral aggregate contact surface of bituminous-stabilized macadam. Construction and Building Materials, 40, pp.622-631. https://doi.org/10.1016/j.conbuildmat.2012.11.059

Zhou, Y.F., Li, J.S., Lu, J.X., Cheeseman, C. and Poon, C.S., 2020. Sewage sludge ash: A comparative evaluation with fly ash for potential use as lime-pozzolan binders. Construction and Building Materials, 242, p.118160. https://doi.org/10.1016/j.conbuildmat.2020.118160

CHAPTER 10 : COPIES OF PUBLISHED SCIENTIFIC PAPERS

COPIES OF PUBLISHED SCIENTIFIC PAPERS

HOSTED BY
ELSEVIER
Available online at www.sciencedirect.com
ScienceDirect
Soils and Foundations 63 (2023) 101351
SOILS AND FOUNDATIONS
www.elsevier.com/locate/sandf

Technical Paper

Correlation between one-dimensional consolidation coefficients and different basalt fiber lengths and RHA-cement contents in fiber-reinforced stabilized expansive soils

Alex Otieno Owino *, Zakaria Hossain

Graduate School of Bioresources, Mie University, Japan

Received 31 August 2022; received in revised form 6 June 2023; accepted 26 June 2023

Abstract

Recently, environmentally friendly soil reinforcement and stabilization techniques, used to reconstitute weak expansive soils, are on the rise, calling for an in-depth analysis of the consolidation projections on the engineering structures built on them. This study investigated one-dimensional consolidation coefficients by conducting a series of oedometer tests on expansive soils reinforced with basalt fibers of different lengths, stabilized with rice husk ash (RHA) as an environmentally friendly cement-reducing aggregate, and nominal dosages of cement in specified combinations. The correlation between the coefficients of consolidation (c_v), volume change (m_v), and permeability (k) and different basalt fiber lengths and RHA-cement contents in ultimate soil composite material was quantified using equations and graphical forms. Furthermore, scanning electron microscopic imagery (SEM) was conducted to examine the structural modifications within the reinforced and stabilized soil specimens upon one-dimensional consolidation. The results showed that basalt fiber-reinforced specimens, comprised of 5% RHA and 3% cement mixtures, showed the lowest one-dimensional consolidation coefficients with a notably greater reduction at high-stress states than the control specimen. Additionally, the coefficients of volume change (m_v) and permeability (k) decreased with the increased compactive effort, with a clear and significant reduction in the basalt fiber-reinforced stabilized soil composites. This study also proposed the best material combination scheme and analytical equations for evaluating the c_v, m_v, and k considering basalt fiber lengths at different pressure levels. The ultimate soil composites had superior properties, and thus, can be used as fill or subbase material for such engineering structures as embankments, pavements, and foundations.

Keywords: Soil consolidation; Basalt fiber; RHA; Coefficient of consolidation; Coefficient of volume change; Permeability coefficient; SEM

1. Introduction

Along with the increase in the built environment, due to urbanization and industrialization, there is a rising demand for infrastructure development in marginalized areas with weak expansive soils, which are considered unsuitable. Expansive soils have been reported to possess weak shear strength and high compressibility and to pose numerous challenges to civil and geotechnical engineers when constructing any engineering structures on them. The instability of expansive soils is due to their high clay contents, which tend to cause the soils to shrink or expand when subjected to a variation in moisture contents. Building on expansive soils can lead to considerable damage to foundations, embankments, and pavements, increasing the cost of constructing durable and safe structures.

Stabilizing and reinforcing these expansive soils in order to improve their geotechnical properties is vital to dealing with these challenges. Conventionally, the incorporation of additives, such as cement, lime, and lime-cement mixtures, has been practiced extensively (Yi et al., 2015;

* Corresponding author.
E-mail address: 520d2s2@m.mie-u.ac (A.O. Owino).

https://doi.org/10.1016/j.sandf.2023.101351

Firoozi et al., 2014; Wang, 2002; Prusinski and Bhattacharja, 1999; Cuisinier et al., 2011; James and Pandian, 2016). However, the over-dependence on cement and lime has proven to degrade the environment, raising environmental concerns such as contributing to 8% to 10% of the global anthropogenic CO_2 emissions from the 4.1 billion metric tonnes produced yearly (Poudyal and Adhikari, 2021). Moreover, CO_2 emissions significantly contribute to global warming, the depletion of natural resources, and the generation of dust from the related manufacturing processes (Ghadir and Ranjbar, 2018; Zhang et al., 2021; Bennett et al., 2022; Hussain et al., 2020; Mo et al., 2016; Blankendaal et al., 2014). In addition to the environmental drawbacks, cement and lime are susceptible to high plastic shrinkage and cracking, affecting the mechanical strength of the stabilized soil (Biswal et al., 2019). To reduce these environmental concerns and enhance the geotechnical properties of expansive soils, the partial replacement of cement and lime with pozzolanic additives, such as rice husk ash (RHA), is gaining research attention. The potential use of RHA in soil stabilization can be attributed to the abundance of rice husks generated worldwide during rice processing (Sandhu and Siddique, 2017) and particularly the presence of highly active amorphous silica (SiO_2) produced during the production of rice husk ash (Chen et al., 2021). However, during the soil stabilization phase, the pozzolanic reactions between the additives and the soil form cementitious systems that need further reinforcement in order to avoid cracking and excessive settlement problems when subjected to extensive loads. Recently, natural fibers, such as basalt fibers, have been used with pozzolanic additives to arrest the formation of weak planes in stabilized soil and to control the consolidation rate while improving the strength (Owino et al., 2022a).

To validate the effectiveness of the reinforcement and stabilization techniques using basalt fibers and RHA, an understanding of the consolidation parameters, namely, the coefficient of consolidation (c_v), coefficient of volume change (m_v), and the ultimate permeability coefficient (k), is critical. The consolidation rate is related to the c_v, while the settlement amount is related to the m_v. Based on experiments, researchers have realized that stabilization and fiber reinforcement techniques have increased strength, enhanced stability, and substantially reduced the rate of consolidation settlement.

While working on fiber-reinforced soil, Abdi et al. (2008) found that increasing the content and length of the fibers significantly reduced the consolidation settlement, swelling, and crack formation. In another study, while investigating the consolidation responses of silty clayey soils stabilized with fly ash, Das and Pal (2012) noted that the coefficient of consolidation (c_v) increased with the fly ash content. As for the coefficient of volume change (m_v), Kar and Pradhan (2011) studied the compressibility trends of polypropylene and coir fiber-reinforced local cohesive soils. Their results showed that the m_v decreased significantly with an increase in the fiber content. In addition, the study concluded that the coefficient of consolidation increased with the fiber content. In their research on the one-dimensional consolidation of expansive soils treated with RHA only, Eberemu and Sada (2013) found that the coefficients of volume change (m_v) and consolidation (c_v) generally decreased with increased loading pressure and RHA treatment up to 8%. Moreover, in the same study, the coefficient of permeability was seen to decrease with the increased RHA content up to 8%.

The use of RHA as a stabilizing agent and fibers as a reinforcing agent has attracted the attention of researchers who have found that RHA and fibers have an advantageous effect in developing the geotechnical properties of the soils under study (Rao et al., 2011; Sabat, 2013; Changizi and Haddad, 2015; Fatahi et al., 2013; Muñoz et al., 2021). However, in the available literature, most articles have been limited to the type of reinforcement material, type of soil, and type of stabilizing agent applied in their particular research. In addition, the testing procedures have been limited to unconfined compression, triaxial, direct shear, and CBR tests. To date, little research has been carried out on expansive soils and no scientific studies can be found on the combined action of RHA and basalt fibers, especially its effect on consolidation settlement, volume change, and permeability.

Within this context, the aim of the present study is to investigate the correlation between the consolidation coefficients and the addition of different basalt fiber lengths and RHA-cement contents in expansive soils. In addition, the proposal of a material combination scheme with superior properties, that could be used as fill or subbase material for engineering structures, such as embankments, pavements, and foundations, is also considered. A series of oedometer tests are conducted on expansive soils reinforced with basalt fibers of different lengths (3, 6, and 12 mm) and stabilized with RHA (5%, 10%, and 15%)-cement (3%) mixtures under the specified combinations. A correlation between the coefficients of consolidation (c_v), volume change (m_v), and permeability (k) and the length of the basalt fibers and the RHA-cement contents in the ultimate soil composite material is determined. Furthermore, scanning electron microscopic imagery (SEM) is conducted to examine the structural modifications within the stabilized and reinforced soil composites upon complete one-dimensional consolidation. The results are presented graphically with correlation equations and pictorial forms to provide additional data and to act as a benchmark in providing solutions to challenges encountered by civil, geotechnical, and geo-environmental engineers working with the new composite material.

2. Materials

2.1. Soil

The soil used in this study was obtained from the Handa area of Mie Prefecture, Japan. The index properties of the

Table 1
Properties of soil.

Property	Value
Specific gravity	2.74
Sand (75 μm–2 mm) (%)	6.14
Silt (5 μm–75 μm) (%)	51.24
Clay (<5 μm) (%)	38.86
Liquid limit LL (%)	58.21
Plastic limit PL (%)	31.05
Plasticity index PI (%)	27.16
Optimum water content (%)	26.02
Maximum dry density (g/cm^3)	1.65
AASHTO classification	A-7–5(2)

soil are shown in Table 1 and the particle size distribution is illustrated in Fig. 1. Based on the American Association of State Highway and Transportation Officials (AASHTO), the soil was classified as A-7–5(2) clayey soil.

2.2. Rice husk ash (RHA)

Rice husk ash is prepared by burning rice husks, a byproduct of rice milling, at temperatures between 650 °C and 700 °C for 27 h (Nahar et al., 2021; Boateng and Skeete, 1990; Tamaki, 2019). These temperatures and time produce high amorphous silica levels (91%), a valuable element for pozzolanic reactions. RHA was adopted for this study due to its potential use as a sustainable and environmentally friendly stabilizer ensuring the proper use of disposed RHA (Behak, 2017). Additionally, RHA has the potential to act as a cement-reducing aggregate, conserving the environment from pollution associated with cement manufacturing (Sandhu and Siddique, 2022). In this study, RHA dosages were set to be between 5% and 15% because the optimal strength of RHA-stabilized soil is achieved when the RHA content is between 5% and 15% (Owino et al., 2022b). This range in RHA content provides the best balance between strength and cost-effectiveness in terms of the costs related to cement reduction, soil stabilization, and RHA disposal.

Moreover, the rate of RHA addition also depends on the properties of the soil. Soils with high plasticity and low permeability require higher rates of RHA addition to improve their strength and stability. Therefore, the range provided in this study ensured a detailed parametric study on the RHA dosage during expansive soil stabilization. Make Integrated Technology Co., Ltd, Osaka, Japan provided the controlled burnt RHA used in this study. The properties of the RHA and the particle size distribution are shown in Table 2 and Fig. 1, respectively.

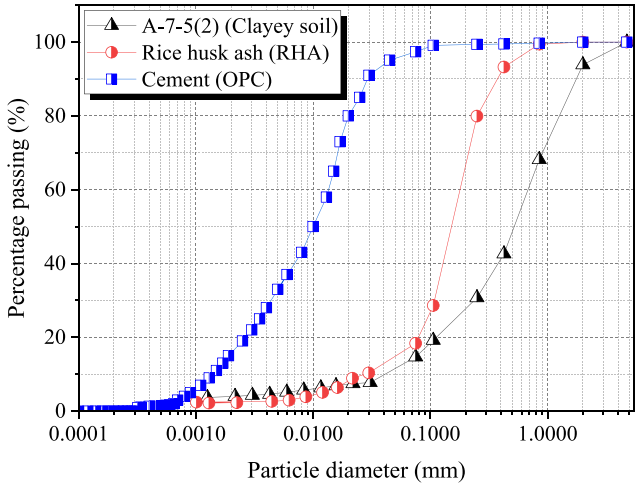

Fig. 1. Particle size distributions of soil, RHA, and OPC.

2.3. Basalt fiber (BF)

Basalt fiber is a material made from fine fibers of natural basalt rock. The production of BF is a one-stage process involving the melting and homogenization of basalt rock and its extrusion through small nozzles to produce continuous filaments of basalt fiber (Hu and Liu, 2010; Dhand et al., 2015). Basalt fibers were used as the primary reinforcing material in this study. The superiority of BF, compared to other conventional fibers, is due to its high tensile strength (4100 to 4840 MPa), high elastic modulus (93.1 to 111.0 GPa), long-term durability, thermal stability, and alkali resistance (Sim and Park, 2005). JCK Corporation provided the fibers in their standardized forms of 3, 6, and 12 mm (https://www.j-c-k.co.jp). The detailed physical, thermal, and chemical properties of the BF used in this study are shown in Table 3.

2.4. Ordinary portland cement (OPC)

The properties of OPC are shown in Table 4 and a detailed particle size distribution is shown in Fig. 1. Minimal dosages of OPC were used as the pozzolanic reaction activator by providing the calcium oxide ions as a binder element. Additionally, the minimum dosage of 3% cement was typically used for the following reasons: (i) Higher cement dosages can have a negative environmental impact, such as increased carbon emissions and depletion of natu-

Table 2
Physical and chemical properties of RHA.

Physical property	Value
Specific gravity	1.47
Average particle size (mm)	0.001 to 0.30
Loss of ignition	4.00 to 6.00
Chemical property	
Oxide compounds	Value (%)
Silica (SiO_2)	91.10
Carbon dioxide (CO_2)	4.35
Potassium oxide (K_2O)	2.40
Calcium oxide (CaO)	0.57
Iron oxide (Fe_2O_3)	0.05
Alumina (Al_2O_3)	0.03
Others	1.50

Table 3
Properties of basalt fibers.

Physical Property	Value
Fiber diameter (μm)	6∼30
Fiber length (mm)	3, 6 & 12
Density (g/cm^3)	2.63∼2.80
Tensile strength (MPa)	4100∼4840
Elastic modulus (GPa)	93.10∼110
Fracture elongation rate (%)	3.1
Thermal property	Value
Heat resistance temperature (°C)	−269∼650
Thermal conductivity (W/mk)	0.03∼0.04
Melting temperature (°C)	1450
Softening temperature (°C)	1050
Chemical property	
Oxides composition	Value (%)
Silicon oxide (SiO_2)	51.6∼59.3
Aluminum oxide (Al_2O_3)	14.6∼18.3
Iron oxide (Fe_2O_3)	9.00∼14.0
Calcium oxide (CaO)	5.90∼9.40
Magnesium oxide (MgO)	3.00∼5.30
Others	0.09∼0.13

Table 4
Properties of OPC.

Physical property	Value
Initial setting time (minutes)	170
Final setting time (minutes)	225
Specific gravity (g/cm^3)	3.15
Specific surface area (m^2/kg)	340
28-day compressive strength (MPa)	33∼53
Loss of ignition (%)	<4
Chemical property	
Oxide composition	Value (%)
Calcium oxide (CaO)	63.40
Silicon dioxide (SiO_2)	21.60
Iron oxide (Fe_2O_3)	5.35
Alumina (Al_2O_3)	4.45
Magnesium oxide (MgO)	1.65
Others	3.55

ral resources during their production. (ii) Using the 3% cement dosage is a cost-effective solution for achieving the required strength and stability if other binding aggregates with cementitious properties, such as RHA, are used. (iii) Cohesive soils, such as expansive soils, require less cement than non-cohesive soils like sand. As discussed in the previous section, the minimal dosages of cement can reduce the overdependence on OPC and enable the application of sustainable cement-reducing alternatives.

3. Experimental apparatus and techniques

3.1. Oedometric cell apparatus

The experimental equipment used in this study is presented in Fig. 2. It consists of an oedometric cell on a rigid base, a loading lever arm, and a dial gauge combined with an LVDT (Linear Variable Differential Transformer). The oedometric cell included a water container, a pressurizing plate fitted with a porous plate at the bottom, a guide ring, a consolidation ring, and a bottom plate equipped with porous media. The guide and consolidation rings were made of stainless steel with a uniform diameter of 60 mm and a height of 20 mm. They were inserted into the bottom plate to ensure high rigidity, thereby minimizing expansion in the radial direction during loading. The porous media on the pressurizing and bottom plates allowed proper drainage through the specimens during one-dimensional consolidation.

3.2. Specimen preparation procedure

During the specimen preparation, one of the primary objectives was to achieve the maximum effect of the fibers, securing their random installation in the soil composite. The dry materials were dry-mixed manually using a spatula before adding water. The dry-mixing process ensured the random distribution of the fibers and aided in preventing the effect of fiber balling, which was checked through physical observation of the mixture before adding water. It is important to note that many factors, including the type of fibers, fiber stiffness, concentration of fibers, and specimen preparation method and time, can influence the distribution of the fibers in a soil specimen. Therefore, it is essential to carefully control these factors to guarantee accurate results. In this case, a visual inspection of the fiber distribution was possible due to the stiffness of the basalt fibers that enabled the random distribution of the individual fibers in the soil.

Each specimen was prepared using soil (200 g), RHA (5%, 10%, or 15% dry weight of the soil), cement (3% dry weight of the soil), and basalt fibers (3, 6, or 12 mm in length and 1% dry weight of the soil for each length) in their specified combination schemes, as shown in Table 5. Water was added to reach initial water contents of 47.81%, 51.53%, and 55.62% for the 5% RHA, 10% RHA, and 15% RHA, respectively. The difference in the initial water contents was due to the high-water affinity for the higher percentages of RHA when mixed with soil, as observed through an optimum moisture content evaluation in a related study (Owino et al., 2022b). The stipulated water contents, just below the liquid limit of the clay soil,

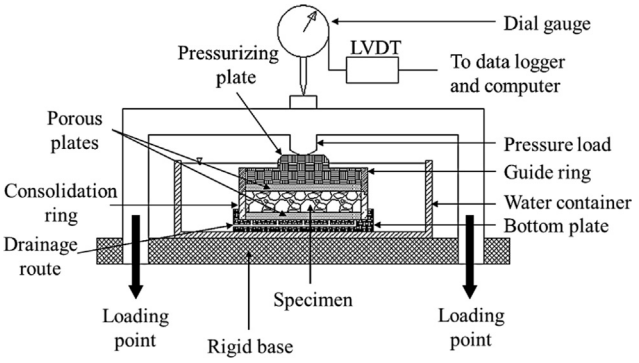

Fig. 2. Components of oedometric cell apparatus.

enhanced the handling and formability of the specimens. The added water increased the water contents of the specimens to within the range of the liquid limit of medium plastic clay (40%–60%), hence simulating pore water pressures similar to those of clay in its natural state (Sridharan and Nagaraj, 2004; Owino et al., 2022a). Preparing the specimens within this liquid limit was essential mainly because it is considered the limiting water content above which the soil almost flows, and it is one of the main parameters dictating the compressibility of soil. Next, the materials were mixed for 10 min using a spatula to obtain a homogeneous paste, rolled by hand into a 30-mm-thick cylindrical shape, and then placed in a desiccator for 24 h to achieve maximum moisture equilibration. Afterward, the specimens were trimmed using the cutting rings (diameter = 60 mm; height = 20 mm), and the excess soil was cut off using a cutting wire before transferring them to the soil consolidation rings. The dimensions of the initial cylindrical specimens were maintained for each combination scheme to minimize the scalability errors for each prepared specimen. The trimmed soil specimens were used to evaluate the initial water content of each specimen.

Concerning the above specimen preparation procedure, it should be noted that the scale effect of the basalt fiber length on the mechanical properties of the specimens is dependent on the dimensions of the soil specimen being tested. In general, longer basalt fibers can provide more reinforcement to the soil composites and can lead to improved mechanical properties. However, the effect of the fiber length on the mechanical properties of basalt fiber-reinforced soil may not be consistent across different specimen sizes. This is because the ratio of fiber length to specimen size can affect how the fibers interact with the soil matrix and with each other. Therefore, it is essential to consider the specimen dimensions, basalt fiber dosage percentages, and length when designing and testing basalt fiber-reinforced soils to ensure that the chosen fiber length is appropriate for the scale of the specimens.

Additionally, the void ratio, density, and degree of saturation of the specimens were calculated, as will be discussed in the subsequent section. Filter paper, with similar dimensions to the consolidation rings, was placed at the top and bottom of each specimen to prevent the soil composite from clogging the porous plates during the loading and drainage processes. A detailed specimen preparation procedure for all ten combinations is shown in Fig. 3. The preparation procedure for the control specimen (Specimen 1) followed the same steps from 1 to 8 minus the additives in Steps 1 and 2.

3.3. Experimental procedure

After transferring the specimens into the consolidation rings, the initial weight and dimensions were determined. The oedometric cell was assembled and filled with water, as shown in Fig. 3 [item (8) Fully assembled oedometric cell]. Afterward, the mechanical loading–unloading cycles were performed in steps with incremental loads of 9.8, 19.6, 39.2, 78.5, 157, 314, 628, and 1256 kPa during the loading cycle and 628, 314, 157, 78.5, 39.2, 19.6, and 9.8 kPa during the unloading cycle. All the load increments/reductions were kept constant for 24 h until the primary consolidation had ceased and the excess pore water pressure had dissipated completely (Ferrari et al., 2016).

Meanwhile, the settlement of each specimen over time was measured using an electronic dial gauge, combined with an LVDT, and connected to a data logger and computer to maintain accuracy among the obtained data sets. Each specimen was consolidated for 16 days, after which it was weighed and oven-dried to calculate the final water content. Finally, a piece of each specimen was collected for the SEM analysis. The testing procedure followed the Japan Industrial Standards (JIS) (JIS A 1217, 2010; JIS A 1227, 2010).

4. Results and discussion

In this section, the states of each specimen before and after consolidation were assessed. Subsequently, the influence of the additives on the one-dimensional consolidation coefficients was analyzed using the time-compression curves from the oedometer tests. The curves were used to

Table 5
Specimen combination schemes.

Specimen	Combination	Code
1	100% S	S
2	100% S + 5%RHA + 3%C + 1%BF3	S:5R:3C:1BF3
3	100% S + 10%RHA + 3%C + 1%BF3	S:10R:3C:1BF3
4	100% S + 15%RHA + 3%C + 1%BF3	S:15R:3C:1BF3
5	100% S + 5%RHA + 3%C + 1%BF6	S:5R:3C:1BF6
6	100% S + 10%RHA + 3%C + 1%BF6	S:10R:3C:1BF6
7	100% S + 15%RHA + 3%C + 1%BF6	S:15R:3C:1BF6
8	100% S + 5%RHA + 3%C + 1%BF12	S:5R:3C:1BF12
9	100% S + 10%RHA + 3%C + 1%BF12	S:10R:3C:1BF12
10	100% S + 15%RHA + 3%C + 1%BF12	S:15R:3C:1BF12

Note: S = Soil, RHA/R = Rice husk ash, C = Cement, BF3 = Basalt fiber 3 mm, BF6 = Basalt fiber 6 mm, BF12 = Basalt fiber 12 mm.

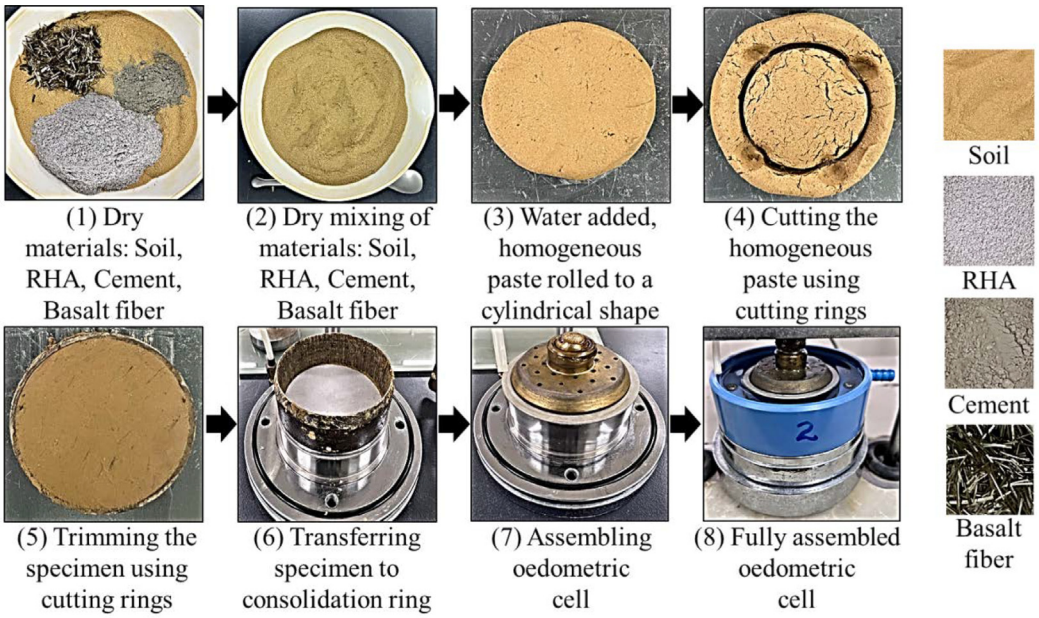

Fig. 3. Specimen preparation procedure and oedometric cell assembly, Note: The surface cracks on the rolled 30-mm-thick cylindrical shape in item (4) were removed by cutting off the extra 10 mm, thus reducing the sample thickness to 20 mm. This procedure ensured a very minimum disturbance to the specimen structure.

assess the coefficient of consolidation (c_v), followed by a series of equations applied to determine the coefficient of volume change (m_v) and the coefficient of permeability (k) at the pre-yield stress, yield stress, and post-yield stress phases. Furthermore, the correlation between the one-dimensional consolidation coefficients with different basalt fiber lengths and RHA-cement contents was analyzed. SEM analyses quantified the structural modifications in the specimens upon consolidation, considering the soil composite structure, fiber reinforcement, and porosity of the specimen combination schemes under study.

4.1. Specimen conditions before and after consolidation

In Fig. 4 and Table 6, the specimen conditions and descriptive statistics of the specimen conditions, respectively, are provided. Equations (1), (2), (3), and (4) were used to calculate the initial water content (w_i), final water content (w_f), void ratio (e), wet density (ρ_t), and saturation level (S_{ro}) of the ten specimen combinations.

$$w_i \text{ or } w_f = \frac{m_i - m_s}{m_s} \times 100 \quad (1)$$

$$e = \frac{H_i}{H_s} - 1;\ H_s = \frac{m_s}{\rho_s \pi D^2/4} \quad (2)$$

$$\rho_t = \frac{m_i}{(A.H_i)};\ A = \pi D^2/4 \quad (3)$$

$$S_{r0} = \frac{w_o \rho_s}{e_o H \rho_w} \quad (4)$$

where w_i is the initial moisture content (%), w_f is the final moisture content (%), m_i is the initial mass of the specimen (g), m_s is the oven-dried mass of the specimen (g), H_i is the initial height of the specimen (cm), H_s is the actual height of the specimen (cm), A is the cross-sectional area of the specimen (cm^2), D is the diameter of the specimen (cm), ρ_s is the density of the soil particles (g/cm^3), and ρ_w is the density of water (g/cm^3).

The mean saturation level of the prepared specimens was 90%, while the mean void ratio and wet density were 1.49 and 1.62 g/cm^3, respectively. The initial states were considered in this study to justify the accuracy of the specimen preparation procedure and can be used to validate the authenticity of the results. Standard deviations in the void ratio, wet density, and saturation were kept to minimum values of 0.11, 0.03, and 1.84, respectively, justifying close standardization in the specimen conditions before testing. However, to achieve the standardized values, it was requisite to adjust the amount of water during the specimen preparation to compensate for the high water affinity of RHA, as demonstrated by the compaction curves in a related study (Owino et al., 2022a). Hence, the standard deviation values for the initial and final moisture contents were 4.12 and 3.99, respectively. It is also noteworthy that increasing the RHA content from 0% to 15% contributed to a slight increase in the void ratios of the specimens due to the porous morphology of the RHA particles (Chen et al., 2021).

4.2. Time-compression curves

According to the theory of one-dimensional consolidation, soil undergoes a time-dependent displacement/deformation when acted upon by an external load. This deformation can lead to the draining of excess pore water

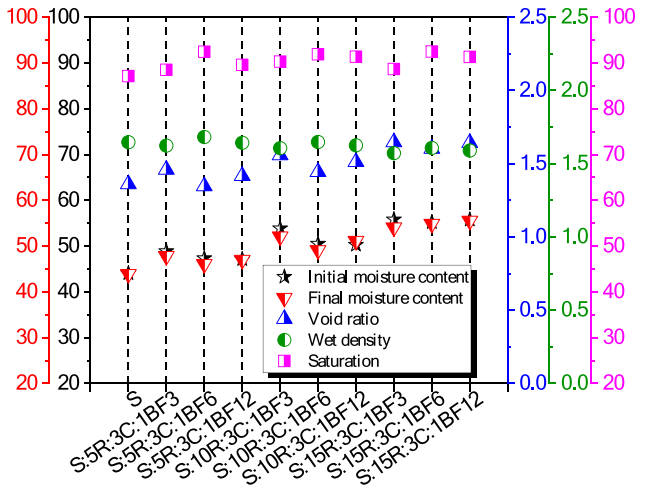

Fig. 4. Specimen conditions before and after consolidation.

pressure due to the gradual transition of the applied loads from the pore water to the soil particles under steady pressure. The notable assumptions in this theory include the following: (1) The soil is linearly elastic. (2) The soil grains and water are incompressible. (3) The load is applied in the vertical direction only. (4) The drainage of the pore water is one-dimensional in the direction of the load. (5) The coefficient of consolidation, the coefficient of volume change, and the coefficient of permeability are constant. (6) The time lag of consolidation is dependent on the low permeability of the expansive soils (Yuan-qiang et al., 2004; Terzaghi, 1943).

Based on this theory, the time-displacement plots of all ten specimen combinations for the load increments in the present study are shown in Fig. 5(a)-(g). In Fig. 5(a), there is no clear distinction between the primary and secondary consolidation phases at low compression pressures. However, as the consolidation pressures increase, a clear contrast between the primary and secondary consolidation phases in the time-displacement curves is evident, owing to the generated exponential curve forms (Fig. 5(b)-(g)). From these plots, the time T_{50} required to reach 50% primary consolidation is evaluated by defining the 0% primary consolidation stage from the early portion of the curve and the 100% primary consolidation stage from the point of intersection between the primary and secondary consolidation segments using the logarithm of the time method (Casagrande and Fadum, 1940). It is noteworthy that time T_{50} in Fig. 5(h) is seen to be highly dependent on the RHA-cement content.. Increasing the RHA content from 5% to 15% decreased the time required to achieve a certain degree of consolidation under the same effective stress. Similar results were also reported by Jain and Puri (2013).

It is also apparent that, for basalt fiber-reinforced and RHA-cement stabilized expansive soils, T_{50} decreased significantly with an increase in consolidation pressure. This decrease prompted a uniform secondary consolidation phase, preventing structural failures from prolonged primary consolidation. Moreover, the addition of different lengths of basalt fibers significantly reduced the T_{50} values compared to the control specimen (S), constituting soil only.

4.3. Coefficient of consolidation (c_v)

The coefficient of consolidation (c_v) measures the rate at which the soil consolidation process proceeds, a basic differential equation developed by Terzaghi (1943). A presentation of the c_v as a function of the average vertical consolidation pressure ($\bar{p}$) is shown in Fig. 6(a). The vertical axis (c_v) is on a logarithmic scale against the horizontal axis, plotted as the geometric mean average consolidation pressure ($\bar{p}$) (with values of 14, 28, 55, 111, 222, 444, and 888 kPa) calculated by Eq. (5). All the analytical equations followed the Japanese Industrial Standards 1217 and 1227.

$$\bar{p} = \sqrt{(p \cdot p')} \tag{5}$$

where p is the pressure increment and p' is the consolidation pressure at the previous loading stage in kPa. The data points corresponding to 14 kPa were omitted in Fig. 6 owing to the non-uniform vertical stress-time responses at low consolidation pressure. The c_v data points are defined by Eq. (6) in cm^2/day for all ten oedometer tests.

$$c_v = 0.197\left(\frac{\bar{H}^2}{2}\right)^2\left(\frac{1440}{T_{50}}\right) \tag{6}$$

where c_v is the coefficient of consolidation in cm^2/day, $\bar{H}$ is the average height of the specimen, 0.197 is the value of the time coefficient at 50% consolidation, and 1440 is the unit conversion factor to cm^2/day. For the ten oedometer tests, the variation in c_v with $\bar{p}$ for the fiber-RHA-cement specimens showed a similar trend to that observed for the control specimen (soil only), as shown in Fig. 6(a). During the first loading phase, at low consolidation pressures ranging from 0 to 28 kPa, non-uniform vertical stress-time

Table 6
Descriptive statistics of specimen conditions in Fig. 4.

Item	Unit	Total number of specimens	Mean	Standard deviation	Coefficient of variation	Minimum	Maximum
Initial moisture content, w_i	%	10	50.8778	4.1284	0.0811	44.0532	55.8053
Final moisture content, w_f	%	10	50.1627	3.9918	0.0795	43.8949	55.5363
Void ratio, e		10	1.49832	0.1108	0.0740	1.34564	1.64647
Wet density	g/cm^3	10	1.62405	0.0320	0.0197	1.57189	1.68152
Saturation	%	10	90.3745	1.8417	0.0203	87.1351	92.4881

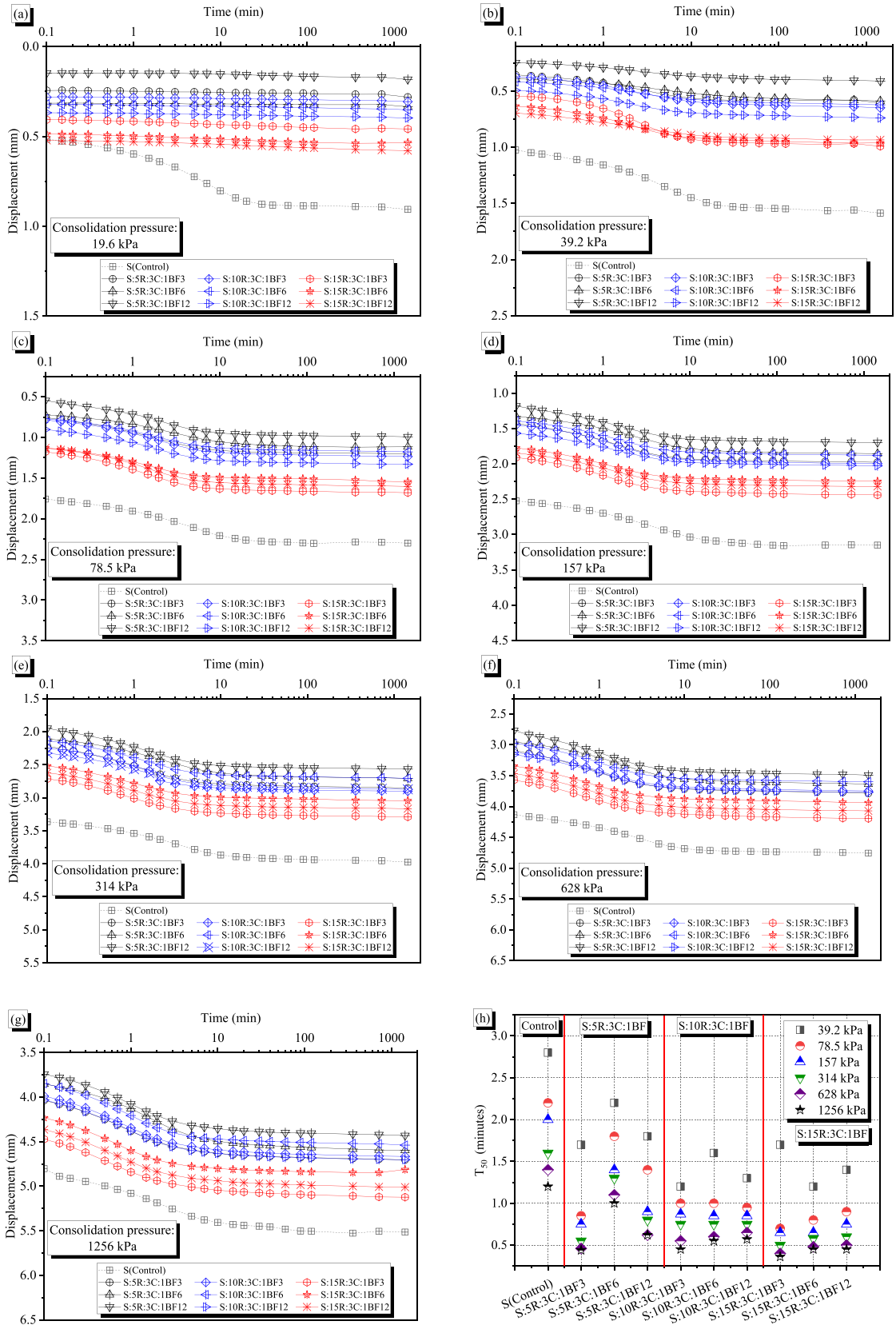

Fig. 5. (a-g) Time-displacement curves and (h) Relationship between T_{50} and specimen combinations schemes.

responses at low consolidation pressure occurred due to shrinkage and swelling, and hence, the difference in the c_v vs. stress values for the specimens compared to the other stress conditions. The data set at 28 kPa are plotted in this figure to show the general trend of the increasing c_v during the pre-yield stress phase. It can also be observed in the figure that the c_v increased as the $\bar{p}$ approached the yield stress.

In contrast, afterward, the value remained approximately constant in the post-yield phase. The yield stress phase (50 to 110 kPa) was evaluated from the void ratio (e) versus effective vertical pressure (log σ_v) compression curves for the reconstituted soil specimens. These yield stresses (σ_y) were estimated from the e vs. log σ_v plots using the Casagrande method (Casagrande, 1936), as discussed in a related study (Owino et al., 2022a), to create the boundary conditions for the yield phases employed in this study. The observed approximate constant values of c_v revealed that the creep effects should be carefully considered when working with basalt fiber-reinforced and RHA-stabilized expansive soils. This trend agrees with the results of Ferrari et al. (2016) observed while working on the one-dimensional consolidation of shales.

Additionally, the increasing c_v trend with $\bar{p}$ was attributed to the enhanced chemical and mechanical properties derived from the RHA stabilization and basalt fiber reinforcements. Robinson and Allam (1998) and Sridharan and Nagaraj (2004) also reported a similar trend of increasing c_v with consolidation pressure when analyzing the role of the mechanical and physio-chemical factors on the c_v trend with $\bar{p}$. It was also evident that the RHA content played a significant role in influencing the trend of the consolidation rate. For example, specimen S:5R:3C:1BF12, with a 5% RHA content, produced the lowest c_v values compared to specimen S:15R:3C:1BF3, with a 15% RHA content, which had the highest c_v values. This increase in the c_v values at 15% RHA was due to the increased hydraulic conductivity associated with the porous structure of RHA and the additional voids created by random fiber intersections. A comparable increase in c_v values with increasing hydraulic conductivity was also reported by Yeo et al. (2005). It is noteworthy that the RHA content influenced the c_v value depending on the degree of pozzolanic activity in the specimen. The complete utilization of RHA during pozzolanic reactions for specimens with 5% and 10% RHA developed their mechanical properties

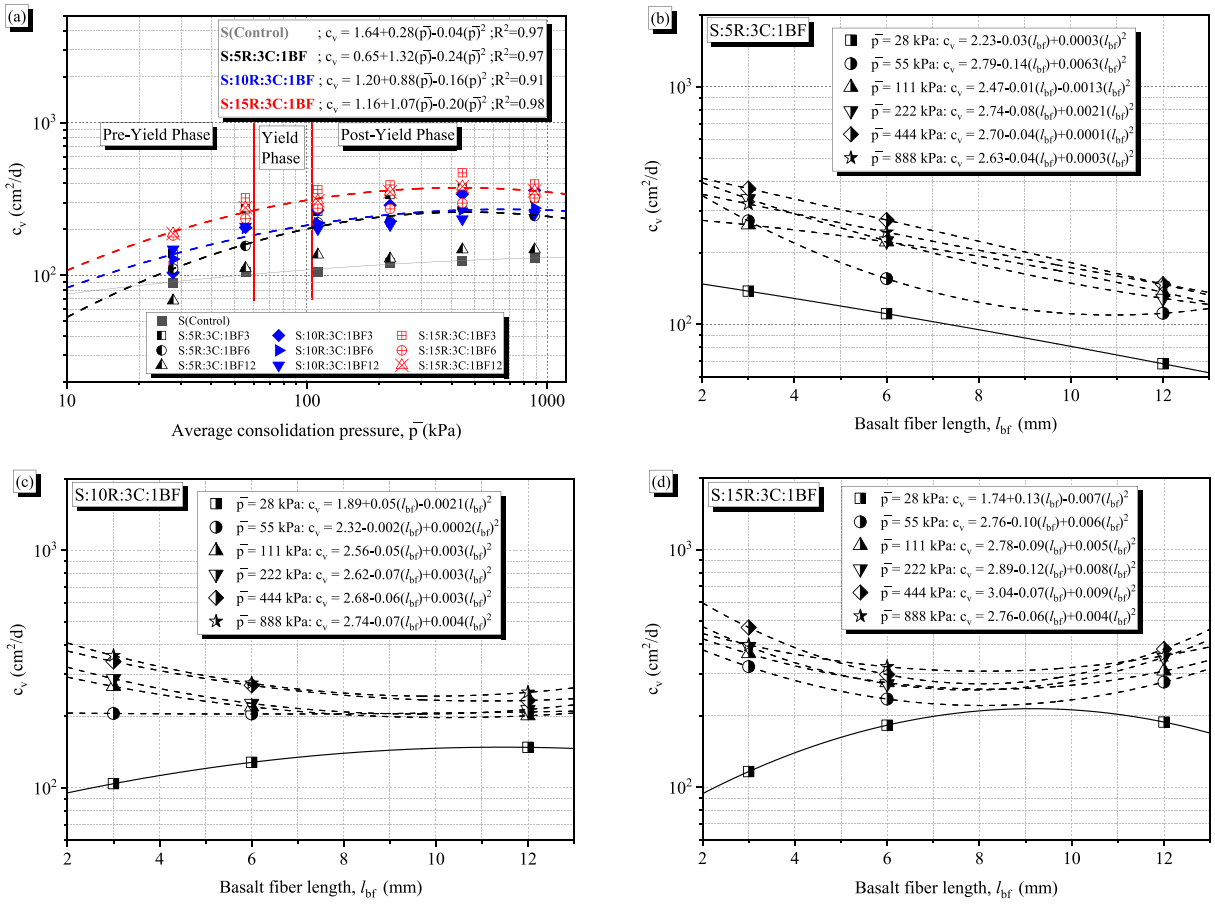

Fig. 6. (a) Relationship between c_v and $\bar{p}$, (b) Correlation between c_v and l_{bf} for 5% RHA specimens, (c) Correlation between c_v and l_{bf} for 10% RHA specimens, and (d) Correlation between c_v and l_{bf} for 15% RHA specimens.

through the improvement in their compressibility behavior, and hence, low c_v values. Moreover, as observed for all the tested specimens, the c_v value varied at the same $\bar{p}$ depending on the RHA content.

Furthermore, to correlate the coefficient of consolidation (c_v) with basalt fiber reinforcement, all the values for the c_v are plotted against the different basalt fiber lengths in Fig. 6(b)-(d). In general, the length of the basalt fibers significantly influences the c_v value, as seen in the correlation plots. The decrease in the c_v was more significant in the specimen containing 12-mm basalt fibers, as shown in Fig. 6(b) and (c), representing RHA compositions of 5% and 10%, respectively. For example, considering the maximum $\bar{p}$ of 888 kPa, with an increase in the basalt fiber length from 3 to 12 mm, the c_v values for the 5% RHA specimen decreased from 321.02 to 147 cm^2/d. A similar reduction in the c_v with the increasing basalt fiber length was further reported for the 10% RHA specimens, with exceptions in the 15% RHA specimens at the basalt fiber length of 12 mm, as revealed in Fig. 6(d). It can be concluded that the RHA content established a boundary condition at 10% RHA, beyond which any further increase in the RHA content increased the c_v value with the increasing fiber content. Moreover, it was evident that the coefficient of consolidation was dependent on the average consolidation pressure during the loading stage, with an apparent inverse relationship.

Furthermore, using the c_v versus length of the basalt fiber plots, the curve-fitting correlation equations are evaluated and presented in Fig. 6(b-d). The equations can predict the c_v values at specific basalt fiber lengths and consolidation pressures for fiber lengths ranging from 3 to 12 mm. Nonetheless, the equations derived herein were based on the responses of the stabilized and fiber-reinforced expansive soil composites; hence, additional studies should be undertaken while working on other types of soils under the same scope. It can be concluded that the longer basalt fibers provided sufficient reinforcements in the specimens by resisting excessive compression during the loading phase, resulting in a reduced consolidation rate.

4.4. Coefficient of volume change (m_v)

In the construction industry, foundation settlement is one of the safety concerns in the geotechnical assessment of engineering structures. Excessive settlement can cause structural damage or significantly reduce the durability of the structure. The coefficient of volume change (m_v) has been demonstrated to be a suitable parameter when calculating the consolidation settlement, providing essential measures to counter the projected soil settlement. The coefficient of volume change can be defined as the change in volume of a soil mass per unit of initial volume when subjected to an increase in effective pressure. According to the Japan Industrial Standards 1217 and 1227, m_v is the ratio of the volume change of the soil to the difference in effective pressure. It is calculated using Eq. (7).

$$m_v = \frac{\Delta\varepsilon/100}{\Delta_p} \tag{7}$$

where $\Delta\varepsilon$ is the compression strain generated at each loading stage [the ratio of the consolidation amount (ΔH) to the average specimen height ($\bar{H}$)], and Δp is the increment in consolidation pressure. The variation in the m_v at different compactive efforts for specimens with different basalt fiber lengths and various RHA contents is shown in Fig. 7(a). The coefficient of volume change was minimum at a low consolidation pressure (14 kPa) due to the high swelling pressure in the expansive soil compared to the applied load. Eberemu et al. (2016) reported a similar response to low consolidation loads. In general, irrespective of the fiber reinforcement length and RHA stabilization, the m_v value showed a reducing trend as the average consolidation pressure increased. This reduction was induced by the compressive forces rearranging and closely packing the composite materials, increasing the bonding forces and yield stress in the specimen, thereby reducing the m_v considerably. A relatable reduction in the m_v with increasing pressure was also realized by Santagata et al. (2008).

Additionally, it is noteworthy that the m_v value was dependent on the specimen composition in the pre-yield and post-yield phases. For instance, considering the basalt fiber reinforcement and RHA-cement content, specimen S:5R:3C:1BF3 showed the lowest m_v value of $1.20 * 10^{-4}$ m^2/kN compared to specimen S:15R:3C:1BF3 with $1.07 * 10^{-3}$ m^2/kN during the pre-yield phase ($p = 14$ kPa). This difference was probably due to the enhanced stiffness and resistance to compressive forces obtained from the complete pozzolanic reactions at 5% RHA than at 15% RHA. For example, at $p = 14$ kPa, the fiber-reinforced specimen with 5% RHA portrayed a direct relationship, with the coefficient of volume change increasing from 1.20×10^{-4} m^2/kN to 1.41×10^{-4} m^2/kN to 2.19×10^{-4} m^2/kN for basalt fiber lengths of 3, 6, and 12 mm, respectively. On the other hand, an inverse relationship was observed for higher RHA-cement contents. The 10% RHA attained m_v values of 5.69×10^{-4} m^2/kN to 2.20×10^{-4} m^2/kN, while the 15% RHA produced values of 1.07×10^{-4} m^2/kN to 3.53×10^{-4} m^2/kN as the length of the basalt fibers increased from 3 to 12 mm.

It was further concluded that RHA and basalt fiber reinforcements slightly increased the m_v with increasing compactive force across all specimens during the pre-yield phase. This slight increase was due to the additional displacements required to reduce the voids created by the porous RHA and the random distribution of basalt fibers. However, in the post-yield state, the ultimate compact structure in the specimen provided resistance to compressive forces leading to a significant reduction in the m_v value with average consolidation pressure. Similar responses

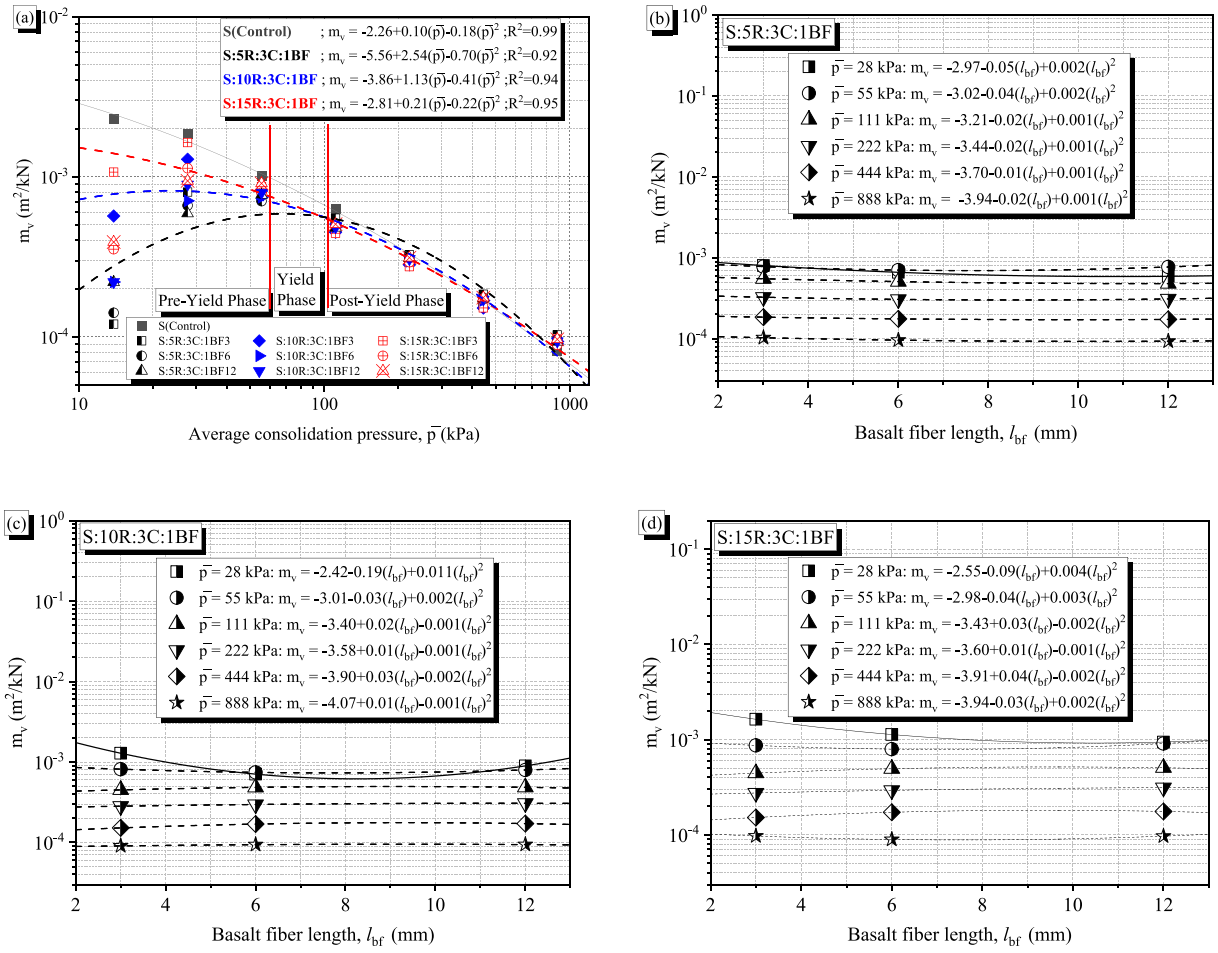

Fig. 7. (a) Relationship between m_v and $\bar{p}$, (b) Correlation between m_v and l_{bf} for 5% RHA specimens, (c) Correlation between m_v and l_{bf} for 10% RHA specimens, and (d) Correlation between m_v and l_{bf} for 15% RHA specimens.

have also been observed by Xu et al. (2020), Eberemu (2011), Eberemu et al. (2016), and Laskar and Pal (2013).

Moreover, a plot of the m_v on the log scale against the basalt fiber length (l_{bf}) is considered to correlate the relationship between the m_v and the length of the basalt fiber, as illustrated in Fig. 7(b), (c), and (d) for specimens S:5R:3C:1BF, S:10R:3C:1BF, and S:15R:3C:1BF, respectively. It is evident from these figures that increasing the length of the basalt fibers in the specimens had a minimal effect on the m_v with increasing consolidation pressures from 55 to 888 kPa. Generally, slightly higher m_v values were recorded for the specimens containing 15% RHA due to the extra volume changes initiated by the high void ratios. Additionally, from the m_v versus length of basalt fiber (l_{bf}) plots, the curve fitting correlation equations to predict the m_v were evaluated and presented across all specimens. These equations can be used to predict the coefficient of volume change (m_v) if the basalt fiber length (lbf) and the average consolidation pressures are provided for fiber lengths ranging from 3 to 12 mm. Similar to the c_v equations in the previous section, the proposed equations were based on the response of stabilized and fiber-reinforced expansive soil composites.

4.5. Permeability coefficient (k)

This section highlights the effects of the basalt fiber length and RHA-cement contents on the permeability coefficient (k) of stabilized expansive soils undergoing one-dimensional consolidation. Permeability describes the rate at which water can move through the pores of a soil medium; it has proven to be an essential parameter influencing soil consolidation and strength. Following the Japan Industrial Standards 1217 and 1227, the coefficient of permeability can be calculated using Eq. (8).

$$k = \frac{c_v m_v \gamma_w}{8.64 \times 10^8} \tag{8}$$

where k is the coefficient of permeability in m/s, c_v is the coefficient of consolidation, m_v is the coefficient of volume change, γ_w is the unit volume weight of water (9.81 kN/m^3), and 8.64 × 10^8 is the conversion parameter of k to m/s. Fig. 8(a) compares the pressure dependence of the reinforced and stabilized expansive soil's permeability coefficient, considering the following factors: length of basalt fibers, RHA-cement content, and average consolidation pressure. It was found that the permeability coefficient var-

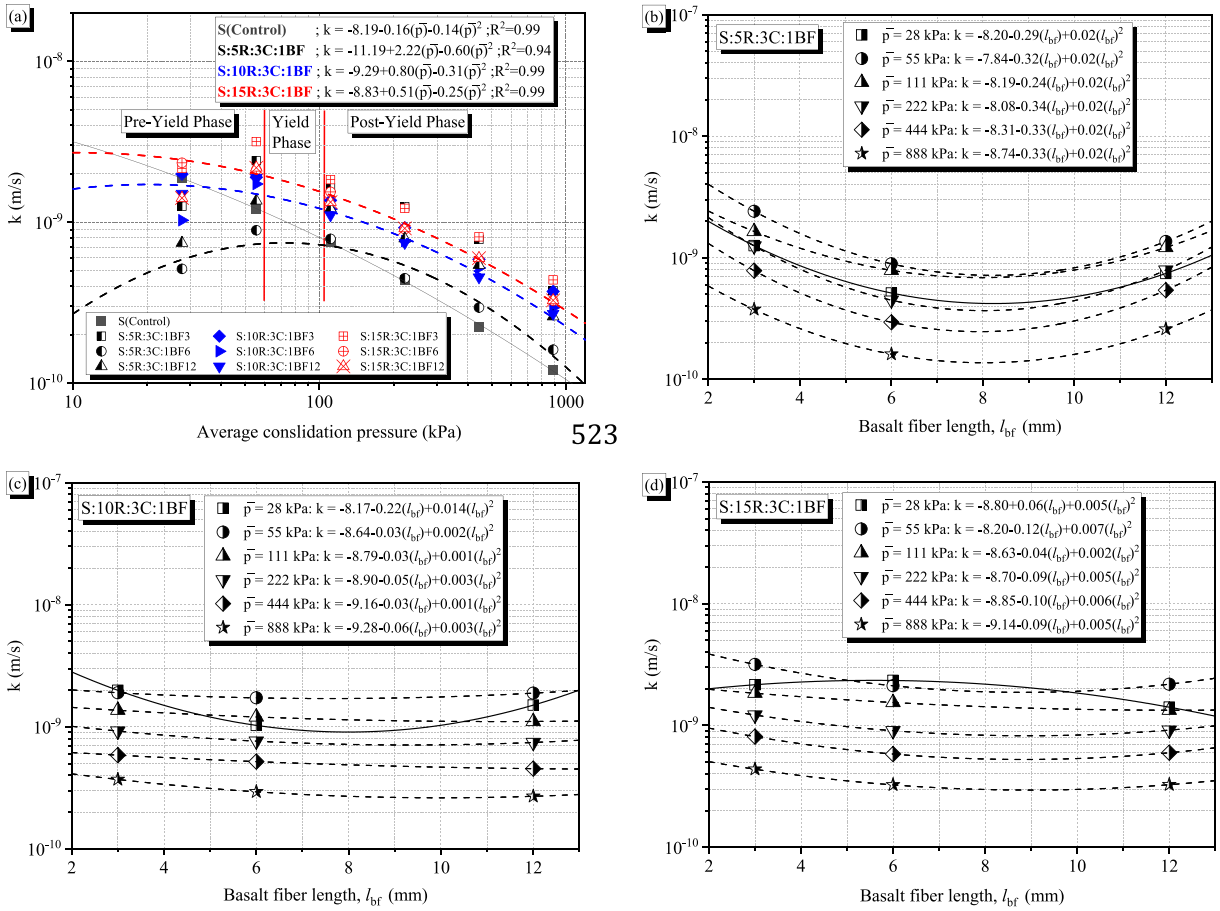

Fig. 8. (a) Relationship between k and $\bar{p}$, (b) Correlation between k and l_{bf} for 5% RHA specimens, (c) Correlation between k and l_{bf} for 10% RHA specimens, (d) Correlation between k and l_{bf} for 15% RHA specimens.

ied in the order of 10^{-10} to 10^{-9} and was greatly influenced by the average consolidation pressure. Moreover, the value of k increased during the pre-yield phase and decreased significantly in the post-yield phase for all the specimens tested. However, the value of k in the observed trend depended on the specimen's RHA-cement content and basalt fiber length.

For instance, the coefficient of permeability increased with the RHA content for all the individual average consolidation pressures, as shown in Fig. 8(a). This increase was due to the high porosity caused by the excess RHA particles and the void networks created by the basalt fibers in the composite specimen. Additionally, the pozzolanic compounds generated by the RHA and cement precipitation enhanced cementation at low RHA-cement contents, and hence, the low k values at 5% RHA. A similar reduction in the permeability coefficient due to the pozzolanic reaction has also been reported in other studies, such as Onyelowe et al. (2021), Jamil et al. (2013), Gupta and Kumar (2017), and Nshimiyimana et al., (2018).

However, as the average consolidation pressure increased, the k value decreased to an almost constant value of order 10^{-10} for all the tested specimens due to the complete removal of the voids and sufficient rearrangement of the soil-RHA-cement and fibers. This relationship between the voids and the permeability indicated that voids played the dominant role in affecting the permeability coefficient. Cheng et al. (2020) also observed a similar relationship while conducting experiments with the consolidation properties of reconstituted clay soils.

Supplementary to the analyses discussed herein, a correlation plot has been considered in terms of the influence of the basalt fiber length on the permeability coefficient, as shown in Fig. 8(b)-(d). In Fig. 8(b), representing a basalt fiber reinforced specimen with 5% RHA and 3% cement, the permeability coefficient decreased with increasing fiber length up to 6 mm. The declining trend of k with the length of the basalt fiber for the 5%RHA-3C specimens can be attributed to the well-defined structural development due to cementation from the adequate pozzolanic reaction and enhanced reinforcement. However, a further increase in the basalt fiber length to 12 mm brought about a slight increase in permeability due to the longer paths for water to drain more quickly through the specimen. The rise in the permeability coefficient with the length of the fiber reinforcements was also observed by Abdi et al.

(2008), while they were investigating the effects of fiber inclusion on the hydraulic conductivity in clay soils. In the case of 10%RHA-3C and 15%RHA-3C, shown in Fig. 8(c) and (d), respectively, a very minimal reduction in the k value was recorded for all the average consolidation pressure increments. From these correlation plots, curve-fitting equations were formulated to assist design engineers in predicting the projected coefficients of permeability for RHA-basalt fiber-stabilized soils for a given average consolidation pressure and length of basalt fiber (3 to 12 mm).

4.6. Microstructural analysis

The effect of basalt fiber reinforcements and stabilization using RHA-cement mixtures on the consolidation coefficients of reconstituted expansive soils can be explained by capturing the microstructural development through scanning electron microscopy (SEM). SEM micrographs at a magnification of X500 and scale of 100 μm, showing the coupling effect of the basalt fibers with the compact cementitious composite soil matrix for the tested specimen combinations, are shown in Figs. 9–11. These SEM images represent the corresponding specimen states at the end of the consolidation process (average consolidation pressure = 888 kPa). This section discusses a detailed analysis to justify the trends of the coefficient of consolidation (c_v) and the coefficient of permeability (k), as mentioned earlier.

Fig. 9(a-c) represent the SEM imagery of the fiber-reinforced 5%RHA-3C composites. The mobilization of basalt fiber reinforcements was driven by the highly significant interfacial contacts developing during the physical connection between the cementitious soil matrix and the fiber surface. In this study, the fiber interfacial contacts referred to the points of physical contact or interaction between the fibers and the soil composites. The interfacial contacts were more pronounced when the length of the basalt fibers increased from 3 to 12 mm due to the increased fiber surface area and the interconnectivity arising from the intense fiber network. Additionally, a clear indication of a cemented compact structure was evident due to the complete utilization of 5% RHA and cement during the pozzolanic reactions. The fiber interfacial contacts were crucial in altering the behavior of the stabilized soil during consolidation by slightly increasing the drainage paths, enhancing the load transfer, and providing the reinforcement effect, hence the improved consolidation characteristics. The synergetic action between the fibers and each cemented specimen structure resisted excess compressibility, reducing the coefficient of consolidation (c_v) for the 5% RHA composites, as shown in Fig. 6(a). At the same

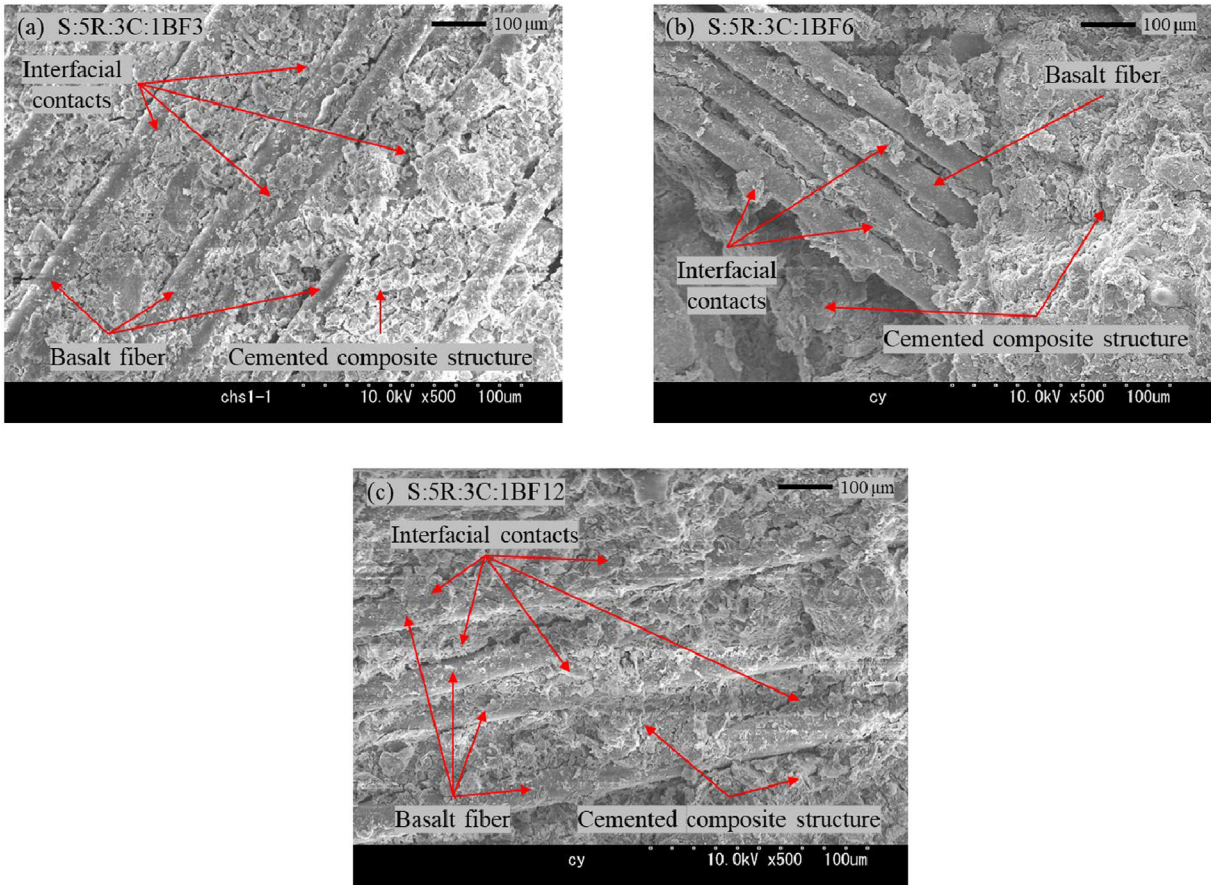

Fig. 9. SEM imagery for 5%RHA-3%C composites: (a) Specimen S:5R:3C:1BF3, (b) Specimen S:5R:3C:1BF6, and (c) Specimen S:5R:3C:1BF12.

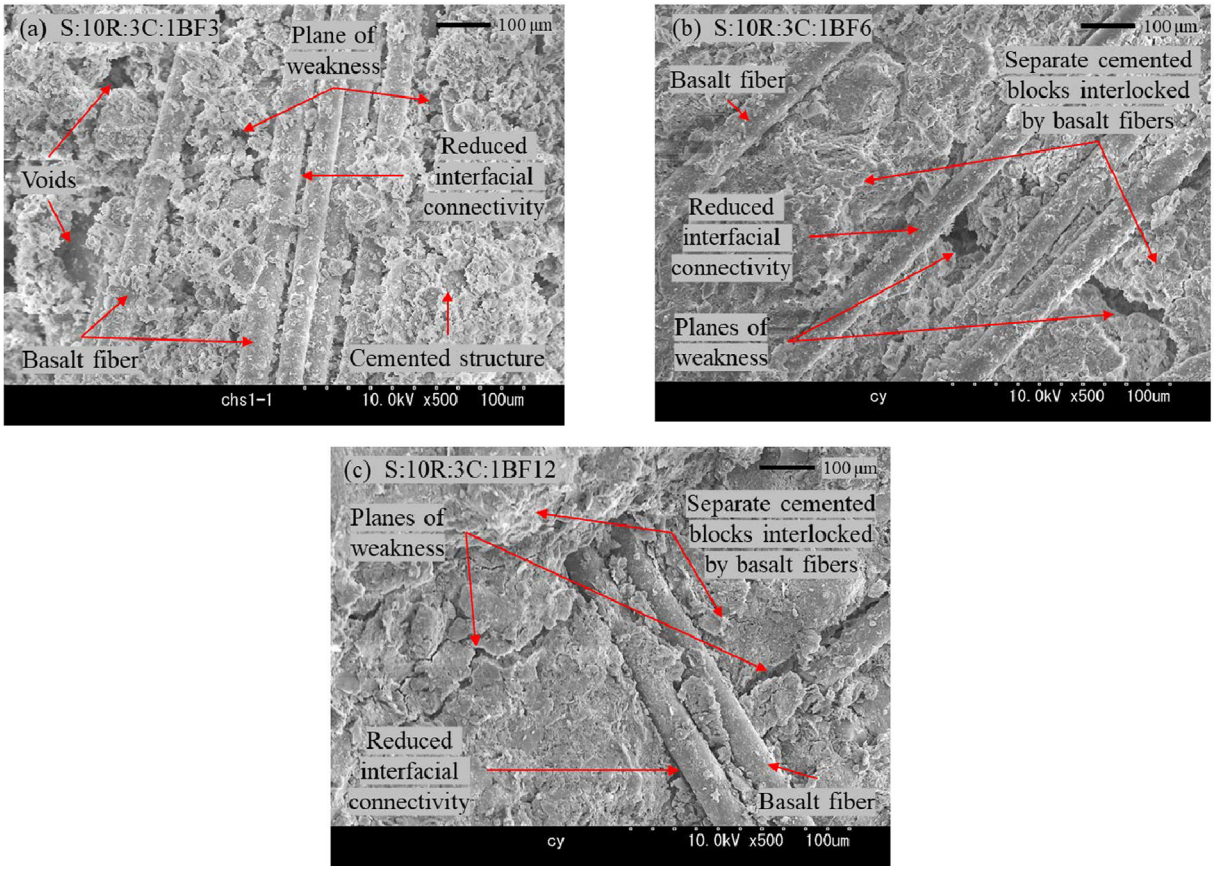

Fig. 10. SEM imagery for 10%RHA-3%C composites: (a) Specimen S:10R:3C:1BF3, (b) Specimen S:10R:3C:1BF6, and (c) Specimen S:10R:3C:1BF12.

time, the cementitious structure eliminated excess voids, leading to the lower permeability coefficient values (k) for the 5%RHA-3%C composites, as presented in Fig. 8(a). The tendency of fiber reinforcement to improve the bonding strength of expansive soils was also observed by Syed et al. (2020) when stabilizing expansive clays using geopolymerization and fiber reinforcement.

Contrarily, the rising trends of c_v and k for the fiber-reinforced specimen containing 10% RHA and 3% C were justified by the occurrence of planes of weakness and voids in the specimens, as displayed in Fig. 10(a-c). The planes of weakness referred to specific planes or surfaces within the soil specimen that exhibited reduced strength or cohesion compared to the surrounding soil mass, such as formed cracks, while the voids refer to the open spaces or gaps within the soil composite that were not filled with solid particles. It was evident that the planes of weakness and voids increased the drainage paths for pore water, and thus, the slightly higher values of c_v and k. However, the discrete distributions of high tensile strength basalt fibers in the specimen structure interlocked the separate cemented blocks, restricting further cracks during consolidation. The interlocking mechanism was more significant with the increasing basalt fiber length from 3 to 12 mm. Moreover, the micro-structural bonding was slightly reduced for these composites due to the inadequate intensity of the interfacial contacts in the specimen structure compared to the 5%RHA-3C specimens.

Considering the basalt fiber-reinforced specimens containing 15% RHA and 3% C, shown in Fig. 11(a-c), it is noteworthy that the influence on the c_v and k depended on the extent of the interfacial contacts and the presence of loose materials, as will be discussed in this section. Up front, it was observed that the smooth basalt fiber surfaces indicated insufficient interfacial contacts between the basalt fibers and the soil-RHA-cement composite compared to the 5%RHA-3%C and 10%RHA-3%C composites. The reduced interfacial connectivity reduced the microstructural bonding, increasing the pore water drainage paths along the fibers. Additionally, this phenomenon led to reduced localized stress concentrations within the specimen, influencing the consolidation process by increasing compressibility and the dissipation of excess pore water pressure, increasing the values of c_v and k considerably. Next, the confirmation of fine loose material in the SEM images indicated high compressibility when subjected to one-dimensional loading. The loose materials were derived from the accumulation of excess fine materials from the high RHA contents. The porous nature of RHA and the reduced particle-to-particle bonding allowed for easy dissipation of more pore water, increasing the values of c_v and k, as shown in Fig. 6(a) and 8(a), respectively.

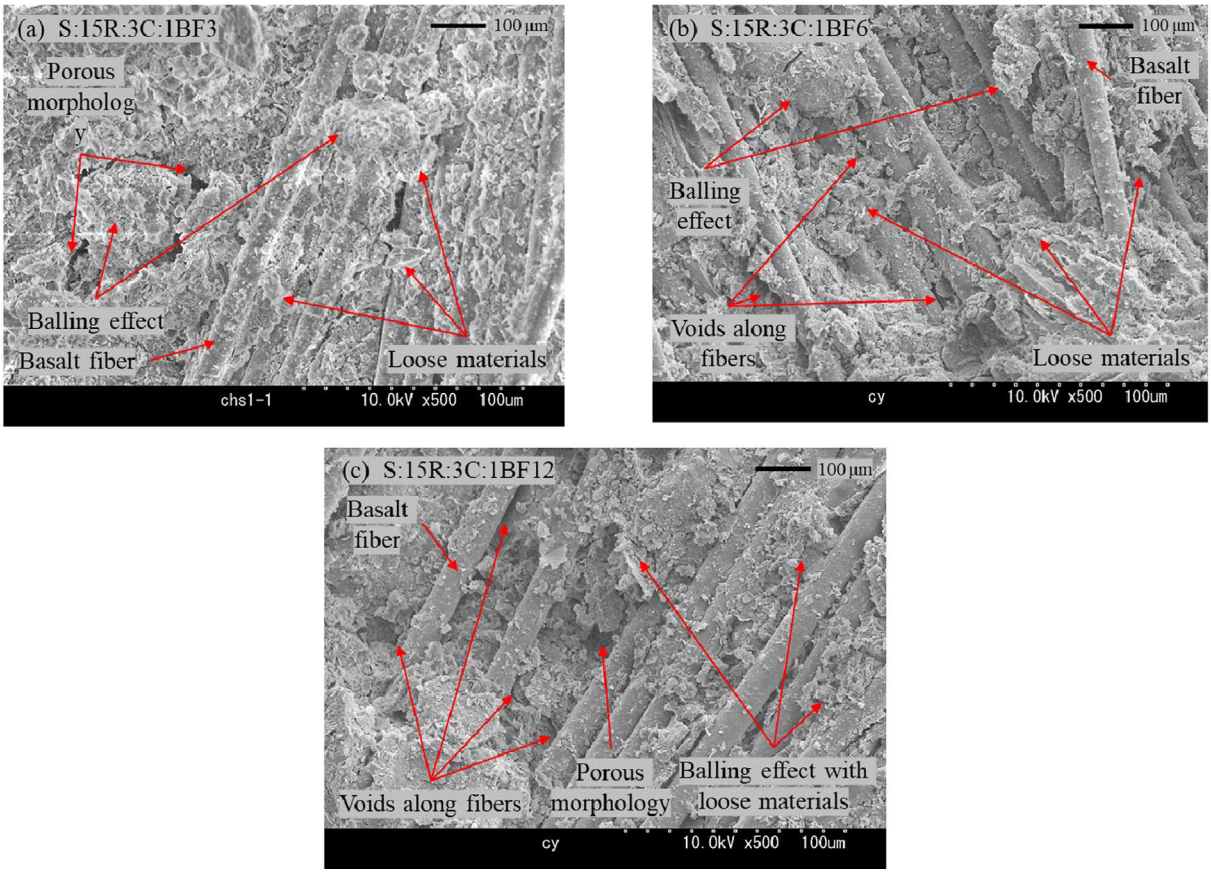

Fig. 11. SEM imagery for 15%RHA-3%C composites: (a) Specimen S:15R:3C:1BF3, (b) Specimen S:15R:3C:1BF6, and (c) Specimen S:15R:3C:1BF12.

Furthermore, the reduced pozzolanic activity at 15% RHA-3%C, due to the excess accumulation of RHA, led to the balling (a process or phenomenon where particles agglomerate or clump together, forming balls or larger aggregates) of the soil-RHA-cement particles around the basalt fibers, and hence, the more notably porous structure. As a result, the void ratios increased, allowing room for considerable particle rearrangement during loading. This balling effect developed a highly compressible and porous specimen structure, increasing the c_v and k values.

5. Conclusion

This paper presented an experimental analysis based on a series of oedometer tests to study the correlation between the one-dimensional consolidation coefficients with different lengths of basalt fibers and RHA-cement contents in fiber-reinforced RHA-treated expansive soils. An effort has been made to explain more rationally the influence that the basalt fiber length and RHA-cement content have on the coefficient of consolidation (c_v), coefficient of volume change (m_v), and coefficient of permeability (k), drawing further justifications through SEM imagery. The following conclusions can be made:

1. Increasing the length of the basalt fibers for each RHA content reduced the coefficient of consolidation (c_v). This reduction was more significant for fiber-reinforced specimens constituting 5% RHA and 10% RHA, with reduction percentages of 54.21% and 30% at the end of consolidation. This response indicated that the degree of consolidation depended on the specimen composition and degree of reinforcement.
2. The coefficient of volume change (m_v) was greatly influenced by the average consolidation pressure rather than the specimen composition (fiber length and RHA-cement content). However, at low consolidation pressures during the pre-yield stage, the fiber-RHA-cement-reinforced specimens displayed lower volume changes than the control specimen. Moreover, a slight increase in the m_v with average consolidation pressure was evident compared to the control specimen.
3. The permeability coefficient (k) of the fiber-reinforced specimen with 5%RHA-3%C decreased with the increasing fiber length. For those with 10%RHA-3%C and 15% RHA-3%C, a very minimal decrease in the k value was recorded with increased fiber length.
4. The curve fitting equations shown in Figs. 6, 7, and 8 were proposed as analytical equations for evaluating the c_v, m_v, and k for basalt fiber lengths ranging from 3 to 12 mm,

RHA-cement contents of 5% to 15%, and the consolidation pressure stage. However, it should be noted that the equations derived herein were based on the responses of stabilized and basalt fiber-reinforced expansive soil composites; hence, additional studies should be undertaken while working on other types of soils.

5. The SEM imagery showed that the random distribution of basalt fibers in the stabilized composite enhanced the reinforcing network within the specimens. Increasing the basalt fiber length from 3 to 12 mm provided a more robust reinforcing phenomenon in the stabilized composite, thereby controlling the interfacial strength. This strength enhancement contributed significantly to the trend of the consolidation coefficients.
6. The relationships discussed in the present study demonstrated that reinforcing expansive soils with 12-mm basalt fibers, 5% RHA, and 3% cement provided superior qualities to the other mixed combinations. Specimen S:5R:3C:1BF12, with a 5% RHA content, produced the lowest c_v values compared to other specimens. Moreover, the 5%RHA-3%C specimens revealed a well-defined structural development due to cementation from the adequate pozzolanic reaction and enhanced reinforcement, as depicted in the SEM images. The slight increase in the k value with 12-mm basalt fibers enhanced the hydraulic conductivity of the stabilized soil compared to the other mixed combinations, indicating improved drainage conditions. The slow rate at which the soil consolidation process proceeds for this combination (i.e., low c_v values) makes it superior to other combinations in this study. Additionally, as indicated in related research (Owino et al., 2022a), this mixed combination had the highest yield stresses and can be considered the optimal value for use in engineering practice as fill material or subgrade to avoid the over-settlement of engineering structures.
7. Thus, the experimental and analytical methodologies presented in this paper are believed to be of great significance for quantifying and interpreting one-dimensional consolidation coefficients and their correlation to fiber reinforcement and RHA-cement stabilization techniques. The correlation equations provided in this study can also be used in design charts for the consolidation and settlement trends of basalt fiber-RHA-cement stabilized expansive soils. The correlation equations were based on the responses of Kaolinite and Montmorillonite-rich expansive soils. Therefore, further investigation and an analysis of the correlation equations for different types of expansive soils are necessary to ascertain their applicability in civil and geotechnical engineering.

CRediT authorship contribution statement

Alex Otieno Owino: Conceptualization, Methodology, Data curation, Writing – original draft. **Zakaria Hossain:** Supervision.

Acknowledgements

The authors would like to express their appreciation to the Japan Ministry of Education, Culture, Sports, Science, and Technology for providing a MEXT scholarship through Mie University, where this study was conducted. This research was also gratefully supported by Make Integrated Technology Limited, which provided experimental materials.

References

Abdi, M.R., Parsapazhouh, A., Arjmand, M., 2008. Effects of random fiber inclusion on consolidation, hydraulic conductivity, swelling, shrinkage limit and desiccation cracking of clays. Int. J. Civ. Eng. 6 (4), 284–292.

Behak, L., 2017. Soil stabilization with rice husk ash. Rice: Technol. Prod. 29. https://doi.org/10.5772/66311.

Bennett, B., Visintin, P., Xie, T., 2022. Global warming potential of recycled aggregate concrete with supplementary cementitious materials. J. Build. Eng. 52. 104394. https://doi.org/10.1016/j.jobe.2022.104394.

Biswal, D.R., Sahoo, U.C., Dash, S.R., 2019. Durability and shrinkage studies of cement stabilized granular lateritic soils. Int. J. Pavement Eng. 20 (12), 1451–1462. https://doi.org/10.1080/10298436.2018.1433830.

Blankendaal, T., Schuur, P., Voordijk, H., 2014. Reducing the environmental impact of concrete and asphalt: a scenario approach. J. Cleaner Prod. 66, 27–36. https://doi.org/10.1016/j.jclepro.2013.10.012.

Boateng, A.A., Skeete, D.A., 1990. Incineration of rice hull for use as a cementitious material: The Guyana experience. Cem. Concr. Res. 20 (5), 795–802. https://doi.org/10.1016/0008-8846(90)90013-N.

Casagrande, A., Fadum, R.E., 1940. Notes on Soil Testing for Engineering Purposes. Harvard University Graduate School Engineering Publication, (8), Massachusetts.

Casagrande, A, 1936. The determination of pre-consolidation load and its practical significance. In: Proc. Int. Conf. Soil Mech. Found. Eng. Cambridge, Mass. vol. 3, pp. 60.

Changizi, F., Haddad, A., 2015. Strength properties of soft clay treated with a mixture of nano-SiO2 and recycled polyester fiber. J. Rock Mech. Geotech. Eng. 7 (4), 367–378. https://doi.org/10.1016/j.jrmge.2015.03.013.

Chen, R., Congress, S.S.C., Cai, G., Duan, W., Liu, S., 2021. Sustainable utilization of biomass waste-rice husk ash as a new solidified material of soil in geotechnical engineering: A review. Constr. Build. Mater. 292. 123219. https://doi.org/10.1016/j.conbuildmat.2021.123219.

Cheng, G., Zhu, H.H., Wen, Y.N., Shi, B., Gao, L., 2020. Experimental investigation of consolidation properties of nano-bentonite mixed clayey soil. Sustainability. 12 (2), 459. https://doi.org/10.3390/su12020459.

Cuisinier, O., Le Borgne, T., Deneele, D., Masrouri, F., 2011. Quantification of the effects of nitrates, phosphates and chlorides on soil stabilization with lime and cement. Eng. Geol. 117 (3–4), 229–235. https://doi.org/10.1016/j.enggeo.2010.11.002.

Das, S., Pal, S.K., 2012. Consolidation Characteristics of Silty-Clay Soil Mixed with Class F Indian Fly Ash. In: Indian Geotech. Conf. December, 13–45.

Dhand, V., Mittal, G., Rhee, K.Y., Park, S.J., Hui, D., 2015. A short review on basalt fiber reinforced polymer composites. Composites Part B: Eng. 73, 166–180. https://doi.org/10.1016/j.compositesb.2014.12.011.

Eberemu, A.O., 2011. Consolidation properties of compacted lateritic soil treated with rice husk ash. Geomaterials 1 (3), 70–78. https://doi.org/10.4236/gm.2011.13011.

Eberemu, A.O., Sada, H., 2013. Compressibility characteristics of compacted black cotton soil treated with rice husk ash. Nigerian J. Technol. 32 (3), 507–521.

Eberemu, A.O., Omajali, D.I., Abdulhamid, Z., 2016. Effect of compactive effort and curing period on the compressibility characteristics of tropical black clay treated with rice husk ash. Geotech. Geol. Eng. 34 (1), 313–322. https://doi.org/10.1007/s10706-015-9946-9.

Fatahi, B., Fatahi, B., Le, T.M., Khabbaz, H., 2013. Small-strain properties of soft clay treated with fibre and cement. Geosynth. Int. 20 (4), 286–300. https://doi.org/10.1680/gein.13.00018.

Ferrari, A., Favero, V., Laloui, L., 2016. One-dimensional compression and consolidation of shales. Int. J. Rock Mech. Min. Sci. 88, 286–300. https://doi.org/10.1016/j.ijrmms.2016.07.030.

Firoozi, A.A., Taha, M.R., Firoozi, A.A., Khan, T.A., 2014. Assessment of nano-zeolite on soil properties. Aust. J. Basic. Appl. Sci. 8 (19), 292–295.

Ghadir, P., Ranjbar, N., 2018. Clayey soil stabilization using geopolymer and Portland cement. Constr. Build. Mater. 188, 361–371. https://doi.org/10.1016/j.conbuildmat.2018.07.207.

Gupta, D., Kumar, A., 2017. Performance evaluation of cement-stabilized pond ash-rice husk ash-clay mixture as a highway construction material. J. Rock Mech. Geotech. Eng. 9 (1), 159–169. https://doi.org/10.1016/j.jrmge.2016.05.010.

Hu, H., Liu, Y., 2010. High modulus, high tenacity yarns. Technical textile yarns. Woodhead Publishing, pp. 329–386. https://doi.org/10.1533/9781845699475.2.329.

Hussain, J., Khan, A., Zhou, K., 2020. The impact of natural resource depletion on energy use and CO2 emission in Belt & Road Initiative countries: A cross-country analysis. Energy 199. 117409. https://doi.org/10.1016/j.energy.2020.117409.

Jain, A., Puri, N., 2013. Consolidation characteristics of highly plastic clay stabilized with rice husk ash. Int. J. Soft Comput. Eng. (IJSCE) 2, 413–418.

James, J., Pandian, P.K., 2016. Industrial wastes as auxiliary additives to cement/lime stabilization of soils. Adv. Civ. Eng. 2016 (1267391), 17. https://doi.org/10.1155/2016/1267391.

Jamil, M., Kaish, A.B.M.A., Raman, S.N., Zain, M.F.M., 2013. Pozzolanic contribution of rice husk ash in cementitious system. Constr. Build. Mater. 47, 588–593. https://doi.org/10.1016/j.conbuildmat.2013.05.088.

JCK Corporation, 2022. Basalt Fiber Materials, Products and Development. バサルト繊維素材、製品、開発はJCK株式会社へ, Accessed 31 August 2022. http://www.j-c-k.co.jp/shohin.html. https://drive.google.com/file/d/1qxw-ZF47EmhUFIJB3IIy6ndejN6pK1D9/view.

JIS A 1217, 2010. Test method for soil consolidation test. Japanese Industrial Standard, Guidance and Basic - Soil Test, The Jpn. Geotech. Soc. 103–120 (in Japanese).

JIS A 1227, 2010. Test method for soil consolidation test. Japanese Industrial Standard, Guidance and Basic - Soil Test, The Jpn. Geotech. Soc. 103–120 (in Japanese).

Kar, R., Pradhan, P., 2011. Strength and compressibility characteristics of randomly distributed fiber-reinforced soil. Int. J. Geotech. Eng. 5 (2), 235–243. https://doi.org/10.3328/IJGE.2011.05.02.235-243.

Laskar, A., Pal, S.K., 2013. Effects of waste plastic fibres on compaction and consolidation behavior of reinforced soil. Electron. J. Geotech. Eng. 18, 1547–1558.

Mo, K.H., Alengaram, U.J., Jumaat, M.Z., Yap, S.P., Lee, S.C., 2016. Green concrete partially comprised of farming waste residues: a review. J. Cleaner Prod. 117, 122–138. https://doi.org/10.1016/j.jclepro.2016.01.022.

Muñoz, Y.O., dos Santos Izzo, R.L., de Almeida, J.L., Baldovino, J.A., Rose, J.L., 2021. The role of rice husk ash, cement and polypropylene fibers on the mechanical behavior of a soil from Guabirotuba formation. Transp. Geotech. 31. 100673. https://doi.org/10.1016/j.trgeo.2021.100673.

Nahar, N., Owino, A.O., Khan, S.K., Hossain, Z., Tamaki, N., 2021. Effects of controlled burn rice husk ash on geotechnical properties of the soil. J. Agri.Eng. 52 (4). https://doi.org/10.4081/jae.2021.1216.

Nshimiyimana, P., Miraucourt, D., Messan, A., Courard, L., 2018. Calcium carbide residue and rice husk ash for improving the compressive strength of compressed earth blocks. MRS Adv. 3 (34–35), 2009–2014. https://doi.org/10.1557/adv.2018.147.

Onyelowe, K.C., Onyia, M.E., Bui Van, D., Baykara, H., Ugwu, H.U., 2021. Pozzolanic reaction in clayey soils for stabilization purposes: a classical overview of sustainable transport geotechnics. Adv. Mater. Sci. Eng. 6 (28). https://doi.org/10.1007/s41204-021-00123-2.

Owino, A.O., Nahar, N., Hossain, Z., Tamaki, N., 2022a. Dimensional influence of basalt fiber reinforcements on the consolidation behavior of rice husk ash stabilized soils. Constr. Build. Mater. 339. 127686. https://doi.org/10.1016/j.conbuildmat.2022.127686.

Owino, A.O., Nahar, N., Hossain, Z., Tamaki, N., 2022b. Effects of basalt fibres on strength and permeability of rice husk ash-treated expansive soils. J Agric. Eng. 53 (1).

Poudyal, L., Adhikari, K., 2021. Environmental sustainability in cement industry: An integrated approach for green and economical cement production. Resour. Environ. Sustainab. 4. 100024. https://doi.org/10.1016/j.resenv.2021.100024.

Prusinski, J.R., Bhattacharja, S., 1999. Effectiveness of Portland cement and lime in stabilizing clay soils. Transp. Res. Rec. 1652 (1), 215–227. https://doi.org/10.3141/1652-28.

Rao, D.K., Pranav, P.R.T., Anusha, M., 2011. Stabilization of expansive soil with rice husk ash, lime and gypsum–an experimental study. Int. J. Eng. Sci. Technol. 3 (11), 8076–8085.

Robinson, R.G., Allam, M.M., 1998. Effect of clay mineralogy on coefficient of consolidation. Clays Clay Miner. 46 (5), 596–600.

Sabat, A.K., 2013. Engineering properties of an expansive soil stabilized with rice husk ash and lime sludge. Int. J. Eng. Technol. 5 (6), 4826–4833.

Sandhu, R.K., Siddique, R., 2017. Influence of rice husk ash (RHA) on the properties of self-compacting concrete: A review. Const. Build. Mater. 153, 751–764. https://doi.org/10.1016/j.conbuildmat.2017.07.165.

Sandhu, R.K., Siddique, R., 2022. Properties of sustainable self-compacting concrete made with rice husk ash. Eur. J. Environ. Civ. Eng. 26 (13), 6670–6694. https://doi.org/10.1080/19648189.2021.1955747.

Santagata, M., Bobet, A., Johnston, C.T., Hwang, J., 2008. One-dimensional compression behavior of a soil with high organic matter content. J. Geotech. Geoenviron. Eng. 134 (1), 1–13. https://doi.org/10.1061/(ASCE)1090-0241(2008)134:1(1).

Sim, J., Park, C., 2005. Characteristics of basalt fiber as a strengthening material for concrete structures. Compos. B 36 (6–7), 504–512. https://doi.org/10.1016/j.compositesb.2005.02.002.

Sridharan, A., Nagaraj, H.B., 2004. Coefficient of consolidation and its correlation with index properties of remolded soils. Geotech. Test. J. 27 (5), 469–474.

Syed, M., GuhaRay, A., Agarwal, S., Kar, A., 2020. Stabilization of expansive clays by combined effects of geopolymerization and fiber reinforcement. J. Inst. Eng. (India) Series A 101 (1), 163–178. https://doi.org/10.1007/s40030-019-00418-3.

Tamaki, N., 2019. Plant-based (rice husk) silica: M.I.T Co., Ltd.: Osaka. Plant-based (rice husk) silica, M.I.T Co., Ltd. Accessed 1 October 2019. https://mit-corp.biz/business/biosilica/.

Terzaghi, K., 1943. Theoretical Soil Mechanics. John Wiley and Sons Inc., New York, N Y.

Wang, L., 2002. Cementitious Stabilization of Soils in the Presence of Sulfate. Louisiana State University and Agricultural & Mechanical College.

Xu, D.S., Huang, M., Zhou, Y., 2020. One-dimensional compression behavior of calcareous sand and marine clay mixtures. Int. J. Geomech. 20 (9), 04020137. https://doi.org/10.1061/(ASCE)GM.1943-5622.0001763.

Yeo, S.S., Shackelford, C.D., Evans, J.C., 2005. Consolidation and hydraulic conductivity of nine model soil-bentonite backfills. J. Geotech. Geoenviron. Eng. 131 (10), 1189–1198. https://doi.org/10.1061/(ASCE)1090-0241(2005)131:10(1189).

Yi, Y., Gu, L., Liu, S., 2015. Microstructural and mechanical properties of marine soft clay stabilized by lime-activated ground granulated blast furnace slag. Appl. Clay Sci. 103, 71–76. https://doi.org/10.1016/j.clay.2014.11.005.

Yuan-qiang, C., Xu, L., Shi-ming, W., 2004. One-dimensional consolidation of layered soils with impeded boundaries under time-dependent loadings. Appl. Math. Mech. 25 (8), 937–944. https://doi.org/10.1007/BF02438802.

Zhang, R., Arrigoni, A., Panesar, D.K., 2021. Could reactive MgO cement be a green solution? The effect of CO2 mineralization and manufacturing route on the potential global warming impact. Cem. Concr. Compos. 124. 104263. https://doi.org/10.1016/j.cemconcomp.2021.104263.

Construction and Building Materials 374 (2023) 130930

Contents lists available at ScienceDirect

Construction and Building Materials

journal homepage: www.elsevier.com/locate/conbuildmat

The influence of basalt fiber filament length on shear strength development of chemically stabilized soils for ground improvement

Alex Otieno Owino *, Zakaria Hossain

Graduate School of Bioresources, Mie University, 1577 Kurimamachiya-Cho, Tsu, Mie 514-8507, Japan

ARTICLE INFO

Keywords:
Basalt fiber
Fiber-reinforcement
Microstructure
Calcium aluminosilicate hydrate
Rice husk ash
Drained triaxial test
SEM
XRD
Ground improvement

ABSTRACT

In recent years, adding fiber reinforcements into chemically stabilized weak soils to resolve brittleness at the post-peak shear strength state is becoming an increasingly popular research area. However, there is little to no research investigating the shear developments initiated through the hybridization of ground improvement techniques using high-strength basalt fibers and sustainable chemical stabilizers such as rice husk ash (RHA). This study investigated how different basalt fiber filament lengths can reinforce and consequently influence shear response in such chemically stabilized soils. A series of triaxial compression tests, scanning electron microscopy (SEM), and X-ray powder diffraction (XRD), considering curing periods, were carried out on fiber-reinforced and unreinforced chemically stabilized specimens containing: weak clay soil, varied lengths of basalt fibers filaments, RHA, and cement in their specified combinations. Based on the results, an increment in basalt fiber filaments length significantly increased the deviatoric stresses, increasing cohesion and angle of internal friction by 81% and 63%, respectively. SEM imagery showed a highly reinforced soil composite at the microstructural level. At the same time, XRD analysis justified the presence of solid calcium aluminosilicate hydrate bonds, a product of pozzolanic activity. The fiber reinforcing mechanism through interfacial contacts between basalt fiber filaments and the new stabilized soil composite was investigated and validated to form a new construction material for use as a base course during ground improvement.

1. Introduction

Since the introduction of ground improvement techniques, improving soil engineering behavior has been a significant concern for geotechnical engineers. To date, many ways to enhance soil engineering properties, such as incorporating reinforcements into the soil to densify the soil structure, using chemical stabilizers (say: cement [1–3] and lime [4]), or replacing the problematic soil with high-strength soil up to a given depth is a common practice [5]. Amongst all these methods, chemical stabilization using cement has been practiced extensively as an effective technique to improve the performance of weak soils. The process of cement manufacture utilizes approximately 1.7 tons of raw material, yielding about 1 ton of CO_2 during the combustion process [6,7]. Therefore, with the increasing environmental concerns from cement manufacture, alternative approaches are under study to partially or fully reduce cement usage [8]. In literature, the development of sustainable high-strength cementitious composites using cement substitutes like RHA is rising, but higher cement percentages (>5%) in these stabilized composites require further examination [9–12]. Additionally, soil stabilization using agricultural wastes such as bagasse ash and stone dust has been proposed to curb this challenge [13].

Recently, one of the potential soil composite combinations gaining research attention is rice husk ash (RHA) mixed with nominal cement dosages [14,15]. The mixture is considered a highly reactive pozzolanic material when amorphous silica (SiO_2) and Al_2O_3 in the RHA react with CaO in cement in the presence of water. The hydration process leads to the formation of a cementitious compound called calcium aluminosilicate hydrate, also known as CSH Gel [16–20]. In literature, adding these cementitious compounds to weak clay soils considerably led to the development in strength and compressibility [21–23]. However, cementitious bonds became brittle during loading at the post-peak strength state, and the residual shear strength significantly diminished [22,24–26].

In this context, using randomly oriented fibers (ROF) to reinforce the cementitious structure of chemically stabilized soil composites is gaining research attention [27–29]. The main advantage of ROF reinforcements is the elimination of weak zones in the stabilized soil structure compared to other conventional reinforcement methods

* Corresponding author.
E-mail address: 520d2s2@m.mie-u.ac.jp (A.O. Owino).

https://doi.org/10.1016/j.conbuildmat.2023.130930
Received 8 December 2022; Received in revised form 1 March 2023; Accepted 2 March 2023
Available online 9 March 2023

[30–33]. Also, fibers are easily mixed with the soil hence a more reliable option for ground improvement in terms of workability [34]. Lima et al. [35], while working on cement and lime-stabilized soils, observed that the compressive strength significantly increased with the addition of fiber reinforcements. Random fibers have also been proven to improve soil stress–strain behavior [36]. The effects of adding rice husk ash, pond ash, cement, and polypropylene fiber on clay's compaction and strength behavior have also been studied. The literature showed that the inclusion of fiber reinforcement within un-cemented and cemented soil caused an increase in the unconfined compressive strength, split tensile strength, and axial strain at failure [37–40]. Also, fibers changed the brittle behavior of cemented soils to a more ductile one [41]. Recently, most studies have only investigated the effects of fiber inclusions in cemented cohesionless soils, with few researchers conducting studies on weak clay soils [34,42]. In addition, there is limited research on how high-strength fiber filaments can influence the ultimate shear strength of RHA-cement stabilized soils.

Based on these deficits, the present study aimed to evaluate the influence of basalt fiber filament lengths, considering its high tensile strength, on the shear strength development of the hybrid stabilized soils composite for ground improvement. A series of triaxial compression tests were carried out on specimens constituting; clay soil, high-strength basalt fibers (filament lengths 3, 6, and 12 mm), 5% RHA, and 3% cement considering curing periods 1 day, 7 days, and 28 days. Scanning electron microscopy (SEM) for the specimens was also analyzed to examine the development of interfacial contacts between basalt fibers and the stabilized soil composite matrix at the microstructural level. At the same time, XDR was used to investigate the crystalline phases in the stabilized soil composite.

The manuscript was organized as follows. Section 2 defined the research significance. Section 3 described the materials and methods, providing details on the materials adopted, material preparation relating to the detailed blend combinations, tests adopted for the compaction characterization, shear strength analysis, and microstructural examination (SEM and XRD). Section 4 reported the results and discussions of the tests conducted to measure the compaction response, stress–strain relationship with the curing period, failure pattern, effects of filament length on shear strength parameters, microstructural analysis (SEM and XRD), and validation of shear strength development. Section 4.4. provided an image-based analysis of the basalt fiber reinforcement mechanism using SEM imagery and XRD analyses, focusing on the interfacial bonding between basalt fibers and the stabilized soil composite. Section 5 identified the limitations of the current study, while in Section 6, conclusions were drawn based on the present experimental results. Finally, in Section 7, future research work was proposed to supplement the data available for future designs in ground improvement applications.

2. Research significance

Fiber filament length and the amounts of sustainable soil stabilizers in cementitious soil composites can effectively improve the shear response of weak expansive soils. The problems of failure mechanism and shear parameters of fiber-reinforced stabilized soils under various loading conditions have been studied quite extensively in the past. Despite the volume of research available, very little or no research is reported on the influence of basalt fiber filament length on the shear strength development of sustainably stabilized soils, even though it presents considerable versatility towards the development of fiber-reinforced cementitious systems for ground improvement in geotechnical engineering. Most soil reinforcements today involve low tensile strength fibers and are degradable with time. Additionally, these fibers are being used together with well-established stabilizers like cement, which has proven hazardous to the global carbon footprint and is uneconomical considering construction costs. For optimal response, therefore, the utilization of natural high-strength fibers and sustainable stabilizers to produce hybrid fiber-reinforced cementitious systems is necessary. Also, it is paramount to investigate the shear development in such composites and to identify the synergistic effects between the blend combinations if present. Additionally, using recyclable aggregates such as RHA can reduce cement usage and disposal problems in an economical and environmentally friendly way through their incorporation into developing new innovative material composites.

3. Material and methods

3.1. Materials

The materials used in this study included clay soil (S) from the Handa area of Mie Prefecture, Japan, basalt fiber (BF), rice husk ash (RHA), and Portland cement (C), as shown in Fig. 1. The soil was classified as A-7–5 (2) clayey soils based on the American Association of State Highway and Transportation Officials (AASHTO). Other soil characteristics included liquid limit (58.21%), plastic limit (31.05%), sand content (6.2%), silt content (52.56%), and clay content (41.24%).

JCK Corporation provided basalt fibers in their standardized forms of 3 mm, 6 mm, and 12 mm to establish a comprehensive parametric study on shear development and reinforcement projections of different basalt fiber filaments in chemically stabilized soils. Basalt fibers are an environmentally friendly material made from melted basalt rock at a high temperature of 1500 °C and then quickly morphed into a continuous fiber by extrusion through 6–30 μm filament nozzles. Upon industrial strength testing, the fibers indicated a high tensile strength of 4100–4840 MPa, elastic modulus 93.1–110 GPa, and a fracture elongation rate of 3.1%.

RHA, with a high silica content of 91.10%, was obtained from Make Integrated Technology Co., Ltd, Osaka, Japan. A detailed grain size analysis for soil, RHA, and cement is shown in Fig. 2a. Where soil had grain sizes ranging from 0.001 to 2 mm, RHA 0.00129 to 0.3 mm, and cement 0.0001 mm to 0.1 mm. Soil, RHA, and cement were subjected to X-ray powder diffraction (XRD) analysis which quantitatively allowed for the determination of the chemical composition of the materials, as illustrated in Fig. 2b. The soil had high crystal peaks of SiO_2 found in sedimentary soils, essential for the soil stabilization processes [43]. RHA had an amorphous phase with a crystalline phase observed at a diffraction angle (2θ) of approximately 21°, corresponding to SiO_2. The crystalline phase in RHA indicated that the burning of rice husks was done at a temperature above 600 °C. The amorphous phase was destroyed at these high temperatures, increasing pozzolanic properties [44,45]. On the other hand, the cement had a composition of alite (Ca_3SiO_5), a major chemical component in Portland cement that defined its high strength. Minimum dosages of Portland cement were chosen for this research to reduce cement usage and due to its availability in the market as an amorphous SiO_2 activator.

3.2. Material preparation

The soil was sieved through the 2 mm sieve and allowed to air dry for two weeks before specimen preparation. The blends were prepared by dry-mixing the air-dried soil with RHA (5% dry weight of soil) and cement (3% dry weight of soil) to a homogeneous mix, as shown in Fig. 3a.

In this study, RHA dosage was set to 5% due to the maximum utilization of the amorphous silica at low percentages [14,15]. On the other hand, minimum dosages of cement reduced cement usage and provided Ca^{+} ions in optimal proportions during pozzolanic reactions. Incorporating RHA as a cement reduction parameter agreed with the environmental conservation and carbon emission reduction goals explained in Section 1.

Next, water was added to the dry mix considering the w_{opt} of each specific combination to initiate the chemical stabilization phase through hydration (Fig. 3b). Basalt fiber (1% dry weight of soil) with filament

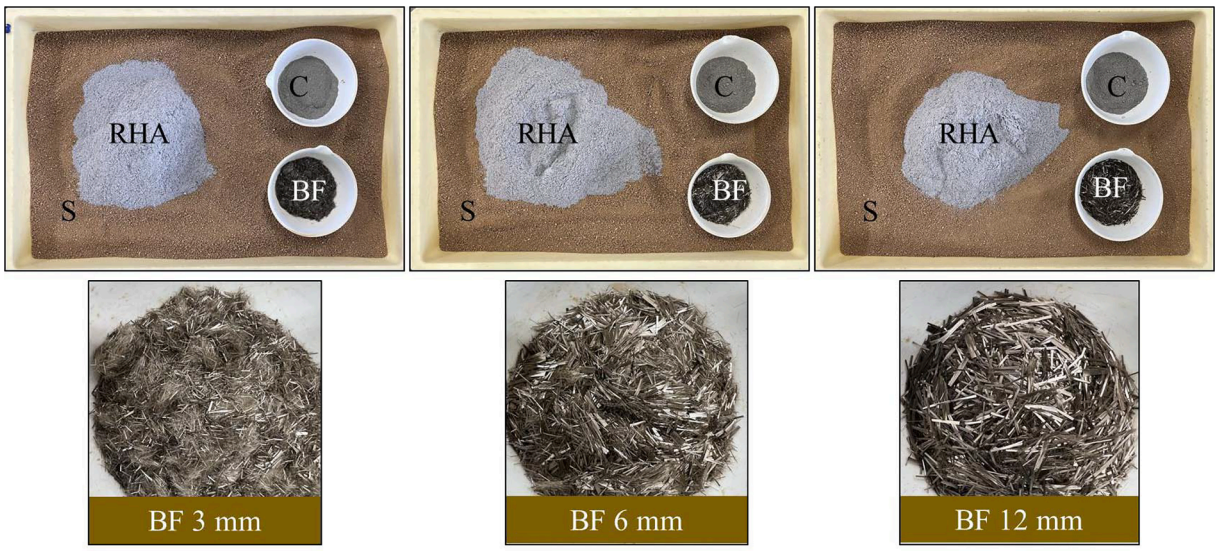

Fig. 1. Experimental materials: S-Soil; RHA-Rice husk ash; C-Cement; BF-Basalt fiber.

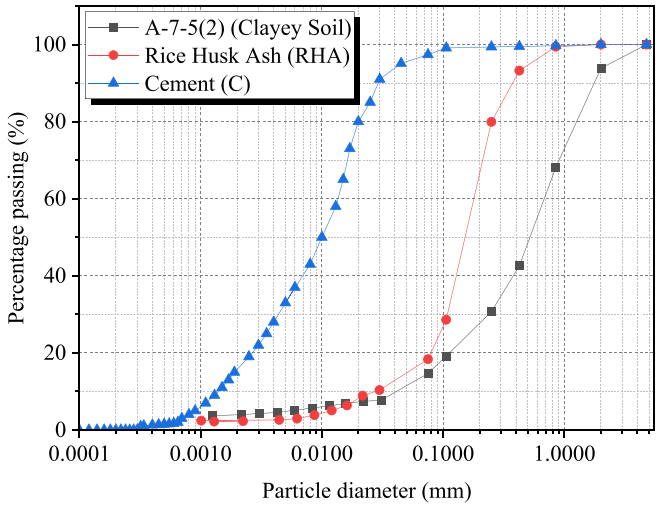

Fig. 2a. Particle size distribution for Soil and RHA.

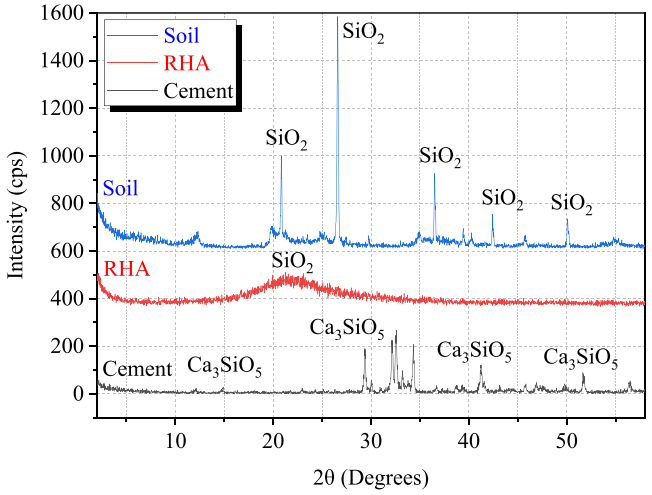

Fig. 2b. X-ray diffraction (XRD) of soil, RHA, and cement.

lengths of 3 mm, 6 mm, and 12 mm were sprinkled on the top surface of the soil-RHA-Cement mixture to ensure random distribution and reduce fiber balling during the next phase of mixing as shown in Fig. 3c. The fiber content was set at 1% to avoid tangling or balling during the specimen preparation, affecting the blends' homogeneity [46]. The manual mixing of all the materials guaranteed an even distribution of basalt fibers within the new composite material, as shown in Fig. 3d.

Blend combinations were prepared at the maximum dry density (ρ_{dmax}) and optimum moisture content (w_{opt}), after which three cylindrical specimens were prepared for each level of confining pressure (Fig. 3e) at −3% OMC and tested after a moist-curing period of 1, 7, and 28 days. The detailed blend combinations used in this study are shown in Table 1.

3.3. Testing methods

3.3.1. Compaction tests

For each material blend shown in Table 1, a standard proctor compaction test was done to determine the optimum moisture content (w_{opt}) and the corresponding maximum dry density (ρ_{dmax}). Each blend was compacted into a cylindrical mold measuring 10 cm in diameter and 12.73 cm in height using a 2.5 kg rammer at a falling height of 30 cm while maintaining a constant compaction effort for each of the three layers. This process was repeated for various known moisture contents, and the dry densities were calculated for each. The plots of the dry density to the moisture content, also called the compaction curves, were then used to obtain the peak points representing the maximum dry density and the optimum moisture content. All testing procedures followed the Japan Industrial Standards (JIS) A 1210 standards [47].

3.3.2. Triaxial compression tests

Following the Japan Geotechnical Society 0520 ~ 0524 standards [48], consolidated drained (CD) triaxial tests were performed on cylindrical specimens measuring 5 cm (in diameter) and 12.5 cm in height. The specimens were prepared by compacting each blend in three layers inside a mold of similar dimensions using a 1 kg rammer at a 30 cm falling height. Each specimen was set up in the triaxial test pressure chamber and sealed with a rubber sleeve, as shown in Fig. 4. The consolidated drained triaxial tests experimental setup consisted of the following major components; (1) load cell to measure the axial load, (2) loading piston to apply the axial loading on top of the specimen, (3) dial gauge to measure the axial displacement, (5) pressure cylinder to contain the chamber fluid, (6) chamber fluid to apply the hydrostatic

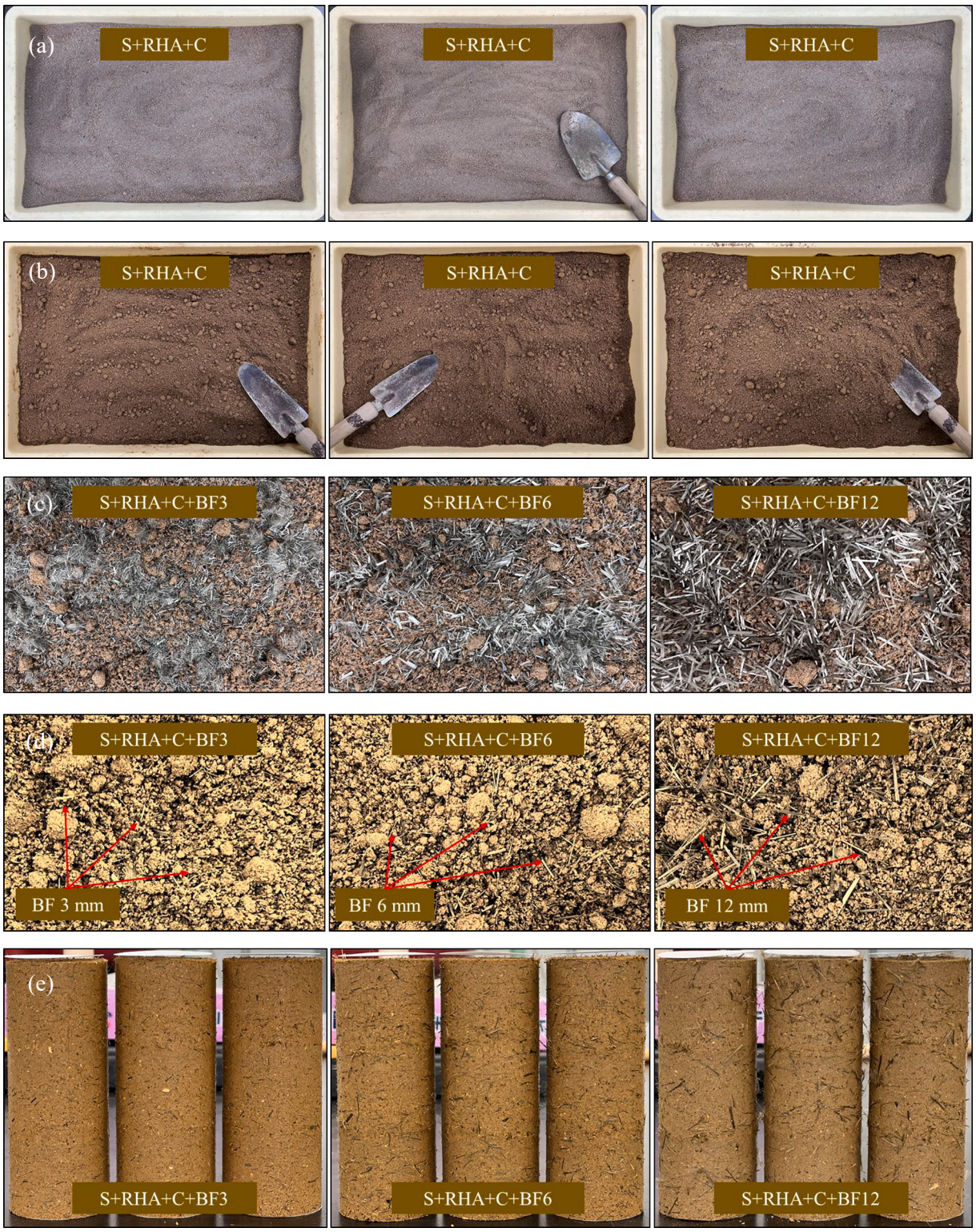

Fig. 3. Preparation of materials and specimen. (a) Step 1: Dry mixing of Soil, RHA, and Cement in specified combinations. (b) Step 2: Addition of water considering the w_{opt} of specified combinations. (c) Step 3: Addition of varied basalt fiber filament lengths in specified combinations. (d) Step 4: Manual mixing of the materials: To ensure the random orientation of the basalt fibers and to achieve a homogeneous mix. (e) Step 5: Specimen preparation- 3 Samples per confining pressure for all specified combinations.

chamber pressure (σ_3), (9) drainage/pore water pressure measurement route, (10) confining fluid supply path and (13) air pressure inlet route. A detailed illustration with well-labeled components is shown in Fig. 4.

In this study, the confining pressures were 50 kPa, 100 kPa, and 150 kPa. The drainage/pore water-pressure measurement route was left open to ensure a drained condition within the specimen. Specimens were allowed to shear slowly enough at a rate of 0.5 mm/minute so that the pore water pressure did not develop within the composite structure. During the experiment, values of deviatoric stresses and axial strains were recorded in a data logger. The experiment was stopped once the

Table 1
Detailed blend combinations.

Blends	Soil, S (%)	RHA (%)	Cement, C (%)	Basalt Fiber, BF (mm)
S-Control	100	0	0	0
S:5R	100	5	0	0
S:5R:3C	100	5	3	0
S:5R:3C:1BF3	100	5	3	3
S:5R:3C:1BF6	100	5	3	6
S:5R:3C:1BF12	100	5	3	12

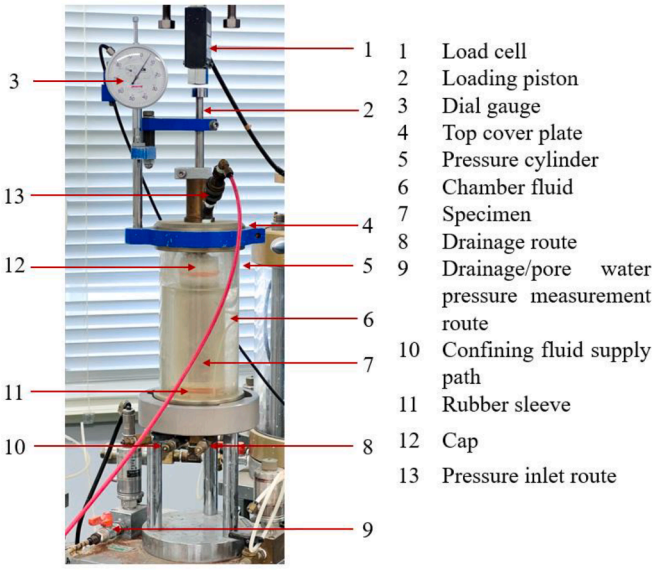

Fig. 4. Triaxial testing apparatus.

peak value of the deviatoric stress was attained and then reduced to two-thirds or at 10% axial strain.

3.3.3. *Microstructural study on shear strength development*

A microstructural examination through scanning electron microscope (SEM) imagery and X-ray powder diffraction (XRD) was essential to validate the mechanical and chemical changes in the reinforced and stabilized soil composite.

SEM imagery was an essential technique for analyzing the soil composite on a micrometer scale by employing low-energy secondary and backscattered electrons to visualize the structural changes in the new composite material [49]. The three-dimensional images from the SEM test showed the role played by the additives in altering the surface morphology of the stabilized soil at a micro-level during the curing period [50,51].

The X-ray powder diffraction (XRD) was used to identify the crystalline patterns that provided a detailed analysis of the degree of incorporation of the chemical stabilizing agents within the stabilized soil composite. Specifically, XRD helped to better understand the various chemical stages in the stabilized soil due to pozzolanic reactions, considering curing periods [52–54].

4. Results and discussion

4.1. *Effects of filament length on compaction characteristics*

The geotechnical properties of soil, such as shear strength, highly depend on the moisture content and the compaction density. The results of optimum moisture content and dry density for soil and the soil blends in this study are shown in Fig. 5. The compaction curves did not pass the saturation line (S_r), establishing the correctness of the relationships

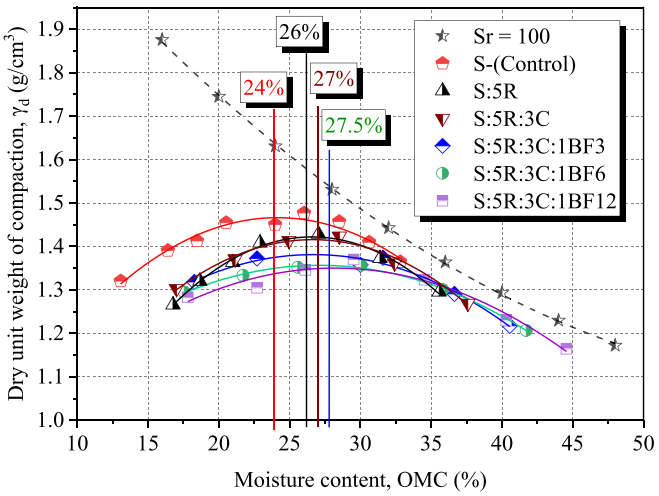

Fig. 5. Effects of RHA, cement, and basalt fiber filament lengths on compaction characteristics.

between w_{opt} and ρ_{dmax}. It was evident from Fig. 5 that the w_{opt} increased from 24% (soil only) to 26% and 27% after adding RHA and RHA-cement to the expansive soil, respectively. Besides, adding basalt fibers filaments to the soil, RHA, and cement composite had minimal effects on the w_{opt}. It was also observed that increasing basalt fiber filament lengths in the soil composite had minimal influence on ρ_{dmax} for all three blends. For instance, w_{opt} was maintained at 27.5% for all combinations while ρ_{dmax} varied slightly with values 1.35 g/cm^3 for specimen S:5R:3C:1BF3 and 1.37 g/cm^3 for both S: 5R:3C:1BF6 and S:5R:3C:1BF12. The increase in w_{opt} was attributed to; the high-water absorption rate of RHA due to its porous structure [55], the additional porosity due to fiber interconnectivity, and water requirements due to the heat of hydration brought about by the cement. Also, the addition of cement and RHA led to volumetric changes in the structure of the aggregates during flocculation, leading to a significant increase in the void ratio hence the rise in moisture content [56]. Further, the maximum dry density (ρ_{dmax}) decreased due to the low specific gravities of RHA and cement compared to the soil [57,58]. A decrease in the maximum dry density compared to the control specimen indicated that low compaction energy is needed; hence an economical compaction cost can be realized [59].

4.2. *Effects of filament length on stress–strain relationship with curing period*

The effects of basalt fiber filament length on the deviatoric stresses ($\Delta\sigma$) and axial strains (ε) acting within the specimens with curing periods are discussed in this section. A series of triaxial tests for confining pressures 50 kPa, 100 kPa, and 150 kPa were conducted, and the results were plotted after 1 day, 7 days, and 28 days of curing. For reference, the stress–strain relationship for the control specimen (soil only) was established in Fig. 6. The control specimen graphs showed that the confining pressures had a minimal influence on the ultimate deviatoric stress ($\Delta\sigma$), with a small increment recorded after 28 days of curing. The low deviatoric stresses were due to the brittleness of the soil and the lack of proper bonding between the soil particles during shearing - a common phenomenon for highly cohesive soils.

However, with the addition of RHA and RHA:cement to the expansive soil, there was a clear distinction between the deviatoric stresses ($\Delta\sigma$) with different confining pressures. The relationship between axial strain (ε) and the deviatoric stress ($\Delta\sigma$) for specimens containing 5 % RHA and 5 %RHA:3%cement have been illustrated in Fig. 7 and Fig. 8, respectively. In both instances, the deviatoric stresses ($\Delta\sigma$) increased with the curing period, with the cement composites recording the

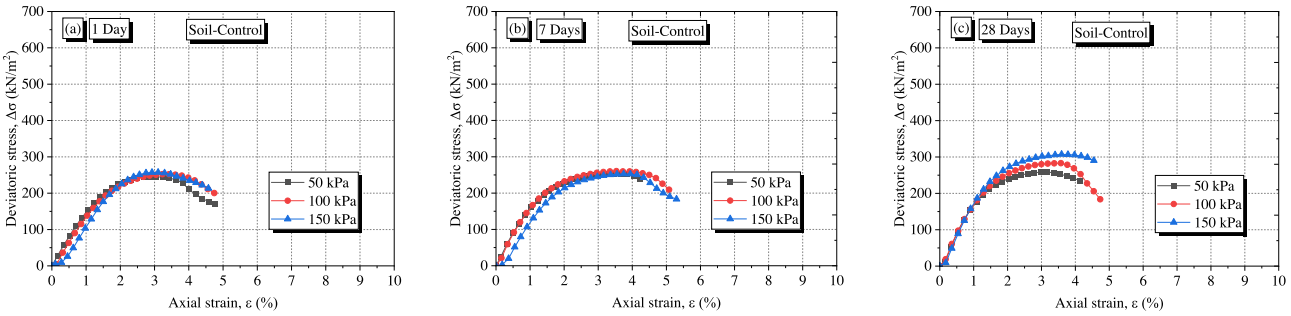

Fig. 6. Stress-Strain relationship for soil only with curing period: (a) 1 day, (b) 7 days, and (c) 28 days.

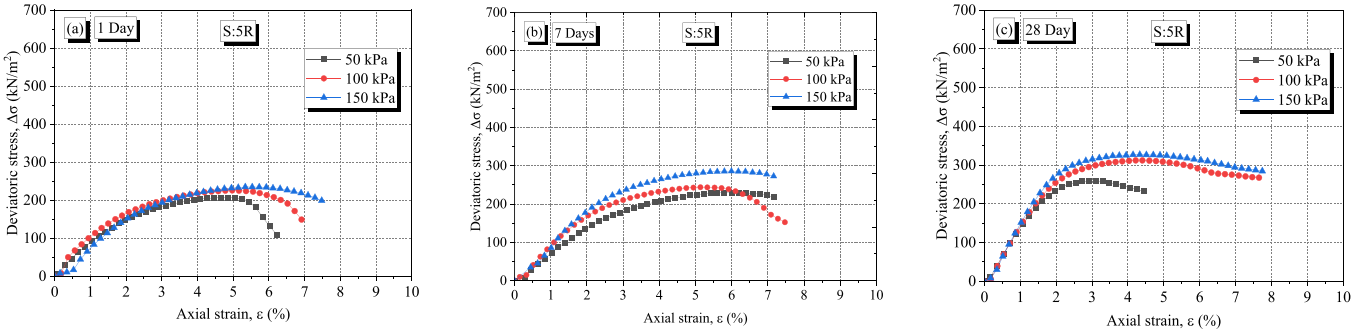

Fig. 7. Stress-Strain relationship for soil:5%RHA with curing period: (a) 1 day, (b) 7 days, and (c) 28 days.

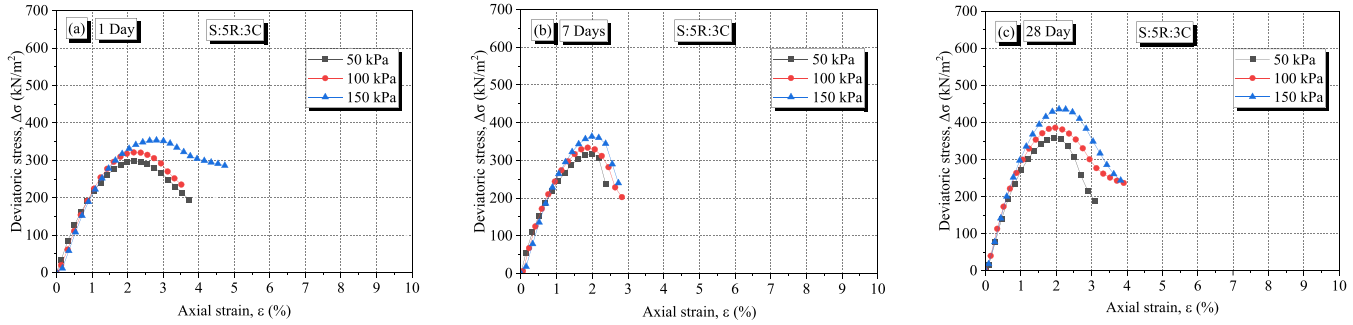

Fig. 8. Stress-Strain relationship for soil:5%RHA:3C with curing period: (a) 1 day, (b) 7 days, and (c) 28 days.

highest values at 150 kPa confining pressures compared to the control. However, it was noteworthy that the addition of cement decreased the axial strains (ε) at maximum deviatoric stresses (Δσ) in the tested specimens. At the same time, a brittle nature was evident on the cement composites due to the sharp decrease in the deviatoric stress (Δσ) after the peak value was realized, as compared to the significant softening behavior on the 5 %RHA specimens.

Figs. 9–11 showed that adding basalt fiber filament lengths into the soil-RHA-cement composite highly influenced the maximum deviatoric stress (Δσ) at failure. The stress-stain relationships after 1 day of curing for specimens reinforced with basalt fiber 3 mm, 6 mm, and 12 mm are plotted in Fig. 9. The increase in deviatoric stress (Δσ) caused by the basalt fibers was consistent and increased with filament length. Also, it was noteworthy that the deviatoric stresses (Δσ) increased with the confining pressure. Besides, varying the basalt fiber filament length from 3 mm to 12 mm increased the axial strain slightly, with a notable 1%

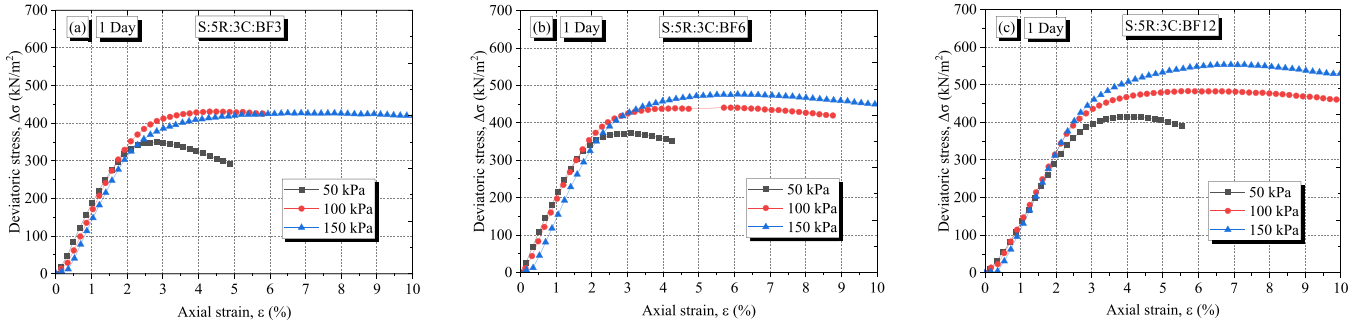

Fig. 9. Stress-Strain relationship after 1 day of curing for specimen reinforced with (a) 3 mm, (b) 6 mm, and (c) 12 mm basalt fiber filament lengths.

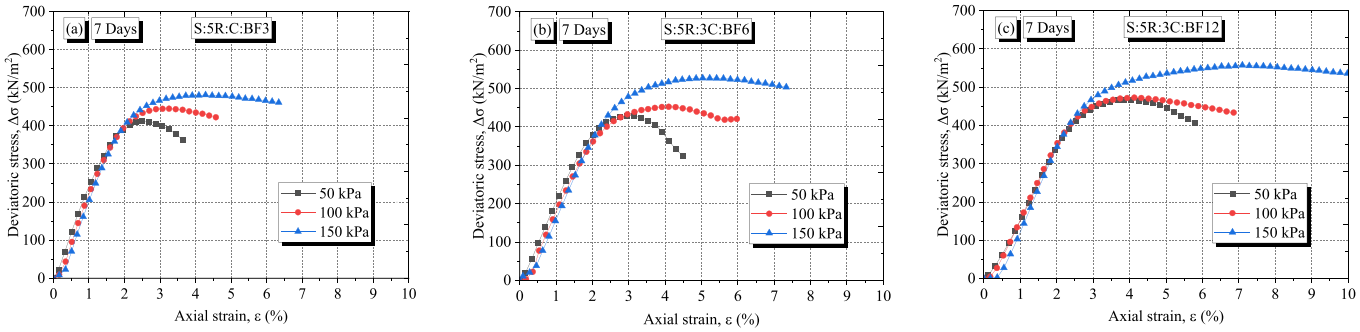

Fig. 10. Stress-Strain relationship after 7 days of curing for specimen reinforced with (a) 3 mm, (b) 6 mm, and (c) 12 mm basalt fiber filament lengths.

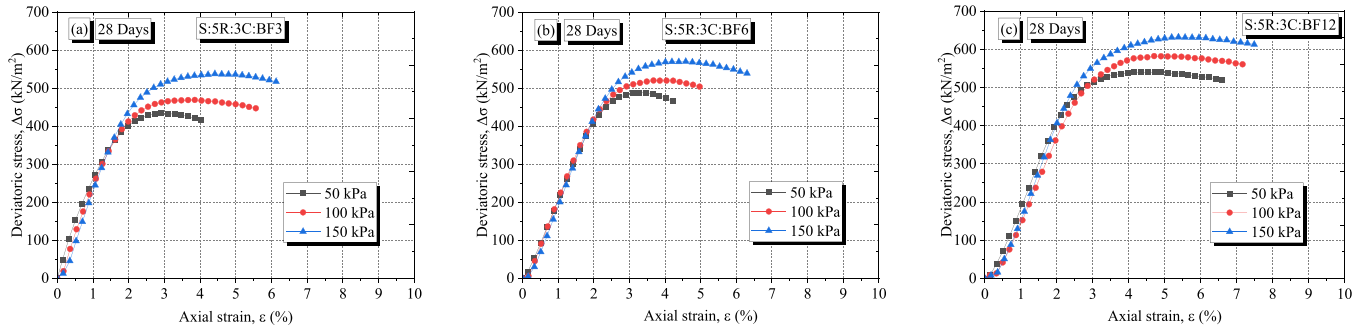

Fig. 11. Stress-Strain relationship after 28 days of curing for specimen reinforced with (a) 3 mm, (b) 6 mm, and (c) 12 mm basalt fiber filament lengths.

increase in axial strain (ε) for the 12 mm specimens at maximum deviatoric stress.

To further clarify the performance of different basalt fiber filament lengths, sets of specimens were moist-cured for 7 and 28 days, followed by testing to examine how the curing period influenced the shear characteristics, as shown in Fig. 10 and Fig. 11 . The results indicated a notable improvement in the deviatoric stresses (Δσ) compared to the 1-day curing results and the control specimen. This increase was due to the additional stiffness initiated by the fiber reinforcements and cementation from the pozzolanic reactions during curing. The curing effect was more dominant after 28 days, where the record-high deviatoric stresses (Δσ) with values 537.33 kN/m^2, 569.91 kN/m^{2,} and 631.86 kN/m^2 for 3 mm, 6 mm, and 12 mm filament length, respectively, were recorded as shown in Fig. 11. These results concluded that the deviatoric stresses (Δσ) increased with the basalt fiber filament length and that significant improvement was highly dependent on the curing period allowed before testing.

On the other hand, adding longer basalt fiber filament lengths increased the value of axial strains (ε) required to achieve maximum deviatoric stresses in the specimens. At such high strain levels, the interfacial forces between the fibers and the soil-RHA-cement composite were progressively mobilized, hence reaching high levels of deviatoric stresses (Δσ) within the specimen [60]. Incorporating longer fiber filament lengths in the specimen enhanced the ductility, thus the ability to withstand maximum deviatoric stresses (Δσ) at high axial strains. Tang et al. [34] and Consoli et al. [61] showed a similar improvement in the ductility of fiber-reinforced soil composites. Additionally, the results depicted that a further increase in the strains after the peak deviatoric stress led to the loss of shear strength. However, the loss of shear strength followed a gradual projection due to the low elastoplastic deformations in the specimen along the failure plane. These deformations triggered the steady softening behavior. Consoli et al. [62] and Heineck et al. [63] also observed a similar gradual loss in shear strength at large shear strains while investigating the performance of fibers in sandy soil.

Furthermore, to understand the mechanical responses to shear for unreinforced and fiber-reinforced specimens, photo data showing the failure patterns for specimens tested after 28 days of moist curing were obtained, as illustrated in Fig. 12a-f. The control specimen (soil only) and the unreinforced specimens experienced a simple shear with well-defined cracks forming along the failure plane, as shown in Fig. 12a-c. This cracking was due to the brittle nature of the soil once the maximum deviatoric stresses were achieved. The addition of basalt fibers arrested the formation of these cracks in the specimen, further enhancing ductility derived from the improved contact friction between basalt fibers and the soil-RHA-cement composite, as shown in Fig. 12d-f. Besides, there was a significant reduction in the visible vertical planes of weakness (cracks) as the filament lengths increased from 3 mm to 6 mm to 12 mm, thus depicting additional elasticity in the specimens. Similar results on the effectiveness of fibers to arrest cracking in fiber-reinforced soil composites were also observed in other studies [34,64–66].

4.3. *Effects of filament length on shear strength parameters*

In this study, shear parameters of the stabilized expansive soil were quantified using the Mohr-Coulomb failure theory, presented in terms of the shear strength (τ) versus effective normal stress (σ). Considering specimens subjected to different stress conditions, simulating the in-situ stress variations with depth, the failure stress circles corresponding to the various stresses (50 kPa, 100 kPa, and 150 kPa) were represented by points A, B, and C, respectively, as illustrated in Fig. 13. A tangent line to the Mohr semi-circles satisfied the general failure criterion, and values of cohesion in kN/m^2 and angle of internal friction in radians were evaluated from the straight-line equation to represent stress states at failure. Representative plots of the Mohr Columb stress circles for the

Fig. 12. Specimens failure planes at 50, 100, and 150 kPa confining pressure after 28 days of curing.

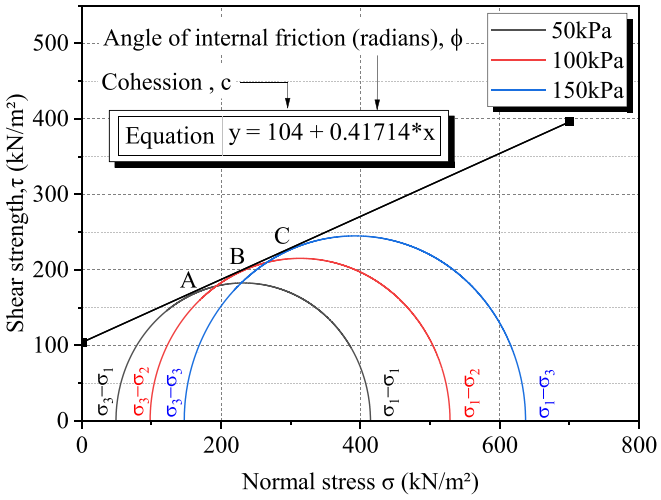

Fig. 13. Stress circles at failure corresponding to different principal stresses.

specimens tested after 28 days of curing were shown in Fig. 14a-f.

The analyses herein emphasized the effects of basalt fiber filaments on the shear parameters of unreinforced and reinforced chemically stabilized soil. They were plotted in terms of cohesion and angle of internal friction, as presented in Fig. 15 and Fig. 16. Each point in the plot corresponded to the average cohesion and average angle of internal friction from the three tested specimens. This average value eliminated the random errors during specimen preparation and in the experimental procedure, giving a more accurate value than when a single investigation was carried out.

In Fig. 15, a correlation of the cohesion values for the unreinforced and fiber-reinforced composites with the curing period was analyzed. From this graph, the S:5R specimens recorded the lowest cohesive strengths due to the limited calcium ions leading to weaker cementitious bonds in the composite matrix. Conversely, the cohesion of the control specimen increased after 7 days of curing. Then it reduced considerably after 28 days of curing due to the degradation of the soil particle bonds. However, upon adding a nominal dosage of cement, a steady increase in the cohesive strength was noted, with c increasing from 108 kN/m^2 to 120 kN/m^2 and ultimately to 124 kN/m^2 for 1 day, 7 days, and 28 days respectively.

On the other hand, basalt fiber addition into the chemically stabilized specimen significantly improved the cohesion at each curing stage. However, the increasing cohesion value depended on the basalt fiber filament length present in the specimens. For instance, the specimens containing 12 mm basalt fiber filaments attained the highest cohesion of 180 kN/m^2 after 28 days of curing compared to the 166 kN/m^2 and 135 kN/m^2 obtained from the 6 mm and 3 mm specimens, respectively. It can be concluded that longer basalt fiber filament lengths strengthened the reinforcement effects by efficiently distributing the loads to adjacent fibers, enabling the stabilized specimen to act as a dense structure through fiber interactions. Using shorter fibers (6 mm and 3 mm) lowered the cohesion due to the reduced fiber contact areas hence a less dense network in the specimen. This phenomenon was observed by other researchers [67].

It was also recognized that the angle of internal friction of the fiber-reinforced specimen improved compared to the unreinforced soil, as shown in Fig. 16. This frictional resistance development can be attributed to the following two factors. Firstly, adding the soil stabilizing agents (RHA and cement) enabled large clusters to form and, in turn, increased the grain-to-grain contact during shearing. Secondly, adding basalt fibers to the stabilized soil composite improved the physical interaction between the soil clusters by anchoring them together to form a denser structural framework that enhanced frictional resistances during shearing.

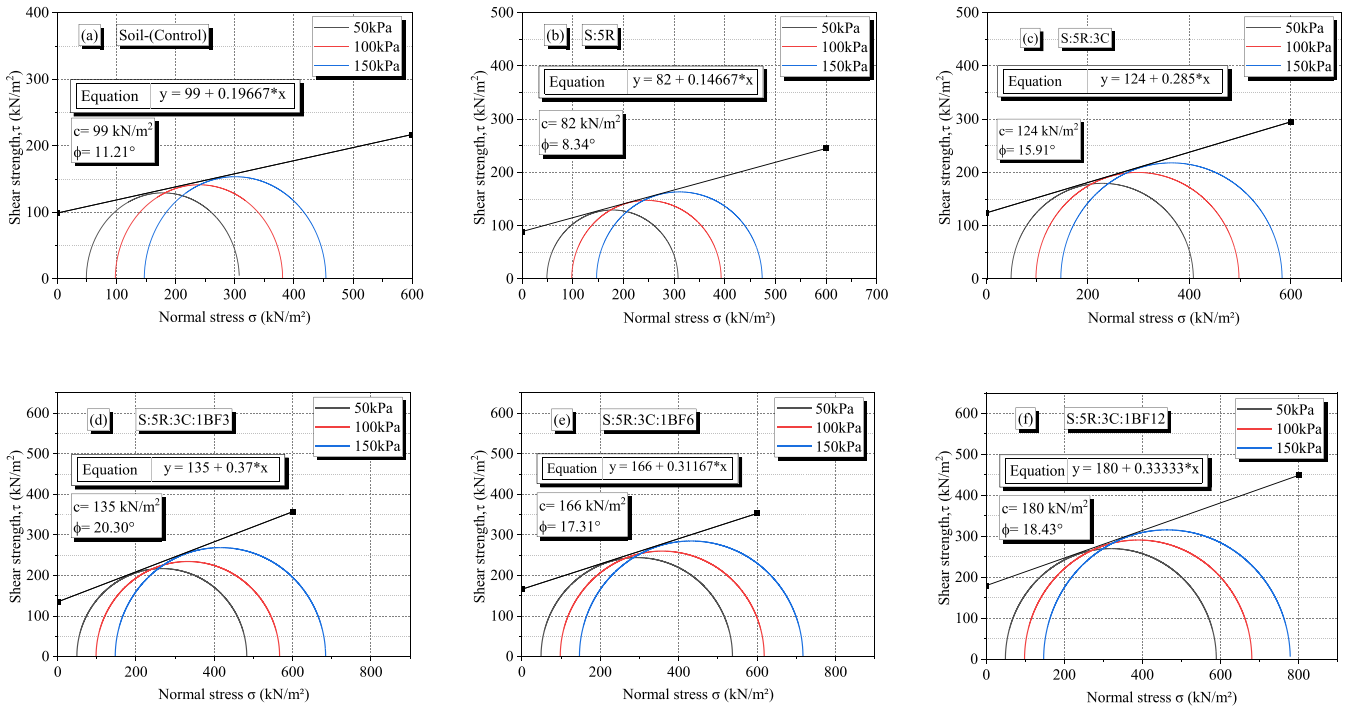

Fig. 14. Mohr Columb stress circles for the specimens after 28 days of curing (a) Soil-(Control) (b) S:5R (c) S:5R:3C (d) S:5R:3C:1BF3 (e) S:5R:3C:1BF6 (f) S:5R:3C:1BF12.

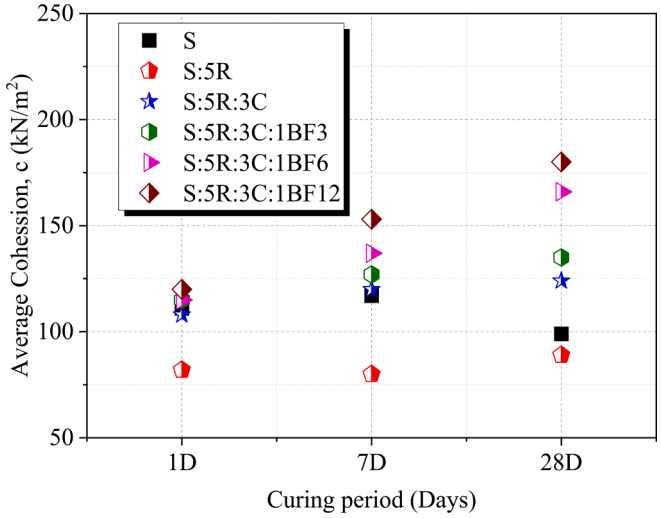

Fig. 15. Effects of basalt fiber filament length on cohesion with curing period.

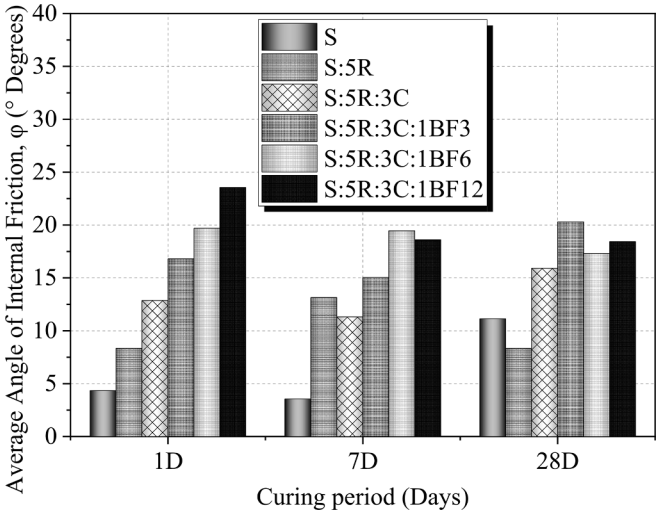

Fig. 16. Effects of basalt fiber filament length on ϕ with curing period.

Further, to uphold the significance of this research, a comparison between the shear strength parameters of this study with other relevant studies was established, considering different types of fibers and stabilization methods as shown in Fig. 17. Notably, the new composite containing 5 %RHA, 3% cement, and 12 mm basalt fibers attained the highest cohesion values compared to the composites reinforced with sisal [68], jute [69], and polypropylene fibers [70] and the unreinforced composites containing RHA [15] and cement [71] as indicated in Fig. 17a. For example, Najmun et al. showed that stabilizing expansive soils with 5% RHA attained a maximum cohesive strength value of 85 kN/m^2 [15]. In another relevant study, Ghadakpour et al. showed that adding nominal cement dosages (2%) increased the cohesive strength to 100 kN/m^2 [71]. However, in this study, adding 12 mm basalt fibers to such composites significantly increased cohesive strength to 180 kN/m^2 with percentage increases of 112% and 80% compared to the 5 %RHA and 2% cement composites, respectively.

Additionally, changes in fiber type showed an increase in cohesive strength by up to 44%, 58%, and 8% for the jute fiber, sisal fiber, and polypropylene fiber, respectively, compared to the cohesive strength of 12 mm basalt fiber reinforced composites.

On the other hand, in Fig.17 (b), the variation in the angle of internal friction was less significant for the fiber-reinforced composites. Jute fiber and sisal fiber showed an average ϕ of 25.8%, indicating a 545% increase compared to the ϕ of the control specimen (S-Control). This study recorded a 350% increase in ϕ, indicating significant developments in ϕ compared to the control specimen (S-Control). However, studies by Najmun et al., Cai et al., and Ghadakpour et al. showed slightly higher ϕ values due to the higher percentages of sand content in the clayey soil used in their study [15,70,71].

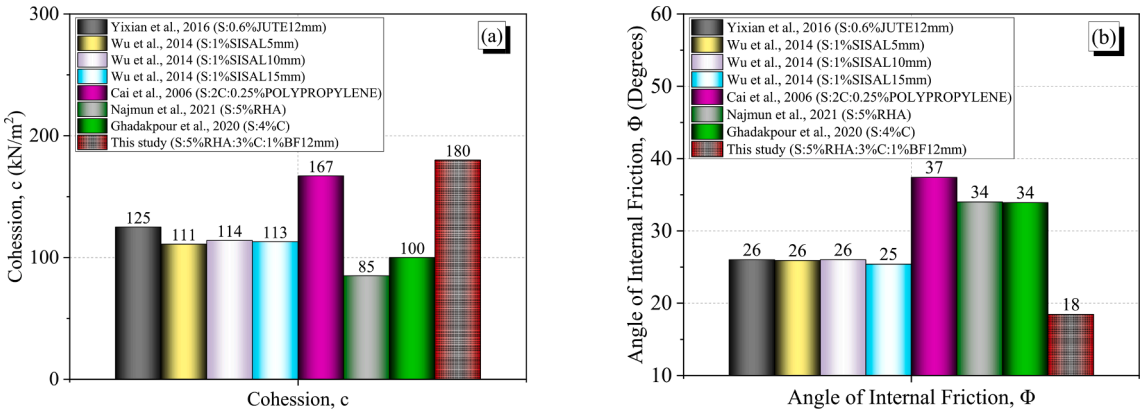

Fig. 17. A comparison between shear strength parameters with relevant studies (a) Cohesion (b) Angle of internal friction.

4.4. Microstructural analysis and validation of shear strength development

The test results discussed above demonstrated that the shear developments in the stabilized specimens were mainly due to the reinforcement extent on the cemented composite structure: influenced by the basalt fiber filament length and pozzolanic activity. This study validated these phenomena through SEM and XRD analyses.

4.4.1. SEM analysis

Firstly, a microstructural examination was conducted to show the structural modification of the soil-only specimen, followed by analyzing the ultimate composite structure after adding RHA and cement. It was evident that micro-crack formation was a common phenomenon in the unreinforced specimens, as shown in Fig. 18, Fig. 19, and Fig. 20 for S-Control, S:5R, and S:5R:3C blends, respectively. In the control specimen (S-Control (Fig. 18a, b), the porous morphology (micro-pores) alongside the micro-cracks indicated a higher potential for shear failure during loading due to the increased planes of weakness in the sample at 7 days and 28 days of curing. However, for the S:5R (Fig. 19a, 19b), a reduction in micro-cracks formation and the development of cemented composite structure after 28 days of curing validated the increase in the cohesion value, as shown in Fig. 15.

Furthermore, adding nominal dosages of cement enhanced the degree of cementation in the composite structure with the curing period, reducing micro-pores and micro-cracks development, as shown in Fig. 20a and 20b. This phenomenon led to a steady increase in cohesion compared to the S-control and S:5R specimens, as indicated earlier.

Moreover, the interactions between the basalt fiber filaments and the cemented composite structure on shear development were verified. The SEM images of the high-strength specimen (S:5R:3C:1BF12) after drained shearing at 150 kN/m^2 confining pressure are presented in Fig. 21a and 21b. It was observed that after 7 days of curing, separate cemented blocks were interlocked together by loosely packed basalt fiber filaments. Further, after 28 days of curing, the interfacial contacts between basalt fiber filaments and the surrounding composite materials increased significantly, improving the bonding degree within the composite structure. As a result, the basalt fiber filaments bridged the gaps between the separate cemented blocks enabling them to withstand higher degrees of stress during the shearing process. This bridging mechanism was a factor of basalt fiber filament length (from 3 mm to 12 mm), as indicated in the progressive increase in the cohesion and angle of internal friction values in Fig. 15 and Fig. 16.

It can be concluded that the consequent increase in c and ϕ was attributed to the reinforcing effect of the basalt fiber filament length.

4.4.2. Basalt fiber reinforcement mechanism

As discussed in this study, adding fibers to the new composite material significantly influenced the failure characteristics during shear. Therefore, understanding the reinforcing mechanism is necessary to justify their potential to arrest the formation of planes of weakness within the composite materials. In this section, a detailed illustration through SEM imagery at a magnification of x2000 was used to illustrate the developments in interfacial bonding and fiber surface frictional resistances with the curing period. It was noteworthy that basalt fibers in their natural form had smooth surfaces, as shown in Fig. 22a. However,

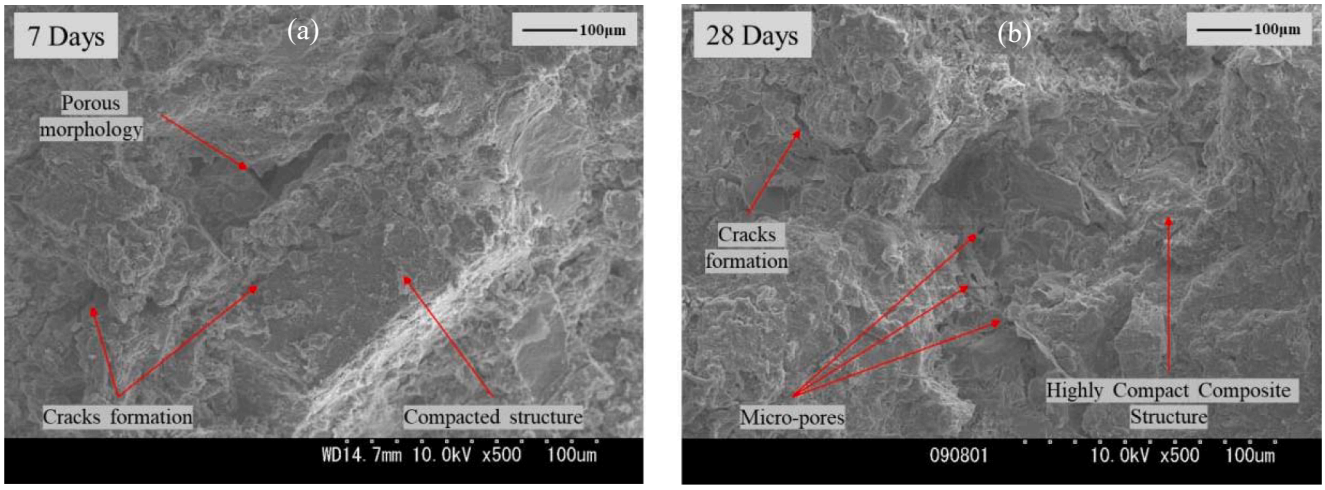

Fig. 18. (a)SEM image for S-Control specimen after 7 days curing at x500. (b) SEM image for S-Control specimen after 28 days curing at x500.

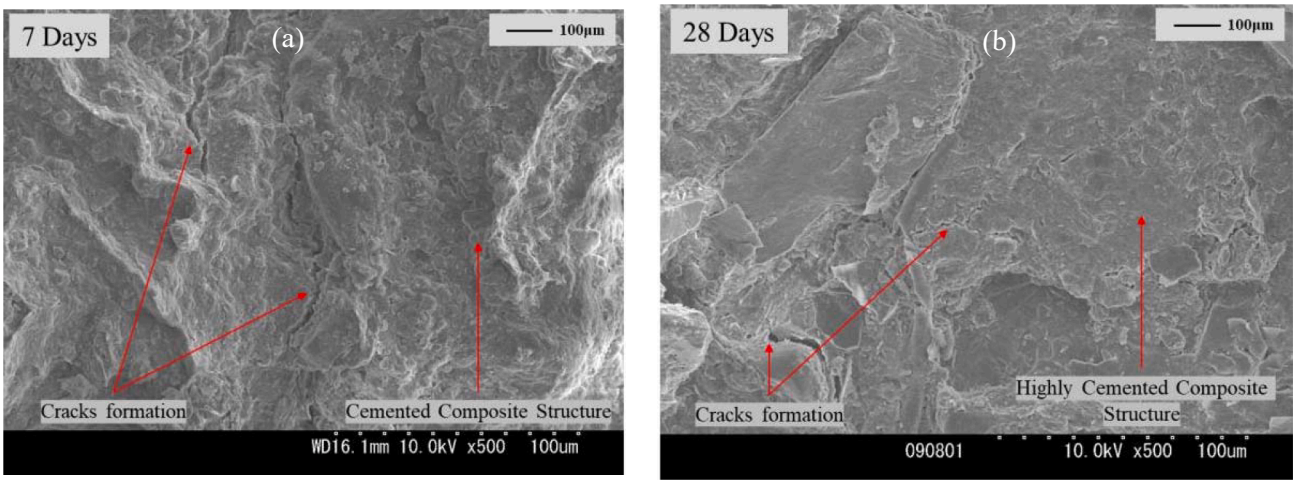

Fig. 19. (a) SEM image for S:5R specimen after 7 days curing at x500. (b) SEM image for S:5R specimen after 28 days curing at x500.

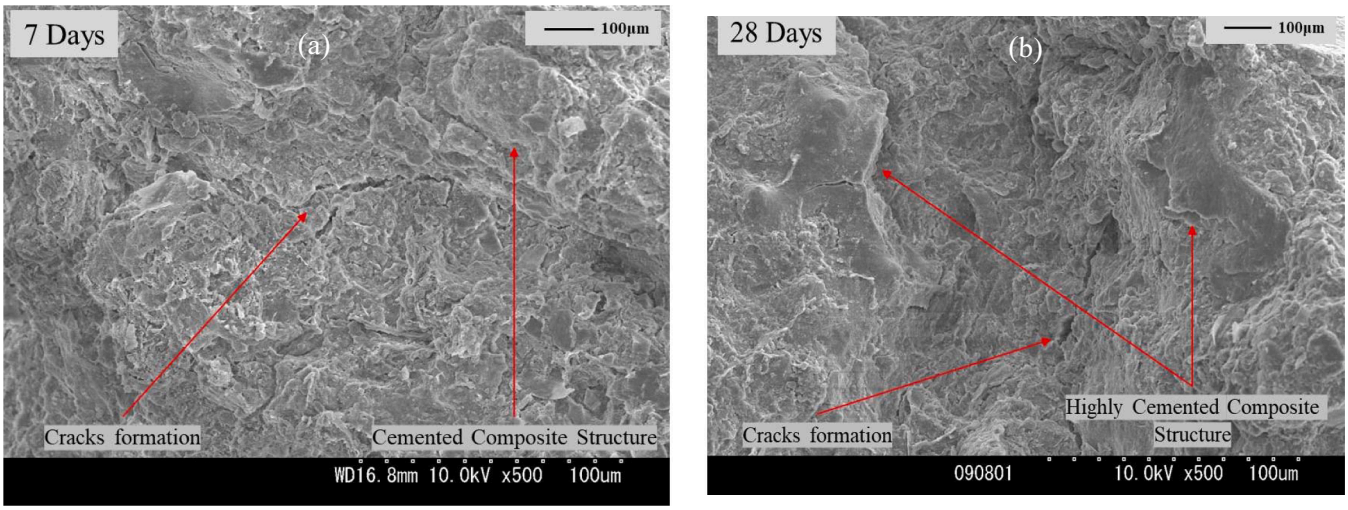

Fig. 20. (a)SEM image for S:5R:3C specimen after 7 days curing at x500. (b) SEM image for S:5R:3C specimen after 28 days curing at x500.

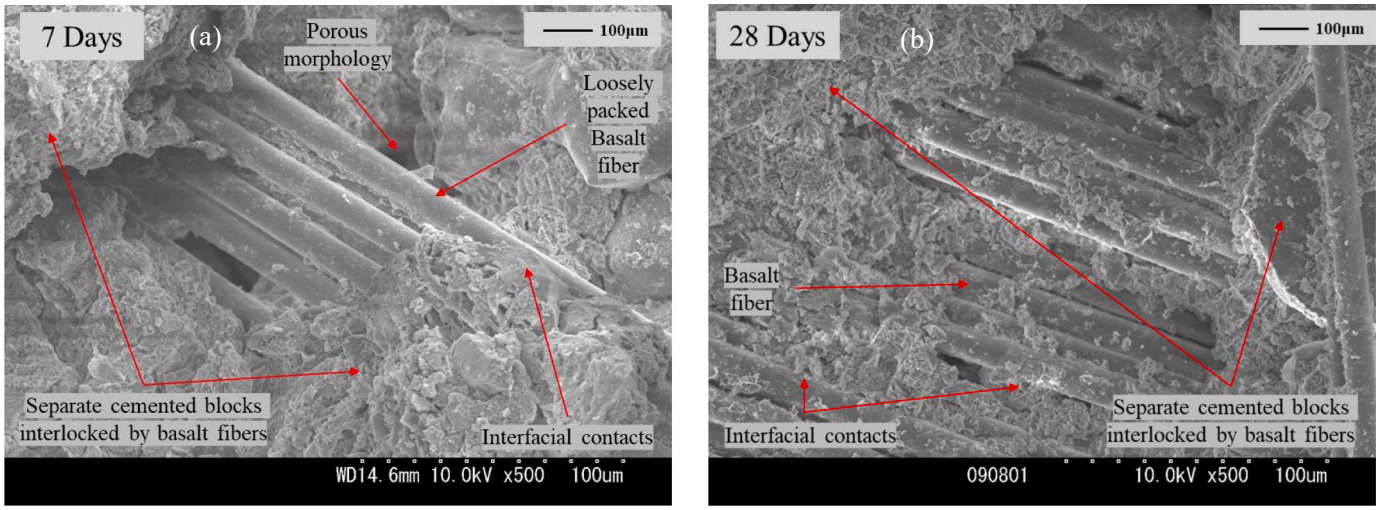

Fig. 21. (a) SEM image for S:5R:3C:1BF specimen after 7 days curing at x500. (b) SEM image for S:5R:3C:1BF specimen after 28 days curing at x500.

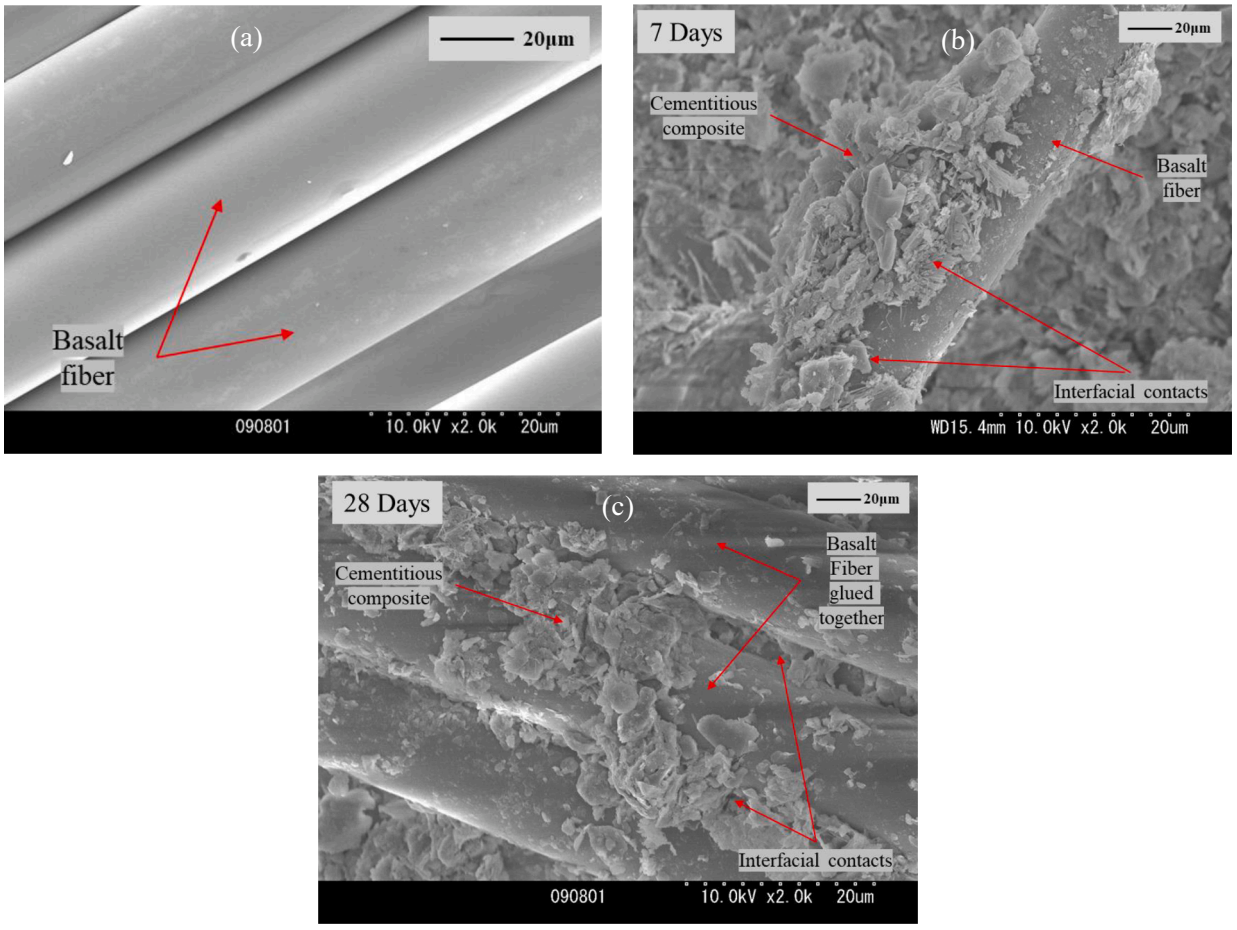

Fig. 22. (a) SEM image for the natural form of basalt fiber. (b) SEM imagery of the interfacial bonds between basalt fiber and S:5R:3C composite after 7 days of curing at x2000. (c) SEM imagery of the interfacial bonds between basalt fiber and S:5R:3C composite after 28 days of curing at x2000.

upon its use in soil reinforcement, rapid developments of interfacial bonds between the fiber filaments and the surrounding soil composite ensued, as shown in Fig. 22b.

Flocculation was evident after 7 days of curing, leading to small soil composite clusters forming around the basalt fiber filaments, as shown in Fig. 22b. Furthermore, as the curing period increased to 28 days, a denser cluster held the fiber filaments in place, displaying a more compact structure within the reinforced specimen, as shown in Fig. 22c. The formation of the large clusters around the basalt fiber filaments was attributed to the fiber's ability to attract the pozzolanic elements from the soil, RHA, and cement. In this state, movements of fiber filaments were restricted under loading, which induced tension into the fibers' body, increasing the shear parameters significantly. These mechanisms were also supported by Tang et al. [34].

Moreover, cementitious products from pozzolanic reactions were attached tightly to the fiber filaments, further increasing the frictional

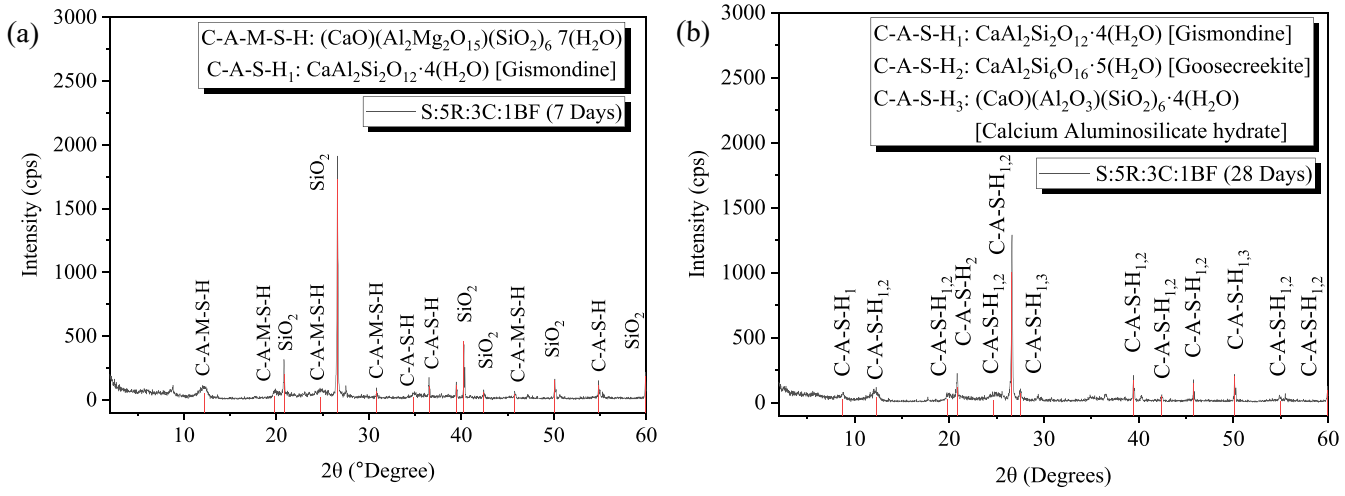

Fig. 23. (a) X-ray diffraction (XRD) analysis of the specimen after 7 days of curing. (b) X-ray diffraction (XRD) analysis of the specimen after 28 days of curing.

resistances in the specimen during shearing. This bonding mechanism within the new composite material ensured sufficient transfer of applied loads from the clusters to the adjacent fibers, thus preventing further cracks within the specimen. These phenomena led to improved shear strength and ductility as reflected in the attained values of deviatoric stress, axial strains, cohesion, and angle of internal friction.

4.4.3. XRD analyses

Through XRD analyses, crystalline peaks of Calcium Silicate Hydrates (C-S-H), a product of the pozzolanic reactions between soil, cement, and amorphous silica found in RHA, were observed. In literature, during the process of C-S-H formation, higher chances of the uptake of other minerals present in the soil composite, such as Magnesium (Mg) and Aluminum (Al) compounds, were observed in the past [72–74]. This study also observed that during the early stages of curing (7 days), when the pH was still low, the emerging C-S-H bonds got decalcified on the surface of the specimen into amorphous silica, which reacted with Mg in the soil composite and yielded traces of Magnesium Silicate Hydrates (M−S−H). This decalcification process led to the formation of Calcium Aluminum-Magnesium Silicate Heptahydrate (C-A-M−S−H [(CaO)$(Al_2Mg_2O_{15})(SiO_2)_6$ 7(H_2O)] in the specimens, which slightly reduced the effectiveness of the C-S-H in stabilizing the soil composite, as shown in Fig. 23a.

However, after 28 days of curing, it was observed that there was no further uptake of Mg ions; instead, continued uptake of Aluminum ions in C-S-H gel was evident. Aluminum ions uptake occurred both in the surface, interlayer, and in the silicate chains, leading to the formation of stronger C-A-S-H gel bonds known as Calcium Alumino Hexasilicate Tetrahydrate [(CaO)$(Al_2O_3)(SiO_2)_6$ 4(H_2O)] as shown in Fig. 23b. This Al uptake at higher pH values were also recorded in other relevant studies [75–79]. The Mg concentrations were reduced due to the increased specimen pH above 10, leading to a much lower aqueous magnesium concentration than calcium, thereby enhancing the formation of stronger C-A-S-H bonds in all the specimens [80,81]. Consequently, the interaction between the tensioned basalt fiber filament lengths and the stronger C-A-S-H bonds validated and dictated the rate of development in shear strength with the curing period.

5. Limitations of the study

This study concentrated mainly on the shear characteristics of expansive soils reinforced and stabilized with basalt fibers and RHA-cement mixtures, demonstrating that the proposed methodologies generally captured the behavior of the composite material under triaxial compression well. However, there is a limitation of the present research work and the proposed methods: The fiber reinforcements and chemical stabilization mechanisms were affixed to a given soil type and, therefore, can create boundaries for the generalization of the results to other soil types in engineering practice. The results herein highly depended on the materials studied, and additional research is necessary to address this gap.

6. Conclusions

In this study, a series of consolidated drained (CD) triaxial tests were carried out on soil composites reinforced with high-strength basalt fiber filaments (filament lengths 3, 6, and 12 mm) and chemically stabilized with RHA-cement mixtures (5% RHA, and 3% cement), considering curing periods 1 day, 7 days, and 28 days. The experimental results were reported, including the compaction test, stress–strain relationship, and ultimate shear strengths. The microstructure interaction and chemical composition were also analyzed using SEM and XRD. The following conclusions can be drawn:

The combined effects of basalt fiber reinforcements and cementation decreased the maximum dry density (ρ_{dmax}) while maintaining the optimum moisture content (w_{opt}), ensuring economical compaction cost.

During shearing, the improved frictional resistances from fiber reinforcements and cementation in the specimens increased the initial deviatoric stress to a maximum value of 631.86 kN/m^2, followed by a gradual softening behavior before failure. This development in the deviatoric stresses during loading led to significant growth in shear strength with cohesion and an angle of internal friction reaching maximum values of 180 kN/m^2 and 18.43°, respectively, for specimens having 12 mm filament lengths (S:5R:3C:1BF12) after a curing period of 28 days.

The experimental results showed that fiber filament length dictated the effectiveness of basalt fibers as a potential ground improvement material. The interaction between the longer fibers (12 mm) and the specimen's cementitious bonds significantly improved the ultimate shear strength compared to the shorter fibers (6 mm and 3 mm). In addition, the 12 mm basalt fiber filaments greatly affected the specimen ductility at peak stresses than the 6 mm and 3 mm filaments. The 12 mm basalt fiber reinforcing mechanism through interfacial contacts within the new stabilized soil composite containing 5 %RHA and 3% cement (S:5R:3C:1BF12) was validated as the optimum filament length and the best combination in choosing the new construction material for use as a base course during ground improvement. However, this conclusion is based on the filament range between 3 mm and 12 mm. Further studies are necessary to evaluate the boundary limits considering basalt fiber dosage and filament length.

SEM analysis showed a compact soil composite structure consisting of clusters of cemented materials (soil:RHA:cement) anchored together with basalt fiber filaments, validating the noteworthy developments in shear strength. Moreover, high levels of strong calcium silicate hydrate chains were recorded through XRD analysis.

As observed, the experimental results in this study were in good agreement with the related studies on reinforced soil composites. Thus, incorporating basalt fibers, RHA, and nominal dosages of cement into weak soils is a practical approach to solving geotechnical engineering challenges during ground improvement.

7. Future research

In the last decade, geotechnical engineers have been driven by a sustainability approach when choosing construction materials, leading to the tendency to use natural fiber reinforcement techniques and new stabilization methods in ground improvement applications, as presented in this study. This approach is essential and can significantly impact the built environment, economy, and natural environment. Based on the extensive analysis in this study and the previous studies, some critical research gaps have been identified, and the future research prospects are listed as follows;

1. It is apparent that experimental laboratory results alone are insufficient to establish the general applicability of the data sets obtained in practical engineering practice. Therefore, a tailored constitutive model based on the experimental results and a theoretical approach using the hypoplastic model has been proposed as future research work to supplement the current study.
2. Future work on narrowing down the specific applicability of the new composite material in engineering practice can be formulated using the simulation results on the practical applications obtained from item no. 1.
3. An evaluation of the associated environmental impacts of the current study is necessary through the Life Cycle Assessment (LCA) methodology, considering the relevance of basalt fiber reinforcements and sustainable chemical stabilization processes for soils against conventional alternatives. LCA can be used to determine and classify the probable environmental impacts associated with all the stages of life

of the final new composite material [82–84]. For example, assessment of the new material from raw material extraction, processing, distribution, use, recycling, and final disposal of the used materials depending on the engineering application proposed in item no. 2.

CRediT authorship contribution statement

Alex Otieno Owino: Conceptualization, Methodology, Data curation, Writing – original draft. **Zakaria Hossain:** Supervision, Writing – review & editing.

Declaration of Competing Interest

The authors declare that they have no known competing financial interests or personal relationships that could have appeared to influence the work reported in this paper.

Data availability

Data will be made available on request.

Acknowledgements

The authors would like to acknowledge the Japan Ministry of Education, Culture, Sports, Science and Technology for providing the MEXT scholarship through Mie University, where this study was conducted. This research was also supported by Make Integrated Technology Limited, which provided the necessary experimental materials.

References

[1] S. Horpibulsuk, R. Rachan, A. Chinkulkijniwat, Y. Raksachon, A. Suddeepong, Analysis of strength development in cement-stabilized silty clay from microstructural considerations, Constr. Build. Mater. 24 (10) (2010) 2011–2021, https://doi.org/10.1016/j.conbuildmat.2010.03.011.
[2] N. Miura, S. Horpibulsuk, T.S. Nagaraj, Engineering behavior of cement stabilized clay at high water content, Soils Found. 41 (5) (2001) 33–45, https://doi.org/10.3208/sandf.41.5_33.
[3] S.Y. Liu, D.W. Zhang, Z.B. Liu, Y.F. Deng, Assessment of unconfined compressive strength of cement stabilized marine clay, Mar. Georesour. Geotechnol. 26 (1) (2008) 19–35, https://doi.org/10.1080/10641190801937916.
[4] I. Saidate, T. Rikioui, Stabilization of Gypsum Clay Soil by Adding Lime, Civ. Eng. J. 8 (11) (2022) 2511–2520, https://doi.org/10.28991/CEJ-2022-08-11-010.
[5] M. Topolnicki, In situ soil mixing, Ground Improv. 2 (2004) 331–428.
[6] H.G. Van Oss, A.C. Padovani, Cement manufacture and the environment: part I: chemistry and technology, J. Ind. Ecol. 6 (1) (2002) 89–105, https://doi.org/10.1162/108819802320971650.
[7] M.Ö.A. Akan, D.G. Dhavale, J. Sarkis, Greenhouse gas emissions in the construction industry: An analysis and evaluation of a concrete supply chain, J. Cleaner Prod. 167 (2017) 1195–1207, https://doi.org/10.1016/j.jclepro.2017.07.225.
[8] M.B. Ali, R. Saidur, M.S. Hossain, A review on emission analysis in cement industries, Renewable Sustainable Energy Rev. 15 (5) (2011) 2252–2261, https://doi.org/10.1016/j.rser.2011.02.014.
[9] Z. Zhang, S. Liu, F. Yang, Y. Weng, S. Qian, Sustainable high strength, high ductility engineered cementitious composites (ECC) with substitution of cement by rice husk ash, J. Cleaner Prod. 317 (2021), 128379, https://doi.org/10.1016/j.jclepro.2021.128379.
[10] G.R. de Sensale, A.B. Ribeiro, A. Gonçalves, Effects of RHA on autogenous shrinkage of Portland cement pastes, Cem. Concr. Compos. 30 (10) (2008) 892–897, https://doi.org/10.1016/j.cemconcomp.2008.06.014.
[11] N. Yoobanpot, P. Jamsawang, Effect of cement replacement by rice husk ash on soft soil stabilization, Agric. Nat. Resour. 48 (2) (2014) 323–332.
[12] I.C. Attah, R.K. Etim, I.N. Usanga, Potentials of cement kiln dust and rice husk ash blend on strength of tropical soil for sustainable road construction material, In IOP Conference Series: Mater. Sci. Eng. 1036 (1) (2021), 012072, https://doi.org/10.1088/1757-899X/1036/1/012072.
[13] S. Basack, G. Goswami, H. Khabbaz, M. Karakouzian, P. Baruah, N. Kalita, A Comparative Study on Soil Stabilization Relevant to Transport Infrastructure using Bagasse Ash and Stone Dust and Cost Effectiveness, Civ. Eng. J. 7 (11) (2021) 1947–1963, https://doi.org/10.28991/cej-2021-03091771.
[14] N. Nahar, Z. Hossain, N. Tamaki, Optimum utilization of rice husk ash waste for ground improvement, Int. Agric. Eng. J. 30 (1) (2021) 1–10.
[15] N. Nahar, A.O. Owino, S.K. Khan, Z. Hossain, N. Tamaki, Effects of controlled burn rice husk ash on geotechnical properties of the soil, J. Agric. Eng. 52 (4) (2021) 1216, https://doi.org/10.4081/jae.2021.1216.
[16] Q. Yu, K. Sawayama, S. Sugita, M. Shoya, Y. Isojima, The reaction between rice husk ash and Ca $(OH)_2$ solution and the nature of its product, Cem. Concr. Res. 29 (1) (1999) 37–43, https://doi.org/10.1016/S0008-8846(98)00172-0.
[17] W. Xu, T.Y. Lo, W. Wang, D. Ouyang, P. Wang, F. Xing, Pozzolanic reactivity of silica fume and ground rice husk ash as reactive silica in a cementitious system: A comparative study, Mater. 9 (3) (2016) 146, https://doi.org/10.3390/ma9030146.
[18] A.N. Givi, S.A. Rashid, F.N.A. Aziz, M.A.M. Salleh, Assessment of the effects of rice husk ash particle size on strength, water permeability and workability of binary blended concrete, Constr. Build. Mater. 24 (11) (2010) 2145–2150, https://doi.org/10.1016/j.conbuildmat.2010.04.045.
[19] Y.J. Patel, N. Shah, Enhancement of the properties of ground granulated blast furnace slag based self compacting geopolymer concrete by incorporating rice husk ash, Constr. Build. Mater. 171 (2018) 654–662, https://doi.org/10.1016/j.conbuildmat.2018.03.166.
[20] F.H. Ali, A. Adnan, C.K. Choy, Geotechnical properties of a chemically stabilized soil from Malaysia with rice husk ash as an additive, Geotech. Geol. Eng. 10 (2) (1992) 117–134.
[21] A.H. Kamruzzaman, S.H. Chew, F.H. Lee, Structuration and destructuration behavior of cement-treated Singapore marine clay, J. Geotech. Geoenviron. Eng. 135 (4) (2009) 573–589, https://doi.org/10.1061/(ASCE)1090-0241(2009)135:4(573).
[22] G.A. Lorenzo, D.T. Bergado, Fundamental characteristics of cement-admixed clay in deep mixing, J. Mater. Civ. Eng. 18 (2) (2006) 161–174, https://doi.org/10.1061/(ASCE)0899-1561(2006)18:2(161).
[23] K. Uddin, A.S. Balasubramaniam, D.T. Bergado, Engineering behavior of cement-treated Bangkok soft clay, Geotech. Eng. 28 (1997) 89–119.
[24] A.P. Panda, S.N. Rao, Undrained strength characteristics of an artificially cemented marine clay, Mar. Georesour. Geotechnol. 16 (4) (1998) 335–353, https://doi.org/10.1080/10641199809379976.
[25] A. Porbaha, S. Shibuya, T. Kishida, State of the art in deep mixing technology. Part III: Geomaterial Characterization, Proc. Inst. Civ. Eng. Ground Improv. 4 (3) (2000) 91–110, https://doi.org/10.1680/grim.2000.4.3.91.
[26] J.H. Yin, Stress-strain-strength characteristics of soft Hong Kong marine deposits without or with cement treatment, Lowland Technol. Int. 3 (1) (2001) 1–13. https://cot.unhas.ac.id/journals/index.php/ialt_lti/article/view/285.
[27] I. Kafodya, F. Okonta, Effects of natural fiber inclusions and pre-compression on the strength properties of lime-fly ash stabilised soil, Const. Build. Mater. 170 (2018) 737–746, https://doi.org/10.1016/j.conbuildmat.2018.02.194.
[28] T.E. de Lima, A.R. de Azevedo, M.T. Marvila, V.S. Candido, R. Fediuk, S. N. Monteiro, Potential of Using Amazon Natural Fibers to Reinforce Cementitious Composites: A Review, Polym. 14 (3) (2022) 647, https://doi.org/10.3390/polym14030647.
[29] S. Gowthaman, K. Nakashima, S. Kawasaki, A state-of-the-art review on soil reinforcement technology using natural plant fiber materials: Past findings, present trends and future directions, Mater. 11 (4) (2018) 553, https://doi.org/10.3390/ma11040553.
[30] H.J. Pincus, M.H. Maher, Y.C. Ho, Behavior of fiber-reinforced cemented sand under static and cyclic loads, Geotech. Test. J. 16 (3) (1993) 330.
[31] S. Dhar, M. Hussain, The strength behaviour of lime-stabilised plastic fibre-reinforced clayey soil, Road Mater. Pavement Des. 20 (8) (2019) 1757–1778, https://doi.org/10.1080/14680629.2018.1468803.
[32] S. Soleimani Kutanaei, A. Janalizadeh Choobbasti, Effects of nanosilica particles and randomly distributed fibers on the ultrasonic pulse velocity and mechanical properties of cemented sand, J. Mater. Civ. Eng. 29 (3) (2017) 04016230, https://doi.org/10.1061/(ASCE)MT.1943-5533.0001761.
[33] H.S. Wang, C.S. Tang, K. Gu, B. Shi, H.I. Inyang, Mechanical behavior of fiber-reinforced, chemically stabilized dredged sludge, Bull. Eng. Geol. Environ. 79 (2) (2020) 629–643, https://doi.org/10.1007/s10064-019-01580-5.
[34] C. Tang, B. Shi, W. Gao, F. Chen, Y. Cai, Strength and mechanical behavior of short polypropylene fiber reinforced and cement stabilized clayey soil, Geotext. Geomembr. 25 (3) (2007) 194–202, https://doi.org/10.1016/j.geotexmem.2006.11.002.
[35] D.C. Lima, B.D.S. Bueno, L. Thomasi,. The mechanical response of soil-lime mixtures reinforced with short synthetic fiber. In Proc., 3rd Int. Symp. on Environ. Geotechnol. 1 (1996)868-877).
[36] N.C. Consoli, M.A. Vendruscolo, P.D.M. Prietto, Behavior of plate load tests on soil layers improved with cement and fiber, J. Geotech. Geoenviron. Eng. 129 (1) (2003) 96–101, https://doi.org/10.1061/(ASCE)1090-0241(2003)129:1(96).
[37] A. Ghorbani, M. Salimzadehshooiili, J. Medzvieckas, R. Kliukas, Strength characteristics of cement-rice husk ash stabilised sand-clay mixture reinforced with polypropylene fibers, Balt. J. Road Bridge Eng. 13 (4) (2018) 447–474, https://doi.org/10.7250/bjrbe.2018-13.428.
[38] R. Chen, S.S. Congress, G. Cai, W. Duan, S. Liu, Sustainable utilization of biomass waste-rice husk ash as a new solidified material of soil in geotechnical engineering: A review, Const. Build. Mater. 19 (292) (2021), 123219, https://doi.org/10.1016/j.conbuildmat.2021.123219.
[39] M.M. Taha, C.P. Feng, S.H. Ahmed, Modification of mechanical properties of expansive soil from north china by using rice husk ash, Mater. 14 (11) (2021) 2789, https://doi.org/10.3390/ma14112789.
[40] A. Ghorbani, M. Salimzadehshooiili, Evaluation of strength behaviour of cement-RHA stabilized and polypropylene fiber reinforced clay-sand mixtures, Civ. Eng J. 30 (4) (2018) 2628–2641, https://doi.org/10.28991/cej-03091187.
[41] A. Kumar, D. Gupta, Behavior of cement-stabilized fiber-reinforced pond ash, rice husk ash–soil mixtures, Geotext. Geomembr. 44 (3) (2016) 466–474, https://doi.org/10.1016/j.geotexmem.2015.07.010.

[42] M. Chen, S.L. Shen, A. Arulrajah, H.N. Wu, D.W. Hou, Y.S. Xu, Laboratory evaluation on the effectiveness of polypropylene fibers on the strength of fiber-reinforced and cement-stabilized Shanghai soft clay, Geotext. Geomembr. 43 (6) (2015) 515–523, https://doi.org/10.1016/j.geotexmem.2015.05.004.
[43] J. de Jesús Arrieta Baldovino, R. dos Santos Izzo, J.L. Rose, M.A. Avanci, Geopolymers Based on Recycled Glass Powder for Soil Stabilization, Geotech Geol Eng 38 (4) (2020) 4013–4031.
[44] A. Chouksey, N. Dev, S. Kumari, Review paper on utilization potential of rice husk ash as supplementary cementitious material. In Sustainable Constr. Build. Mater. (2019)673-684. Springer, Singapore. 10.1007/978-981-13-3317-0_60.
[45] Y.O. Muñoz, R.L. dos Santos Izzo, J.L. de Almeida, J.A. Baldovino, J.L. Rose, The role of rice husk ash, cement and polypropylene fibers on the mechanical behavior of a soil from Guabirotuba formation, Transp. Geotech. 31 (2021), 100673, https://doi.org/10.1016/j.trgeo.2021.100673.
[46] S.M. Hejazi, M. Sheikhzadeh, S.M. Abtahi, A. Zadhoush, A simple review of soil reinforcement by using natural and synthetic fibers, Constr. Build. Mater. 30 (2012) 100–116, https://doi.org/10.1016/j.conbuildmat.2011.11.045.
[47] JIS A 1210, Test method for soil compaction using a rammer. Japanese Industrial Standard, Guidance and Basic - Soil Test, The Jpn. Geotech. Soc. (in Japanese) (2010)71-78.
[48] JGS 0524, Method for consolidated-drained triaxial compression test on soils, Jpn. Geotech. Soc. Dositsu Shiken Hou Dositsu Kogakkai: (2001)233-43. [In Japanese].
[49] R. Polo-Mendoza, G. Martinez-Arguelles, L.F. Walubita, F. Moreno-Navarro, F. Giustozzi, L. Fuentes, T. Navarro-Donado, Ultraviolet ageing of bituminous materials: A comprehensive literature review from 2011 to 2022, Constr. Build. Mater. 350 (2022), 128889, https://doi.org/10.1016/j.conbuildmat.2022.128889.
[50] G. Cheraghian, M. Wistuba, Ultraviolet aging study on bitumen modified by a composite of clay and fumed silica nanoparticles, Sci. Rep. 10 (11216) (2020) 1–17, https://doi.org/10.1038/s41598-020-68007-0.
[51] M. Mazumder, R. Ahmed, A. Wajahat Ali, S.-J. Lee, SEM and ESEM techniques used for analysis of asphalt binder and mixture: A state of the art review, Constr. Build. Mater. 186 (2018) 313–329, https://doi.org/10.1016/j.conbuildmat.2018.07.126.
[52] F.E. Jalal, Y. Xu, B. Jamhiri, S.A. Memon, On the recent trends in expansive soil stabilization using calcium-based stabilizer materials (CSMs): a comprehensive review. Adv. Mater. Sci. Eng. (2020)2020. 10.1155/2020/1510969.
[53] Y. Li, S. Wu, Y. Dai, L. Pang, Q. Liu, J. Xie, D. Kong, Investigation of sodium stearate organically modified LDHs effect on the anti-aging properties of asphalt binder, Constr. Build. Mater. 172 (2018) 509–518.
[54] A. Ahmed, Compressive strength and microstructure of soft clay soil stabilized with recycled basanite, Appl. Clay Sci. 104 (2015) 27–35, https://doi.org/10.1016/j.clay.2014.11.031.
[55] M.H. Zhang, R. Lastra, V.M. Malhotra, Rice-husk ash paste and concrete: some aspects of hydration and the microstructure of the interfacial zone between the aggregate and paste, Cem. Concr. Res. 26 (6) (1996) 963–977, https://doi.org/10.1016/0008-8846(96)00061-0.
[56] E.A. Basha, R. Hashim, H.B. Mahmud, A.S. Muntohar, Stabilization of residual soil with rice husk ash and cement, Constr. Build. Mater. 19 (6) (2005) 448–453, https://doi.org/10.1016/j.conbuildmat.2004.08.001.
[57] J.N. Jha, K.S. Gill, Effect of rice husk ash on lime stabilization of soil, J. Inst. Eng. (India), Part CV, Civil Engineering Division 87 (2006) 33–39.
[58] A.S. Muntohar, G. Hantoro, Influence of rice husk ash and lime on engineering properties of a clayey subgrade Electron, J. Geotech. Eng. 5 (2000) (2000) 1–13.
[59] C. Li, Mechanical response of fiber-reinforced soil, The University of Texas at Austin. (2005) 212.
[60] N.C. Consoli, P.D.M. Prietto, L.A. Ulbrich, The behaviour of a fibre-reinforced cemented soil, Proc. Inst. Civ. Eng. Ground Improv. 3 (1) (1999) 21–30, https://doi.org/10.1680/gi.1999.030103.
[61] N.C. Consoli, M.D.T. Casagrande, M.R. Coop, Performance of a fibre-reinforced sand at large shear strains, Geotech. 57 (9) (2007) 751–756, https://doi.org/10.1680/geot.2007.57.9.751.
[62] K.S. Heineck, M.R. Coop, N.C. Consoli, effect of micro reinforcement of soils from very small to large shear strains, J. Geotech. Geoenviron. Eng. 131 (8) (2005) 1024–1033, https://doi.org/10.1061/(ASCE)1090-0241(2005)131:8(1024).
[63] A. Ghorbani, M. Salimzadehshooiili, Dynamic characterization of sand stabilized with cement and RHA and reinforced with polypropylene fiber, J. Mater. Civ. Eng. 31 (7) (2019) 04019095, https://doi.org/10.1061/(ASCE)MT.1943-5533.0002727.
[64] J.S. Yadav, S.K. Tiwari, P. Shekhwat, Strength behaviour of clayey soil mixed with pond ash, cement and randomly distributed fibres, Transp. Infrastruct. Geotechnol. 5 (3) (2018) 191–209, https://doi.org/10.1007/s40515-018-0056-z.
[65] M.J. Khattak, M. Alrashidi, Durability and mechanistic characteristics of fiber reinforced soil-cement mixtures, Int. J. Pavement Eng. 7 (1) (2006) 53–62, https://doi.org/10.1080/10298430500489207.
[66] L. Nguyen, B. Fatahi, Behaviour of clay treated with cement & fibre while capturing cementation degradation and fibre failure–C3F model, Int. J. Plast. 81 (2016) 168–195, https://doi.org/10.1016/j.ijplas.2016.01.015.
[67] Y. Wu, Y. Li, B. Niu, Assessment of the mechanical properties of sisal fiber-reinforced silty clay using triaxial shear tests, Sci. World J. (2014), https://doi.org/10.1155/2014/436231.
[68] W. Yixian, G. Panpan, S. Shengbiao, Y. Haiping, Y. Binxiang, Study on strength influence mechanism of fiber-reinforced expansive soil using jute, Geotech. Geol. Eng. 34 (2016) 1079–1088, https://doi.org/10.1007/s10706-016-0028-4.
[69] Y. Cai, B. Shi, C.W. Ng, C.S. Tang, Effect of polypropylene fibre and lime admixture on engineering properties of clayey soil, Eng. Geol. 87 (3–4) (2006) 230–240, https://doi.org/10.1016/j.enggeo.2006.07.007.
[70] M. Ghadakpour, A.J. Choobbasti, S.S. Kutanaei, Experimental study of impact of cement treatment on the shear behavior of loess and clay, Arabian J. Geosci. 13 (2020) 1–11, https://doi.org/10.1007/s12517-020-5181-7.
[71] D. Bonen, M.D. Cohen, Magnesium sulfate attack on Portland cement paste-I, Microstructural analysis. Cem. Concr. Res. 22 (1) (1992) 169–180, https://doi.org/10.1016/0008-8846(92)90147-N.
[72] R.S. Gollop, H.F.W. Taylor, Microstructural and microanalytical studies of sulfate attack. I. Ordinary Portland cement paste, Cem. Concr. Res. 22 (6) (1992) 1027–1038, https://doi.org/10.1016/0008-8846(92)90033-R.
[73] M. Santhanam, M.D. Cohen, J. Olek, Mechanism of sulfate attack: A fresh look: Part 1: Summary of experimental results, Cem. Concr. Res. 32 (6) (2002) 915–921, https://doi.org/10.1016/S0008-8846(02)00724-X.
[74] T.T.H. Bach, E. Chabas, I. Pochard, C.C.D. Coumes, J. Haas, F. Frizon, A. Nonat, Retention of alkali ions by hydrated low-pH cements: Mechanism and Na+/K+ selectivity, Cem. Concr. Res. 51 (2013) 14–21, https://doi.org/10.1016/j.cemconres.2013.04.010.
[75] E. L'Hôpital, B. Lothenbach, G. Le Saout, D. Kulik, K. Scrivener, Incorporation of aluminium in calcium-silicate-hydrates, Cem. Concr. Res. 75 (2015) 91–103, https://doi.org/10.1016/j.cemconres.2015.04.007.
[76] B. Lothenbach, A. Nonat, Calcium silicate hydrates: Solid and liquid phase composition, Cem. Concr. Res. 78 (2015) 57–70, https://doi.org/10.1016/j.cemconres.2015.03.019.
[77] I.G. Richardson, A.R. Brough, R. Brydson, G.W. Groves, C.M. Dobson, Location of aluminum in substituted calcium silicate hydrate (C-S-H) gels as determined by 29Si and 27Al NMR and EELS, J. Am. Ceram. Soc. 76 (9) (1993) 2285–2288, https://doi.org/10.1111/j.1151-2916.1993.tb07765.x.
[78] I.G. Richardson, The calcium silicate hydrates, Cem. Concr. Res. 38 (2) (2008) 137–158, https://doi.org/10.1016/j.cemconres.2007.11.005.
[79] E. Bernard, B. Lothenbach, F. Le Goff, I. Pochard, A. Dauzères, Effect of magnesium on calcium silicate hydrate (CSH), Cem. Concr. Res. 97 (2017) 61–72, https://doi.org/10.1016/j.cemconres.2017.03.012.
[80] B. Lothenbach, D. Nied, E. L'Hôpital, G. Achiedo, A. Dauzères, Magnesium and calcium silicate hydrates, Cem. Concr. Res. 77 (2015) 60–68, https://doi.org/10.1016/j.cemconres.2015.06.007.
[81] L.F. Walubita, G. Martinez-Arguelles, R. Polo-Mendoza, S. Ick-Lee, L. Fuentes, Comparative Environmental Assessment of Rigid, Flexible, and Perpetual Pavements: A Case Study of Texas, Sustainability. 14 (16) (2022) 9983, https://doi.org/10.3390/su14169983.
[82] R. Polo-Mendoza, G. Martinez-Arguelles, R. Peñabaena-Niebles, A multi-objective optimization based on genetic algorithms for the sustainable design of Warm Mix Asphalt (WMA), Int. J. Pavement Eng. (2022) 1–21, https://doi.org/10.1080/10298436.2022.2074417.
[83] R. Polo-Mendoza, R. Penabaena-Niebles, F. Giustozzi, G. Martinez-Arguelles, Eco-friendly design of Warm mix asphalt (WMA) with recycled concrete aggregate (RCA): A case study from a developing country, Const. Build. Mater. 326 (2022), 126890, https://doi.org/10.1016/j.conbuildmat.2022.126890.

Construction and Building Materials 339 (2022) 127686

Contents lists available at ScienceDirect

Construction and Building Materials

journal homepage: www.elsevier.com/locate/conbuildmat

Dimensional influence of basalt fiber reinforcements on the consolidation behaviour of rice husk ash stabilized soils

Alex Otieno Owino [a,*], Najmun Nahar [a,b], Zakaria Hossain [a], Noma Tamaki [c]

[a] Graduate School of Bioresources, Mie University, 1577 Kurimamachiya-Cho, Tsu, Mie 514-8507, Japan
[b] Life and Earth sciences, Jagannath University, Bangladesh
[c] Make Integrated Technology Company, Osaka, Japan

ARTICLE INFO

Keywords:
Consolidation curves
Basalt fibers
Expansive soil
Rice husk ash
Compressibility
Swelling
SEM
XRD

ABSTRACT

The development of reinforcement techniques in soils with various fibers has been a common practice since the early days. Recently, fibers and materials considered waste are being used to develop sustainable solutions in designing new soil reinforcing and stabilizing materials. In this paper, an investigation has been carried out to evaluate the dimensional influence of basalt fiber on the compressibility and swelling of soils stabilized with rice husk ash (RHA) and cement. Incorporating a nominal dosage of basalt fibers into the soil–cement-RHA composite produces a strong composite with smart material properties. Specimen containing expansive clay soil, basalt fibers (lengths 3 mm, 6 mm, 12 mm), RHA (5%, 10%, and 15%), and cement (3%), in their specified combinations, were prepared and tested. The influence of fiber length and variation of RHA-cement content was quantified using the consolidation curves (compression curves and normalized compression curves), compression index, and swelling index, which provided a detailed behavioral modification upon consolidation. Scanning Electron Microscopy (SEM) and X-ray powder diffraction (XRD) were also used to examine the reconstituted soil structure and chemical components. It is demonstrated that a reconstituted clay soil combination of 12 mm basalt fibers, 5% RHA, and 3% cement, enhanced the ultimate yield pressures and the resistance to excessive swelling. This paper emphasized the projected responses during the loading and unloading phases on the specimen and discussed the consolidation characteristics of the newly reconstituted soil composites.

1. Introduction

Construction of engineering infrastructures such as roads, embankments, bridges, and buildings on clay soils is often discouraged due to the weak structural framework. Therefore, reconstituting such soils with various stabilizing additives and reinforcements is extensively practiced to curb this challenge. The effects of the stabilization techniques in such reconstituted soils can be quantified in terms of consolidation behavior and bearing capacity. Upon which, the consolidation behavior helps analyze the deformation projections of geotechnical structures built on the reconstituted clays and model the soil behavior (for example, settlement, swelling, excessive shrinkage, and cracking) [1,2].

In engineering practice, chemical additives such as cement and rice husk ash (RHA) have been used to enhance the soil structure of such expansive clay soils because of the associated pozzolanic activity during the stabilization process [3-5]. Furthermore, stabilizing expansive soil using RHA and fly ash has also considerably reduced swelling between the foundation footing and subgrade [6]. Also, in literature, using RHA, lime, and gypsum as additives to expansive soil has resulted in significant development in the strength characteristics of weak expansive soil [7]. These investigations disclosed that adding cement or lime to RHA might accelerate the strength properties. However, cement-treated soils are more prone to shrinkage and cracking when used as a base course [8,9].

To control this shrinkage and cracking, the utilization of fibers is gaining focus due to the reinforcements added to the soil mass. Fiber inclusions significantly modify and improve the mechanical behavior of these types of soils [10-18]. Recently several pieces of research on fiber reinforced soils have been carried out to examine the compressibility responses and strength parameters. Drained triaxial compression tests have indicated increased peak strength in sandy soils stabilized with cement and randomly oriented fiberglass [19]. In a separate study, Consoli et al. demonstrated that utilizing randomly distributed polyethylene fibers obtained from plastic wastes and combined with rapid

* Corresponding author.
E-mail addresses: 520d2s2@m.mie-u.ac.jp, owinoalex55@gmail.com, 520d2s2@m.mie-u.ac.jp (A. Otieno Owino).

https://doi.org/10.1016/j.conbuildmat.2022.127686
Received 2 February 2022; Received in revised form 19 April 2022; Accepted 26 April 2022
Available online 4 May 2022

hardening Portland cement improved the engineering behavior of uniform sand [20]. Moreover, the combined use of different types of fibers, for example, polypropylene and glass fiber, to reinforce weak soils have also attracted research attention [21]. Syed and Guha conducted a simulation to determine the reliability index of using two kinds of fibers and found out that the amounts of fibers present in the stabilized composite are essential factors in determining the ultimate strength.

Regarding the consolidation response of soils, Abdi et al. [22] found out that the addition of randomly distributed polypropylene fibers substantially reduced the consolidation settlement of clay soil [22]. The literature cited a study on the consolidation settlement and swelling characteristics of clays, including 5, 10, and 15 mm polypropylene fibers at the fiber content of 1, 2, 4, and 8% by weight of soil. Das and Pal [23] tested the consolidation characteristics of silty-clay soil mixed with fly ash and concluded that the compression index decreased significantly with increased fly ash content. Kar and Pradhan [24], in a study on strength and compressibility characteristics of local cohesive soil (CL) with random inclusion of polypropylene and coir fibers, observed that compression index and the coefficient of volume change decreased with an increase in the fiber content. Many relatable approaches have been suggested to investigate soils with various fiber reinforcements [25-30]. Even though experimental studies have utilized fibers and cement composites to stabilize soils and analyze the consolidation characteristics in literature, information about the dimensional effects of environmentally friendly fiber such as basalt fiber is scarce.

Furthermore, the interaction between basalt fibers and sustainable stabilization techniques using RHA with nominal cement dosages is also scarce. The superiority of basalt fibers over conventional fibers is derived from the high tensile strength and the natural occurrence from basalt rocks which gives it more versatility in enhancing the compressive capabilities of expansive soil composites. Therefore, the analysis of reconstituted weak expansive soils with basalt fibers is necessary to ensure its validation for vast applications due to the enhanced geotechnical behavior. On the other hand, using RHA as a sustainable means of chemically stabilizing expansive soils addresses the environmental pollution concern while maintaining sustainable geotechnical applications in engineering construction works.

This investigation, therefore, aims to generate information on the overall consolidation response of reconstituted expansive clay soil composites reinforced with varied basalt fiber lengths and RHA-cement mixtures in their specified combinations. It also evaluates the optimal combination appropriate for engineering applications. Odometer tests on specimens containing basalt fibers (lengths: 3 mm, 6 mm, 12 mm), RHA (5%, 10%, and 15%), and cement (3%), and in their specified combinations were carried out. The consolidation curves demonstrated the effects of basalt fiber length, RHA content, and minimal cement dosage. Results of consolidation yield stress (σ'), SEM, XRD, compression index (C_c), swelling index (C_s,) and assessment of compression curves at pre-and post-yield states of the reconstituted clay soil were studied and depicted in graphical form for the sake of convenient design of such soil composites during engineering applications.

2. Materials and methods

2.1. Materials

2.1.1. Soil

The soil used in this research was collected from Handa Area, Mie Prefecture, Japan. The soil was air-dried for 3 weeks and then sieved through the 200 mm sieve, after which sieve analysis, hydrometer analysis, liquid limit, and plastic limit analysis were conducted to classify the soil. The liquid and plastic limits were 58.21% and 31.05%, respectively. The soil consisted of 6.2% sand, 52.56% silt, and 41.24% clay. Also, based on the American Association of State Highway and Transportation Officials (AASHTO), the soil was classified as A-7–5(2) clayey soils. The soil compositions above rank the soil as expansive clay soil. Testing procedures followed Japan Industrial Standards JIS A 1204 for the sieve and hydrometer test and JIS A 1205 for the liquid and plastic limit tests. Additional geotechnical properties are shown in Table 1.

2.1.2. Rice husk ash

A controlled burned RHA at 650–700 °C with high silica content of 91.10% was provided by Make Integrated Technology Co., Ltd, Osaka, Japan. The high silica content was obtained by burning the rice husks for 27 h in a computer-controlled industrial incinerator. The RHA particles sizes ranged from 0.07 to 0.3 mm. Detailed particle size distribution of soil and RHA is shown in Fig. 1. A detailed physical and chemical property chart for rice husk ash is illustrated in Table 1.

2.1.3. Basalt fiber

Basalt fiber used in this research had a tensile strength of between 4100 ~ 4840 MPa, high elastic modulus ranging from 93.1 ~ 110GPa, and lengths of 3 mm, 6 mm, and 12 mm. Other physical properties include fiber diameter; 6 ~ 30 μm, fiber density; 2.63 ~ 2.8 g/cm^3, and a fracture elongation rate of 3.1%.

2.1.4. Portland cement

Ordinary Portland Cement (OPC) was also used as a binder element. The physical and chemical properties of OPC cement are illustrated in Table 2.

2.2. Specimen preparation and testing method

To prepare the specimen, 200 g of the air-dried soil passing through the 0.425 mm sieve was mixed with basalt fiber, RHA, and cement in the specified combinations, as shown in Table 3. Specimen were prepared using soil (200 g), basalt fiber (3 mm, 6 mm, and 12 mm), RHA (5%, 10%, and 15% dry weight of soil), and cement (3% dry weight of soil). The nominal dosage of OPC used in this study provided the necessary Calcium ions required to enhance the pozzolanic reactions within the prepared specimen. Water was then added to an initial water content of approximately 45%, 50%, and 55% for 5%RHA, 10%RHA, and 15% RHA, respectively, due to the high-water affinity for the higher percentages of RHA. The added water increased the water content of the dry soil to slightly above the liquid limit hence simulating pore water pressures similar to clay in its natural state. Each soil, basalt fiber, RHA, and cement combination was then mixed for 5 min to achieve a

Table 1
Properties of Soil and RHA.

Materials	Property	Value
Soil Properties	Specific Gravity, g/cm^3	2.74
	Maximum dry density, g/cm^3	1.65
	Saturation, %	87.14
	Sand (75 μm − 2 mm), %	6.20
	Silt (5–75 μm), %	52.56
	Clay < 5 μm, %	41.24
	Liquid limit, LL, %	58.21
	Plastic limit, PL, %	31.05
	Plasticity Index, PI, %	27.16
	AASHTO classification	A-7–5(2)
RHA Properties	Average Particle Size, mm	0.001 to 0.3
	Loss of Ignition, %	4–6
	Specific Gravity, g/cm^3	2.12
	Burning Temperature, °C	650–700
	Burning time, hour	27
	Silica (SiO_2), %	91.10
	Carbon dioxide (CO_2) %	4.35
	Potassium Oxide (K_2O), %	2.40
	Calcium Oxide (CaO), %	0.57
	Iron Oxide (Fe_2O_3), %	0.05
	Alumina (Al_2O_3), %	0.03
	Others, %	1.50

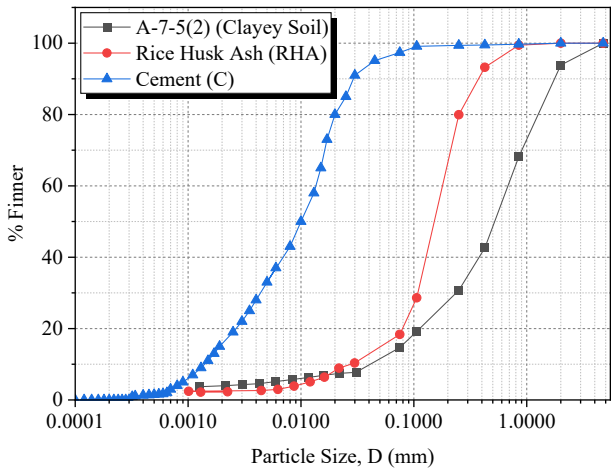

Fig. 1. Particle size distribution for soil and RHA.

Table 2
Properties of OPC.

Materials	Property	Value
Cement Properties	Initial setting time, minutes	170
	Final setting time, minutes	225
	Specific gravity, g/cm^3	3.15
	Specific surface area, m^2/kg	340
	28-day compressive strength, MPa	33–53
	Calcium Oxide (CaO), %	63.40
	Silicon dioxide(SiO_2), %	21.60
	Iron Oxide (Fe_2O_3), %	5.35
	Alumina (Al_2O_3), %	4.45
	Sulfur trioxide (SO_3), %	1.92
	Magnesium oxide (MgO), %	1.65
	Sodium oxide (Na_2O), %	0.11
	Potassium oxide (K_2O), %	0.22
	Loss of ignition, %	<4

Table 3
Experimental specimen codes and specified combinations.

Specimen Code	Soil, S (g)	Basalt Fiber, BF (mm)	RHA (%)	Cement, C (%)
S-Control	200	0	0	3
S:5R:3C	200	0	5	3
S:10R:3C	200	0	10	3
S:15R:3C	200	0	15	3
S:5R:3C:1BF3	200	3	5	3
S:10R:3C:1BF3	200	3	10	3
S:15R:3C:1BF3	200	3	15	3
S:5R:3C:1BF6	200	6	5	3
S:10R:3C:1BF6	200	6	10	3
S:15R:3C:1BF6	200	6	15	3
S:5R:3C:1BF12	200	12	5	3
S:10R:3C:1BF12	200	12	10	3
S:15R:3C:1BF12	200	12	15	3

homogeneous mixture. The homogeneous mix was then transferred to the soil cutting rings (diameter 60 mm and height 20 mm) and trimmed to fit the odometer test rings of similar dimensions. After setting the specimen in the odometer testing machine, they were then subjected to incremental loads of 9.8, 19.6, 39.2, 78.5, 157, 314, 628, and 1256 kN/m^2 during the loading phase and 628, 314, 157, 78.5, 39.2, 19.6 and 9.8 kN/m^2 during the unloading phase. Each load increment/reduction was kept constant for 24 h until the primary consolidation had seized [31]. The testing procedures followed the Japan Industrial Standards [32,33].

3. Consolidation framework

In geotechnical engineering, chemically stabilized soils possess an artificial soils structure due to the hydration effect of cement and the pozzolanic reactions present [34-38]. Therefore, during the loading/reloading phase on such artificially structured soils, the compression index is low until the yield pressure (σ') is realized due to the resistances attributed to the soil structure. An ideal illustration of the consolidation behavior of soils is shown in Fig. 2.

Beyond this yield pressure (σ'), compressibility is significantly increased due to the loss of soil structure, also known as destructuring [2,39-43]. During destructuring, the additional void ratio (e_s) declines with the increasing effective vertical pressure(σ_v) due to the soil structure. Hence, with a further rise in σ_v, the compression curve of the artificially structured clay tends to meet the compression curve of remolded/destructured clay, also known as the Intrinsic Compression Line (ICL) [1,44]. This variation in the void ratio can be expressed as:

$e = e_R + e_s$ (1).

Where e: represents the void ratio of the artificially structured soil, e_R: represents the void ratio of the remolded/destructured clay, and lastly, e_s: the additional void ratio attributed to the soil structure destruction [45]. Burland [1] suggested the ICL as a reference point for interpreting the responses of all artificially structured clays when the effective stresses were between 10 kPa and 4000 kPa in all testing conditions. The ICL was plotted in terms of a void ratio *e* given by the Eqs. (2–3), versus the log of the effective vertical pressure, log σ_v.

$e = I_v C_c^* + e^*_{100}$ (2).

$I_v = 2.45–1.285 log\ \sigma_v + 0.179\ \log\ \sigma_v^3$ (3) Where C_c^* is the intrinsic compression index defined by the difference between the void ratio of the remolded clay at 100 kPa (e^*_{100}) and 1000 kPa (e^*_{1000}) and I_v: the intrinsic void index. It was resolved that, for normally consolidated clay, the position of consolidation curves to the ICL line depends on the clay soil's structural composition [1]. In addition, Hong et al. [46] found that when the stress levels were higher than the remolded/reconstituted soils' yield pressure, the compression curves of remolded/ reconstituted clay normalized well with the ICL. The validity of this consolidation framework is illustrated in this study for the proposed reconstituted clay

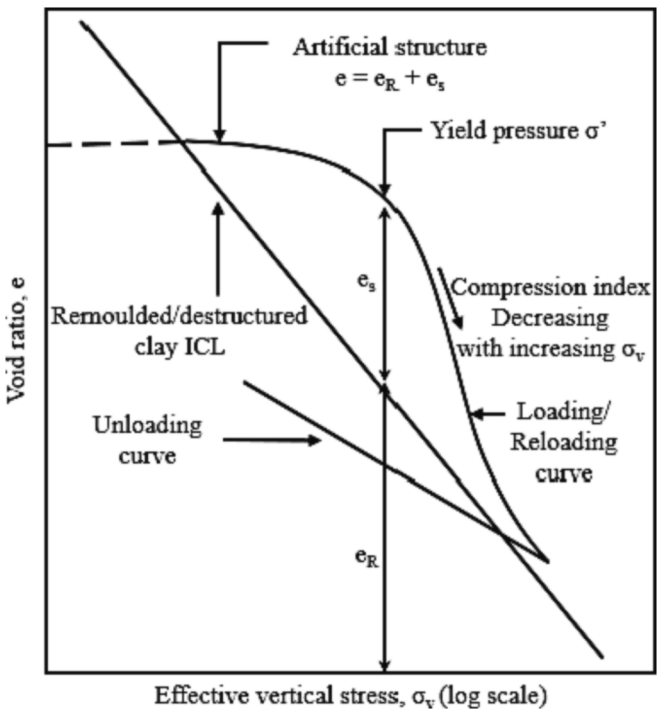

Fig. 2. Consolidation behavior of soil. (modified from Du et al., [38]).

soil composite, as will be discussed in the next section.

4. Results and discussion

4.1. Compression curves

The void ratio (e) versus effective vertical pressure (log σ_v) compression curves for the reconstituted soil specimens at RHA contents of 5, 10, and 15% are shown in Fig. 3a, Fig. 3b, and Fig. 3c, respectively. The influence of varying the basalt fiber length from 3 mm to 6 mm to 12 mm is also shown in each RHA content. In all the figures presented in this study, the symbol S denotes soil, *i*R denotes a specimen with an RHA content of *i*%; *i*C denotes cement content of *i*%, while BF*i* denotes a specimen with basalt fiber length *i*mm. It can be seen from Figs. 3a, 3b, and 3c that the compression curves of all S*i*R*i*CBF*i* reconstituted soil specimens lie above that of the corresponding soil specimen and show a typical concave shape due to the effects of soil-structure [46,47]. When the effective vertical pressure (σ_v) is lower than the yield pressure (σ'), slight compressibility is realized due to the resistances initiated by the soil structure [48]. After the yield pressure, the compressibility of the reconstituted and stabilized soils increases significantly due to the gradual collapse of the soil structure at higher effective vertical pressure levels.

Meanwhile, it is noteworthy that the relationship between the void ratios and the effective vertical pressure is highly dependent on the length of basalt fiber, RHA content, and cement content, with higher void ratios in the S:15R:3C:1BF specimens. It is noticeable that the void ratio decreases as the effective vertical pressure increases for all instances. The yield pressure (σ') can be estimated from these plots using the Casagrande method [49].

The relationship between yield pressure (σ') and various lengths of basalt fiber is shown in Fig. 4. It can be observed that increasing the length of basalt fibers from 0 mm to 12 mm improves the yield pressure of the reconstituted soil composite for all the RHA- cement mix ratios. The random fiber inclusion and the orientation of basalt fibers increase the specimen's stiffness hence improving the yield pressure (σ'). Additionally, scanning electron microscopy (SEM) shows a dense network of basalt fibers in the stabilized soil, as shown in Fig. 5a, 5b, and 5c for the high strength specimens S:5R:3C:1BF12, S:10R:3C:1BF12, and S:15R:3C:1BF12 respectively. From this phenomenon, it can be concluded that the random inclusion of high tensile strength fibers enhances the mechanical interaction between the fibers and the surrounding reconstituted soil composite through an anchoring effect and is more significant as the length of basalt fibers increases from 0 mm to 12 mm.

Furthermore, the increment in yield pressure was due to the resistance to compression pressures initiated by the pozzolanic reaction in the soil structure [50]. For example, at low RHA contents of 5%, there was a significant improvement in reconstituted soil structure due to the complete utilization of RHA and cement during the pozzolanic reactions. This structural development and basalt fiber reinforcements formed a

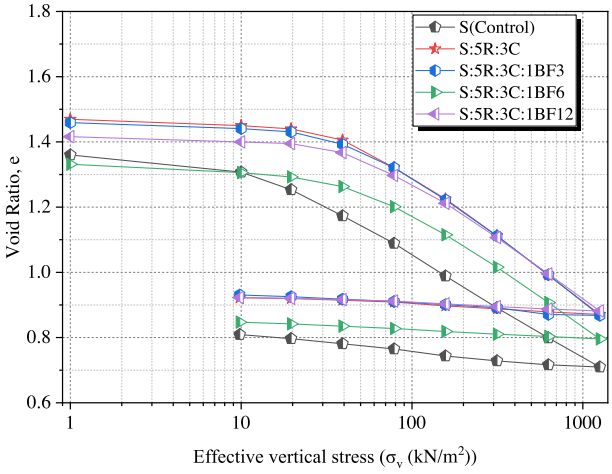

Fig. 3a. Compression curve for basalt fiber reinforced soil at 5%RHA.

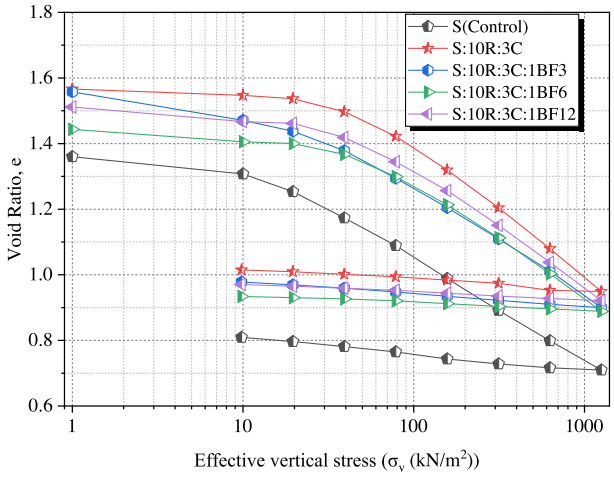

Fig. 3b. Compression curve for basalt fiber reinforced soil at 10%RHA.

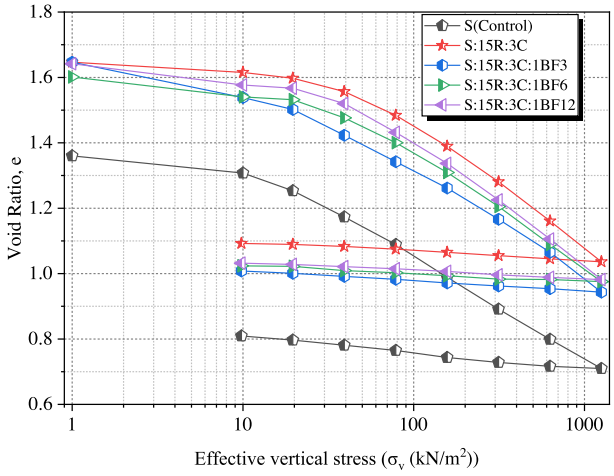

Fig. 3c. Compression curve for basalt fiber reinforced soil at 15%RHA.

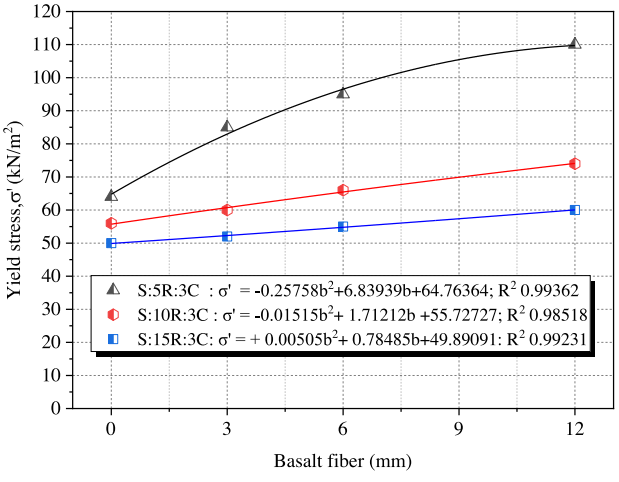

Fig. 4. Relationship between yield pressure (σ') and basalt fiber length.

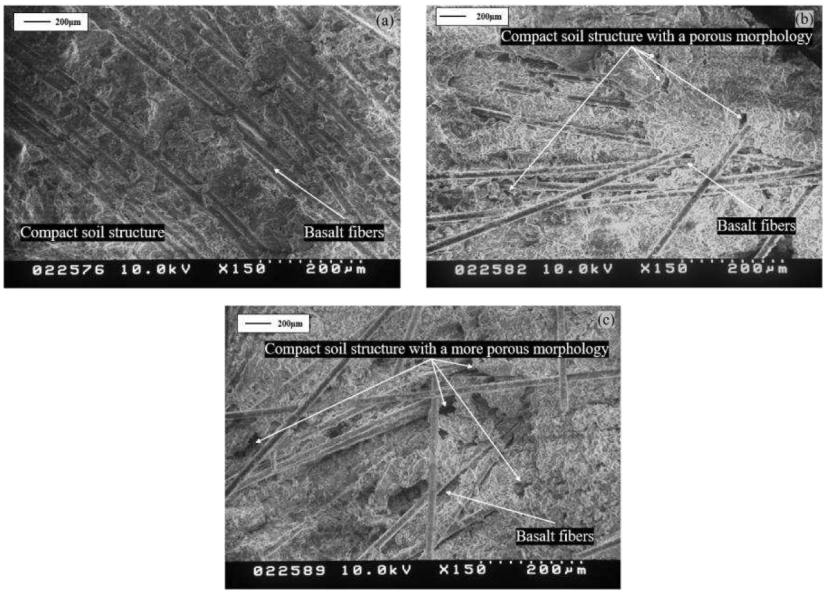

Fig. 5. Quantification of the increase in yield pressure by SEM imagery: (a) S:5R:3C:1BF12 specimen, (b) S:5R:3C:1BF12 specimen, (c) S:5R:3C:1BF12 specimen.

highly compact reconstituted soil structure with almost no visible porous morphology, as illustrated in Fig. 5a. On the other hand, increasing the RHA content to 10% and 15% led to excess RHA within the reconstituted soil composite, producing a more porous soil composite structure, as shown in Fig. 5b and Fig. 5c. The porous morphology was more susceptible to compressive pressures; thus, the noteworthy reduction in yield pressure as compared to 5% RHA content.

In this study, the presence of pozzolanic elements is quantified using X-ray powder diffraction (XRD) analyses, as shown in Fig. 6. In Fig. 6a, the XRD analysis of 5%RHA reconstituted soil composites shows high peaks of Calcium Aluminohexasilicate Tetrahydrate {$(CaO)(Al_2O_3)(SiO_2)_6$ $4(H_2O)$} and SiO_2, also known as CSH Gel. The presence of alumina in the CHS gel significantly increases the stability of the reconstituted soil composites hence improving yield pressures of up to 110kN/m^2 (for BF12mm) [51]. Correspondingly, increasing the RHA contents to10% and 15% leads to the formation of CSH gel, but, with a fragile dicalcium silicate hydrate {Ca2(SiO3OH) (OH)} composition due to the absence of alumina compounds in the reconstituted soil composite as shown in Fig. 6b and 6c [52]. The fragility of the 10% and 15% RHA composites are quantified by the reduced maximum yield pressures of 74kN/m^2 and 60kN/m^2, respectively. However, with the addition of basalt fibers, the 10% and 15% RHA reconstituted soil composites

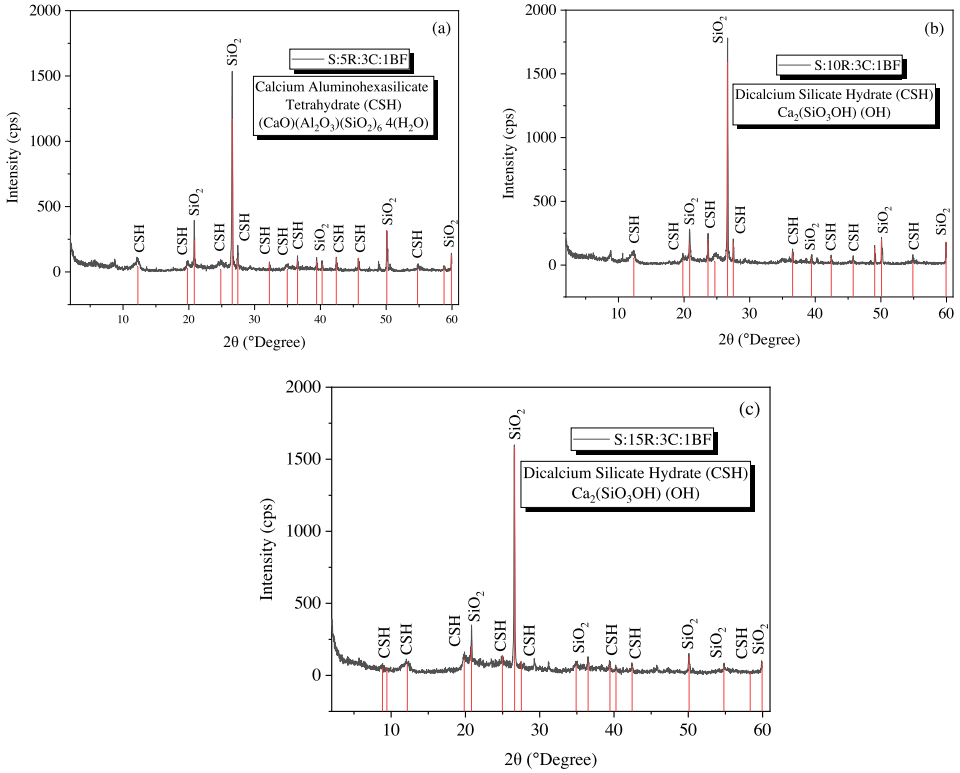

Fig. 6. Quantification of the pozzolanic elements by XRD analyses: (a) S:5R:3C:1BF12 specimen, (b) S:10R:3C:1BF12 specimen, (c) S:15R:3C:1BF12 specimen.

showed improved characteristics than the control specimens.

4.2. Normalized compression curve

Burland [1] introduced the normalizing void index (I_v) to correlate the compression curves of various remolded clay with the initial water contents ranging between 0.6 and 4.5 times the liquid limit. This correlation reported that the compression curves normalized well with the void index of reconstituted clays at initial water contents 1.0–1.5 times the liquid limits. Therefore, a unique line named the ICL was suggested to express the normalized compression curve in terms of the void index versus effective vertical pressures. The normalized compression curves of reconstituted soil composites for S:5R:3C:1BF and S:10R:3C:1BF specimens are shown in Fig. 7a and Fig. 7b, respectively, calculated using Eq. (3). Despite the discrepancy in basalt fiber lengths in the specimens, the compression curves of the reconstituted soil composite normalized perfectly with the ICL after the yield pressure phase, as suggested by Hong et al. [46]. The perfect normalization illustrated the presence of significant bonding in the new stabilized soil composite [53]. In addition, the higher effective vertical pressures (ranging from 100 to 1200kN/m^2) accelerated the rearrangement of the soil-RHA-cement particles and the basalt fibers relative to each other, resulting in a compact reconstituted soil structure.

On the other hand, the normalized curves for S:15R:3C:BF6 and S:15R:3C:BF12 are positioned below the ICL at vertical pressures above 100kN/m^2 due to high RHA content in the reconstituted clay soil, as illustrated in Fig. 7c. The inadequate pozzolanic reactions and destructuring can bring about such behavior in the soil at high loading pressures.

4.3. Compression Index, C_c

The compression index (C_c) is a fundamental parameter in determining the one-dimensional consolidation settlement of reconstituted clays. The greater the C_c value, the higher the chances of one-dimensional consolidation. The index is calculated from the normal consolidation phase (Loading phase) of the compression curves due to the elastic behavior of the soil. The compression index can be easily obtained by extending the straight-line portion of the normal consolidation region of the compression curves in Fig. 3a, Fig. 3b, and Fig. 3c. Then, taking the difference in the void ratio(e) divided by the change in effective vertical pressure (σ') in the log scale as shown in Eq. (4).

$$c_c = \left[\frac{e_a - e_b}{log(\sigma_b^1 - \sigma_a^1}\right] \quad (4)$$

The C_c value varies with the lengths of the basalt fiber included in the reconstituted soil composite for a given soil-RHA-cement content, as shown in Fig. 8. The specimen without basalt fibers shows C_c values ranging between 0.39 and 0.41 as the RHA content increases from 5% to 15%. Adding basalt fiber into the reconstituted soil composite reduces the compression index values by approximately 16% to values between 0.329 and 0.351; 0.33–0.345; 0.35–0.37 for basalt fiber lengths 3 mm, 6

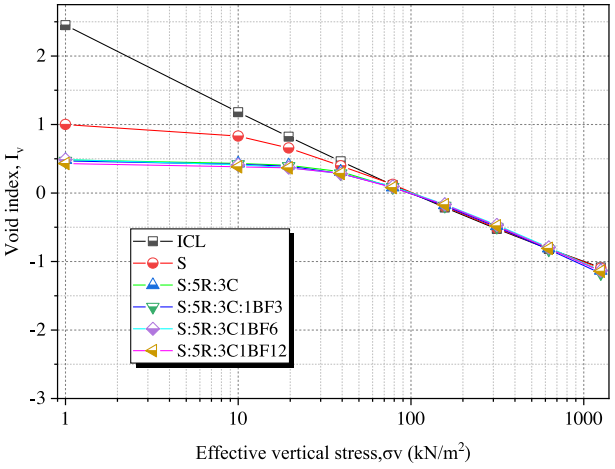

Fig. 7a. Normalized compression curves at 5% RHA.

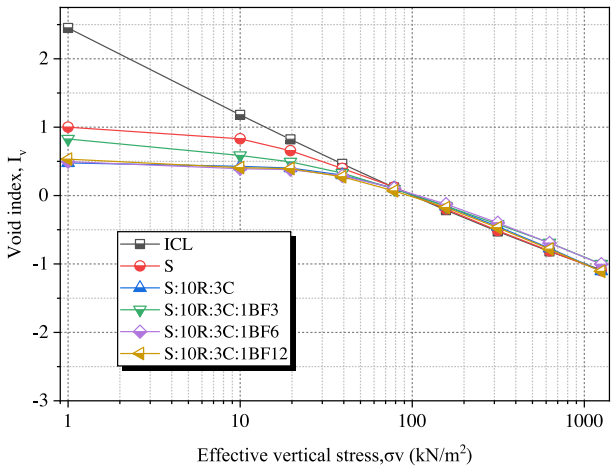

Fig. 7b. Normalized compression curves at 10% RHA.

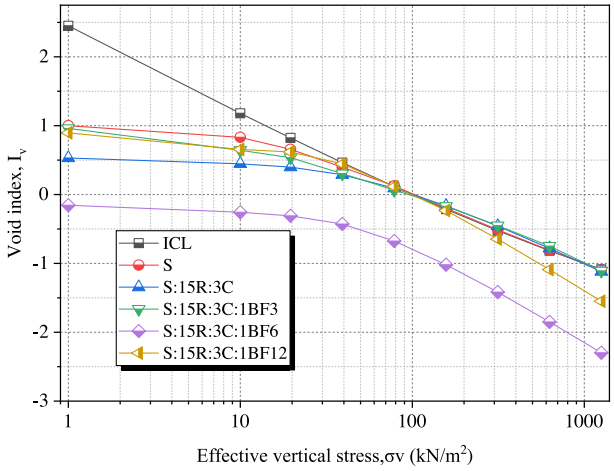

Fig. 7c. Normalized compression curves at 15% RHA.

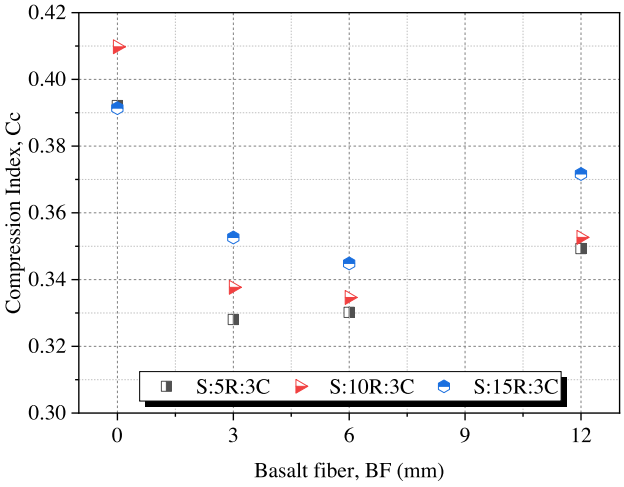

Fig. 8. Compression index C_c versus length of basalt fibers.

mm, 12 mm, respectively. A comparable reduction in compression index values when fibers are supplemented into a soil composite was noted by Kar and Pradhan [23]. It is also apparent from Fig. 8 that the degree of compression is dependent on the length of basalt fibers in the specimen. For example, an increase in basalt fiber length from 3 mm to 6 mm gives an insignificant rise in compression index compared to the notable development at 12 mm. Moreover, it is noteworthy that compression index values are kept to an average value of 0.3 for the 5% RHA-3% cement specimen, and a nominal increase is achieved as the RHA content rises to 10% and 15%-3% cement. This nominal increase in the compression index was due to the mobilized rearrangement of the particles in the reconstituted soil composite due to the additional porosity formed by the excess RHA in the soil-RHA-cement composite.

4.4. Swelling Index, C_s

Expansive clay soils have great swelling potential due to the dominant clay minerals that change volume when moisture changes ensue. Using fibers, methods to solve this swelling problem have recently gained research attention [24,25,54]. In this study, the dimensional influence of basalt fiber to curb the swelling of reconstituted clay soils is presented as shown in Fig. 9 using Eq. (4) and the unloading compression curves in Fig. 3a, Fig. 3b, and Fig. 3c.

The reconstituted soil composite without basalt fibers depicts high swelling indexes due to the absence of particle anchorage mechanism brought about by the fiber reinforcements. Upon basalt fiber addition, the swelling index of the 5% RHA-3% cement reconstituted soil specimen reduces from 0.0339 (for BF3mm) to 0.028 (for BF12mm), and a similar trend is observed for 10% and 15% RHA specimens as illustrated in Fig. 9. It is evident that longer fibers (BF12mm) substantially reduce the swelling index. For instance, reconstituted soils composites with 3 mm basalt fibers have a swelling index of 0.0326, 0.0322, and 0.0312 for 5%, 10%, and 15% RHA, respectively. While reconstituted soil specimen with 12 mm basalt fibers attained 0.028, 0.0265, and 0.0261 for 5%, 10%, and 15% RHA, respectively. The intensity of fiber interaction within the specimen arrests the interparticle movements hence the reduced swelling potential during the unloading phase compared to the specimen without fibers.

Furthermore, it is seen that the influence of basalt fiber reinforcements on the swell index is more significant at higher rice husk ash content. The high RHA contents mixed with nominal cement dosages produce a low-plastic material with a high water absorption rate. Hence, the decreases in swelling index with increased rice husk ash content [55,56].

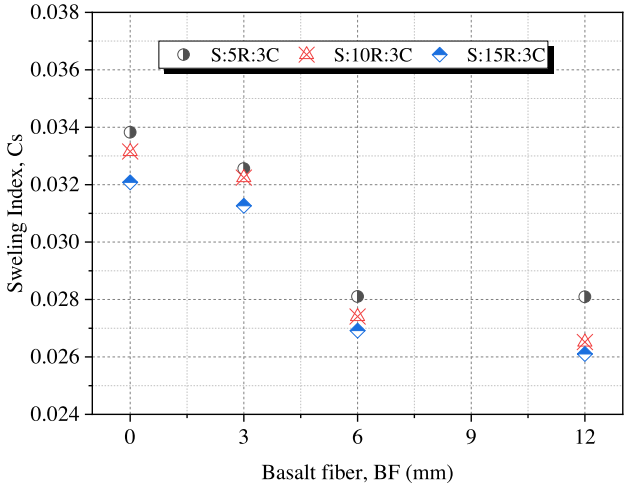

Fig. 9. The relationship between swelling index (C_s) and length of basalt fiber.

4.5. Assessment of compression curves

The test results in this study demonstrate that the compressibility of clay soils reinforced with basalt fiber and stabilized with RHA and cement can be determined by three parameters: length of basalt fibers, yield pressure (σ'), and RHA-cement content. It is also evident that the compressibility rate is directly related to the degree of bonding as reflected by the yield pressure (σ') [33,38]. In this study, this bonding phenomenon is attributed to the pozzolanic reactions (between soil, RHA, cement) and basalt fiber reinforcements. For example, considering the S:5R:3C:1BF12 specimen, the yield stresses increase to 110kN/m^2, reducing the compressive index from 0.392 to 0.35, as shown in Fig. 10a. Also, a reduction in compression index as yield pressure increases is observed for S:10R:3C:1BF12 and S:15R:3C:1BF12 with values of 0.354 and 0.37, respectively. The curve fitting equations illustrating the relationship between the compressive index and yield stress, based on the experimental data of clay soils reinforced with different lengths of basalt fibers and stabilized with RHA, are therefore expressed as follows:

$C_c = 0.00007\sigma'^2 - 0.0147\,\sigma' + 1.008$; for S:5R:3C:*i*BF composites (5).

$C_c = 0.00066\sigma'^2 - 0.0890\,\sigma' + 3.301$; for S:10R:3C:*i*BF composites (6).

$C_c = 0.00159\,\sigma'^2 - 0.1768\,\sigma' + 5.245$; for S:15R:3C:*i*BF composites (7).

Where, C_c is the compression index and σ' is the yield pressure of the reconstituted soil composite. The correlation coefficients (R^2) of the yield pressure versus the compression index shows high reliability of the test data as illustrated in Fig. 10a, Fig. 10b and Fig. 10c with values 0.99, 0.86 and 0.94 respectively.

5. Conclusions

A series of oedometer tests were performed to investigate the dimensional influence of basalt fibers reinforcements on the consolidation behavior of RHA-cement stabilized soils. The dimensional effects of basalt fibers and the RHA-cement content on the consolidation yield pressure(σ'), compression index (C_c), and swelling index (C_s) at the pre- and post-yield state are discussed. The concept of the intrinsic compression line is adopted to assess the compression curves of the new fiber reinforced soil composite. The following conclusions can be drawn from this study:

1. Increasing the length of basalt fiber in the reconstituted clay soil composite improves the consolidation yield pressure (σ'). This increase in yield pressure is also dependent on the RHA-cement content in the reconstituted soil structure. This behavior suggests that the composition of soil structure mainly governs the degree of yield

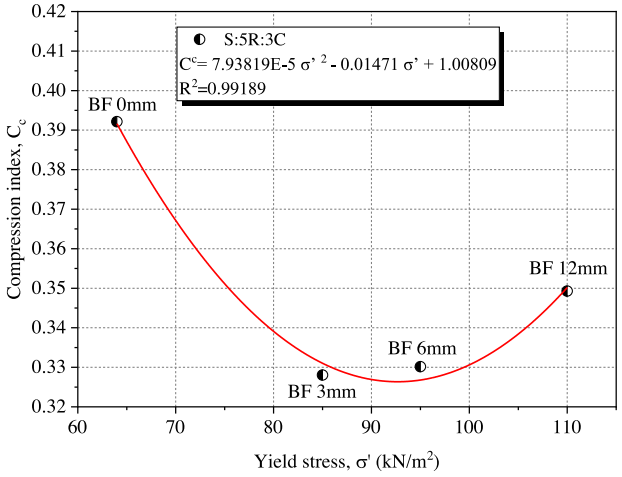

Fig. 10a. Relationship between σ' and C_c for 5%RHA soil composites.

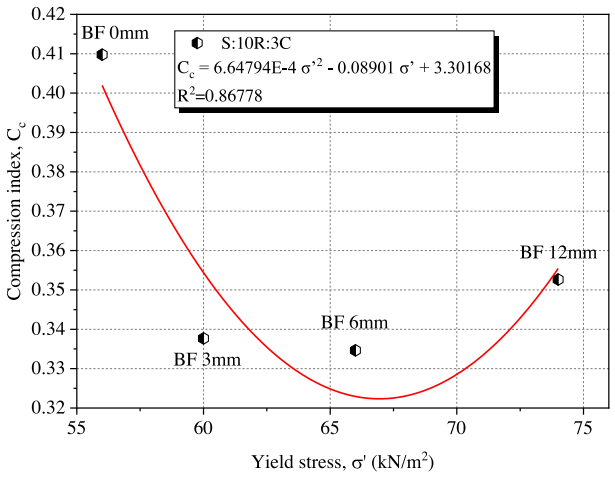

Fig. 10b. Relationship between σ' and Cc for 10%RHA soil composites.

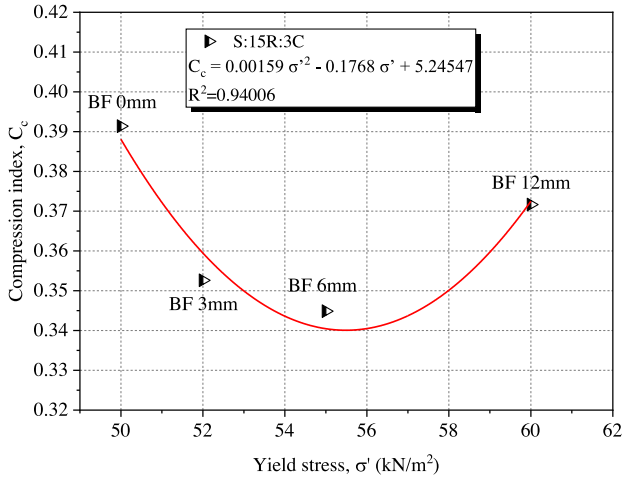

Fig. 10c. Relationship between σ' and C_c for 15%RHA soil composites.

pressure. The reconstituted clay soil composite with 12 mm basalt fibers, 5%RHA content (RHA), and 3% cement had a highly cemented and reinforced structure hence the high σ' of 110kN/m^2 as confirmed in the SEM and XRD analysis.

2. Adding basalt fiber to RHA stabilized soils significantly reduces the compression index (C_c). In this study, a 16% reduction is observed compared to the control specimen. As the length of basalt fiber increases from 3 mm to 6 mm, there is a 0.6% increase in the compression index, and at 12 mm, the C_c increases by 6% but is still lower than the C_c of the control specimens. This response illustrates that basalt fibers can improve the compressive index hence improving consolidation yield stress, σ'.
3. The swell index for basalt fiber reinforced RHA-cement stabilized soils decreased with fiber length and RHA content increment. The reduction in the swelling index indicates improved stability of the reinforced soil composite.
4. The curve fitting empirical relationships between C_c and σ' is proposed. These equations can be used for compressibility analysis in soils reinforced with basalt fibers ranging from 0 to 12 mm to estimate the projected compression index if the yield pressure and the length of basalt fibers are known.
5. This study concludes that a reconstituted clay soil composite with 1% 12 mm basalt fibers, 5% RHA, and 3% cement considerably improves consolidation behavior. This composite has an enhanced yield pressure of 110kN/m^2, compression index of 0.349, and swelling index of 0.0281. The improved consolidation characteristics make the new composite suitable for use in foundation fills as it can resist excessive settlement when subjected to structural loads.

Declaration of Competing Interest

The authors declare that they have no known competing financial interests or personal relationships that could have appeared to influence the work reported in this paper.

Acknowledgements

The authors would like to acknowledge the Japan Ministry of Education, Culture, Sports, Science and Technology for providing the MEXT scholarship through Mie University, where this study was conducted.

References

[1] J.B. Burland, On the compressibility and shear strength of natural soils, Geotech. 40 (3) (1990) 329–378, https://doi.org/10.1680/geot.1990.40.3.329.
[2] S. Horpibulsuk, M.D. Liu, D.S. Liyanapathirana, J. Suebsuk, Behaviour of cemented clay simulated via the theoretical framework of the structured cam clay model, Comput. Geotech. 37 (2010) 1–9, https://doi.org/10.1016/j.compgeo.2009.06.007.
[3] M.Y. Fattah, F.H. Rahil, K.Y.H. Al-Soudan, Improvement of clayey soil characteristics using Rice Husk Ash, J. Civ. Eng. and Urban. JCEU, ISSN-2252-0430 3 (1) (2013) 12–18.
[4] M.A. Rahman, Effect of cement rice husk ash mixtures on geotechnical properties of lateritic soils, J. Soils. Found. (JSSMF) 27 (2) (1987) 61–65, https://doi.org/10.3208/sandf1972.27.2_61.
[5] G. Sarkar, M.R. Islam, D.M. Alamgir, D.M. Rokonuzzaman, Interpretation of Rice Husk Ash on Geotechnical Properties of Cohesive Soil, Global J. Res. in Eng.: Civ Struct. Eng. 12 (2-A) (2012).
[6] R.M. Brooks, Soil Stabilization with Fly ash and Rice Husk Ash, Int. J. Res. Rev. in Appl. Sci. 1 (3) (2009) 209–217.
[7] R.D. Koteswara, P.R.T. Pranav, M. Anusha, Stabilization of Expansive Soil with Rice Husk Ash, Lime, and Gypsum –An Experimental Study, Int. J. of Eng. Sci. Tech. 3 (11) (2011) 8076–8085.
[8] S. Sebesta, Use of microcracking to reduce shrinkage cracking in cement-treated bases, Transportation research record (1936) (1) (2005) 2-11. 10.1177/0361198105193600101.
[9] D.N. Little, Comparison of in-situ resilient moduli of aggregate base courses with and without low percentages of lime stabilization, In Innovations and Uses for Lime, ASTM Int, 1992.
[10] D. Gupta, A. Kumar, Strength characterization of cement stabilized and fiber reinforced clay–pond ash mixes, Int. J. of Geosynth. Gr. Eng., (2)(4) (2016) 1-11. 10.1007/s40891-016-0069-z.
[11] M.D.T. Casagrande, M.R. Coop, N.C. Consoli, Behaviour of fiber reinforced bentonite at large shear displacement, J. Geotech. Geoenviron. Eng. 132 (11) (2006) 1505–1508, https://doi.org/10.1061/(ASCE)1090-0241(2006)132:11(1505).
[12] M.D.T. Casagrande, N.C. Consoli, M.R. Coop, Performance of a fiber reinforced sand at shear strains, Geotech. 57 (2007) 751–756, https://doi.org/10.1680/geot.2007.57.9.751.
[13] M.D.T. Casagrande, N.C. Consoli, K.S. Hieneck, M.R. Coop, Shear strength behavior of fiber-reinforced sand considering triaxial tests under distinct stress paths, J. Geotech. Geoenviron. Eng 133 (11) (2007) 1466–1469, https://doi.org/10.1061/(ASCE)1090-0241(2007)133:11(1466).
[14] B. Fatahi, H. Khabbaz, B. Fatahi, Mechanical characteristics of soft clay treated with fibre and cement, Geosynth. Int. 19 (3) (2012) 252–262, https://doi.org/10.1680/gein.12.00012.
[15] P. Divya, B. Viswananham, J. Gourc, Evaluation of tensile strength-strain characteristics of fiber reinforced soil through laboratory tests, J. Mater. Civ. Eng. 26 (1) (2014) 14–23, https://doi.org/10.1061/(ASCE)MT.1943-5533.0000772.
[16] J. Li, C. Tang, D. Wang, X. Pei, B. Shi, Effect of discrete fiber reinforcement on soil tensile strength, J. Rock Mech Geotech. Eng. 6 (2) (2014) 133–137, https://doi.org/10.1016/j.jrmge.2014.01.003.
[17] V. Anggraini, A. Asadi, B.B. Huat, H. Nahazanan, Effects of coir fibers on tensile and compressive strength of lime treated soft soil, Measurement. 59 (2015) 372–381, https://doi.org/10.1016/j.measurement.2014.09.059.
[18] E. Botero, A. Ossa, G. Sherwell, E. Ovando-Shelley, Stress strain behavior of a silty soil reinforced with polyethylene terephthalate (PET), Geotext. Geomembr. Press 1–7 (2015), https://doi.org/10.1016/j.geotexmem.2015.04.003.
[19] N.C. Consoli, P.D.M. Prietto, L.A. Ulbrich, Influence of fiber and cement addition on behavior of sandy soil, J. Geotech. Geoenviron. Eng. 124 (12) (1998) 1211–1214, https://doi.org/10.1061/(ASCE)1090-0241(1998)124:12(1211).
[20] N.C. Consoli, J.P. Montardo, P.D.M. Prietto, G.S. Pasa, Engineering behavior of sand reinforced with plastic waste, J. Geotech. Geoenviron. Eng. 128 (6) (2002) 462–472, https://doi.org/10.1061/(ASCE)1090-0241(2002)128:6(462).

[21] M. Syed, A.GuhaRay, Effect of fiber reinforcement on mechanical behavior of alkali-activated binder-treated expansive soil: reliability-based approach, Int. J. Geomech. 20(12)(2020) 04020225. 10.1061/(ASCE)GM.1943-5622.0001871.
[22] M.R. Abdi, P. Ali, M.A. Arjomand, Effects of random fiber inclusion on consolidation, hydraulic conductivity, swelling, shrinkage limit and desiccation cracking of clays, Int. J. Civ. Eng. 6 (4) (2008) 284–292. http://ijce.iust.ac.ir/article-1-174-en.html.
[23] S. Das, S.K. Pal, Consolidation Characteristics of Silty-Clay Soil Mixed with Class F Indian Fly Ash, Indian Geotech. Con. Delhi (2012) 13–45.
[24] R.K. Kar, P.K. Pradhan, Strength and Compressibility Characteristics of Randomly Distributed Fibre-Reinforced Soil, Int. J. Geotech. Eng. (IJGE) 5 (2) (2011) 235–243, https://doi.org/10.3328/IJGE.2011.05.02.235-243.
[25] G.L.S. Babu, A.K. Vasuvedan, M.K. Sayida, Use of coir fibres for improving the engineering properties of expansive soils, J Nat Fibres 5 (1) (2008) 61–75, https://doi.org/10.1080/15440470801901522.
[26] N.M. Al-Akhras, M.F. Attom, K.M. Al-Akhras, A.I.H. Malkawi, Influence of fibres on swelling properties of clayey soils, Geosynth. Int J 15 (4) (2008) 304–309, https://doi.org/10.1680/gein.2008.15.4.304.
[27] S. Cyrus, T.J Babu, Consolidation characteristics of coir reinforced Cochin marine clays, In: Proc. '05 Indian Geotech. Con. Ahmedabad, India, (2005) 125-128.
[28] B.V.S. Viswanadham, B.R. Phanikumar, R.V. Mukherjee, Swelling behaviour of a geofiber-reinforced expansive soil, Geotext. Geomembr. 27 (1) (2009) 73–76, https://doi.org/10.1016/j.geotexmem.2008.06.002.
[29] A. Laskar, S.K. Pal, Effects of waste plastic fibres on compaction and consolidation behavior of reinforced soil, EJGE 18 (2013) 1547–1558.
[30] H. Trouzine, M. Bekhiti, A. Asroun, Effects of scrap tyre rubber fibre on swelling behaviour of two clayey soils in Algeria, Geosynth. Int. 19 (2) (2012) 124–132, https://doi.org/10.1680/gein.2012.19.2.124.
[31] A. Sridharan, H.B. Nagaraj, Compressibility behaviour of remoulded, fine-grained soils and correlation with index properties, Can. Geotech. J. 37 (3) (2000) 712–722, https://doi.org/10.1139/t99-128.
[32] JIS A 1217, Test method for soil consolidation test. Japanese Industrial Standard, Guidance and Basic - Soil Test, The Jpn. Geotech. Soc. (in Japanese) (2010) 215-227.
[33] JIS A 1227, Test method for soil consolidation test. Japanese Industrial Standard, Guidance and Basic - Soil Test, The Jpn. Geotech. Soc. (in Japanese) (2010) 215-227.
[34] S. Horpibulsuk, D.T. Bergado, G.A. Lorenzo, Compressibility of cement admixed clays at high water content, Geotech. 54 (2) (2004) 151–154, https://doi.org/10.1680/geot.2004.54.2.151.
[35] S. Horpibulsuk, N. Miura, D.T. Bergado, Undrained shear behavior of cement admixed clay at high water content, J. Geotech. Geoenviron. (130) (10) (2004b) 1096-1105. 10.1061/(asce)1090-0241(2004)130:10(1096).
[36] J. Suebsuk, S. Horpibulsuk, M.D. Liu, Modified structured cam clay: a generalized critical state model for destructured, naturally structured and artificially structured clays, Comput. Geotech. (37) (7-8) (2010) 956–968. 10.1016/j.compgeo.2010.08.002.
[37] Y.J. Du, M.L. Wei, F. Jin, Z.B. Liu, Stress-strain relation and strength characteristics of cement treated zinc-contaminated clay, Eng. Geol. 167 (2013) 20–26, https://doi.org/10.1016/j.enggeo.2013.10.005.
[38] Y.J. Du, S. Horpibulsuk, M.L. Wei, C. Suksiripattanapong, M.D. Liu, Modeling compression behavior of cement-treated zinc-contaminated clayey soils, Soils Found. 54 (5) (2014) 1018–1026, https://doi.org/10.1016/j.sandf.2014.09.007.
[39] N. Miura, S. Horpibulsuk, T.S. Nagaraj, Engineering behavior of cement stabilized clay at high water content, Soils Found. 41 (5) (2001) 33–45, https://doi.org/10.3208/sandf.41.5_33.
[40] H. Tremblay, S. Leroueil, J. Locat, Mechanical improvement and vertical yield stress prediction of clayey soils from eastern Canada treated with lime or cement, Can. Geotech. J. 38 (3) (2001) 567–579, https://doi.org/10.1139/t00-119.
[41] A.H.M. Kamruzzaman, S.H. Chew, F.H. Lee, Structuration and destructuration behavior of cement-treated Singapore marine clay, J. Geotech. Geoenviron. 135 (4) (2009) 573–589, https://doi.org/10.1061/(asce)1090-0241(2009)135:4(573).
[42] C.F. Chiu, W. Zhu, C.L. Zhang, Yielding and shear behaviour of cement-treated dredged materials, Eng. Geol. 103 (1) (2009) 1–12, https://doi.org/10.1016/j.enggeo.2008.07.007.
[43] D. Wang, N.E. Abriak, R. Zentar, Strength and deformation properties of Dunkirk marine sediments solidified with cement, lime and fly ash, Eng. Geol. 166 (2013) 90–99, https://doi.org/10.1016/j.enggeo.2013.09.007.
[44] T.S. Nagaraj, N.S. Pandian, P.S.R. Narasimha Raju, Compressibility behavior of soft cemented soils, Geotech. 48 (2) (1998) 281–287, https://doi.org/10.1680/geot.1998.48.2.281.
[45] M.D. Liu, J.P. Carter, Virgin compression of structured soils, Geotech. 49) (4 (1999) 43–57, https://doi.org/10.1680/geot.1999.49.1.43.
[46] Z.S. Hong, J. Yin, Y.J. Cui, Compression behaviour of reconstituted soils at high initial water contents, Geotech. 60 (9) (2010) 691–700, https://doi.org/10.1680/geot.09.P.059.
[47] Z.S. Hong, L.L. Zeng, Y.J. Cui, Y.Q. Cai, C. Lin, Compression behaviour of natural and reconstituted clays, Geotech. 62 (4) (2012) 291–301, https://doi.org/10.1680/geot.10.P.046.
[48] S. Leroueil, P.R. Vaughan, The general and congruent effects of structure in natural soils and weak rocks, Géotech. 40 (3) (1990) 467–488, https://doi.org/10.1680/geot.1990.40.3.467.
[49] A Casagrande, The determination of pre-consolidation load and its practical significance, In Proc. Int. Conf. Soil Mech. Found. Eng. Cambridge, Mass., (3) (1936) 60.
[50] S. Sasanian, T.A. Newson, Basic parameters governing the behaviour of cement-treated clays, Soils Found. 54 (2) (2014) 209–224, https://doi.org/10.1016/j.sandf.2014.02.011.
[51] N. Meller, K. Kyritsis, C. Hall, The mineralogy of the CaO–Al2O3–SiO2–H2O (CASH) hydroceramic system from 200 to 350 C, Cem. Concrete Res. 39 (1) (2009) 45–53, https://doi.org/10.1016/j.cemconres.2008.10.002.
[52] M.R. Hansen, H.J. Jakobsen, J. Skibsted, 29Si chemical shift anisotropies in calcium silicates from high-field 29Si MAS NMR spectroscopy, Inorg. Chem. 42 (7) (2003) 2368–2377, https://doi.org/10.1021/ic020647f.
[53] J. Burland, J.R. Standing, R.J. Mair, L.F. Linney, F.M. Jardine, A collaborative research programme on subsidence damage to buildings: prediction, protection and repair, In Geotech. Aspc. Underground Const. Soft Gnd. (1996) 773–778.
[54] M. Malekzadeh, H. Bisel, Swell and compressibility of fibre reinforced expansive soils, Int. J. Adv. Technol. Civ. Eng. 1 (2) (2012) 42–45.
[55] A Muntohar, Utilization of Uncontrolled Burnt Rice Husk Ash in Soil Improvement, Civ. Eng. Dimen. (4) (2) (2002) 100-105. 10.9744/ced.4.2.pp.%20100-105.
[56] A.O. Eberemu, D.I. Omajali, Z. Abdulhamid, Effect of compactive effort and curing period on the compressibility characteristics of tropical black clay treated with rice husk ash, Geotech. Geol. Eng. 34 (1) (2016) 313–322, https://doi.org/10.1007/s10706-015-9946-9.

Effects of basalt fibres on strength and permeability of rice husk ash-treated expansive soils

Alex Otieno Owino,[1] Najmun Nahar,[1,2] Zakaria Hossain,[1] Noma Tamaki[3]

[1]Graduate School of Bioresources, Mie University, Japan; [2]Life and Earth sciences, Jagannath University, Bangladesh; [3]Make Integrated Technology Company, Osaka, Japan

Abstract

The application of stabilised soil in agricultural construction works such as shallow foundation fills and subgrade material for farm roads is in demand due to the improved geotechnical properties. This study focused on improving the compressive capabilities and the permeability characteristics of rice husk ash (RHA)-treated clayey soils using basalt fibre. Basalt fibres are made from naturally occurring basalt rock, yet their use in soil stabilisation has not been realised due to limited research for its validation in ground stabilisation. Essential variables in the stabilised soil matrix included basalt fibre length (3 mm, 6 mm, and 12 mm), RHA percentages (5%, 10%, and 15%), and cement percentage (3%). In addition, the optimum moisture content of each admixture was determined by standard proctor compaction tests and reduced by 3% to prepare the specimens for unconfined compression strength test, constant head permeability test, and scanning electron microscope (SEM) test. It was observed that the unconfined compression strength of the RHA-basalt fibre stabilised clayey significantly increased when the specimens wet cure for 28 days.

Similarly, adding fibres into the soil improved the permeability coefficient. The SEM test showed a porous morphology that increased permeability. Furthermore, through SEM, the randomly oriented basalt fibres' portrayed the reinforcing phenomenon related to improved compressive strength and sufficient bearing capacity to support structures built upon this class of soils.

Correspondence: Alex Otieno Owino, Graduate School of Bioresources, Mie University, Japan. E-mail: 520d2s2@m.mie-u.ac.jp

Key words: Basalt fibre; soil stabilisation; permeability coefficient; unconfined compression strength; scanning electron microscope.

Acknowledgements: the authors would like to acknowledge the Japan Ministry of Education, Culture, Sports, Science and Technology for providing the MEXT scholarship through Mie University, where this study was conducted.

Contributions: AOO, methodology, data processing, and original draft writing; NN, manuscript review, and editing; ZH, supervisor of the Ph.D. student, funding acquisition, and research coordination.

Received for publication: 3 December 2021.
Accepted for publication: 25 January 2022.

Journal of Agricultural Engineering 2022; LIII:1315
doi:10.4081/jae.2022.1315

Introduction

Ground improvement is a fundamental step in geotechnical engineering to improve the strength of naturally occurring soils. The application of such improved soils is in the rise in areas like the subgrade layers (Crockford, 1993), fill material (Festugato *et al*., 2013), and stability for shallow foundations (Mitchell, 1981; Ibraim *et al*., 2013). Major parameters such as strength, modulus of deformations, failure planes, permeability, and the soil microstructure interaction must be examined to support engineering structures. Several methods have been proposed to produce high-strength soils for engineering construction purposes within the last decade. Soil improvement can be made by modifying the existing properties or by stabilisation (Fattah, 2013). Stabilisation methods include densification techniques using cement-rich mixtures, pozzolans to stabilise the soil chemically, and reinforcement techniques using different types of fibres. The use of densification practices by cement has been more and more considered worldwide, but this has led to a tremendous increase in construction costs and environmental impacts associated with cement manufacture (Alhassan, 2008). This encounter has led to the sustainable use of industrial wastes like rice husk ash (RHA) and fibres as potential replacements or reduction aggregates to conventional cement densification techniques, as described in the next section.

The pozzolanic stabilisation technique

One of the predominant pozzolanic materials in engineering use today is RHA. Rice husk is a by-product of the rice grain production process. Upon the controlled and open burning of rice husks, we obtain RHA, which is extensively used to improve soils' geotechnical properties due to its abundance and is superiorly inexpensive compared to other conventional stabilising agents such as cement and lime (Aprianti, 2015). Pozzolans are those materials that are rich in siliceous and aluminous compounds and which in themselves have very minimal cementitious properties until chemically reacted with calcium hydroxide from materials such as cement (Malhotra and Mehta, 2004; Basha *et al*., 2005). Therefore, using RHA in soil stabilisation is advantageous for improving soil strength and durability. In addition, environmental impacts related to the uncontrolled disposal of agricultural waste and excess carbon dioxide emissions from uncontrolled burning of these wastes in the fields (Ali, 1992) can be diminished.

Rahman (1986), in his research on the effects of rice husk ash

alone on the unconfined compressive strength (UCS) of stabilised soils, showed that an increase of RHA to 20% increased the UCS of lateritic soils, after which they started to decrease. Noor (1993) also examined the RHA-cement ratios and how they positively influenced the proposed mix ratios, UCS, and durability. Muntohar's (2004) results showed that mixing RHA with 6% lime significantly reduced swelling and increased durability on such improved soils. The literature also showed that RHA had an optimum percentage above which the UCS of improved soils decreased. Alhassan (2008) showed that adding RHA percentages between 0 to 4% to clay soils and lime specimens significantly increased the UCS value at specified lime contents. On the other hand, from the same research, increasing rice husk ash percentages from 6 to 8% decreased the UCS value considering the curing period in both cases.

Soil stabilisation by RHA involves a pozzolanic reaction between the Ca $(OH)_2$ rich cement or lime and the SiO_2 rich RHA ash in an alkaline environment leading to the formation of calcium silicate hydrate (CSH) gel (Rogers and Glendinning, 2000). James and Rao (1986) investigated the setting process for a lime-excess and a lime-deficient mixture. The reaction product showed the CSH gel by a combination of thermal analysis, XRD, and electron microscopy. In a nutshell, the formation of CSH gel accounted for the strength of lime-RHA and cement, as shown in Eq. (1).

$$Ca\ (OH)_2 + SiO_2 = CaO_{0.8\text{-}1.5}SiO_2\ (H_2O)_{1.0\text{-}2.5} + CaO_{1.5\text{-}2.0}SiO_2.2(H_2O) \quad (1)$$

Fibre stabilisation techniques

Fibre inclusion in a soil matrix has proved to add more intensification in the compressive abilities of soils due to the reinforcing technique between the soil particles. Therefore, several pieces of research have been investigated considering different fibres and their applicability in enhancing soil strength from literature. For example, Kumar (2006) studied the UCS gain on the soil by mixing polyester fibres and soft clay and observed that the compaction degree affected fibre reinforcement. Also, the unconfined compressive strength of clay increased with the addition of fibres, and it further increased when fibres were mixed in the clay-sand mixture.

Hossain (2011) also examined the structural improvement on cement-based matrices using varied carbon fibre lengths, improving durability and compressive strength. With the diversity in the fibre available for soil stabilisation, polypropylene and recycled carpet have also been used before. Where bender element tests on 126 cylindrical specimens of cement-treated clay with various cement and fibre contents were analysed to distinguish the relationships between fibre and cement content and the small-strain mechanical properties (Fatahi *et al*., 2013). Park (2009) further showed that compacting polyvinyl alcohol (PVA) fibre in different layers inside a cylindrical river sand specimen improved the compressive strength as the number of fibre layers increased. With fibres evenly distributed throughout the five layers a reinforced model was twice as strong as a non-fibre-reinforced specimen. A more comparable study to this research was done by Cristelo *et al*. (2015). In their study, the influence of discrete fibre reinforcement on the uniaxial compression response found that sandy clay reinforced with polypropylene fibres and cement increased the stiffness, modulus of deformation, and compression strength of the mixtures for every cement content. Similar results were also determined by Maher and Gray (1990) and Consoli *et al*. (1998).

Therefore, the present study focuses on stabilisation by pozzolanic reactivity of RHA and reinforcement technique by randomly distributed basalt fibre in the proposed hybrid fibre composite. Compressive tests and permeability tests on soil composites with basalt fibres (lengths 3 mm, 6 mm, and 12 mm), cement (3% of the dry weight of soil), and rice husk ash (5%, 10%, and 15% of the dry weight of soil) were carried out. The influence of these stabilisation aggregates was demonstrated by stress-strain curves and associated geotechnical properties presented in graphical form to aid future designs and relevant construction applications.

Research significance

Using fibres and chemical stabilising agents in weak soils can be very effective in arresting cracks on such soils when used in engineering construction applications. The problem associated with the soil failure phenomenon and the bearing capacity factors has been studied in the past. Literature quotes various techniques used to curb the engineering challenges when dealing with low-strength soils. Despite such data, little to no technical literature is available on the dimensional influence of basalt fibres on the unconfined compressive strength and permeability of such chemically stabilised soils. Therefore, investigations can be conducted to examine the optimal stress-strain response of the hybrid fibre composites at micro and macro levels, using different basalt fibre dimensions. This study explores the impacts of these different basalt fibre lengths on the engineering properties of hybrid fibre composites for ground improvement if present.

Materials and methods

Material properties

The materials used in this research included soil, RHA, cement, and basalt fibre (BF). Figure 1 is a pictorial representation of the engineering materials. A detailed explanation of the properties of the materials is as discussed below.

Soil

The soil used in this research was collected from Handa Area, Mie Prefecture, Japan. The soil was air-dried for 3 weeks then sieved through the 2mm sieve, after which sieve analysis and hydrometer analysis were conducted on a 500 grams specimen to

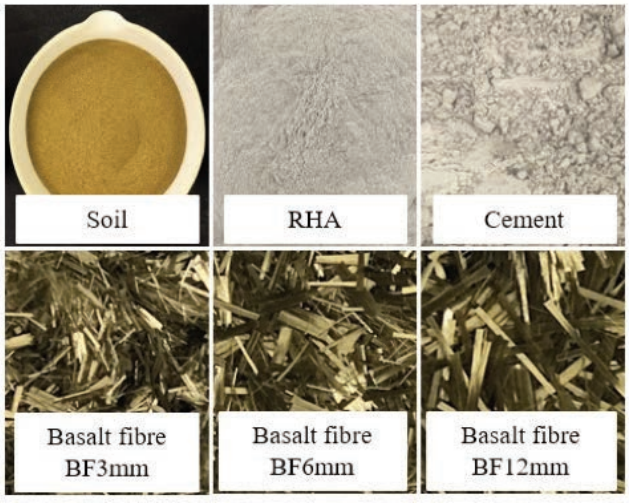

Figure 1. Experimental materials. RHA, rice husk ash.

classify the soil. According to the American Association of State Highway and Transportation Officials (AASHTO), the soil was classified as A-7-5(2) clayey soils with 6.2% coarse sand, 54.58% medium sand, 39.2% clay, and 2.215 group index. More detailed properties are shown in Table 1.

Rice husk ash properties

RHA was obtained from Make Integrated Technology Co., Ltd, Osaka, Japan. The RHA was controlled-burned ash at 650-700°C with a high silica content of 91.10%. In this research, unground ash was used, keeping it in its natural particle size distribution of 0.07 to 0.3 mm. As a result, the most dominant particles were between 0.07 and 0.106 mm. Table 1 shows the rice husk ash's detailed physical and chemical properties.

The particle distribution curves developed from sieve analysis and hydrometer analysis for soil and sieve analysis only for RHA are shown in Figure 2A.

Basalt fibre properties

Basalt fibre is (BF) made from basalt rock. The basalt rock is washed and melted, then extruded through small nozzles to produce the continuous filaments called basalt fibres (Lopresto *et al*., 2011). Its application in engineering construction reinforcement works is derived from the high tensile strength of between 4100-4840 MPa, high elastic modulus ranging from 93.1-110 GPa (Berozashvili, 2001), durability, alkali resistance, and thermal stability compared to other fibres (Sim and Park, 2005). Table 1 illustrates the fundamental properties related to this study.

Ordinary Portland cement

Ordinary Portland cement (OPC) cement was chosen for this study due to its availability in the market.

Table 1. Properties of the experimental materials.

Materials	Parameters	Values
Soil properties	Specific gravity, (g/cm^3)	2.75
	Maximum dry density, (g/cm^3)	1.64
	Optimum water content, %	24.00
	Sand (75 μm - 2 mm), %	6.20
	Silt (5-75 μm), %	54.58
	Clay <5 μm, %	39.22
	Liquid limit, LL, %	58.20
	Plastic limit, PL, %	31.05
	Plasticity Index, PI, %	27.15
	AASHTO classification	A-7-5(2)
RHA Properties	Average particle size, mm	0.001 to 0.3
	Loss of ignition, %	4-6
	Specific gravity, g/cm^3	2.12
	Burning temperature, °C	650-700
	Burning time, hour	27
	Silica (SiO_2), %	91.10
	Carbon dioxide (CO_2), %	4.35
	Potassium oxide (K_2O), %	2.40
	Calcium oxide (CaO), %	0.57
	Iron oxide (Fe_2O_3), %	0.05
	Alumina (Al_2O_3), %	0.03
	Others, %	1.50
Basalt fibre properties	Fibre diameter, (μm)	6～30
	Density, (g/cm^3)	2.63～2.8
	Tensile strength, (MPa)	4100～4840
	Elastic modulus, (GPa)	93.1～110
	Fibre lengths, (mm)	3, 6 and 12
	Fracture elongation rate, (%)	3.1

Testing methods

Standard proctor compaction test

A standard proctor test was done following the JIS A 1210 (2010) standards to evaluate the specimens' maximum dry unit weight (MDD) and the optimum moisture content (OMC). The soil specimen (herein, specimen refers to a mixture of soil, RHA, cement, and basalt fibre in varied ratios) were compacted in three layers inside the compaction mould measuring 10cm diameter and 12.68 cm height, using a 2.5 kg rammer at a falling height of 30 cm. A record of 25 blows was registered for each layer. A representative specimen was taken and tested for moisture content, and the process was repeated for all water increments. The codes for the specimen under study are explained in Table 2.

Unconfined compressive strength test

Unconfined compressive strength (UCS) test was done on a cylindrical specimen with dimensions 5cm diameter and 12.5 cm height to examine the compressibility behaviour of the mix ratios above. The specimens were prepared using a cylindrical mould and a rammer weighing 1 kg at a falling height of 30 cm. All specimens were set at the optimum moisture content obtained from compaction tests and wet cured for 1 day, 7 days, and 28 days at a constant temperature of 25 degrees Celsius before testing. The data sets obtained from each specimen were then analysed in the stress-

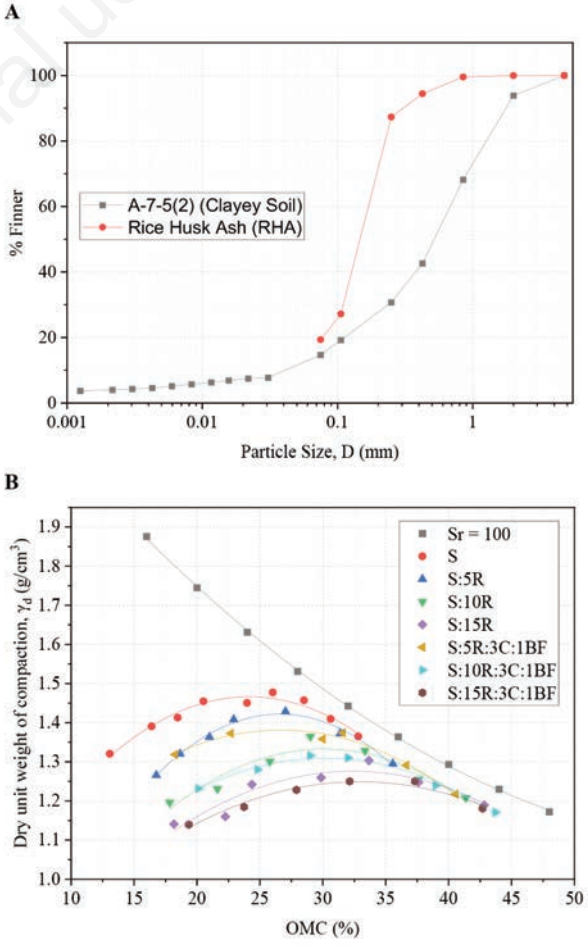

Figure 2. A) Particle size distribution for soil and of rice husk ash (RHA). B) Compaction curves for the mixing ratios. OMC, optimum moisture content.

strain curve plots to evaluate the compressive stress (q_u) and axial strain (Ɛ) relationship and the modulus of deformation, E_{50}. The testing procedures followed the Japan standards, JIS A 1216 (2010).

Permeability test

In this study, a constant head permeability test was carried out to examine the coefficient of permeability, k, for all the specimens considering curing periods 1 day, 7 days, and 28 days. Each specimen was compacted in three layers in the compaction mould (10.4 cm diameter and 6.3 cm height) at 20 blows per layer to maintain constant compaction energy. The specimens were wet cured while retaining the water content at OMC, which allowed for enough hydration and pozzolanic activity. The constant water head was maintained at 45 m, simulated by the air pressure of 0.45 MPa in the water chamber on top of the specimen. Water flowed through the specimen until it was saturated before the first reading. Then, four readings were taken by measuring the volume of percolated water and the corresponding time for flow. Afterward, the average k of each flow was used to evaluate the final permeability coefficient (k). The experimental procedures followed Japan standards, JIS A 1218 (2010).

Scanning electron microscope

Microscopic examination was necessary to understand the macro and microstructure interaction of the proposed hybrid composite. Therefore, a scanning electron microscope was used on a specimen with dimensions 3 mm by 3 mm by 0.5 mm collected from the centre of the cylindrical specimen used during the UCS test. Soil-RHA microstructure was examined at a magnification of ×500. At the same time, the soil-RHA-cement-basalt fibre

Table 2. Specimen codes and mixing ratios.

Specimen code	Description of the mixing ratios
S	Soil only (control specimen)
S:5R	Soil+5%RHA
S:10R	Soil+10%RHA
S:15R	Soil+15%RHA
S:5R:3C:1BF3	Soil+5%RHA+3%cement+1%basalt fibre 3 mm
S:10R:3C:1BF3	Soil+10%RHA+3%cement+1%basalt fibre 3 mm
S:15R:3C:1BF3	Soil+15%RHA+3%cement+1%basalt fibre 3 mm
S:5R:3C:1BF6	Soil+5%RHA+3%cement+1%basalt fibre 6 mm
S:10R:3C:1BF6	Soil+10%RHA+3%cement+1%basalt fibre 6 mm
S:15R:3C:1BF6	Soil+15%RHA+3%cement+1%basalt fibre 6 mm
S:5R:3C:1BF12	Soil+5%RHA+3%cement+1%basalt fibre 12 mm
S:10R:3C:1BF12	Soil+10%RHA+3%cement+1%basalt fibre 12 mm
S:15R:3C:1BF12	Soil+15%RHA+3%cement+1%basalt fibre 12 mm

RHA, rice husk ash.

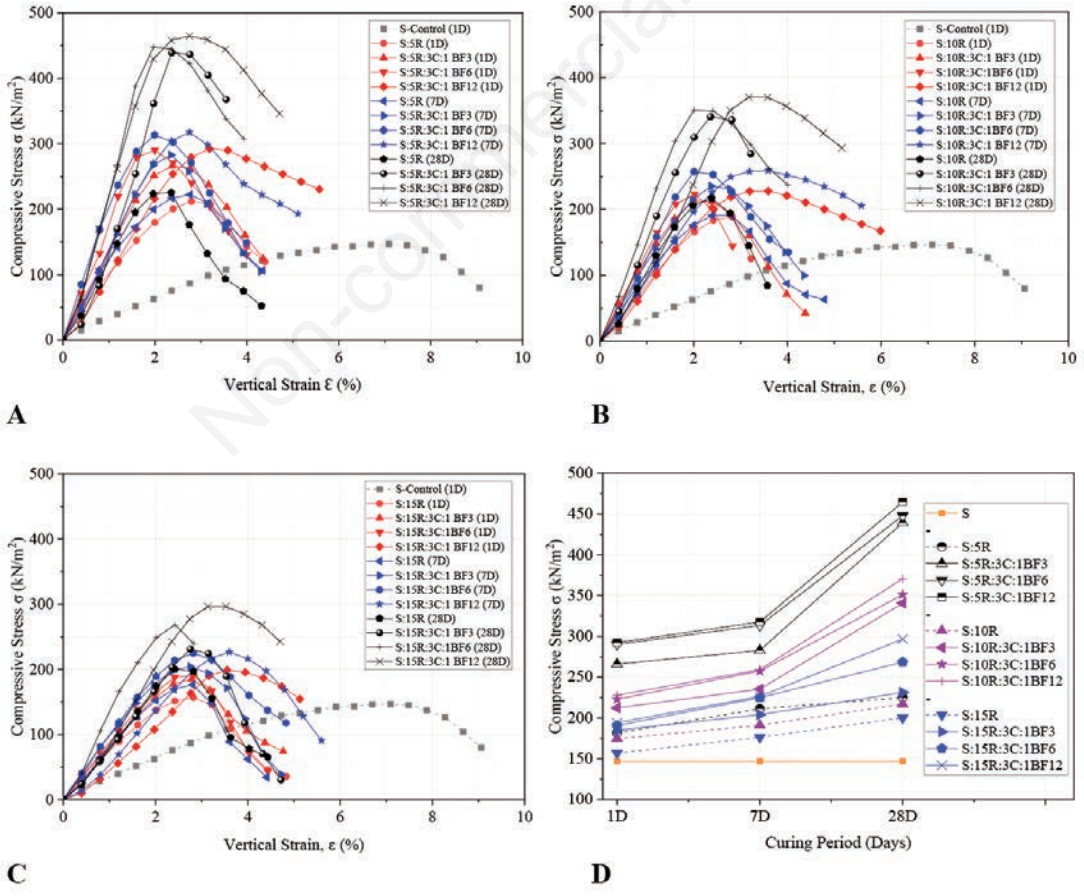

Figure 3. A) Stress-strain relationships for 5% of rice husk ash (RHA) and basalt fibre. B) Stress-strain relationships for 10% RHA and basalt fibre. C) Stress-Strain relationships for 15% RHA and basalt fibre. D) Variation of compressive stress with curing period.

macrostructure was observed at a magnification of ×150 to provide a wider area for spotting the basalt fibres' random distribution in the soil composite matrix.

Results and discussion

Standard Proctor compaction test results

Compaction test refers to soil densification by removing air and rearranging the soil particles through mechanical energy. The degree of compaction is measured in terms of the maximum dry density, $\gamma_{dmax,}$ and the optimum moisture content, OMC (Robert, 2008). Figure 2B shows a plot of the compaction curves and the saturation line Sr, emphasising the maximum values for the OMC and the dry unit weight γ_{dmax} for all the specimen mix ratios. In this study, compaction curves did not pass the saturation line, showing the correctness of the relationships between OMC and γ_{dmax}. The optimum water content increased with an increased percentage of RHA. Similarly, upon adding cement into the mix ratios, there was a further increase in the OMC.

The dry unit weight decreased with the addition of RHA and cement. The increase in OMC was due to the high-water affinity by the increasing percentage of RHA and the hydration effect with cement mixtures (Anupam, 2012). Furthermore, the decrease in dry density was attributed to flocculation and cementitious compounds in the new composite soil mixtures.

Unconfined compressive strength test results

This section shows the relationship between compressive stress, $q_{u,}$ and axial strain, ε for RHA percentages (5%, 10%, and 15%), and basalt fibre lengths (3 mm, 6 mm, and 12 mm). In Figure 3A, the maximum compressive stresses, $q_{u,}$ were achieved with 5% RHA specimen at lower axial strains, ε compared to control. In Figure 3B and C, adding RHA to 10% and 15%, respectively, reduced the compressive stresses with a slight increase in the axial strain for all basalt fibre lengths. A similar trend on axial strain versus RHA was also observed by Basha (2005) and Rao *et al*. (2011). Compressive stress reduction can be attributed to the reduced cementitious properties due to excess RHA, hence less bonding of soil particles and basalt fibres, leading to increased axial displacements. Nevertheless, all 10% RHA and 15% RHA specimens produced significantly more stress-bearing than the control specimen.

Correspondingly, the curing period was considered for 1 day, 7 days, and 28 days as shown in Figure 3D. A slight improvement in q_u was observed from the graph for all the specimens after 7 days of curing. For example, specimen S:5R:3C:1BF12 had an unconfined compressive strength (UCS) of 292 kN/m^2 after one day, and the value increased to 318 kN/m^2 at 7 days of curing. After 28 days of curing, there was a significant increase in the UCS value for S:5R:3C:1BF3, S:5R:3C:1BF6 and S:5R:3C:1BF12 specimen with values 438 kN/m^2, 453 kN/m^2 and 463 kN/m^2 respectively.

The soil matrix also gained strength with an increase in the length of basalt fibres which enhanced the bonding of soil particles by anchoring them together. The highest compressive strengths

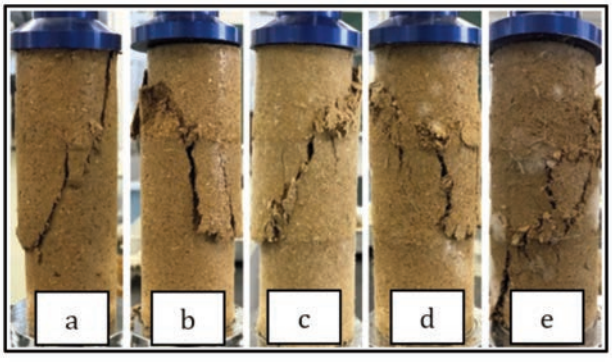

Figure 4. Failure patterns (a) S, (b) S:5R, (c) S:5R:3C:1BF3, (d) S:5R:3C:1BF6, (e) S:5R:3C:1BF12.

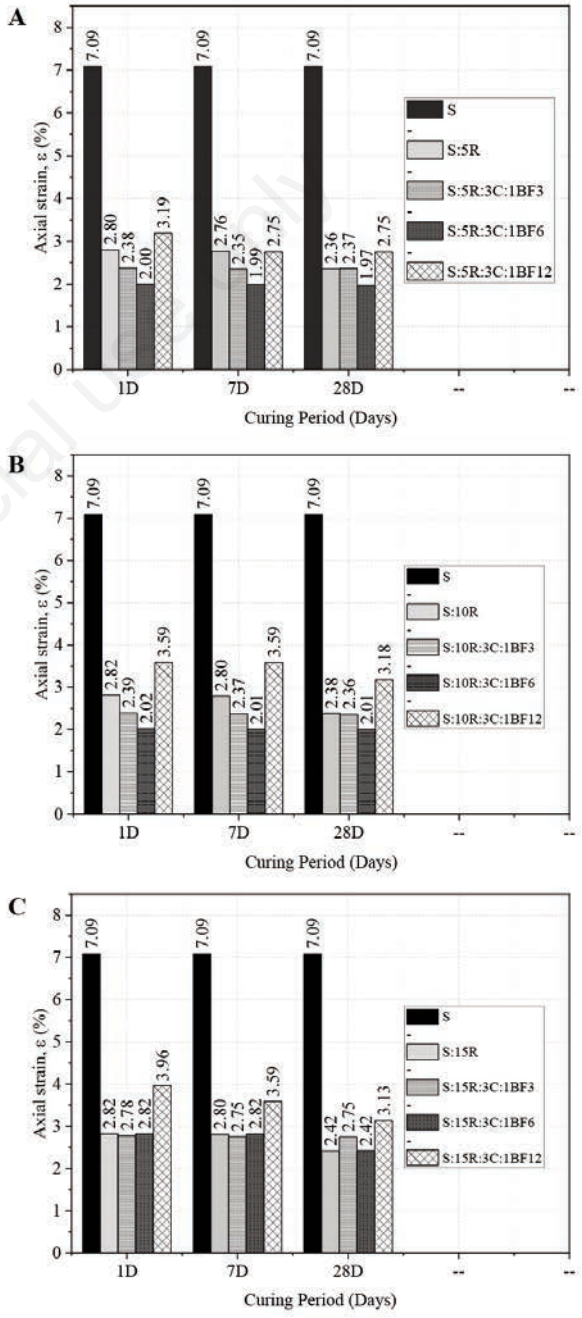

Figure 5. A) Strain *vs* curing periods for 5% of rice husk ash (RHA) and basalt fibre. B) Strain *vs* curing periods for 10% RHA and basalt fibre. C) Strain *vs* curing periods for 15% RHA and basalt fibre.

considering basalt fibre length were obtained from S:5R:3C:1BF12 (463 kN/m^2), S:10R:3C:1BF12 (362 kN/m^2), S:15R:3C:1BF12 (297 kN/m^2) compared to the control specimens' 147 kN/m^2. The UCS increased due to the basalt fibre reinforcements as seen in this study and chemical reaction in the soil matrix, leading to silica gel formation (Kumar *et al*., 2006). Das (1994) classified the quality of subgrade based on UCS value with hard sub-base having UCS values greater than 380 kN/m^2. From this study, S:5R:3C:1BF12 produced a compressive strength of 463 kN/m^2 and can be used as subgrade material for construction works

Figure 4 summarises the failure planes for control specimen, S and the 5% RHA specimen (S:5R, S:5R:3C:1BF3, S:5R:3C:1BF6, and S:5R:3C:1BF12). The first three *specimens*, *a*, *b* and *c*, experienced a simple shear failure with a diagonal failure plane on the upper layers upon maximum compression load. The higher strength mix ratios S:5R:3C:1BF6 and S:5R:3C:1BF12 showed a tension failure with an almost vertical failure plane cutting across all three layers.

It was observed that cracks occurred in the vertical plane for *specimen a* at a strain of 7%, and this strain value reduced considerably to less than 3% for *specimens b*, *c*, and *d* after adding basalt fibres. This reduction in axial strain is shown in Figure 5 for 5%, 10%, and 15% RHA, respectively. Amongst the basalt fibre specimen, 12 mm long fibres had a 1% increase in axial strain compared to BF 3 mm and BF 6 mm. The increase was due to the slight extra deformations during compression, required to tension the randomly placed 12mm long basalt fibres in the specimen structure before the reinforcing benefits were realised. Lawton *et al*. (1993) reported a relatable increase in strain value using multi-oriented geosynthetics. The axial strains reduced slightly after 28 days of curing, signifying shear strength and stiffness development in the soil specimen.

For better clarification on the field use of the results, Figure 6A shows the relationship between the modulus of deformation, E_{50}, and curing period. Adding RHA, cement, and basalt fibre had a tremendous influence on E_{50}. A significant increase was observed after 28 days of curing with 5% mix ratios giving the highest E_{50}. For mix ratios, 5R, S:5R:3C:1BF3, S:5R:3C:1BF6, S:5R:3C:1BF12 the modulus of deformations were 16 MPa, 20 Mpa, 26 MPa, and 29 MPa, respectively, which were much higher compared to control specimen (3 MPa). Specimen S:5R:3C:1BF12 gave the maximum E_{50} due to the high compressive stress of 463 kN/m^2 and additional reinforcing effect after the tensioning of the longer fibres compared to the fibre lengths 3 mm and 6 mm. The dimensional configurations of the basalt fibres and the random dis-

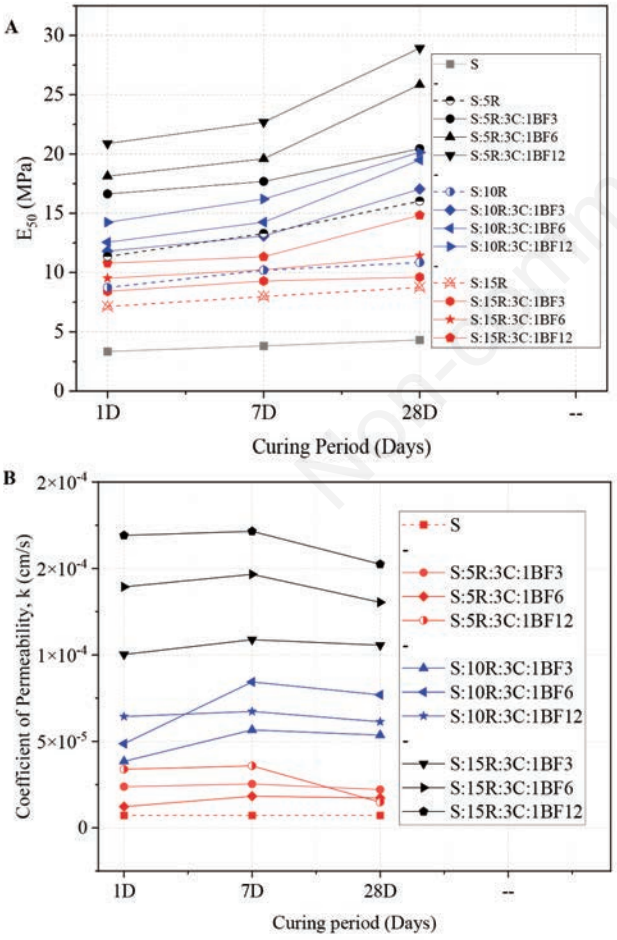

Figure 6. A) Relationship between E_{50} and curing period. B) Coefficient of permeability, k *vs* curing periods.

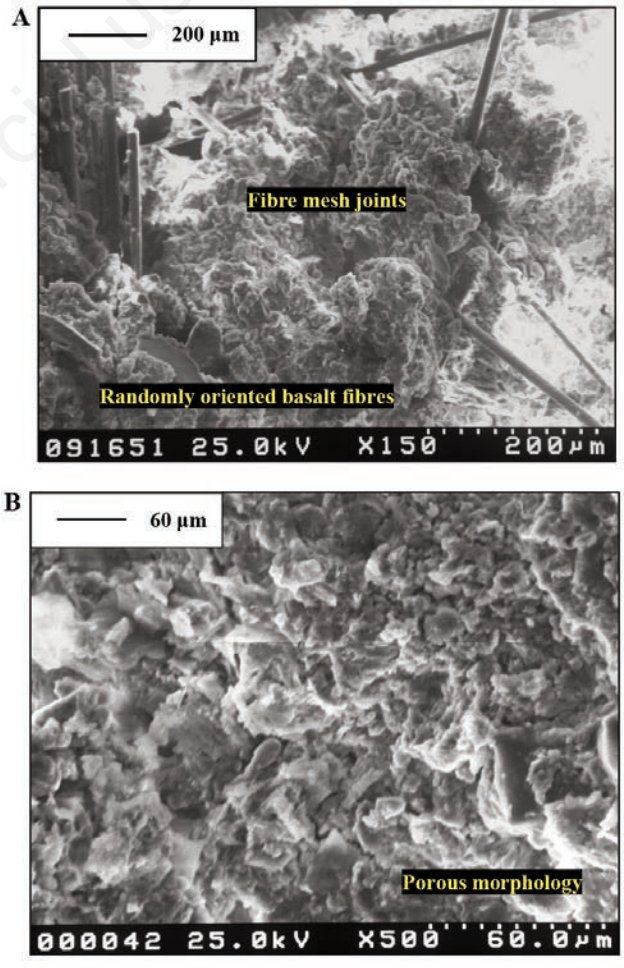

Figure 7. A) Scanning electron microscope (SEM) of magnification ×150. B) SEM of magnification ×500.

tribution of the 12 mm fibres reinforced a larger area in the soil composite structure than the shorter 3 mm and 6 mm upon full tensioning during compression.

Permeability test results

Permeability test examines the water flow rate through a soil medium and is expressed as the coefficient of permeability, k. This water flow rate significantly impacts soils' physical properties when it comes to drainage of subgrade material. In this study, the soil had a very low permeability of 7.1×10^{-6} cm/s, which was not considered suitable for subgrade or shallow foundation use - adding basalt fibres into the soil increased k to 10^{-5} cm/s for all 5% to 10%RHA specimen and 10^{-4} cm/s for 15% RHA specimen, as shown in Figure 6B. From 1 day to 7 days of curing, k increased due to the rapid flocculation of particles in the specimens (Hossain and Sakai, 2008; Wong, 2008) that led to the formation of larger voids in addition to the gaps created by basalt fibres. It was also evident that k declined at 28 days of curing due to the cementation effect that enhanced the binding of the particles in the specimen (Wong *et al*., 2008). This study found out that adding basalt fibres to RHA treated soil increased the value of k, thus improving the drainage potential of the stabilised expansive soil.

Scanning electron microscope

The bonding phenomenon can be validated using SEM images with different magnifications to examine the specimen at both macro-level (Figure 7A) and micro-level (Figure 7B). Figure 7 shows a representative high strength specimen sample with the combinations S:5R:3C:1BF12. The macro-level examination of the specimens (×150) showed the anchoring effect of the basalt fibres, while the micro-level (×500) exhibited the porous morphology in the soil composite structure. This anchoring effect confirmed the increase in compressive strength within the specimens compared to the control. Furthermore, the chemical reaction between soil, RHA, and cement combined with the reinforcing behaviour of basalt fibres form the porous morphology that increased permeability substantially.

Conclusions

The effects of basalt fibre as a potential reinforcing material to RHA-treated soils for ground stabilisation were investigated in this paper. From the results and discussions above, the following conclusions can be drawn. Unconfined compressive strength of compressible clay having 5% rice husk ash increased with the addition of basalt fibres from BF 3 mm to BF 6 mm to BF 12 mm. An increase in UCS value was also evident for 10% and 15% RHA which had UCS values higher than the control specimen but lower than the 5% RHA specimen. Basalt fibres (BF) and the cementitious soil mass improved compressibility and permeability. Notably, the dimensional considerations of the basalt fibre had a significant influence on the compressive strength, with the 12 mm fibres specimen, S:5R:3C:1BF12, showing the top q_u of 463 (kN/m^2) and E_{50} of 29(MN/m^2) after 28 days of curing at 25°C.

In general, the inclusions of randomly oriented Basalt fibre into the soil, combined with the rapidly hardening CSH gel, improved the geotechnical engineering behaviour of the new material and can be proposed for use as a subgrade material for farm roads, pavements, and as fill material in shallow foundations.

References

Alhassan M. 2008. Potentials of rice husk ash for soil stabilization. Assumption Univ. J. Tech. 11:246-50.

Alhassan M. 2008. Permeability of lateritic soil treated with lime and rice husk ash. Assumption Univer. J. Thailand 12:115-20.

Ali F.H., Adnan A., Choy C.K., 1992. Geotechnical Properties of a chemically stabilized soil from Malaysia with rice husk ash as an additive. Geotech. Geol. Eng. 10:117-34.

Anupam A.K., Kumar P., Ransinchung G.D. 2012. Permeability study on fly ash and rice husk ash admixes with subgrade soil for pavement construction. In Proc. of Int. l Conf. on Adv. Archit. Civ. Eng. 21:489.

Aprianti E., Shafigh P., Bahri S., Farahani J.N. 2015. Supplementary cementitious materials origin from agricultural wastes - A review. Constr. Build. Mater. 74:176-87.

Basha E.A., Hashim R., Mahmud H.B., Muntohar A. S., 2005. Stabilization of residual soil with rice husk ash and cement. Constr. Build. Mater. 19:448-53.

Berozashvili M. 2001, Continuous reinforcing fibers are being offered for construction, civil engineering, and other composites applications. Adv. Mater. Com. News. Compos Worldwide. 6:5-6.

Consoli N.C., Prietto P.D., Ulbrich L.A. 1998. Influence of fiber and cement addition on behavior of sandy soil. J. Geotech. Geoenviron. Eng. 124:1211-4.

Cristelo N., Cunha V.M., Dias M., Gomes A.T., Miranda T., Araújo, N. 2015. Influence of discrete fiber reinforcement on the uniaxial compression response and seismic wave velocity of a cement-stabilized sandy-clay. Geotext. Geomembr. 43:1-13.

Crockford W.W. 1993. Strength and life of stabilized pavement layers containing fibrillated polypropylene. In Grogan, W.P. and Chill, D.S. Publ. N. 1418.

Das B.M. 1994. Principles of geotechnical engineering, 3rd edn. PWS-Kent Publishing Company, Boston.

Fatahi B., Fatahi B., Le T.M., Khabbaz H. 2013. Small-strain properties of soft clay treated with fiber and cement. Geosynth. Int. 20:286-300.

Fattah M.Y., Rahil F.H., Al-Soudany K.Y. 2013. Improvement of clayey soil characteristics using rice husk ash. J. Civ. Eng. Urb. 3:12-8.

Festugato L., Fourie A., Consoli N.C. 2013. Cyclic shear response of fibre-reinforced cemented paste backfill. Géotech. Lett. 3:5-12.

Hossain M.Z., Awal A.A. 2011. Flexural response of hybrid carbon fiber thin cement composites. Constr. Build. Mater. 25:670-7.

Hossain M.Z., Sakai T. 2008. The effectiveness of nominal dosage of ordinary cement on strength and permeability of clayey soil. J. Jpn Soc. Soil Phys. 110:25-35.

Ibraim E., Diambra A., Wood D.M., Russell A.R. 2010. Static liquefaction of fibre reinforced sand under monotonic loading. Geotext. Geomembr. 28:374-85.

James J., Rao M. S. 1986. Reaction product of lime and silica from rice husk ash. Cem. Concr. Res. 16:67-73.

JIS A 1210. 2010. Test method for soil compaction using a rammer. Japanese Industrial Standard, Guidance and Basic - Soil Test, The Jpn. Geotech. Soc. pp. 71-78. [in Japanese].

JIS A 1216. 2010. Method for unconfined compression test of soils. Japanese Industrial Standard, Guidance and Basic - Soil Test, The Jpn. Geotech. Soc. pp. 151-158. [in Japanese].

JIS A 1216. 2010. Permeability test of soils. Japanese Industrial

Standard, Guidance and Basic - Soil Test, The Jpn. Geotech. Soc. pp. 91-102. [in Japanese].
Kumar A., Walia B.S., Mohan J. 2006. Compressive strength of fiber-reinforced highly compressible clay. Constr. Build. Mater. 20:1063-8.
Lawton E.C., Khire M.V., Fox N.S. 1993. Reinforcement of soils by multioriented geosynthetic inclusions. J. Geotech. Eng. 119:257-75.
Lopresto V., Leone C., De Iorio I. 2011. Mechanical characterization of basalt fiber reinforced plastic. Compos. Part B. 42:717-23.
Maher M.H., Gray D.H. 1990. Static response of sands reinforced with randomly distributed fibers. J. Geotechn. Engine. 116:1661-77.
Malhotra V.M., Mehta P.K. 2004. Pozzolanic and cementitious materials. CRC Press, Boca Raton, FL, USA.
Mitchell J.K. 1981. Soil improvement-state of the art report. In Proc., 11th Int. Conf. on SMFE. 4:509-65.
Muntohar A.S. 2004. Uses of RHA to enhance lime-stabilized clay soil. pp 356-357 in Int. Conf. Geotech. Eng. Univ. of Sharjah, United Arab Emirate.
Noor M.J.M.M., Aziz A.A., Suhadi R.U.R. 1993. Effects of cement-rice husk ash mixtures on compaction, strength, and durability of Melaka Series lateritic soil. Prof. J. Inst. Surveyors Malaysia 28:61-7.
Park S. 2009. Effect of fiber reinforcement and distribution on unconfined compressive strength of fiber-reinforced cemented sand. Geotext. Geomembr. 27:162-6.
Rahman M.D.A. 1986. The potentials of some stabilizers for the use of lateritic soil in construction. Build. Environ. 21:57-61.
Rao D.K., Pranav P.R.T., Anusha M. 2011. Stabilization of expansive soil with rice husk ash, lime and gypsum-an experimental study. Int. J. Eng. Sci. Tech. 3:8076-85.
Robert W.D. 2008. Soil testing manual: procedures, classification data, and sampling practices. Press of Ohio, OH, USA.
Rogers C.D., Glendinning S. 2000. Lime requirement for stabilization. Transp. Res. Rec. 1721:9-18.
Sim J., Park C. 2005. Characteristics of basalt fiber as a strengthening material for concrete structures. Compos. Part B. 36:504-12.
Wong L.S., Hashim R., Ali F.H. 2008. Strength and permeability of stabilized peat soil. J. Appl. Sci. 8: 3986-90.